Creation and *In Vivo* Evaluation of a Porous Electrode for Pacing in a Coronary Vein: An Assessment of the Potential for Improved Electrical Performance and Chronic Stability of Coronary Venous Pacing Leads

A DISSERTATION
SUBMITTED TO THE FACULTY OF THE GRADUATE SCHOOL
OF THE UNIVERSITY OF MINNESOTA
BY

Brendan Early Koop

IN PARTIAL FULFILLMENT OF THE REQUIREMENTS
FOR THE DEGREE OF
DOCTOR OF PHILOSOPHY

Prof. Art Erdman

May, 2009

Acknowledgements

I would like to acknowledge my advisor, Prof. Art Erdman, for taking me on as an advisee and providing me sound advice throughout my doctoral studies. I was not a typical doctoral student in that I did not perform research for Dr. Erdman specifically, nor was I funded through him. However, due to Dr. Erdman's profound interest in the good of his students and his complimentary interests in medical devices and in fostering productive ties between the University of Minnesota and industry, he agreed to advise me in my doctoral studies and for this I am profoundly grateful. I would also like to acknowledge the rest of my doctoral thesis committee members for their service and advice: Prof. Will Durfee, Prof. Joachim Heberlein, and Prof. Chun Wang.

Many personnel at Boston Scientific CRM were of great help to me, though a few are of special note. Lili Liu, MD, performed many of the lead implants for my chronic animal study and also provided a second set of eyes in determining lead retractions via x-rays. Bill Stoffregen, DVM, PhD performed tissue slicing and histology for my study and was extremely helpful to me in interpreting the results. Mitchell Springer assisted with characterization of the porous electrodes and also with calculations of surface area and did fine work in using cyclic voltammetry for these calculations. I would also like to acknowledge Boston Scientific CRM as a whole and express my deepest gratitude for funding my research, supporting me through my doctoral education, and most especially for always showing confidence in me and my abilities. I hope that the research I have conducted and documented in this thesis will not only prove to be of general scientific value, but also prove to be of great value to the company.

Dedication

I dedicate this work to my wife, Molly, and our children, Clara, Aidan, Eleanor, Maximilian, and Henry, and all our future children. Molly, you have always supported me in any endeavor that I thought was important, and your support throughout my doctoral work involved great sacrifice on your part. I thank you so much for being the wonderful, selfless, and loving wife that you are and I can only hope to catch up to you in holiness some day. I love you! And to all my children, I hope that my work and perseverance throughout all of my education, and my sincere desire to glorify God through my efforts, will inspire you to do the same in whatever God calls you to do or be.

I thank also my parents, Steven and Debra, for instilling a profound love of learning in me that has compelled me through to the end of my formal education and will enrich the rest of my life with new experiences and wonder at God's creation.

Finally, I thank the Lord most deeply for allowing me to start, and complete, my doctoral work. He always orders things for the good of my soul, and I am humbled that He saw fit to include this work in His plan for me.

Ad majorem Dei gloriam

Abstract

In this work, a porous electrode was fabricated and evaluated in a chronic animal study on a coronary venous pacing lead in order to assess its potential for mitigating chronic lead dislodgements and reducing the characteristic rise in pacing thresholds after implant, both of which being important issues that impact safety and efficacy of implanted cardiac resynchronization therapy systems. Eight test leads were assembled with a porous tip electrode with an average pore size of approximately 30 μm, created via a novel fabrication method, and eight control leads were assembled with a standard solid tip electrode design. Both groups were created without steroid-eluting collars and without a capacitive coating on the tip electrodes in order to isolate the affects of electrode porosity. Leads were implanted in canines, and electrical data and x-rays of lead position were taken regularly throughout the 60-day study. Tissue histology was performed for each lead.

Significantly lower ($p<0.05$) mean rise in pacing threshold after implant was observed at day 3 and day 21 for the test group leads (with porous electrodes) as compared to the control group leads. Despite the higher surface area of the porous tip electrodes, pacing impedance was not statistically different between the groups throughout the study, a result likely due to decreased chronic inflammatory response at the surface of porous electrodes. The test group had no lead retractions after day 3 as determined by inspection of x-ray radiographs, while 3-6 (of 8) control group leads retracted after day 3, a result likely due to anchoring of the lead tip due to observed tissue growth into porous electrodes. Mean fibrous capsule thickness at pre-defined measurement points on the tip electrode was not statistically different between the

groups, which correlates with the nearly equal mean pacing thresholds for the groups at day 60. The lack of lead retractions for the test groups leads after day 3 is a promising result which should be investigated further, along with investigations of lead extraction force and further electrical data evaluations, using larger sample sizes and more challenging implant conditions.

Table of Contents

1 Introduction

Electrodes are essential components in implantable electrical devices for transmitting electrical stimuli to the *in vivo* environment and sensing intrinsic signals in the surrounding tissue. Uses of electrodes in implantable devices range from neurological devices for the treatment of tremors resulting from Parkinson's disease, to cardiac devices for the treatment of arrhythmias, to chronic diagnostic catheters, just to name a few. However, in all applications there still remain significant challenges to creating safe and effective electrodes that allow the device to operate as intended. The surface of the electrode, the interface between device and biological environment, is of primary importance in mitigating these challenges.

Understanding the electrode surface, and the manner in which the body responds to that surface, is critical for designing an electrode to function as intended in the body. The foreign body response, or the response of the body to the implantation of a foreign object such as a medical device, is often the environmental issue that has the most impact on electrode performance due to the eventual formation of a fibrotic capsule around the surface of the device [1,2]. The chronic growth of the fibrous capsule, which is typically made up of tightly packed collagen type I and type III fibers and fibroblasts [2], serves to separate the electrode surface from the surrounding tissue with which it was meant to interact and thus degrades electrical function. Detailed knowledge of the process by which this capsule forms, the timescale and stages of its formation, and the resulting effect on electrical function is a requirement for intelligently designing medical device electrodes that can operate as intended in this

extremely complex environment. As a specific example, pacemaker lead electrodes, the subject of this work, cannot be the conduit for effective delivery of what is often life-sustaining therapy without being designed with a thorough knowledge of the body's acute and chronic response to the lead and electrode surface.

1.1 The Foreign Body Response

The foreign body response is initiated by local injury to tissue surrounding an implanted device due to the introduction of that device into the body, and thus is very difficult to prevent [3]. When a medical device is introduced into the body and is exposed to blood, either by implanting the device within the venous or arterial system itself, or by implanting in blood-perfused tissues and causing local injury, it is labeled by the body as a foreign object within seconds through non-specific protein adsorption (also call "opsonization") [2]. Certain proteins that normally circulate within the blood in an inactivated state immediately bind to the device and denature into an activated configuration. This activated configuration sets off a cascade of subsequent protein activations (called the "complement system") that alerts the body to the presence of the foreign object [4]. Attachment of phagocytic cells, such as neutrophils and monocytes (which also normally circulate in the blood), ensues through directed movement along chemical gradients toward the implanted device ("chemotaxis"), eventually resulting in recognition of the adsorbed proteins and attachment to the implant surface [2]. Neutrophils (a type of white blood cell) are first to the site of the implant, replaced later by monocytes, which eventually differentiate into macrophages via activation by adsorbed proteins [2]. Recruitment of these phagocytic cells is enhanced by increased vascular permeability during the first few days after device implant, which floods the

area with fluids [1].

Phagocytic cells attack and digest (through a process called "phagocytosis") any foreign objects within the body, such as particulate matter, bacteria, or other nonviable items such as dead cells. Normally such material is small enough that the cells can fully surround the object and digest it. However, in the presence of a much larger foreign object like a medical device, the attempts of macrophages (for example) to surround the device result in "frustrated phagocytosis," which causes more release of inflammatory stimuli and agglomeration of macrophages into larger, multinuclear cells call foreign body giant cells (FBGC's) [4]. A layer of macrophages and FBGC's often persists adjacent to the device surface for the life of the implant, persistently attempting to heal the area (chronic inflammation) [5]. Macrophages also recruit fibroblasts to the area which form an extracellular matrix of primarily collagen (the fibrous capsule), typically 50-200 μm thick, which serves to wall off the device from the rest of the body [5]. This can be considered the chronic steady state of the foreign body response. For reference, an outline of the events just discussed with relative timing is given in Figure 1 [5]:

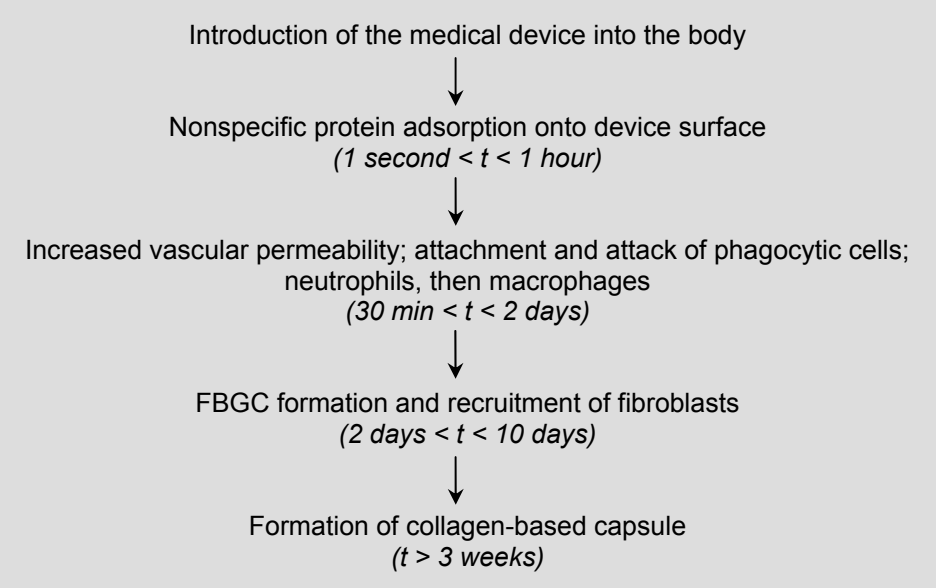

Figure 1: Outline of the biological response to implantation of a foreign body (such as a medical device) [5].

Though this discussion of the foreign body response is brief, it is key to eventually understanding the root causes for differing levels of response to different implants.

1.2 Pacing Leads, Porous Electrodes, and the Foreign Body Response

Implantation of an artificial pacemaker for the treatment of bradycardia and other cardiac conditions has a long history that spans decades. Modern pacemakers are typically implanted subcutaneously near the left or right shoulder and connected to leads that are implanted transvenously into the right chambers of the heart. Figure 2 shows a diagram of a typical implant configuration of a dual-chamber pacemaker; that is, one that is intended to pace and/or sense from both the right atrium and right ventricle.

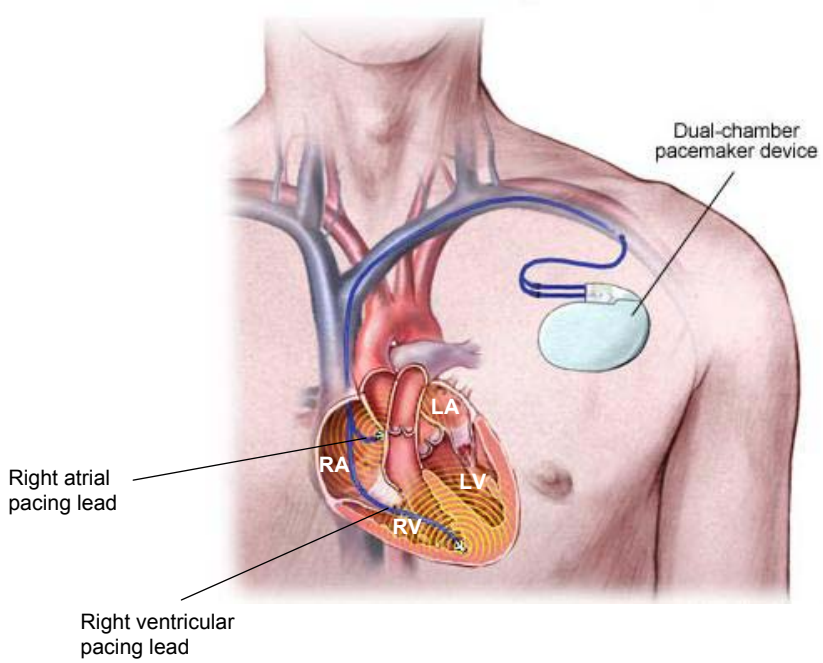

Figure 2: Diagram of a typical implant configuration of a dual chamber pacemaker. The heart's right atrium (RA), right ventricle (RV), left atrium (LA), and left ventricle (LV) are also shown. [6]

As can be seen in Figure 2, the pacing leads are the only components of the pacing system that physically and electrically interact with the heart itself. More specifically, the pacing lead electrodes are critically important in delivery of therapy from the pacemaker to the heart as the electrode/tissue interface is the only means of communication between the device and the heart. Leads, which are insulated conductors connecting the pacemaker to the desired site in the heart, provide the means of transmitting electrical stimuli and sensing the intrinsic cardiac signal. Stability, electrical performance, and reliability of leads are just of few of the important factors that are critical to the ability of the pacemaker to properly deliver appropriate and timely therapy.

Notwithstanding the introduction of a pharmacological agent for active

intervention, certain factors relating to the mechanical design of the electrode can be controlled to minimize fibrotic capsule thickness. An example of one such factor is porosity of the electrode surface for facilitation of tissue in-growth, a design that has been employed in various ways in right atrial (RA) and right ventricular (RV) pacing leads and has been shown to reduce fibrotic capsule thickness at the electrode [7-11]. Though porosity in pacing electrodes was initially thought to improve electrical performance only as a consequence of increased charge densities [12], it has also been hypothesized that tissue in-growth into appropriately sized pores has the effect of stabilizing the interface between tissue and electrode during cardiac motion, resulting in decreased chronic tissue irritation and a smaller fibrotic capsule thickness [8,13,14]. Accordingly, further electrical performance benefits ensue, as the distance from electrode surface to excitable myocardial tissue is reduced commensurate with the decrease in fibrotic capsule thickness.

From at least the mid 1970's, researchers have been interested in creating porosity on pacing electrode surfaces to address poor lead electrical performance, chronic stability, and electrode biocompatibility [8,12]. The electrodes generally consisted of either porous-surface electrodes, created by sintering of metal microspheres on the electrode surface, or porous-mesh electrodes, created by sintering of metal fibers in a hemispherical shape to form the electrode as a whole [7-9]. Platinum or platinum iridium were typically used to form the porous surface or mesh, given that the vast majority of pacing lead electrodes were constructed of these biocompatible materials (and still are today). The applications for these electrodes were limited to RA and RV

pacing leads and RV defibrillation leads, which were the extent of cardiac lead applications until roughly the year 2001.

Porous electrodes were mainly investigated for their hypothesized benefits to electrical performance, with the main goal being to increase the active surface area of the electrode while maintaining the same geometrical size. Increasing the electrically active surface area was found to reduce polarization losses at the electrode surface caused in the charging and discharging of the ion double layer that forms when the electrode is positively or negatively charged [15]. This electrochemical benefit of increased active surface area was one of the main hypotheses for decreased stimulation threshold voltages that were found for both porous-surface and porous-mesh electrodes compared to solid electrodes of the same size [8,9,11]. This is a highly desirable outcome as decreasing pacing thresholds, or the minimum voltage required to depolarize myocardial tissue, improves the longevity of the PG by extending battery life since less voltage is used to pace the heart.

However, upon histological evaluation of the tissue surrounding (and grown into) porous electrodes, it became apparent that electrochemistry alone could not fully account for the improved electrical performance of these electrodes. Researchers that performed histology on porous pacing electrodes discovered that the thickness of the fibrous capsule surrounding the electrode was markedly decreased compared to a solid electrode [7-11]. Researchers also found that chronic lead stability was improved, as evidenced by significantly fewer dislodgements of leads having a porous electrode when evaluated *in vivo* [8-10,16]. The main hypothesis for the reduction in fibrous capsule thickness was the integration of tissue into the electrode itself, which reduces or

eliminates motion, and thus irritation, between the tissue and electrode at the interface due to cyclic cardiac motion [9,10,16]. This phenomenon at the same time can account for reduced lead dislodgements as compared to a solid electrode due to the enhanced tissue attachment and increased mechanical stability generated thereafter. No matter the cause, it was apparent that the main reason for the reduced pacing thresholds of porous electrodes vis-à-vis solid electrodes was actually the reduced thickness of fibrous encapsulation [9,10,16]. The reason the thickness of the fibrous capsule has such an effect on pacing threshold is only apparent from the basic electrical theory of depolarization of myocardial cells via a pacing electrode.

1.3 The Effect of Fibrous Encapsulation on Pacing Threshold and Impedance

A pacemaker causes a contraction in the chamber in which the lead is implanted by creating an electric field between the lead cathode and lead anode (in the case of a bipolar lead; in the case of a unipolar lead the anode is the pacemaker), with enough strength and for a long enough period of time to depolarize the cells in the surrounding myocardium [17]. Though modern implantable pacemakers and defibrillators operate as constant voltage sources, it is not specifically the voltage that causes myocardial depolarization but rather the density of current flow between the cathode and anode of the lead [18,19]. Direct injection of current into the extracellular matrix and through cell membranes can raise the potential difference between the inside and outside of myocardial cells (trans-membrane potential) to depolarization threshold as positive ions, for example, flow toward the lead cathode [20]. The higher the density of current flow, the more readily the myocyte trans-membrane potential is altered.

In order to cause depolarization, the resting trans-membrane potential difference of -90 mV maintained by the myocardial cell with respect to the extracellular matrix is raised to a threshold potential difference of approximately -60 to -70 mV, which triggers opening of ion channels in the cell membrane and allows an influx of sodium ions (Na^+) [21]. Thus, after reaching the threshold potential, the cell is activated and the balance of the myocardial action potential proceeds independent of any external stimulus, reversing the polarity of the cell (up to approximately +20 mV) via exchange of ions through the cell membrane [17,21]. Calcium ions (Ca^{2+}), which enter the cell after sodium ion influx, specifically cause the contraction of the cell by mediation of actin/myosin cross-bridge formation through activation of the protein troponin [22]. Ion exchange within a myocardial cell also influences the potential of neighboring cells through cell-to-cell junctions, causing their depolarization and continuing likewise cell to cell like a wave, causing contraction of the full chamber where the lead is implanted [17]. This contraction pumps the volume of blood in the chamber out through a valve and into the ventricle (in the case of an atrial contraction) or into the greater venous or arterial systems (in the case of a ventricular contraction).

Most often both electric field strength and current density play a role in causing myocardial cell depolarization via external stimulation by a pacing lead [22]. In either case, the proximity of the electrode surface to excitable myocardial cells affects the minimum voltage necessary at the lead electrode to cause depolarization. The distance from electrode surface to excitable myocardial cells is affected by the degree of inflammation and foreign body response that occurs at the surface of the pacing lead electrode. During the course of acute inflammation and the chronic foreign body

response that occurs after implant of the lead, myocardial tissue near the electrode surface is remodeled and becomes non-excitable [17]. That is, the attachment of phagocytic cells, as well as the recruitment of fibroblasts and the creation of a collagenous extracellular matrix, replaces excitable myocardial cells with non-excitable cells/tissue. The remodeled area can conduct ionic currents, but the cells do not depolarize and contract in response to the electric field created by the lead electrode (like myocardial tissue). In effect, a new, larger, "virtual" surface area of the electrode is created, the "surface" that is the interface of excitable and non-excitable tissue, requiring a higher voltage to be created at the physical electrode surface in order to create a strong enough electric field with enough current density at this tissue interface to depolarize the myocardium [17].

In order to understand the dependence of electric field strength on the distance from the source of the field, one need only look at the equation for electric field at a point outside of a uniformly-charged spherical shell (Gauss's Law). The case of a uniformly charged spherical shell, or even a point charge for that matter, is an appropriate analog to a uniformly-charged hemispherical tip electrode on a pacing lead.

$$\vec{E} = \frac{1}{4\pi\varepsilon_0}\frac{q}{r^2}\hat{r}$$

q: Total charge on the sphere
r: Distance from the surface of the sphere to the point of measurement
$\hat{r}$: Unit vector normal to the surface of the sphere

The strength of the electric field ($\vec{E}$) is inversely proportional to the square of the distance away from the charged sphere (r). So, as one moves further away from the surface of the charged sphere, the electric field strength falls off dramatically. Gauss's

Law also gives us the relationship of the potential (V) to the distance away from the surface of a charged spherical shell, which is shown below.

$$V = \frac{1}{4\pi\varepsilon_0}\frac{q}{r}$$

noting that $\vec{E} = -\nabla V$

Here we also see that the potential (V) also is inversely proportional to the distance away from the surface of the charged shell (r), and that the electric field is simply the negative gradient of the potential. Finally, we also can also deduce the dependence of current density ($\vec{J}$) on the distance from the charged surface (r) from the flux of current through a spherical surface.

$$I = \int_S \vec{J} \cdot dA$$

I: Electric current
A: Area of hypothetical surface through which current is passing

If the current density on the surface area A is assumed to be uniform, then we have,

$$I = JA$$

$$J = \frac{I}{A}$$

$$J = \frac{I}{4\pi r^2}$$

r: Distance from the surface of the charged sphere to the spherical surface at which the current density is being evaluated

So the current density also falls off dramatically with increasing distance away from the electrode surface.

In the case of depolarization of cardiac myocytes, where the trans-membrane potential can be dependent on E and J, it is apparent that proximity of the electrode

surface to these excitable cells is the most important driving factor in minimizing the amount of voltage necessary at the electrode surface to induce depolarization. The greater the thickness of surrounding acute inflammation and the eventual fibrous capsule, the higher the voltage necessary at the electrode to create the required *E* and *J* for cellular depolarization. Higher voltage at the electrode causes more charge to be drained from the battery of the pacemaker, decreasing battery life. Figure 3 schematically depicts a tip electrode of a right-sided, passive-fixation pacing lead and the manner in which acute inflammation and the eventual chronic foreign body response (fibrous capsule) causes higher pacing thresholds by increasing the distance from the electrode surface to excitable myocardial tissue.

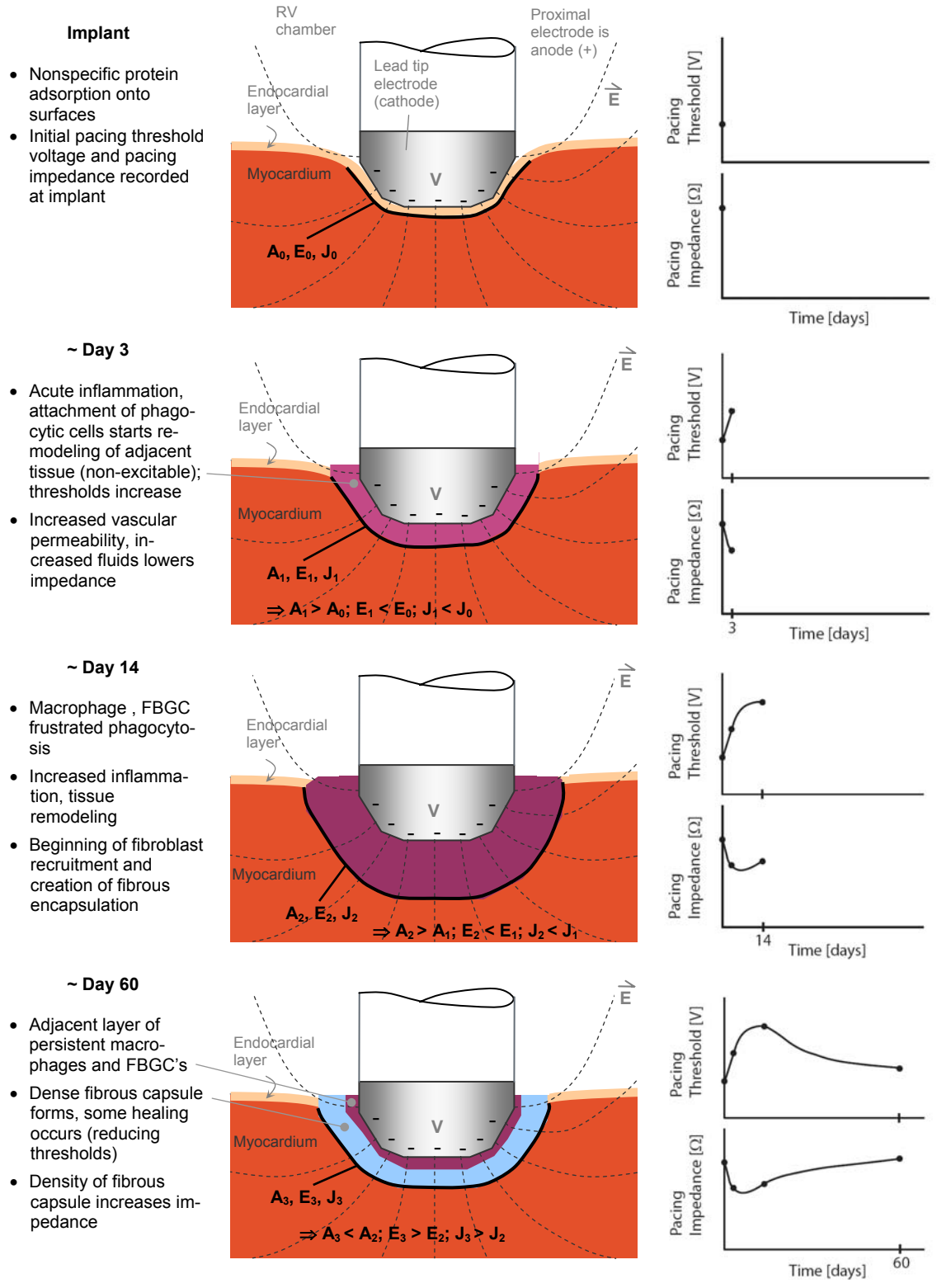

Figure 3: Schematic representation of the acute and chronic foreign body response and the resulting effect on pacing threshold and impedance.

There are a number of things that should be noted in regard to Figure 3. The first is that the main causal factor driving fluctuation in pacing thresholds is the increasing virtual "surface area" of the electrode caused by tissue remodeling, which can alternately be thought of as the increasing distance from the electrode surface to excitable myocardial cells [21]. As the distance from the electrode surface to the myocardium becomes larger between implant and day 14, the pacing threshold increases accordingly. And as acute inflammation subsides and is at least partly replaced by the fibrous capsule, which decreases the distance from electrode surface to the myocardium, the pacing threshold also decreases accordingly. This relationship between the distance to excitable tissue and pacing threshold is simply due to the reduced current density and electric field strength at the interface of myocardial tissue, which requires a higher voltage difference between the lead cathode and anode in order to depolarize the myocardial cells [21].

The second observation to note in regard to Figure 3 is that the pacing impedance is not influenced by the distance to myocardial tissue like the pacing threshold, but rather is mediated by the impedance properties of the actual cells/tissues that are adjacent to the electrode at any point in time as part of the foreign body response. There is an immediate decrease in pacing impedance after implant that is caused by an increase in vascular permeability and subsequent flooding of the local area with fluids [1]. After day 4 or so, vascular permeability is reduced, and this decrease in local fluids along with an increase in the number of phagocytic cells adjacent to the electrode cause impedance to increase (even while pacing thresholds are still increasing, illustrating that thresholds and impedance are mediated by different causal factors) [1].

Impedance continues to increase as the fibrous capsule, tightly packed with collagen, is created after about day 14, since the capsule itself is of relatively higher impedance than the layer of phagocytic inflammatory cells [1]. From about day 14 forward, the extent of impedance increase is related to the level of "biocompatibility" of the electrode. The existence, and thickness, of any chronically persisting layer of macrophages and FBGC's adjacent to the electrode surface serves to keep impedance lower due to the ability of those cells to conduct through cell membranes (in contrast to the higher impedance fibrous capsule, which is relatively acellular) [1]. However, if fewer macrophages and FBGC's persist chronically, adjacent to the electrode surface, impedance can rise at a faster rate. This is a desirable outcome, as the higher the pacing impedance the more battery life is conserved and the longer the pacemaker remains in service before needing replacement.

1.4 Coronary Venous Pacing Leads

Right-sided pacing leads utilizing porous electrode designs are generally considered "passive" fixation mechanisms in that the lead is utilizing either the porosity of the electrode itself or another mechanism, such as silicone tines near the lead tip, to anchor itself to the endocardial surface of the chamber being paced. In contrast, an "active" fixation mechanism would penetrate the endocardial surface into the myocardium to anchor the lead. Leads using active fixation mechanisms, such as an extendable/retractable helix, have become widely popular for physicians implanting right-sided pacing and defibrillation leads. The advent of an active fixation mechanism largely negated the need for porosity to anchor the lead tip, while another innovation, steroid elution near the tip electrode, decreased the need for porosity to lower fibrous

capsule thickness for low pacing thresholds [23,24]. Steroid elution, or elution of a glucocorticosteroid such as dexamethasone phosphate from a silicone binder, attenuates the inflammatory response near the electrode through the action of the drug, decreasing the fibrotic capsule thickness and consequently also pacing thresholds [23,24]. The current state of the art in RA and RV pacing leads largely does not make use of porous electrodes except in a minority of passive fixation lead models, which some doctors prefer for their handling characteristics during implantation (or for other reasons). However, a different pacing technology, coronary venous pacing leads, offers the potential for a new application of porosity in electrodes to mitigate issues specific to these leads.

Coronary venous pacing leads are relatively new innovations that have expanded the indications for pacemakers and implantable cardioverter defibrillators (ICD's). First introduced in the U. S. in 2001 for use in cardiac resynchronization therapy pacemakers (CRT-P), and in 2002 for use in cardiac resynchronization therapy defibrillators (CRT-D), coronary venous pacing leads are used for treating conditions such as heart failure resulting from mechanical dissynchrony of the right and left ventricles. In these applications, coronary venous leads are often called "left ventricular" leads, or "LV" leads, because they are used to pace the left ventricle such that its contractions are synchronized with those of the right ventricle ("resynchronization therapy").

Implantation of a pacing lead within the actual chambers of the left side of the heart is inadvisable not only because the pressure and forces in the left side are much higher than the right side, but also because if a thrombus were to form on the lead surface and detached it could be pumped to sensitive areas of the body (such as the

brain) and cut off oxygen to tissue by blocking blood flow within an artery. The coronary veins allow access to the left-ventricular myocardium without having to implant a lead inside the LA or LV chambers themselves. Figure 4 shows a computer model of the human heart with the ventricles removed, leaving only the cardiac veins visible. One can see that the coronary sinus, the main return path for deoxygenated blood from the myocardial tissues in the heart, provides a singular point through which the veins on the left ventricle can be accessed. The coronary sinus empties into the right atrium, and thus the access point for placement of a lead in the LV veins is through the coronary sinus "os" (mouth or opening) in the right atrium.

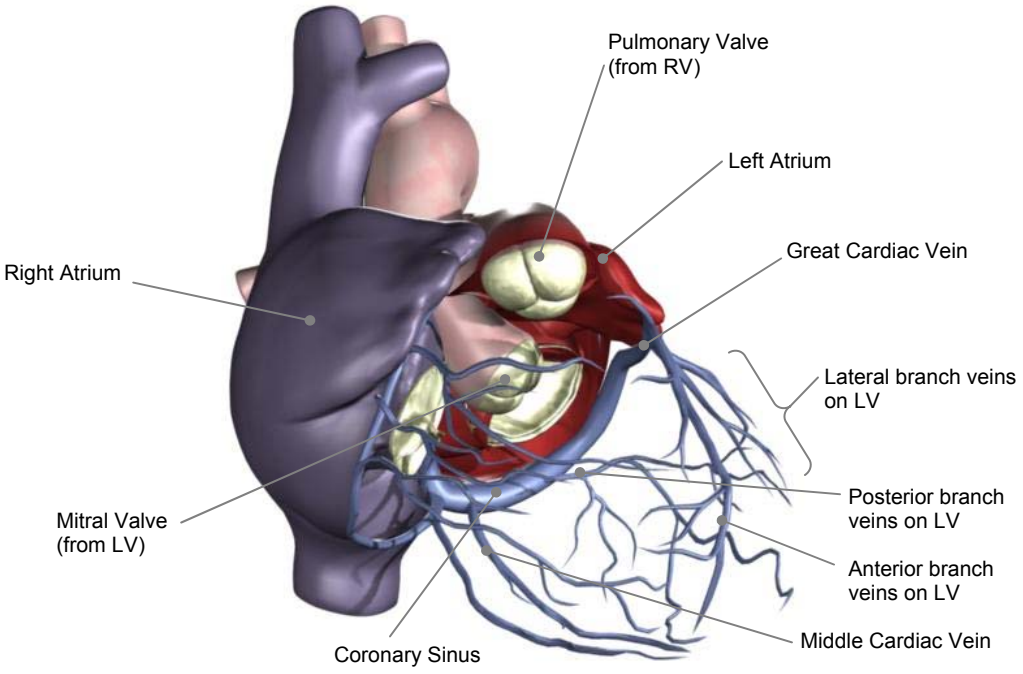

Figure 4: A computer model of the human heart in right anterior oblique (RAO) view, with the ventricles removed leaving only the coronary veins visible. The venous anatomy shown is example, as there is some variation from person-to-person, especially in the smaller branch veins. (Adapted from [25]).

For further information on the anatomy of the coronary veins, reference [26] provides an excellent summary.

A coronary venous lead is placed in a coronary vein in the left ventricular myocardium with the aid of a guiding catheter and a stylet or guide wire via access of the coronary sinus in the right atrium (as shown in Figure 5).

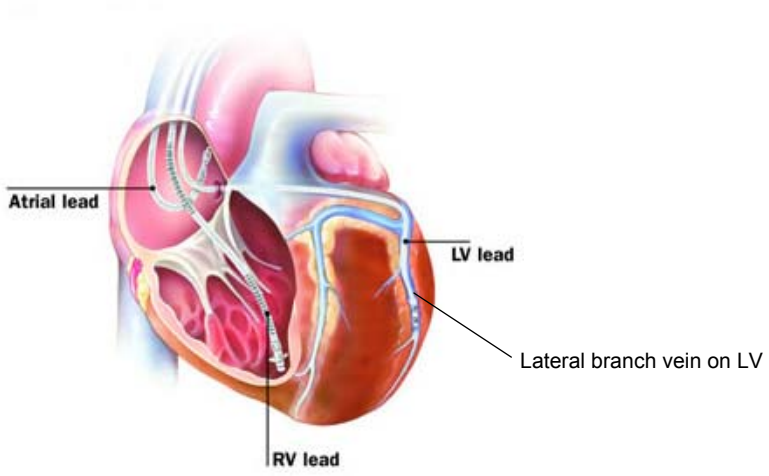

Figure 5: Schematic of anterior of heart in anterior/posterior (AP) view, with right atrium and right ventricle shown in cutaway view. Typical placements of RA, RV, and LV leads are shown for an implanted CRT-D device (not shown) for the treatment of heart failure. (Adapted from [27]).

In order to provide fixation *in situ*, the coronary venous lead is typically designed with tines at the tip of the lead that allow the lead to be wedged in the vein. Alternately, the distal end (i.e. towards the tip) of the lead can be designed with a pre-formed shape (via a shape memory alloy conductor such as MP35N) that presses up against the walls of the vein. Examples of such designs are shown in Figure 6.

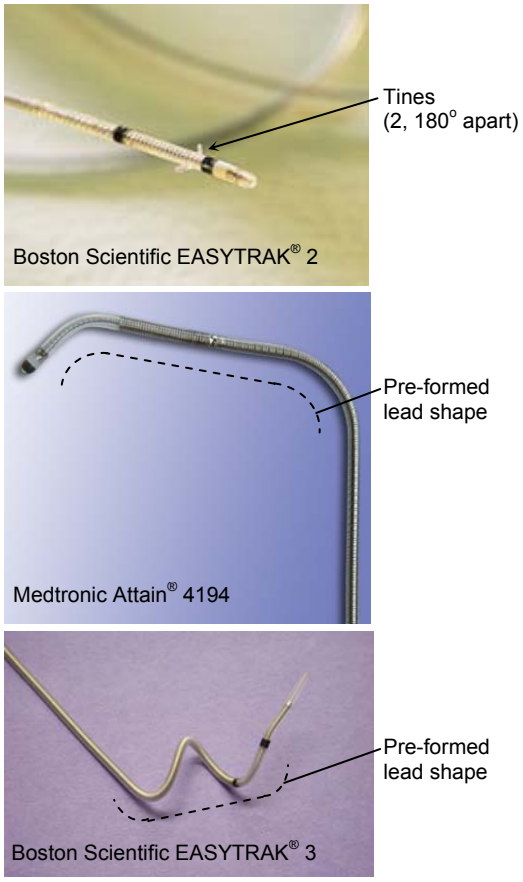

Figure 6: Examples of coronary venous lead fixation mechanisms. [28-30]

These passive fixation mechanisms do not guarantee the lead will stay in its original implant position, and they can also make it more difficult to deliver the lead to the desired vein during implant (as compared to a hypothetical straight lead with no protrusions or shapes). However, an active fixation mechanism (such as a helix electrode that would puncture the vein wall to hold the lead in place) is not a desirable option due to safety concerns.

2 The Problem

In the United States alone, approximately five million people have heart failure with an additional 550,000 diagnosed each year [31]. Thousands of these heart failure patients are implanted with either a CRT-P or CRT-D system every year, which include a coronary venous pacing lead for delivery of therapy to the left ventricle specifically for treatment of heat failure. Stability of coronary venous leads within the vein, both acute (at implant and within the first few days afterward) and chronic (after about day 3), is one of the biggest challenges facing lead designers and physicians today. The designer of coronary venous leads must balance deliverability of the lead, which requires optimized stiffness in the lead body and a high degree of flexibility in the distal end, with creating a reliable lead fixation mechanism, which has thus far required protrusions and pre-formed shapes that can negatively affect deliverability. Clinical trial data to date has also revealed high rates of dislodgements for coronary venous leads, which have been recorded to be in the 3-10% incidence range after the initial implant of the CRT-P or CRT-D system (e.g. [32,33]). Many such dislodgements require the physician to reposition the lead, putting the patient through another surgery, additional mental distress, and further risk of serious complications, including infection. It goes without saying that any advance in coronary venous lead technology that would decrease dislodgement rates would provide a significant benefit to patients and physicians.

Though not as high-impact as stability, there are also significant challenges to creating coronary venous leads that have favorable electrical performance. The

electrode or electrodes of the coronary venous lead reside at the distal end and are typically constructed of 90/10 platinum iridium alloy with a capacitive coating deposited on the outer surface. Most RA and RV leads also utilize these same materials and coatings. However, the tip electrode of RA and RV leads is placed in intimate contact with the endocardial surface of the heart (in the case of a passive fixation lead) or directly into the myocardium of the heart (in the case of an active fixation lead). In contrast, a coronary venous lead is placed in the lumen (or interior) of a coronary vein and where there typically exists a larger distance from the electrode surface to excitable myocardial tissue simply due to anatomy, causing higher pacing thresholds than typically found in RA or RV leads. The foreign body response to the lead in the vein increases the distance to excitable tissue even further as the fibrous capsule forms. Example clinical trial data for a steroid-eluting, endocardial pacing lead show average RA and RV pacing thresholds of 0.7 and 0.6 V at implant, and 0.7 and 0.8 V at 3 months, respectively [34], while Alonso *et al* studied coronary venous leads and reported average pacing thresholds of 1.1 V at implant, increasing to an average of 1.9 V at 3 months [35]. The impact of higher pacing thresholds in coronary venous leads is a greater drain on the battery in the PG, and more frequent surgeries for patients for PG replacement. Thus, another welcome advance in coronary venous leads would be technologies that can reduce chronic pacing thresholds and improve longevity of the PG.

Porous electrodes, with carefully designed porosity, have the potential for addressing issues such as chronic lead stability and high pacing thresholds in coronary venous pacing leads. As discussed previously, there is some evidence that porous

electrodes (depending on the design) can facilitate growth of tissue into the electrode itself. This effect on a coronary venous lead could serve to anchor the lead within the vein and stabilize against the typical forces it experiences in the body, reducing dislodgements. This hypothesized benefit would only occur after tissue grew into the electrode, and so would not have an acute benefit (e.g. during implant or in the period of time between implant and mature tissue in-growth). However, even elimination of chronic dislodgments would be of great benefit, as a significant fraction of coronary venous lead dislodgements occur after, for example, two weeks post-implant [32,33]. Additionally, porous structures, be they electrodes or other types of implants, have been shown to reduce the thickness of fibrous encapsulation due to the foreign body response (e.g. see [10,36,37]). Since reduction of fibrous encapsulation can reduce the distance between the surface of the electrode and excitable myocardial tissue, porous electrodes also have the potential for reducing the voltage threshold necessary to depolarize surrounding myocardial tissue. Therefore, it is the object of this work to design and fabricate a porous electrode capable of use on a coronary venous pacing lead in order to investigate, through chronic animal implants, the potential of such an electrode to reduce chronic lead dislodgements and lower pacing thresholds.

3 Review of Relevant Literature

As of the writing of this thesis, no published literature could be found on any investigations of the effect of porosity in a coronary venous pacing lead electrode on lead stability, fibrous capsule thickness, or pacing thresholds. Even further, published literature on the effect of porosity in a rigid metallic structure in a vessel on local tissue response is extremely sparse. What literature there is on local tissue response to porous structures in vessels mostly focuses on materials used in vascular grafts, such as woven or mesh ePTFE and other polymers (e.g. see [36]). Therefore, this work will constitute an important contribution to the understanding of the biological response to a porous metallic structure in a vessel, as well as contribute to understanding of the potential clinical benefits of such a structure when used as an electrode on a coronary venous pacing lead.

In order to design a porous electrode for use in a coronary venous pacing lead that would cause a favorable biological response (tissue in-growth, thin fibrous encapsulation, among others), it is desirable to know the characteristics of the porous structure that mediate such a response. Not only have the importance (or lack thereof) of certain characteristics been debated, but so also the optimal values of the characteristics in question. The single characteristic of porous structures most often assigned significant importance in the literature in regard to mediating a favorable biological response is average pore size.

Considering for a moment the extremes of pore size, it can certainly be ascertained that as average pore size of a porous structure approaches zero, the

biological response to that structure will, either gradually or abruptly, approach that for a solid structure of the same material. And as average pore size of a porous structure becomes larger and larger, the biological response will also, either gradually or abruptly, approach that for a solid structure of the same material (since the pores would eventually be so large that their local geometry would be indistinguishable to that of a solid surface). Somewhere between these two extremes is an optimum average pore size or range of sizes that mediates the desired biological response. This "optimum" may differ depending on the biological environment and tissue surrounding the implanted porous structure, but in whatever the implant environment of interest, the optimum average pore size should be discoverable. Knowledge of the optimum pore size for porous structures implanted into soft tissues, or even more specifically veins, would be especially useful in designing the porous electrode for this work. Other factors that may influence favorable biological response are also of interest.

Though it is certainly true that different optimal average pore sizes have been reported for significantly different implant environments (such as bone versus soft tissue) [38], even the more specific question of optimal pore size for implant into soft tissues has generated widely varying results from researchers. Table 1 shows a variety of reported results for porous structures that have been implanted into soft tissues, or tested *in vitro* in soft tissue cellular matrices. The reported optimal average pore sizes for tissue in-growth and/or minimum fibrous capsule thickness in Table 1 are worthy of consideration when attempting to create and test a porous electrode on a coronary venous lead. However, from consideration of Table 1, an optimal average pore size would seem to be somewhere between 1-200 μm (a range that covers two orders of

magnitude). No published work could be found that directly reports an optimal average pore size for a rigid metallic porous structure in a vessel (since no such investigation could be found), though studies done on polymer meshes in veins and arteries and studies done on rigid metallic surfaces in endocardium are shown in Table 1.

Table 1: A selection of literature investigating soft tissue in-growth into porous structures, noting the pore sizes that were found to best encourage tissue or cellular in-growth and/or thin fibrous encapsulation.

Author(s)	Reference	Porous Structure Tested	Tissue/Implant Site	Pore Size* [μm]
Zhang *et al*	[36]	Polyurethane vascular graft	Arterial lumen (endothelium)	~30
Park *et al*	[37]	Polymer scaffold	Cultured cardiac myocytes (*in vitro*)	30-200
Campbell and von Recum	[14]	Microporous polymer filter	Subcutaneous implant	1-3
Hishorn *et al*	[13]	Porous Ti surface on Ti electrode	RV endocardial implant	~125
Guarda *et al*	[10]	Porous Pt surface on Pt/Ir electrode	RV endocardial implant	~40
Bobyn *et al*	[7]	Porous Elgiloy surface on Elgiloy electrode	RV endocardial implant	<25
Bobyn *et al*	[7]	Porous Pt/Ir mesh electrode	RV endocardial implant	100-150
Amundson *et al*	[8]	Porous Pt/Ir mesh electrode	RV endocardial implant	~150
Beard *et al*	[12]	Porous Pd and porous Pt/Ir electrodes	Subcutaneous implant	45-100

** Pore size reported to have facilitated a favorable biological response (such as tissue in-growth, low fibrous capsule thickness, etc.).*

There are a number of problems with the studies listed in Table 1 in terms of the validity of the reported average pore size or range of pore sizes for each porous structure studied. First, there is no consistently-defined standard geometry of a "pore." Some porous structures investigated are made of sintered metal in different forms, some

are woven polymer strands, and there are still other geometries. It is not clear what is meant by the term "pore" in each case, much less the "size" of such features. Consider, for example, the porous platinum iridium mesh electrode of Amundson *et al* [8]. The electrode is fabricated by taking platinum iridium wire of a certain diameter and length and manually forming the wire into a tangled, sphere-like structure. This structure is placed within a woven screen of the same wire and the assembly is sintered together. Such a randomly oriented structure does not have a clear "pore" geometry, nor is it clear how the size of the "pores" would be quantified and consistently measured. And yet an average pore size of 150 μm is reported by Amundson *et al*, with no mention of how this value was calculated [8].

Further, even in cases such as the work of Beard *et al* [12] where pore size was measured through conducting BET gas sorption analysis in order to determine a distribution or range of pore sizes within the porous construct, such analysis involves simplifying assumptions regarding pore geometry. Both BET gas sorption analysis and mercury porosimetry (another frequently-used method of measuring metrics of porous structures, such as in [39]) assume that a pore is of cylindrical geometry, where the diameter of the cylindrical pore would be the pore size [40]. One could easily consider this assumption to be invalid for each of the porous structures studied in Table 1 based on the morphologies of the structures. Perhaps total porosity (the volume fraction of the electrode that is void space) would be a more reasonable comparative metric, though it's not known if total porosity correlates to biological response.

Though the porous constructs studied in Table 1 had irregular pore geometries and questionable reported pore sizes, there have been methods reported for making porous

constructs that result in well-defined pore geometries with measureable sizes. One such method is sphere-templating, as reported in the work by Marshall and Ratner [41]. Marshall and Ratner used the method of sphere-templating to create a material image from a template made of a sintered network of microspheres, where the diameter range of the microspheres is chosen based on the desired pore diameter to be created in the material image. The template, or "positive" template, is made of a material capable of being removed through heat or chemical digestion such that only the material image, or "negative" image, is left behind. Figure 7 schematically displays the method of sphere-templating used to make porous hydrogels for tissue engineering [41] and for study of biological response to different pore size materials [42,43].

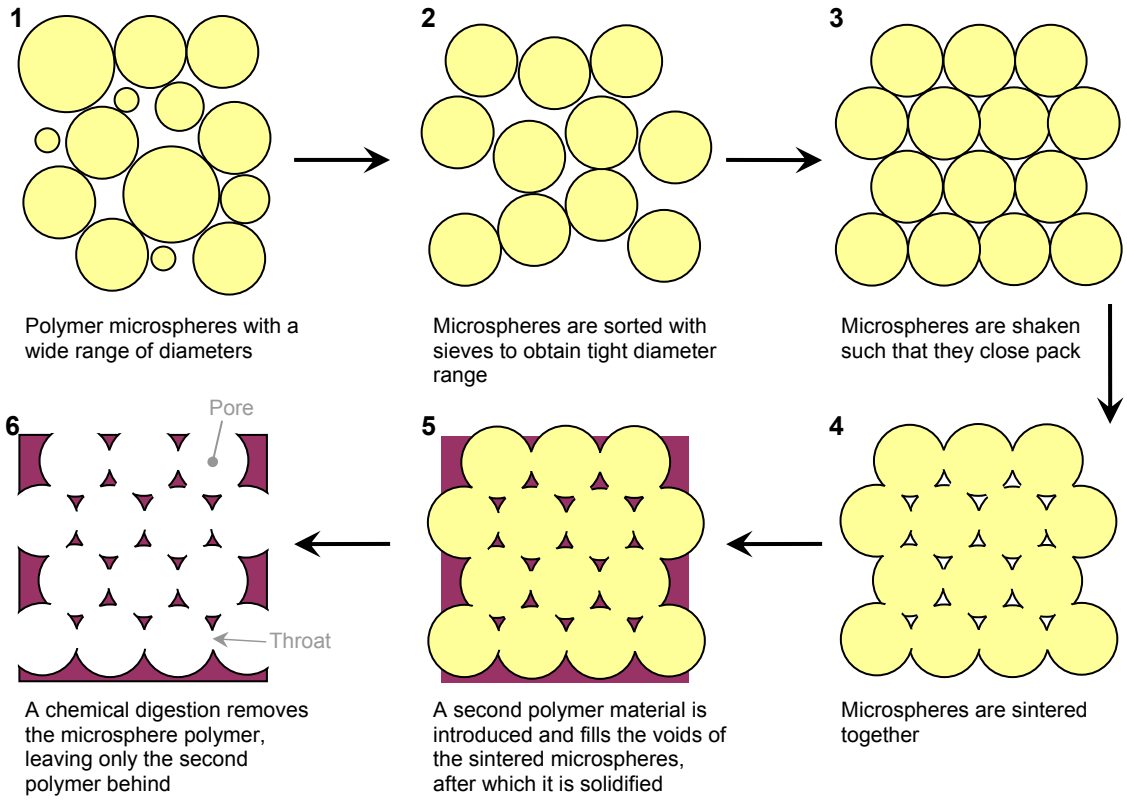

Figure 7: Two-dimensional schematic representation of a sphere-templating method for creating a polymer porous structure with consistent pore size. An actual three-dimensional porous structure fabricated with this method would have spherical pores, defined in size by the pore diameter, interconnected by smaller sized "throats" created where the template microspheres were sintered together [41].

The distinctive feature of the porous structure created via sphere-templating, as shown in step 6 of Figure 7, is the spherical shape of the pores and the consistent pore diameter throughout the structure. Since microspheres of a known diameter range were used to make the positive template (from which the porous structure was made), the size of the pores of the negative image mirror the microsphere diameters (assuming no expansion or contraction of the material occurs). The pores are connected to each other by smaller-sized "throats", which are created by points of coalescence between microspheres of the positive template during sintering, ensuring that the network of

pores is fully interconnected and capable of supporting tissue in-growth.

The sphere-templating method was used by Marshall and co-workers [42,43] to make biopolymer implants with differing pore sizes for implant in soft tissues. Porous silicone structures were created with nominal pore diameters of 20, 35, 50, 70, and 90 μm, respectively, and implanted subcutaneously in mice for one month in order to determine whether an optimal pore size exists for low fibrous capsule thickness and growth of blood vessels within the porous implant ("angiogenesis"). Histological evaluation of the implants showed that the 35 μm pore diameter implant appeared to be the optimum for encouraging angiogenesis within the pores [42,43]. Vascular density within the 35 μm implant pores was roughly double that of the 20 μm and 90 μm pore diameter implants [42,43]. Fibrous capsule thickness was also lowest for the 35 μm pore diameter implant (approximately 14 μm mean capsule thickness), as compared to implants with pore sizes of 20 μm or less (approximately 27 μm mean capsule thickness) or implants with pore sizes of 50 μm or more (approximately 34 μm mean capsule thickness) [44].

Of highest interest in regard to the results just discussed is an explanation for why a specific pore diameter would be preferred for optimal biocompatibility (at least for implants in mice, as discussed above). One potential explanation is that the pore diameter affects the expression of certain phenotypes of cells that have an impact on biological response to the implant, such as macrophages and endothelial cells [44]. It has only recently been appreciated that macrophages have at least two distinct paradigms of cell phenotype, or morphology, which in turn have an effect on the chemical signals released by the macrophage and the ensuing biological response to the

foreign body [45,46]. The so-called "M1" phenotype of macrophages is associated with release of reactive nitrogen and oxygen for attack and digestion of foreign bodies, as well as pro-inflammatory signaling and complement system activation [45]. The "M2" macrophage phenotype, a generic label for multiple types of activated macrophages that are different from M1, is associated with promotion of tissue growth and remodeling [45].

The three-dimensional spatial environment of the pores of a porous implant may mediate the phenotype of macrophages and other cells. It has been reported that the phenotype of macrophages is influenced by the micro-architecture of the implant by Padera and Colton [47], who studied porous membrane implants with differing pore sizes and the ensuing biological response. Padera and Colton observed macrophages in a "round" morpohology, indicative of M2 phenotype, infiltrating porous matrices with pore sizes greater than 8 μm, while implants with smaller pore sizes showed greater numbers of macrophages with a "flat" morphology, indicative of M1 phenotype, on the outer surface of the implant [47]. In regard to the work of Marshall *et al*, Ratner (doctoral thesis advisor to Marshall) has hypothesized that the 35 μm pore diameter structure is most efficient at activating macrophages to a "round" M2 phenotype [44]. Ratner has reported histology slides of the various pore diameter materials in the work of Marshall *et al* [42,43] stained with BM8 macrophage marker showing the 35 μm pore diameter material having a very high density of infiltrated macrophages as compared to both smaller and larger pore sizes [44]. It makes sense that if a solid implant influences macrophages to express a flat (M1) phenotype, an implant with either very small pores or very large pores would appear locally to be similar to a solid

surface. An optimal spatial environment for expression of the round (M2) macrophage phenotype would exist at a pore size between these two extremes. Interestingly, endothelial cells also have been shown to have a polarized expression of phenotypes similar to macrophages, and their "spreading" phenotype has been associated with less tissue growth and remodeling at the surface of bio-implants [48,49].

While at this point the evidence is preliminary and somewhat circumstantial, expression of phenotypes of macrophages (or endothelial cells, or possibly others) that are beneficial to tissue growth and remodeling may offer an important key to understanding the thin surrounding fibrous capsules and increased vascularization of certain porous implants, and the "optimal" response to a specific pore size. However, mediated expression of cell phenotypes may not be the only driver of biological response to porous implants. For instance, it is not known the relative role that mechanical interlocking of implant and surrounding tissue might play in reduced fibrous capsule thickness. Rosengren *et al* hypothesized that motion of the implant surface relative to surrounding tissue mechanically shears nearby cells, causing cell necrosis and higher levels of chronic inflammation and fibrous encapsulation [50]. The implication is that a porous implant that encourages tissue in-growth and eliminates relative motion of the implant surface and surrounding tissue can reduce fibrous encapsulation simply due to better mechanical integration. This potential driver of better porous implant biocompatibility is not exclusive of the potential role of phenotype expression of macrophages or other cells. Both of these factors, and potentially other unknown factors, may contribute to enhanced bio-integration of porous implants.

The literature reviewed here forms an important context for interpretation of the results of the work of this thesis. As noted at the end of Section 2, it is the object of this work to design and fabricate a porous electrode capable of use on a coronary venous pacing lead in order to investigate, through chronic animal implants, the potential of such an electrode to reduce chronic lead dislodgements and lower pacing thresholds. No equivalent study can be found in the literature as of the writing of this thesis. It is not the purpose of this work to find the optimal pore size for a coronary venous pacing lead electrode, or to answer every question raised in this literature review. Rather, the reviewed literature informs the design of the porous electrode evaluated in this work, and also provides the context in which the results of this work can be more properly interpreted. The relevant literature also informs the recommendations for future work in order to build on the results of this thesis.

4 Methods

4.1 Porous Electrode Design

In considering the design of a prototype porous electrode for use in a coronary venous pacing lead, there are number of factors that can affect the successful evaluation of such an electrode. The distal end of coronary venous pacing lead can vary in radial position within the lumen of the vein in which it is implanted, simply due to differences in venous anatomy between test subjects. This potential variation in venous wall contact adds a significant variable to evaluating the effects of porosity on an electrode. Ideally the porous electrode under evaluation would be forced into contact with the lumenal surface of the vein in order to eliminate radial position as a variable that affects electrode/tissue integration. This is just one consideration in design of the electrode itself, as well as selection of the lead design onto which the electrode will be assembled.

Further, there are other important design considerations, such as the placement of the porosity that is created on or in the electrode in order to ensure that it will not be affected by assembly onto the lead. Placing porous areas away from sections of the electrode that are used as points of assembly onto the lead helps to mitigate potential damage to the porosity. Additionally, depending on the thickness of the porosity desired on the electrode, the electrode design must allow for porosity to be created such that there are not significant physical differences between the porous electrode and a control electrode without any porosity. For instance, if incorporating porosity into an electrode design caused it to have a larger diameter than the control electrode, such a physical difference would make isolating the contributions of the porosity to the

performance of the electrode more difficult. All of these factors make design of the porous electrode critical in assuring that the effects of having porosity in an electrode in a coronary vein can be studied meaningfully.

With all of these considerations in mind, the distal electrode of the ACUITY™ Steerable coronary venous pacing lead (manufactured by Boston Scientific Corporation) was chosen as the ideal research case in that its design fulfills all of the desirable attributes discussed above. The ACUITY™ Steerable lead is designed such that the distal end of the lead (approximately the distal 5-7 cm) is formed into a "J" shape so that once deployed in the target vein the shape forces the distal electrode into the vein wall. A guide wire or stylet advanced through the lumen of the lead straightens the "J" during delivery, while removing the guide wire or stylet deploys the "J" in the vein. Deployment of the "J" shape in the vein ensures good contact between the distal electrode and the lumenal surface of the vein in addition to providing a frictional force to hold the lead in place chronically. Figure 8 shows the distal end of the ACUITY™ Steerable lead.

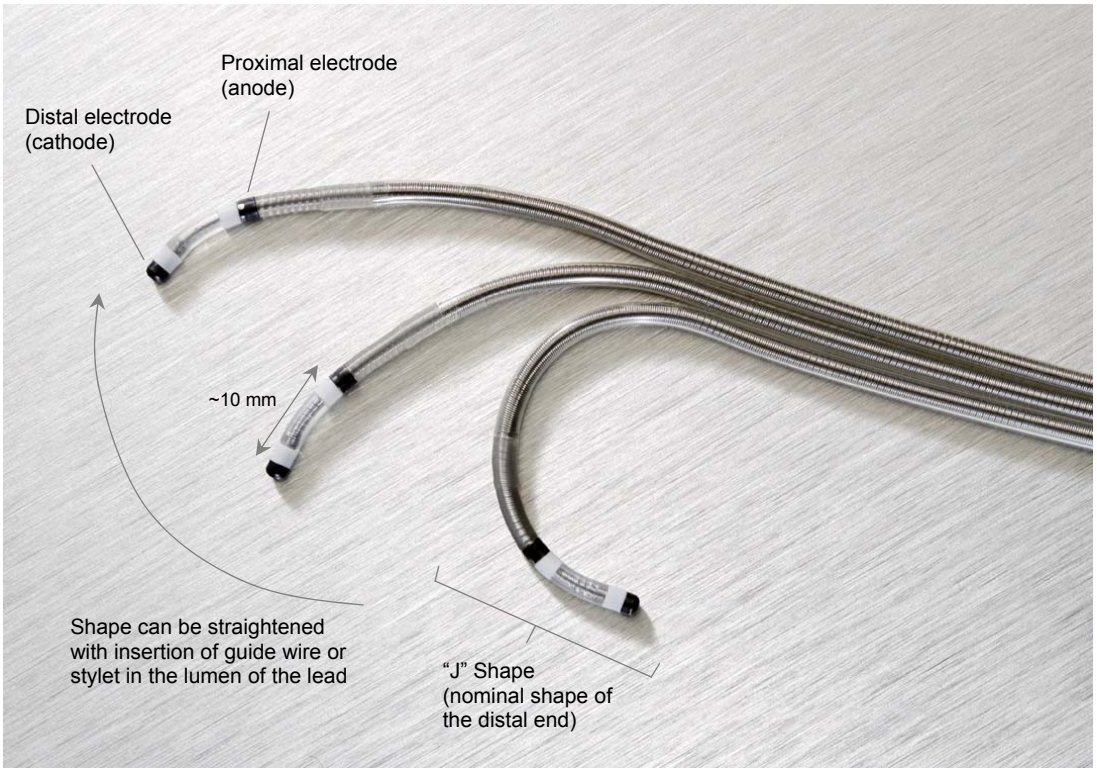

Figure 8: Picture of the distal end of the ACUITY^{TM} Steerable coronary venous pacing lead, manufactured by Boston Scientific Corporation, in three degrees of deployment of the "J" shape [51]. As a point of reference, the spacing between the electrodes is approximately 10 mm in length.

As can be seen in Figure 8, the distal electrode is a "tip electrode" in that it actually forms the tip of the lead. The placement of this electrode at the tip of the lead allows it to be designed with a hemispherical shape that forms a large volume of material which can be used for creation of porosity. This is in contrast to the proximal electrode, which is a thin ring of material with little to no volume that could be sacrificed for porosity. Figure 9 shows a computer aided design (CAD) model of the outer portion of the distal electrode in cross-section.

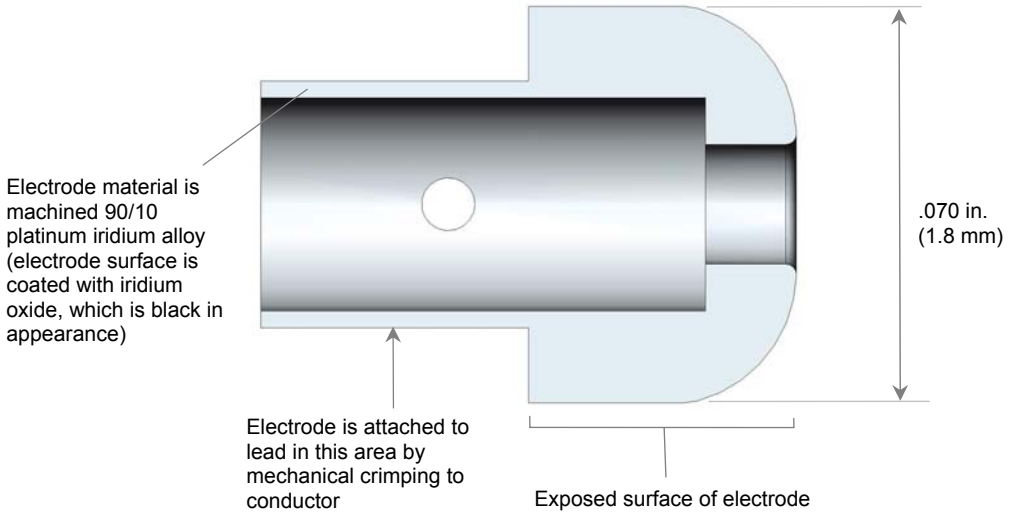

Figure 9: Axial cross-section of a CAD model of the ACUITY™ Steerable distal electrode.

Not only is it apparent in Figure 9 the large volume of material available for creating porosity in the hemispherical tip of the electrode, but one can also see that the area of the electrode used for attachment to the lead conductor is entirely separate from this volume, which is ideal for protecting the porous areas.

Though Figure 9 displays the distal electrode of the ACUITY™ Steerable lead in its nominal form, in order to allow space for creation of porous areas a new electrode needed to be designed to serve as the "base" onto which a porous network of material could be created (hereafter referred to as the "electrode base"). Once the porous areas are added to the electrode base, the porous version of this electrode should approximate the nominal form. Figure 10 outlines the design of the electrode base.

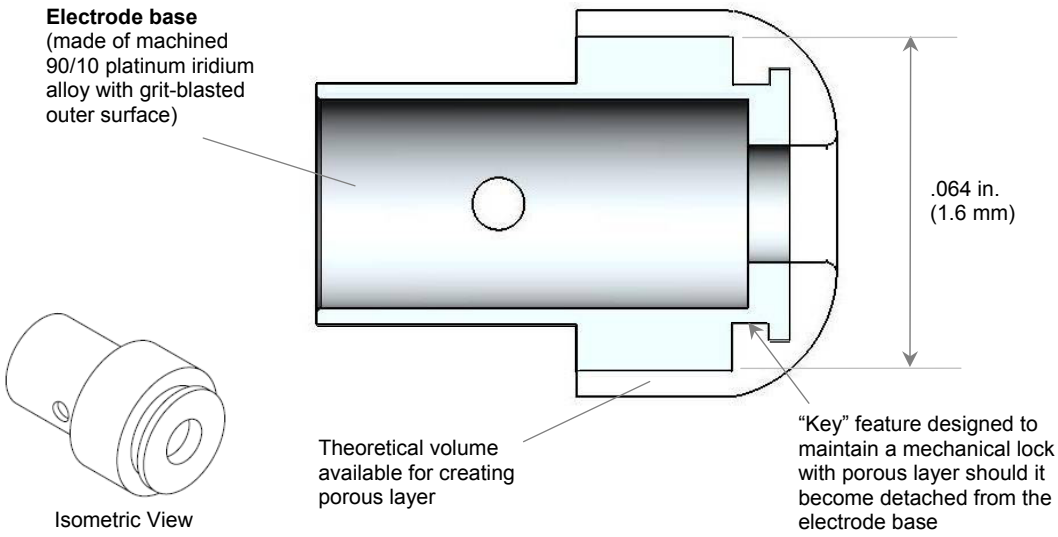

Figure 10: Axial cross-section of a CAD model of a custom-designed electrode base, with additional isometric view. The electrode base is designed for eventual creation of a porous network of material that would fill in the volume as denoted in the figure, creating a finished electrode that is similar to the nominal form of the ACUITY^{TM} Steerable distal electrode.

As can be seen in Figure 10, once the porous areas are added to the electrode base, the design of the base allows multiple thicknesses of the porosity to be created and studied. Ideally the amount of tissue integration as a function of porous layer thickness could be evaluated with this design.

The final important factor in design of the porous electrode is the actual design of the porosity. This investigation required a specific set of imposed requirements to guide design and fabrication of the electrode such that the porous structure would be robust and the performance of the electrode could be analyzed in light of previous work with right-sided pacing leads. One such imposed requirement was that the material which forms the porous network should be the same material as the electrode base. Such a requirement ensures both the ability for a robust attachment to the base and consistency of material for comparison to the nominal solid electrode design. Another

imposed requirement was that the average pore size be greater than 10 μm and less than 150 μm, based on the published literature on optimal pore size for tissue in-growth (see Table 1 in Section 3). In practice, an average pore size of roughly 35 μm was desired based on the work of Marshall and co-workers, as discussed in Section 3 [41,43,44,52].

Though there are a number of possibilities for creating porosity that is integrated with a solid metal surface, the most efficient means of fulfilling the requirements given above through a manual fabrication process suitable for small batches (as utilized by the author of this work) was identified to be sintering of metallic microspheres onto the surface of the electrode base. This type of structure will give an irregularly-shaped pore geometry and a wide distribution of void sizes, which does not mimic the tight distribution of spherical pore diameters of a sphere-templated material such as that of Marshall and co-workers [41,43,52]. However, Marshall and co-workers produced only polymeric porous implants with the sphere-templating method. A methodology to produce a similar sphere-templated structure with a metal (as is necessary for an electrode) in the size scale of a pacing lead electrode is not known, and is outside of the scope of this work to develop. Though a sintered microsphere structure will not have consistent pore geometry, it was still the design intent to select the size of the microspheres to give an approximate pore size after sintering. Metallic microspheres are readily available and can be ordered easily to a specified range of diameters, and also can be made of 90/10 platinum iridium alloy.

Other possibilities were considered for creating the porosity, but ultimately their drawbacks outweighed any potential advantages. For instance, plasma spray coating of platinum iridium was considered, but coating thicknesses are typically very difficult to

control at the scale of electrode bases to be coated, and the amorphous nature of the coating would make estimation of metrics such as surface area and average pore size quite difficult. Such metrics are useful in interpreting the *in vivo* performance of a porous electrode, and in comparing to other published literature. Other potential options also included sintering of a mesh of small wire onto the electrode base, or electro-spinning of material onto the electrode base, but both of these options had drawbacks similar to plasma spray coating in terms of the amorphous nature of the pores being created.

4.2 Porous Electrode Fabrication

The first step in fabrication of the porous electrodes was acquisition of the electrode bases and the microspheres for creating the porosity. Electrode bases were custom manufactured by RMS Medical (Minneapolis, MN), where they were precision machined from 90/10 platinum iridium via an automated machining process. Platinum iridium (90/10) microspheres were sourced from Johnson Matthey Plc (London, UK), where a variety of sizes were available off-the-shelf or for custom manufacture. Cost of such microspheres is driven both by the price of raw materials (platinum being a precious metal) and the manufacturing process of the microspheres, which involves a significant amount of waste. Sieves are also required to sort the microspheres such that only the desired range of diameters is provided. Deviations in desired particle size ranges from that which can be provided by off-the-shelf sieves require custom sieves to be made, which can increase cost significantly. In order to keep cost down, 20 grams of platinum iridium microspheres were ordered with a specified diameter range of 25-45

μm (which allowed use of stock sieves and provided a relatively tight diameter range). Though there existed no *a priori* knowledge of the best microsphere size for producing an approximately 35 μm average pore size (and the cost of such a study would be significant), it was hypothesized that the average diameter of the microspheres would approximate the eventual average pore size. Thus, the diameter range of the microspheres was deemed to be appropriate for fabrication of the porous electrodes, though it was recognized that the average pore size may be deviate from a value 35 μm depending on the packing of the microspheres and other factors.

Multiple methods were attempted to affix the microspheres to the electrode base so that the final sintering operation could be performed. Copper powder (50 μm max particle size; Goodfellow Corporation, Cambridge, UK) was used in place of the platinum iridium microspheres during method development in order to save on cost. The first attempt to attach the copper powder to the electrode base was via a molding process. A binder was created from Hexyl CARBITOL^{TM} Solvent (Dow Chemical, Midland, MI) mixed with a cellulosic thickener (Klucel® hydroxypropylcellulose, Hercules Inc., Wilmington, DE) to form a paste, which was then added to the copper powder and packed into a mold. The mold was designed in CAD software and created via stereo lithography, while a core pin was machined from 316L stainless steel. The intention was to mold the powder/binder paste to the electrode base, forming the desired hemispherical shape, and then to heat the mold to 50^{o}C to set the binder. Unfortunately, despite repeated attempts, this process proved unreliable as the structure was frequently damaged when removing from the mold.

The second method attempted was spray coating of the copper powder to the electrode base. In this method, a liquid polymer binder was selected (Nicrobraz Cement 680; Wall Colmonoy Corporation, Madison Heights, MI) and mixed with the copper powder to form a viscous mixture. This mixture was then fed into an airbrush (Eclipse HP-BCS, Iwata-Medea, Portland, OR) and sprayed onto the electrode base, after which the electrode base was heated via a heat gun (Master-Mite Model 10008, Master Appliance Corp., Racine, WI) to set the binder (taking only matter of seconds). It was discovered that several coats were necessary to build up the required thickness of the porous areas, which were relatively uneven from sample to sample, and though the method was feasible it resulted in unacceptable waste. Only a small fraction of the volume of sprayed powder/binder mixture actually ended up on the electrode base itself, and therefore this method was abandoned.

The final method attempted was dip coating. The same liquid polymer binder used in the spray-coating process was also utilized here, with the exception that once the powder/binder mixture was formed it was placed in an open container such that the electrode base could be vertically dipped into the mixture. Much experimentation with Cu powder-to-binder mix ratio was required to find the right viscosity for optimum coating adhesion and surface tension for formation of the tip. Once optimized, however, the dip coating process proved to be the most efficient in use of the powder while also producing the best results. Figure 11 summarizes all of the methods attempted, and includes an example photo of a successfully coated electrode base utilizing the dip-coating process after setting of the binder.

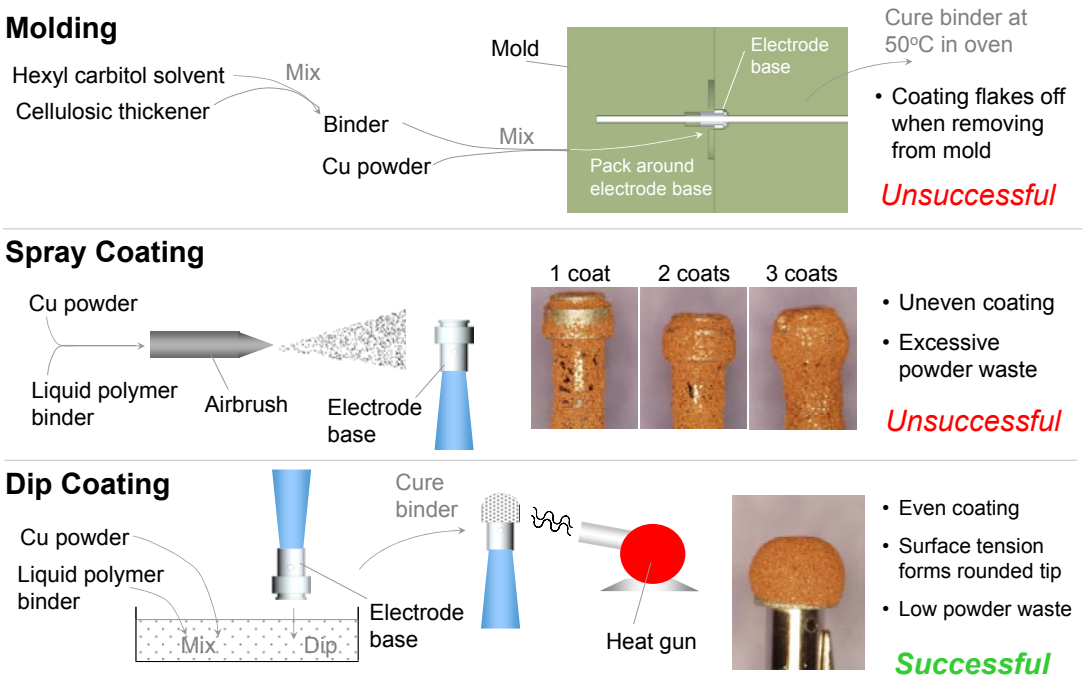

Figure 11: A summary of the methods attempted for affixing a metallic powder to the electrode base in preparation for sintering. In this case copper powder was used as a surrogate for the platinum iridium microspheres during development to save on cost.

The dip coating method was similarly successful using the platinum iridium microspheres, though the mix ratio of binder to microspheres had to be altered (roughly 1 g of platinum iridium microspheres to 30 μL of binder proved optimal). An example of an electrode base coated with platinum iridium microspheres after setting of the binder is shown in Figure 12.

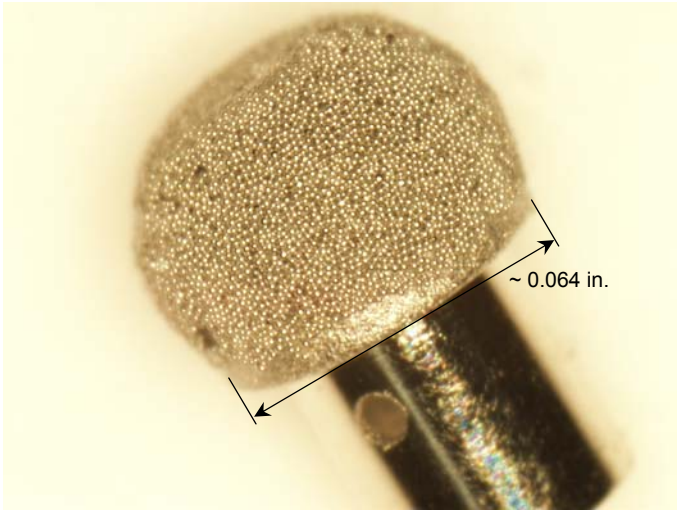

Figure 12: Image taken under light microscopy of an example electrode base successfully coated with platinum iridium microspheres after setting of the binder.

After applying the platinum iridium microspheres to the base electrode in a binder, the next step was to sinter the microspheres in order to weld the microspheres to the electrode base and to each other. Sintering is a common process used for welding together particles of material (in this case metal), typically at a temperature less than the melting temperature of the material. For this application, the sintering operation also creates the porosity in the electrode as the polymer binder surrounding the platinum iridium microspheres is vaporized during sintering, leaving behind voids in the spaces previously occupied by the binder. Nicrobraz Cement volatilizes completely during heating before temperatures reach approximately 550^{o}C [53], while much higher temperatures would be required to sinter platinum iridium without additional compression or packing of the microspheres [54].

There are multiple ways in which to accomplish sintering, since the degree of coalescence of particles can depend on both temperature and the time duration at which the electrode is held at a certain temperature (pressure can also be used to alter sintering

process parameters, but here there was no additional pressure utilized for sintering). For instance, sintering of particles can be accomplished at a lower temperature if time duration or hold-time is increased. Conversely, sintering can be done in a shorter amount of time if temperature is increased. Temperature, time, and pressure influence atomic diffusion between contacting particles, among other factors. Despite this understanding, it was outside the scope of this thesis to specifically study different methods of sintering and the affects on the final structure of the electrode. The requirements for the porous electrodes being fabricated were simply that the sintered particles be well-adhered to the base electrode and to each other (such that handling of the electrode would not damage the porosity, and the implant process would also not impart damage) and also that the pores not be significantly occluded by coalescing material during sintering. Undoubtedly a number of different sintering processes could have produced a final electrode that met these requirements.

In this case, for ease of process experimentation and iteration of process parameters, it was desired that the time duration of the sintering process be as short as possible. This ruled out heating in a high-temperature furnace since the time required to reach a steady state temperature near the melting point of platinum iridium was on the order of minutes, including as much as an hour in total process time for a single run with much experimentation required to obtain the optimum hold time. A much faster and controllable method of heating of a metallic workpiece is inductive heating, and this was the method ultimately selected to sinter the porous electrodes.

A typical inductive heating system utilizes water-cooled copper tubing in a coiled configuration with an AC driving current (in the radio frequency range) to create

a fluctuating magnetic field and induce eddy currents in the workpiece (i.e. the electrode) [55]. Eddy currents circulating within the workpiece cause resistive heating. Inductive systems can heat metals to temperatures near or beyond melting within seconds, and thus are a very efficient method to experiment with optimization of processing parameters for a robust sintering of the porous electrode. Factors such as the frequency of the AC current, the power of the inductive heating system, the magnetic and electrical properties of the workpiece material, the amount of heat loss via conduction through the fixture holding the workpiece (among many other factors) all affect the speed and depth of heating in the workpiece [55]. Though absolute optimization of the process was not sought in this case (as long as the sintered electrode met the aforementioned requirements), a significant amount of experimentation was required to develop a sintering process that was repeatable and resulted in a robust electrode.

The experimental set-up used to sinter the porous electrodes for this work consisted of a benchtop induction heating system with a maximum power output of 3 kW and a frequency range of 400-700 kHz (Model 1TM, SEIT Elettronica, Valdobbiadene, TV, Italy) connected to a coolant water pump (Model R-1100V, RDO Enterprises Inc., Washington, NJ), with input power to the heating system automatically regulated by an AC voltage regulator (Seven Star® Model ATVR-5000, Supreme Premium Products Inc., New York, NY). A fixture to hold the electrode during the sintering process, which must withstand the extremely high temperature of the electrode, was machined from boron nitride ceramic (1”x12” rod, 99% pure, Aremco Products, Inc., Valley Cottage, NY). Light microscopy was used to view the electrode

during sintering, and all processing was done in ambient air due to the robust resistance of platinum and platinum alloys to oxidation [56]. Figure 13 gives a depiction of an electrode being sintered within the induction coil of the heating system.

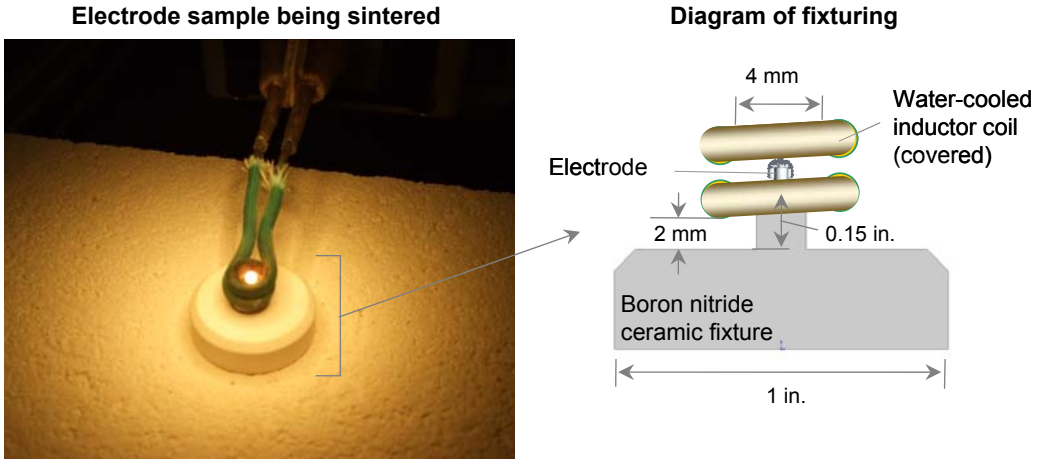

Figure 13: Close-up photo of an electrode sample being sintered, along with a schematic representation of the fixturing for holding the electrode in the inductor coil. Photo was taken approximately 5 seconds into the sintering process.

In order to sinter the platinum iridium microspheres without additional pressure (i.e. relying completely on heating to weld the particles together and to the base), the temperature of the electrode needs to be heated near the melting temperature of 90/10 platinum iridium, depending on the time duration of the process. Longer process time durations can utilize a lower temperature, relying on solid state diffusion as the primary mode of material coalescence between contacting microspheres. For shorter process durations, higher temperatures are necessary to initiate faster diffusion of atoms. The solidus temperature (the point at which the solid starts to liquefy with rising temperature) for 90/10 platinum iridium is approximately 1780^{o}C, while the liquidus temperature (the point of complete liquification) is approximately 1800^{o}C [57]. In

order to cause sintering of contacting microspheres on the electrode base in a relatively short time duration, a temperature relatively near the solidus temperature (approximately 1500-1700^{o}C) would need to be achieved to begin to cause sintering through diffusion of atoms at the outer surfaces of the microspheres on the electrode base and initiate coalescence. However, in this case direct measurement of temperature was not done during the sintering process due to the difficulty involved in actually obtaining an accurate measurement at the surface of the electrode (where temperature is highest for inductive heating [55]) with a thermocouple or other direct-contact means. Specialized infrared temperature measurement equipment was the best option for accurately measuring temperature during sintering, though such equipment was not available for this work. Despite the lack of temperature information, other parameters such as the power level of the inductive heating system, the time duration of the process, and the location of the electrode within the induction coil could be controlled to affect the level of sintering accomplished in the electrode.

Much experimentation was required to optimize the parameters of the sintering process in order to produce an electrode with a fully adhered porous network of microspheres. Parameters with particular impact on sintering results were the power level of the inductive heating system and the time duration of the process. Setting the power level too high resulted in a sintered network of microspheres that was not adhered to the base or a completely melted electrode tip, depending on the time duration of the process. Conversely, setting the power level too low resulted in lack of adequate sintering altogether, no matter the time duration of the process. Further, the location of the electrode within the inductor coil also had to be controlled for an optimal process.

The focal point of highest heating occurs in the center (vertically and horizontally) of the inductor coil, and it was advantageous to place the affixed microspheres at the electrode tip somewhat above this center point such that the electrode base was heated as much as possible to increase adhesion of microspheres to the base. After all process optimization, final parameter settings of 55% power (corresponding to 1.65 kW), time duration of 60.0±0.5 seconds, and electrode placement as detailed in Figure 13 were used to produce all sintered electrodes for use in the chronic animal study. Two boron nitride fixtures were alternately used for holding the electrode during sintering, rotating after each process. The heat transferred to the boron nitride fixture during sintering was so significant that stored heat would adversely alter the results of subsequent processes without allowing the fixture sufficient time to cool to room temperature.

4.3 Characterization of Porous Electrodes

Sintered electrodes were initially characterized by imaging with scanning electron microscopy (SEM) to visualize the sintered microspheres and their connections using a JEOL Model JSM-7000 Field Emission Scanning Electron Microscope. Figure 14 displays images from one representative electrode sample.

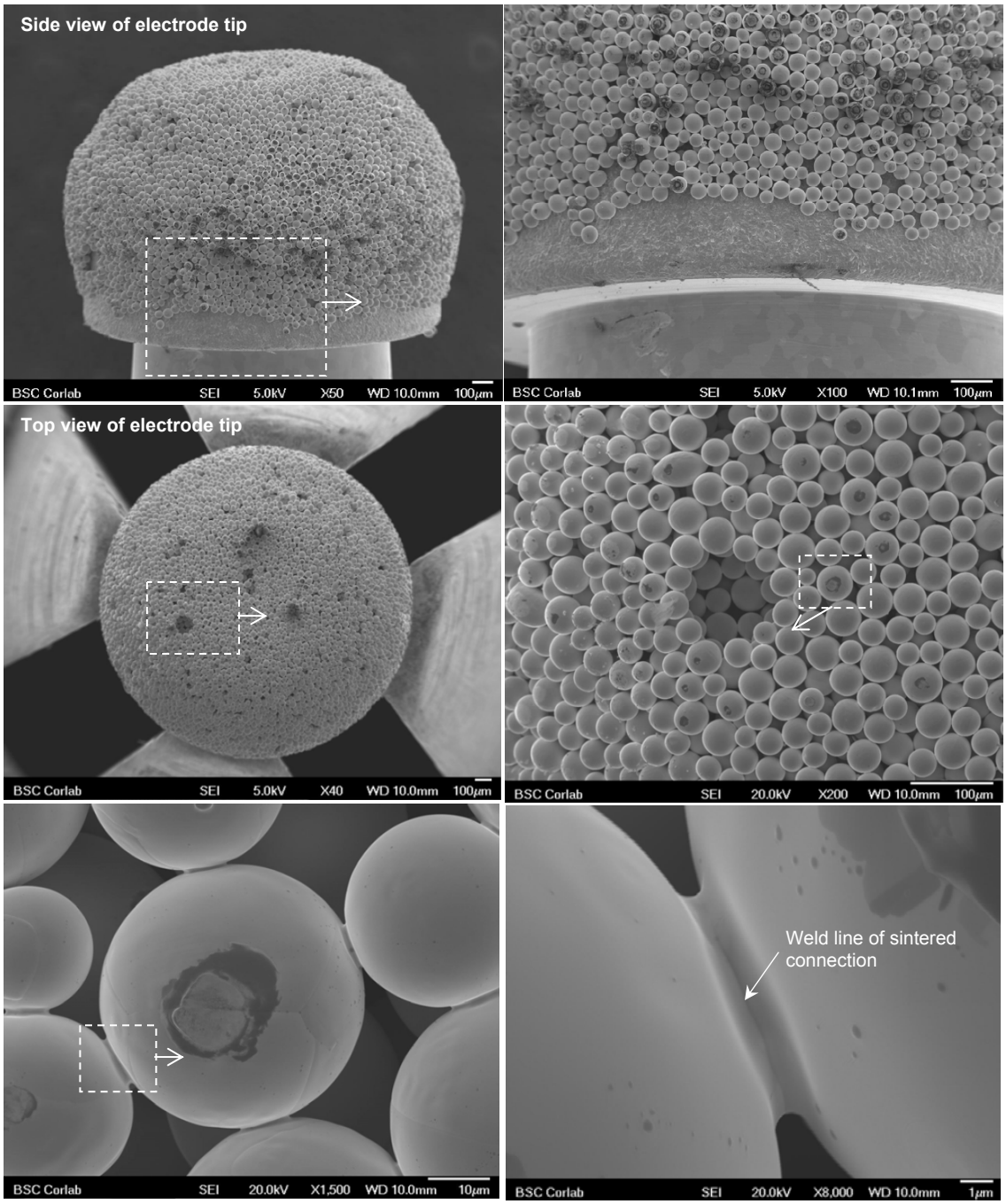

Figure 14: Images of a sintered porous electrode taken using SEM at various levels of magnification.

Grain boundaries in the metal can be noted on the surfaces of the microspheres in Figure 14, particularly in the bottom left image. Darker areas of material can also be noted on the outer surface of some of the microspheres in the images in Figure 14,

likely being a limited amount of oxided iridium or platinum that formed and then coalesced during the sintering and cooling process. In order to characterize the electrode surface, any residues, and any contamination, further SEM imaging was done in backscatter mode coupled with an energy dispersive spectrometer (SEM-EDS). Figure 15 shows that some amount of contamination was found on the electrode.

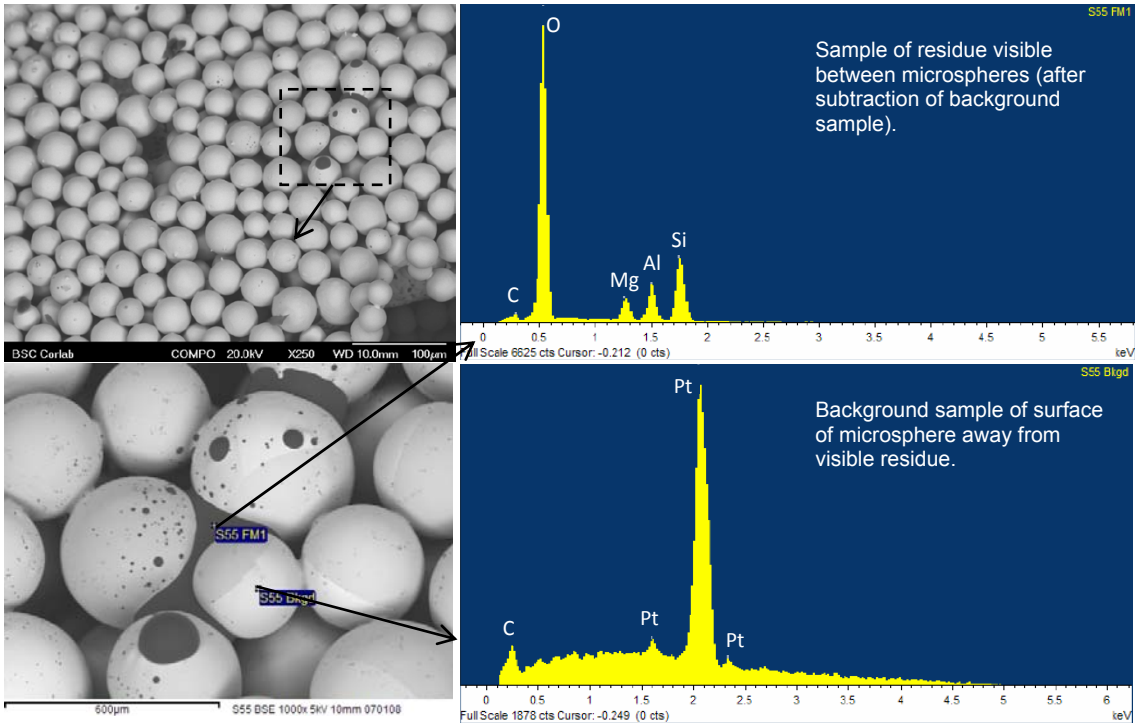

Figure 15: SEM-EDS analysis of surface residues in one location on the surface of a sintered electrode sample. The background data show mostly platinum, with some carbon. Data from a visible residue between microspheres show mostly oxygen, carbon, magnesium, aluminum, and silicon.

Though EDS data shown in Figure 15 are only from one location on one electrode sample, other data were taken in the same manner on other electrode samples and found to be consistent with these data. Contaminants appear to be a combination of magnesium, aluminum, and silicon, with carbon and oxygen from the high temperature sintering process. These contaminants are likely drawn from the wrap encasing the

copper tubing of the inductive heating system (which surrounds the electrode). Some electrode samples were ejected from their position in the ceramic holding fixture during sintering and contacted this wrap while continuing to heat. The caused at least one hole in the wrap to form and some of the wrap material to contaminate the ceramic fixturing. Though there were some contaminants present on the surfaces of the electrodes analyzed, the electrodes were cleaned in isopropyl alcohol in an ultrasonic cleaning system prior to being assembled onto pacing leads for the chronic animal study. This step was done to remove surface contamination such that contaminants did not have an effect on the study results.

In order to obtain an interior view of the sintered network of microspheres, another sintered electrode sample was encapsulated in epoxy, cross-sectioned, and polished, followed by examination via SEM. Figure 16 displays an image of this electrode cross-section.

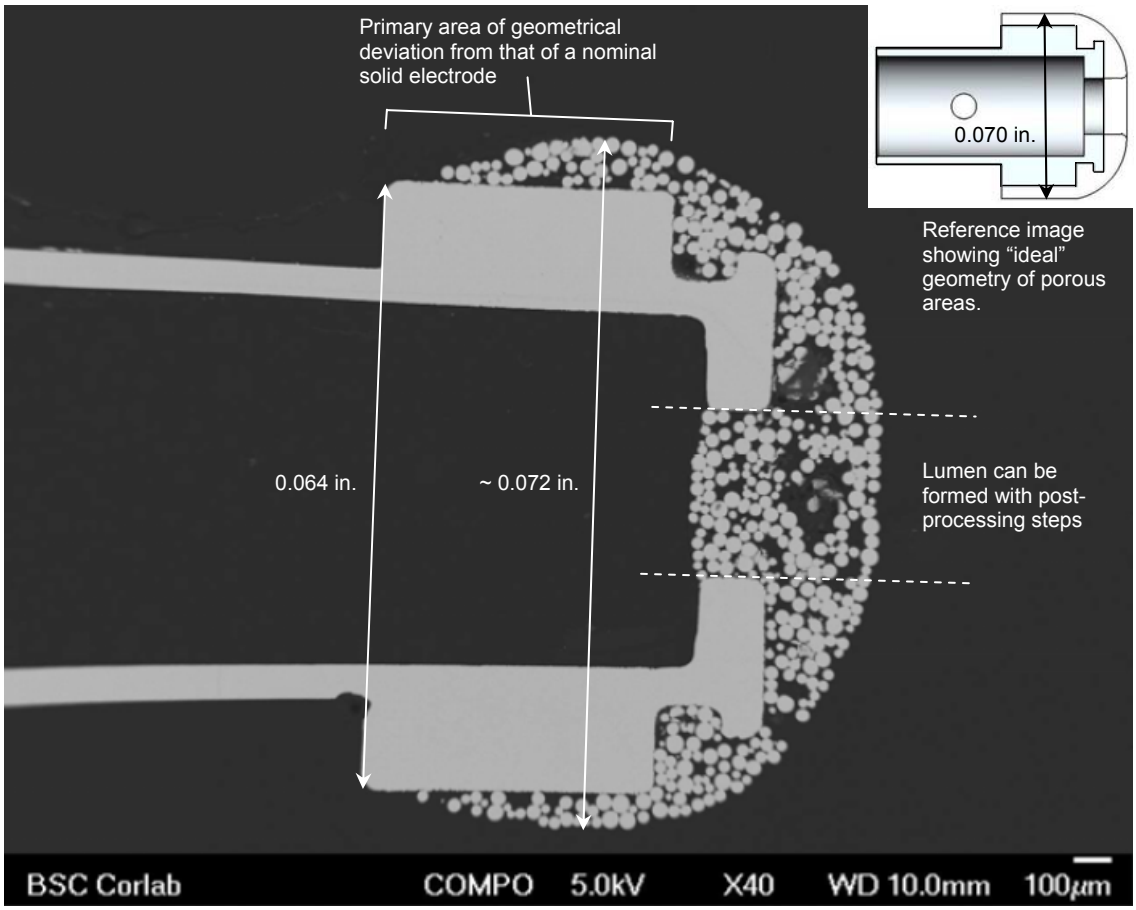

Figure 16: SEM image of a cross-sectioned porous electrode sample. Also shown is a reference schematic showing an "ideal" geometry of the porous areas which would match that of a nominal solid electrode (image from Figure 10).

As can be seen in Figure 16, despite the success of using the dip-coating method to affix the microspheres to the electrode base, the geometry of the hemispherical tip could not be controlled as much as desired and does not exactly match the nominal design of the solid electrode. The surface tension of the binder is utilized to form the hemispherical shape, resulting in the tip being slightly more bulbous and rounded than the nominal electrode geometry.

Nonetheless, the nominal electrode geometry is reasonably approximated with the dip-coating method of affixing the microspheres. Measurements of the outer

diameter of 10 sintered porous electrodes (taking the average of the maximum and minimum value found with an optical comparator) gave an average value of 0.072 in. with a standard deviation of 0.0015 in. This compares to the "ideal" value of 0.070 +/- 0.0005 in., which is the nominal outer diameter and tolerance of the solid electrode design. However, the proximal edge of the hemispherical tip of the porous electrode samples is typically near the diameter of the base electrode, 0.064 in., while the ideal case would be a smoothly-maintained 0.070 in. diameter all the way to this edge, as with the solid electrode. Figure 16 is labeled with the diameter values for reference.

Another point noted in Figure 16 is that a lumen can be created through mechanical post-processing after sintering of the electrode, though it is not shown in the cross-section. One option for creating a lumen is through drilling, though the actual method used was a mechanical punch with a 0.019 in. diameter stainless steel mandrel. Figure 17 shows an image taken under light microscopy showing a sample with a lumen created.

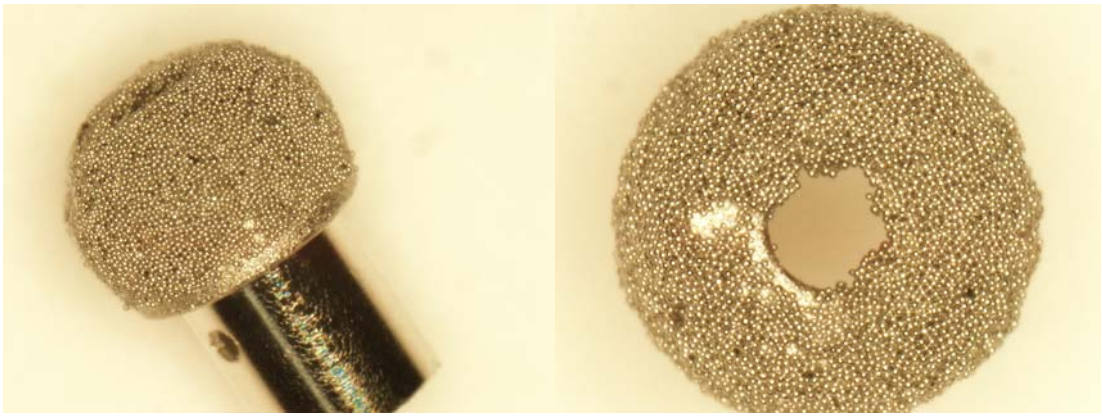

Figure 17: Example of sintered porous electrode with lumen created after sintering. Additional manual removal of some sintered microspheres in the lumen inner diameter was necessary before assembly onto full leads for use in the chronic animal study in order to ensure the lumen was fully clear and would not inhibit delivery using a guide wire.

Some of the most useful parameters for assessing the sintered porous electrodes, and eventual comparison on chronic animal study results to other published literature, were those of average pore size and total porosity. A parameter of additional importance in assessing the potential electrochemical benefits of such an electrode was surface area. Attempts were made to measure all of these parameters, with varying levels of success. For average pore size, mercury porosimetry and BET gas sorption analysis, both widely used methods for measuring parameters of porous materials [40], were attempted on electrode samples. In both cases no results were generated because the size of the electrodes was not large enough for enough mercury intrusion (in the case of mercury porosimetry) or for accurate results using BET gas sorption analysis. Multiple electrodes would have needed to be grouped together for the analysis, though it was unclear how many would be required to get accurate results, and in the case of mercury porosimetry the test was destructive. Instead of these methods it was decided to rely on other ways of calculating surface area and total porosity, and hopefully be able to determine a useful estimation of average pore size through direct measurement.

A means of calculating the total porosity in an electrode sample was established using SEM images of the electrode cross-section (such as in Figure 16). The electrode cross section was divided into three separate zones for calculation of total porosity, termed “outer surface,” “corner,” and “tip”. Multiple SEM images were taken within each of these zones for a representative electrode specimen, with each image being processed to separate the solid metal from the pores and then calculate the area of each. The total porosity is then calculated as the percent of cross-sectional area made up of porous area, averaged over the images taken. Figure 18 exemplifies this process for

calculating total porosity, along with data from each of the three designated porous zones of the electrode. All work was completed with a JEOL model JSM-7000 Field Emission Scanning Electron Microscope system.

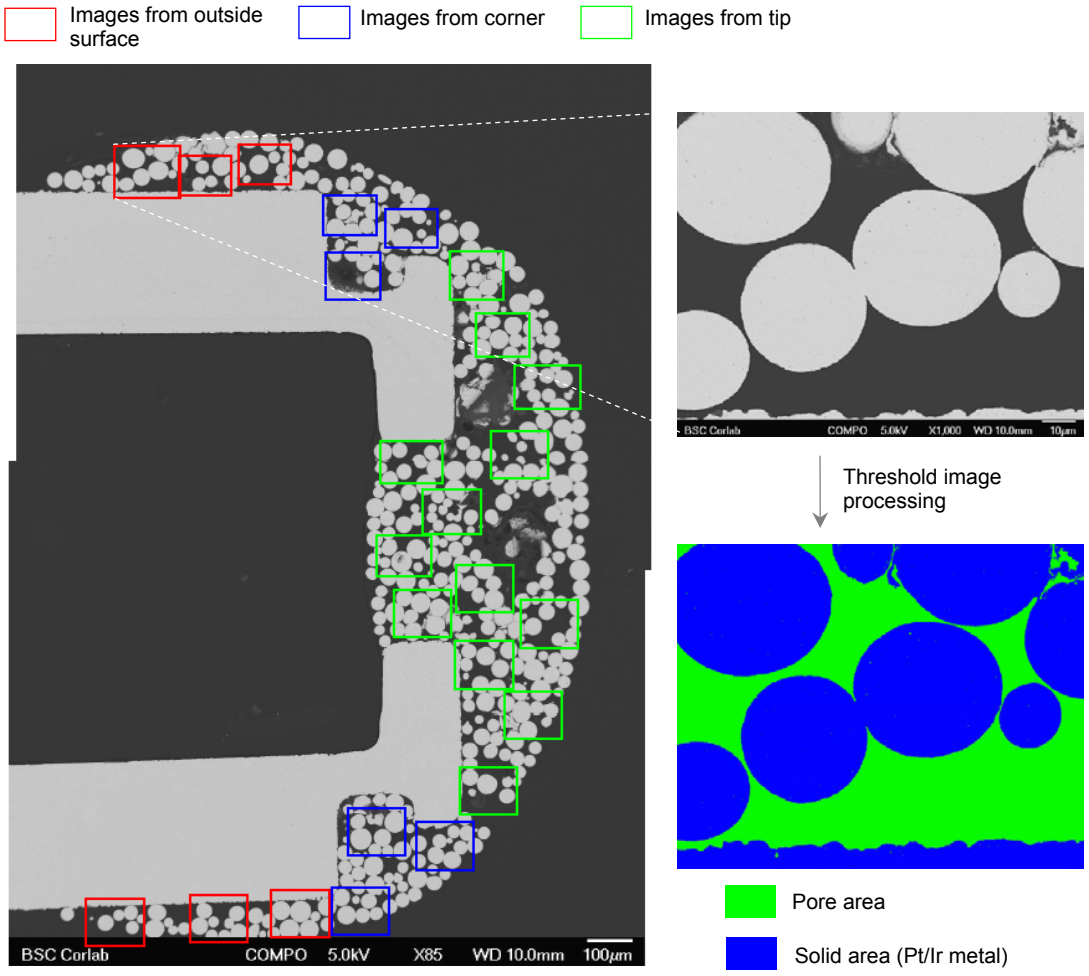

	Outside Surface	Corner	Tip	All Regions	
Average Pore Area [%]	36.8	34.6	37.9	36.8	← Total Porosity
Average Solid Area [%]	63.2	65.5	62.1	63.2	
# measurements	n=6	n=6	n=13	n=25	

Figure 18: Method of calculation of total porosity and porosity within certain regions of the electrode via SEM images of an electrode cross-section.

Figure 18 shows the porosity to be very consistent throughout the volume of sintered microspheres, varying between 34.6 and 37.9% across the three denoted regions measured, with an overall average value of 36.8%. Certainly the calculated total porosity can be treated as an estimate, as the value can be influenced by the location of the images utilized in the calculation. Additionally, since the porosity measurement is based on a two-dimensional slice through the electrode it cannot be treated the same as a volume fraction of void space (which perhaps is a better definition of total porosity). In theory the percent cross-sectional area that is void space should overestimate the percent of the volume of the porous area that is void space, since the spheres are rarely sliced at their center in the cross-section (making the cross-sectional void area appear larger on a percentage basis as compared to a true volume percent). However, the porosity calculation based on cross-sectional area is useful in that it showed the relatively low variation in distribution of the spheres throughout the electrode, which should also apply to volume fraction of void space.

Estimation of the average pore size is difficult given the irregular geometry of the pores. However, the two-dimensional image in Figure 18 was utilized to measure the size of voids that occurred between groups of microspheres of three or more. When this was done for the upper half of the image and all line lengths were normalized to the 100 μm benchmark, the histogram in Figure 19 was generated.

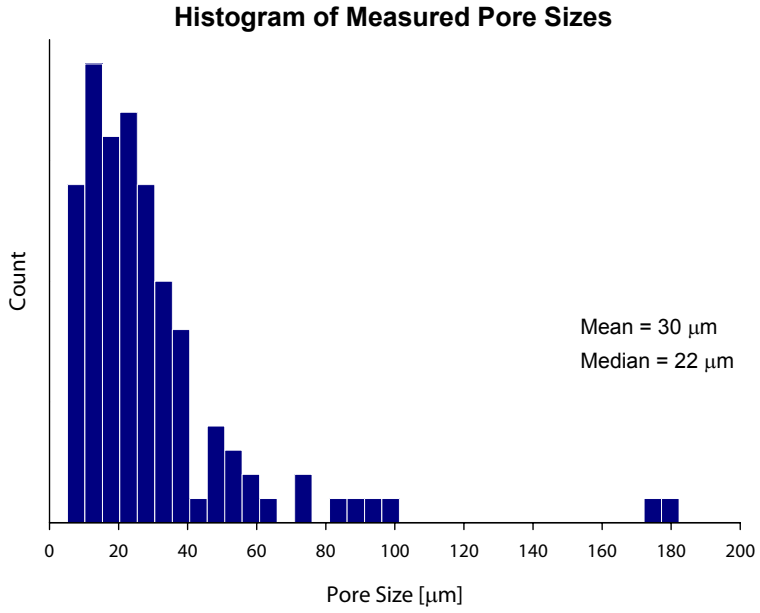

Figure 19: Histogram of pore sizes measured in the upper half of the two-dimensional cross-section image in Figure 18. Pore sizes were obtained by measuring the width at the center of voids that occurred between three or more microspheres.

Measured pore sizes fit a lognormal distribution as one would expect (since the lower end is bounded by zero), with the mean and median pore size being 30 μm and 22 μm, respectively. Certainly the mean and median values can be treated as estimates due to the aforementioned limitations of using a two-dimensional image to estimate three-dimensional spaces. However, these measurements do provide some confirmation that the 25-45 μm range of diameters of the microspheres produced a mean void size somewhat smaller than the mean microsphere diameter of 35 μm.

In order to estimate the surface area of the porous electrodes for comparison to the standard solid electrode surface area, a simple calculation was done that made use of the measured weight of porous electrodes after addition of the microspheres. This method is shown below.

Weight for 30 electrode base samples (base electrode prior to adding microspheres):

Mean = $0.0323\ g$
St. Dev. = $0.000388\ g$

Weight for 10 porous electrode samples with sintered microspheres:

Mean = $0.0391\ g$
St. Dev. = $0.00123\ g$

For an assumed mean microsphere diameter of 35 μm (assumed from known range of microsphere diameters being 25-45 μm):

Mass of one sphere = $\frac{4}{3}\pi R^3 \cdot \left(\rho_{90/10\,PtIr}\right) = 4.83\times10^{-7}\ g$

where $\rho_{90/10PtIr} = 21.35\ \text{kg/m}^3$

The difference between the mean porous electrode and electrode base weights was taken (equaling the mean total mass of microspheres on a porous electrode) and the mean number of microspheres on each electrode was calculated:

$$\frac{\left\langle m_{spheres,total}\right\rangle}{\left\langle m_{sphere}\right\rangle} = \frac{0.00706g}{21.35kg/m^3} = \left\langle N_{spheres,total}\right\rangle = 14{,}600$$

The mean surface area added to the electrode base by the microspheres is:

$$SA_{spheres,total} = 4\pi R^2 \cdot \left\langle N_{spheres,total}\right\rangle = 56.2mm^2$$

The mean electro-active surface area of a porous electrode (the exposed electrode surface area once assembled onto a pacing lead, neglecting the lumen surface area) is given below. A CAD model of the electrode base was used to calculate the area of electrode base surfaces that contribute and this was included in the estimate.

$$\left\langle SA_{\text{exp}osed}\right\rangle = 63.6mm^2$$ (719% increase over standard solid tip electrode)

Including all surfaces of the electrode (calculated via CAD model) the total surface area of the porous electrode is:

$$\left\langle SA_{total}\right\rangle = 77.0mm^2$$ (251% increase over standard solid tip electrode)

The percent increase over the standard solid tip electrode is calculated by comparing against values for the solid electrode exposed surface area of 7.76 mm^2, and solid electrode total surface area of 21.9 mm^2, obtained via CAD model.

Cyclic voltammetry was used in order to validate these theoretical estimates per the method of [58]. Cyclic voltammetry is an electrochemical test designed to examine the electrochemical reactions that occur for a given workpart (in this case, the porous electrode samples) in solution over a range of applied voltages. The test is performed in

a cell containing an electrolyte, which in this case was 0.5 mol/L sulfuric acid. A potentiostat applies a range of voltages between the reference electrode and the workpart, and measures current between the workpart and the counter electrode during the voltage sweep. During the course of the applied voltages the total charge of adsorbed hydrogen is calculated by integration of the monolayer hydrogen adsorption region of the current vs. voltage plot. This value is then divided by 210 $\mu C/cm^2$, which corresponds the amount of charge transferred per unit surface area during adsorption or desorption of a monolayer of hydrogen ions on a platinum surface [53], resulting in the calculated surface area of the workpart. For more information, Appendix A gives details regarding the test set-up.

Ten porous electrode samples were tested individually using the cyclic voltammetry method described above. Prior to the tests, each porous electrode was subjected to sonic agitation in deionized water for five minutes in order to remove any air bubbles trapped within the electrode pores. For all tests using the cyclic voltammetry method the total surface area of the electrode is measured (all surfaces were exposed). Mean measured surface area for the porous electrodes was 75.2 mm^2, with a standard deviation of 13.6 mm^2. This mean measured surface area is extremely close to the theoretical surface area calculated earlier (77.0 mm^2), which not only validates the surface area value but so also the assumption of a mean microsphere diameter of 35 μm (which was used in the theoretical surface area calculation). As a control, nine solid electrode samples were also tested using the cyclic voltammetry method, resulting in a mean measured surface area of 19.4 mm^2, with a standard

deviation of 2.8 mm^2. This is also very close to the theoretical value of 21.9 mm^2 calculated from a CAD model of the electrode.

4.4 In Vivo Evaluation of Porous Electrodes

4.4.1 Study Purpose

Chronic implant in animals was deemed the most relevant and useful means of evaluating the biological affects of inclusion of porosity onto a coronary venous pacing lead electrode. Only the *in vivo* environment can provide opportunities for histological evaluation of the implants and correlation to other chronic performance aspects of the electrodes. Therefore, the primary purpose of this study was to evaluate the histology of coronary venous leads with porous electrodes after 60-day chronic implant in canines to determine the level of tissue in-growth and fibrous capsule thickness around the electrodes. Performance of leads with porous electrodes was to be compared to control leads with solid electrodes that underwent the same implant procedure and underwent the same analysis. A secondary purpose of this study was to compare the chronic electrical performance and stability of leads with porous electrodes and non-porous controls and to correlate their *in vivo* performance to fibrous capsule thickness and tissue in-growth.

4.4.2 Research Questions and Hypotheses

For this study, there were multiple research questions intended to be addressed via data gathered both during and after the study. Below are given the research questions, hypotheses as to the results for each of the questions, and the data that was intended to answer the research question. Going into the study, the primary research question was the following:

Research Question 1

After 60-day chronic implant, are there significant differences notable in biological response for the porous electrode as compared to the solid (control) electrode?

Hypothesis

It was hypothesized that data collected from histological evaluation of the biological response near the two electrode types would show that the thickness of the fibrous capsules surrounding porous electrodes was thinner than those surrounding solid electrodes.

Means of Answering Research Question

Slicing of heart tissue for histological evaluation was done with the leads in place in order to visualize the lead/tissue interface without disruption. Through multiple slices of each lead distal end, and after appropriate staining to mark collagenous tissue, the thickness of the fibrous capsule was measured at multiple points for comparison among lead samples.

For research question 1, "biological response" was intended to encompass a number of different measures, including thickness of the fibrous capsule that forms after implant, cellular response at the implant surface, density of fibrous encapsulation, and others.

In addition to the primary research question, there were also secondary research questions that the study was intended to address. The second research question dealt with electrical performance of the implanted leads.

Research Question 2

Are there significant differences notable in electrical performance (voltage thresholds, impedance, sensed R-wave amplitude) between leads with the porous electrode as compared to leads with the solid (control) electrode?

Hypothesis

It was hypothesized that if indeed there were differences between study groups in thickness of fibrous encapsulation, there in fact would be differences in voltage threshold (with porous electrodes requiring less voltage to pace the left ventricle). However, due to the small sample sizes inherently involved in chronic animal evaluation, it was also hypothesized that such a difference would not be observed with statistical significance in the study. Pacing impedance of porous electrode leads was expected to be lower due to the increased surface

area of the electrode as compared to the solid electrode. No differences between study groups were expected in terms of sensed R-wave amplitudes.

Means of Answering Research Question

At implant and at regularly scheduled intervals throughout the study, the animal was sedated and electrical measurements were taken via an implanted pacemaker.

The hypothesized result for research question 2 and the unlikelihood of statistically significant results relate to inherent challenges in using animal implants to prove effectiveness. Animal implants most often are used to display safety of a medical device and not effectiveness due to the large number of animals that would be necessary to show significant differences between study groups. Chronic animal studies are expensive to perform due to the facilities necessary, the labor involved in follow-up evaluations and histology, and other factors, and so large sample sizes make the study even more expensive and impractical. Nonetheless, this study was useful even for assessing further research opportunities, and therefore evaluating electrical performance between study groups was a worthwhile exercise.

Another secondary research question dealt with evaluation of lead stability over the course of the study.

Research Question 3

Are there significant differences notable in stability of leads with the porous electrode as compared to leads with the solid (control) electrode?

Hypothesis

It was hypothesized that tissue in-growth into the porous electrode would help anchor the lead tip in the vein and, with large sample sizes, a difference would be noted in rate of lead retraction and dislodgement between study groups. However, due to the small sample sizes inherently involved in chronic animal evaluation, it was also hypothesized that such a difference would not be observed with statistical significance in the study.

Means of Answering Research Question

At implant and at regularly scheduled intervals throughout the study the animal was sedated and radiographic x-ray images were taken in both anterior/posterior and lateral views. The radiographs were then used to determine whether the tip of the lead had moved proximally from its original implant position, and approximate distance values were recorded for any observed lead movements by comparison to the 1 cm length between the tip electrode and proximal ring electrode on the lead.

In regard to research question 3, despite any concerns about statistical power to resolve differences between study groups, this question was also worthwhile to evaluate due to the ability to correlate lead movement to histological images.

4.4.3 Overview of Study Design

This 60-day canine study evaluated the *in vivo* pacing threshold performance, lead stability, and post mortem histology of two groups: one control group and one experimental group. The control group consisted of standard ACUITY^{TM} Steerable leads with two modifications: an uncoated (i.e. no iridium oxide, as would normally be added) solid distal tip electrode and no steroid-eluting collar. The experimental group consisted of standard ACUITY^{TM} Steerable leads with two modifications: a porous distal tip electrode and no steroid-eluting collar. For both groups the proximal electrode was the standard iridium oxide-coated ring electrode. Electrical performance data (left-ventricular pacing thresholds, pacing impedances, and sensed R-wave amplitudes) were collected from all study animals at day 0, 3, 7, 14, 21, 28, 42 and 60 post-implantation. Radiographic confirmation of lead position in the coronary vein was also performed throughout the study. Gross necropsy and histology were assessed at termination.

The entire study was to enroll a minimum of sixteen (16) and a maximum of twenty (20) animals. Animals could be rejected due to insufficient coronary vein size or

geometry, or replaced due to lead retraction/dislodgement; therefore, additional animals were made available for this protocol. The study director (author) and/or implanting surgeon or facility veterinarian determined the suitability of the animal's vascular geometry for implant of the control and experimental leads by assessing the ease or difficulty of the implant procedure and the final location of the lead's tip electrode and fixation shape within the branch vein.

4.4.4 Study Justification

It was deemed necessary to implant test articles in large animals (canines) for this study since the most relevant environment in which performance of the test articles could be evaluated was *in vivo*. A bench or *in vitro* test would not give the biological responses that this study was intended to characterize. Additionally, small animals such as mice or rats were not suitable for this study due to the size of the pacing leads and the necessity to do voltage threshold testing. The canine model provides stable electrical performance while maintaining a stable weight, which, for example, is a difficulty with the porcine model over the course of a 60-day study. Gross changes in animal size and weight during the study can affect the ability to gather data and even result in lead dislodgement.

In compliance with USDA Policy #12 [59], a literature search was performed to verify that this research was not redundant and that animal testing was appropriate. Using predetermined keywords and wildcard variations, the titles, abstracts and major descriptor fields of three online databases (MEDLINE, EMBASE, and Biosis Previews) were searched by a Boston Scientific CRM technical librarian on March 17, 2008. The search terms used can be viewed in Appendix B. After reviewing the results of the

database searches, no published account was found through the online literature search that duplicated this study.

4.4.5 Test Articles

In this study, porous tip electrodes were fabricated for inclusion on the ACUITY™ Steerable left-ventricular lead design in order to evaluate chronic fixation stability and electrical performance as compared to that of ACUITY™ Steerable leads with solid tip electrodes. These porous tip electrodes were assembled onto eight ACUITY™ Steerable model 4554 leads in place of the standard iridium oxide-coated tip electrode. Additionally, in order to isolate the effects of the porous electrode on the chronic inflammatory response in the vein, both of the steroid eluting collars normally assembled onto ACUITY™ Steerable leads (one near each electrode) to mitigate chronic inflammatory response were replaced with short sections of silicone tubing with no loaded drug (i.e. dummy collars). Test group leads were assembled in the Boston Scientific Puerto Rico manufacturing facility and sterilized for chronic implant.

Upon completion of assembly of the porous electrodes onto ACUITY™ Steerable leads, pictures of the lead tip were taken under magnification in order to characterize any damage to the porosity that occurred. These pictures were used to sort leads and choose those with tip electrodes in an undamaged state or with minimal damage for inclusion in the study. Figure 20 displays a picture of an undamaged lead tip (representing most of the leads included in the study) and also displays a picture of a lead tip with some amount of damage to the porosity. This latter case represents the worst case for the leads included in the study (other rejected leads all had worse damage, and thus the best eight leads were selected for the study).

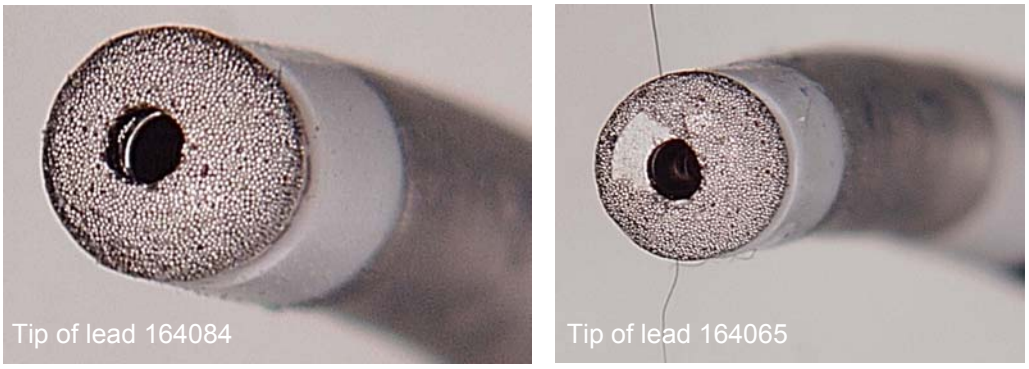

Figure 20: Example images taken under magnification after assembly of porous tip electrodes onto ACUITY™ Steerable leads. The left-hand image is representative of the state most of the porous tip leads included in the study. The right-hand image is representative of the worst-case damage of any porous tip lead included in the study. Though steroid collars can be seen just proximal to the tip electrodes in these pictures (they were initially assembled onto the leads in error) these collars were later removed and replaced with silicone tubing.

For reference, Appendix C includes pictures of the tip of each porous electrode lead included in the study.

Subsequent to the assembly of the leads to be implanted for the animal study, work was done to increase the strength of the porous network by further optimizing the sintering time (resulting in a longer sintering process and slightly larger coalescence of microspheres). This work could be leveraged in any future studies in order to prevent porous electrode damage during assembly. However, despite the minor damage incurred to some of the porous tip electrodes assembled onto study leads, the effect on the outcome of this study was likely negligible. Even for the worst-damaged lead tip most of the volume of porosity remained in place.

In addition to test group leads, eight control group leads were also implanted as part of the study for performance comparison. Control articles consisted of ACUITY™ Steerable model 4554 leads with a solid, uncoated, "as-machined" tip electrode in place of the standard iridium oxide-coated tip electrode. Additionally, in order to isolate the

chronic inflammatory response in the vein from any effect of steroid, both of the steroid-eluting collars normally assembled onto ACUITY™ Steerable leads were replaced with short sections of silicone tubing with no drug (i.e. dummy collars). Control group leads were assembled in the Boston Scientific Puerto Rico manufacturing facility and sterilized for chronic implant.

Implantable pulse generators used in the study were from the Boston Scientific INSIGNIA™ family of pacemakers. The coronary venous leads included in this study were connected to the right-ventricular port in the INSIGNIA™ device at implant (connection to the right-ventricular port still allows data to be accurately recorded from an implanted left-ventricular lead), and the device was interrogated during scheduled checks in order to record electrical data. These pacemakers were not used to stimulate the heart between data checks. An image of an INSIGNIA™ model pacemaker used in this study is included in Figure 21.

Figure 21: Image of INSIGNIA™ model pacemaker utilized for electrical data acquisition in the chronic animal study.

4.4.6 Animal Model

Details about the animal model chosen for this study are included in Table 2.

Table 2: Details regarding animal model selected for study implants.

Animal Species	Canine (purpose-bred mongrel or mongrel-cross)
Total Animals Required	Minimum of 16 and maximum of 20
Sex Required	Either male or female
Age of Animals Required	Age appropriate for weight
Body Weight Range	> 20 kg
Source	Boston Scientific CRM approved source
System of Identification	Ear-tag, tattoo, or other number assigned at time of experiment
Selection Criteria	Approved for use by Boston Scientific CRM veterinarian based on physical exam, appropriate blood work, EKG, and parasite screen

4.4.7 Animal Care and Handling

Boston Scientific CRM complies with all animal use regulations as set forth in the Animal Welfare Act, Title 9, CFR, Chapter 1, Subchapter A and adheres to the principles outlined in the "Guide for the Care and Use of Animals," National Institutes of Health Publication [60]. Boston Scientific CRM preclinical studies area procedures were followed during the conduct of all studies, as appropriate.

Any drugs which may alter the local inflammatory response of the heart to the lead were restricted. Restricted medications for the animal species in this study were:

- NSAIDS
- Corticosteroids
- Tetracycline
- Systemic antihistamines
- Omega 3/6 fatty acids

Further, the drugs listed below were restricted if their effect overlapped the time at which pacing thresholds were taken.

- Epinephrine
- Verapamil

- Lidocaine
- Procainamide
- Propanalol

Refer to Table 3 for antibiotic formularies specific to the species in this study.

Table 3: Antibiotics

Phase	Drug	Dose	Route/ Frequency
Peri-operative	Cefazolin	~25-30 mg/kg	IV given in prep, at least 30 minutes prior to surgical incisions and then again after 1.5-2 hrs
Post-operative	Amoxicillin/Clavulanic Acid	~20-22 mg/kg	Starting in afternoon the day of surgery and continuing for 7days.*
Note: Prescription medication could be changed at the discretion of a facility veterinarian with appropriate justification documentation. * If an animal was unable to take the oral antibiotic on a particular day, Cefazolin ~25mg/kg IM or SQ g 8hr may have been substituted and the dosing schedule for Amoxicillin/Clavulanic acid appropriately adjusted.			

Refer to Table 4 for sedation and induction formularies specific to the species in this study.

Table 4: Anesthesia

Phase	Drug	Dose	Route/ Frequency
Sedation	Morphine sulfate	~ 0.5 mg/kg	Subcutaneous
Induction	Ketamine Diazepam	~ 6-11 mg/kg ~ 0.4-0.5 mg/kg up to 10 mg total	Intravenous
Peri-operative	Isoflurane	To effect	Inhalant
Note: Prescription medication could be changed at the discretion of a facility veterinarian with appropriate justification documentation.			

Refer to Table 5 for analgesia formularies specific to the species in this study.

Table 5: Analgesia

Phase	Drug	Dose	Route/ Frequency
Intra-operative	Morphine sulfate	~ 0.5 mg/kg	Subcutaneous; repeat intra-operative if greater than 4 hours from pre-operative dose
Post-operative	Morphine sulfate	~0.25-0.5mg/kg	Subcutaneous; the day of surgery
	Tramadol	~ 4mg/kg	Beginning in the afternoon the day of surgery and continuing for 3 days.*
Note: Prescription medication could be changed at the discretion of a facility veterinarian with appropriate justification documentation. * If an animal was unable to take oral medication, morphine could be substituted at ~ 0.25 to 0.5 mg/kg SQ and the schedule of tramadol adjusted appropriately.			

The drugs listed in Table 6 were allowed for use interoperatively as needed to maintain physiological homeostasis.

Table 6: Interoperative drugs

Reason	Drug	Dose
Isotonic fluids	0.9% NaCl or LRS	As maintenance fluids
Bradycardia	Atropine	~0.02-0.04 mg/kg
Low Blood pressure	Hetastarch 6%	~25-50 cc ~up to 20ml/kg/24 hours
	Phenylephrine	~0.25 to 3.0 µg/kg/min
Low blood sugar	5% dextrose	As needed per blood glucose values

Additionally, in order to facilitate data collection and radiographs at designated lead check time points, animals were allowed to be sedated with IV xylazine, up to 1.1 mg/kg total dose.

4.4.8 Animal Replacement

Animals with health complications or insufficient vascular geometry as estimated by the study director (author) and/or implanting surgeon or facility veterinarian during visualization of a baseline venogram at implant could be removed from the study and replaced at the discretion of the study director.

4.4.9 End of Study

At the end of the 60-day study, the animals enrolled in the study were euthanized for necropsy and histology examination. The euthanasia complied with the "2000 Report of the AVMA Panel on Euthanasia" [61] and was carried out as follows: Prior to euthanasia, the animal was given an approximately 200 IU/kg heparin IV bolus. Euthanasia was performed by an overdose of barbiturates, inhalant anesthetics or KCl in conjunction with general anesthesia.

4.4.10 Surgical Approach

Leads were implanted using standard coronary venous lead implantation techniques and accessories, and in a randomized order and blinded to the implanting surgeon and follow-up technician. A summary of the surgical approach is as follows:

- The animal was sterilely scrubbed and draped. Ioban drape was used.
- Under sterile conditions, a cut down to the right jugular vein was performed, and the vein isolated and ligated proximally.
- A venogram was acquired by inserting an Arrow 6 Fr balloon catheter (or equivalent) into the ostium of the coronary sinus. The balloon was temporarily inflated to block outflow of the sinus while a bolus of contrast agent (~ 5 mL) was injected through the catheter to illuminate the coronary venous tree. Alternatively, a guiding catheter was introduced into the coronary sinus first followed by subsequent insertion of the balloon catheter through the guide.
- Once the venogram was stored, the balloon catheter was removed. If the balloon catheter was introduced without the guide catheter, the guide catheter

was inserted at that time. A small bolus of contrast was used to confirm the position of the guide catheter coaxial with the lumen of the coronary sinus.

- The venogram was visually evaluated for coronary venous diameter, length, and geometry conducive to a coronary venous lead implant. This information was recorded in the animal record or appropriate data collection form. If it was determined by the implanting surgeon, facility veterinarian, or study director (author) that the anatomy was not conducive to LV implant, the animal was rejected for this study.
- The test or control article lead was inserted through a guide catheter by tracking over a guide wire or using a delivery stylet.
- The lead was advanced as far as possible to a stable position within the target vein (i.e. tip electrode was "wedged" in the distal end of the vein) so that in the final lead position as much of the "J" fixation shape as possible resided within the branch vein and the tip electrode had good vein wall contact.
- When the lead was in the desired position, the guide wire or stylet was removed while applying gentle forward pressure on the lead until the "J" fixation engaged.
- The lead was electrically tested for sensing and pacing criteria for both the tip electrode and ring electrode. Recommended acceptance criteria at implant were voltage threshold of < 2.5V, impedance between 200 – 2000 ohms, and R-wave amplitude ≥ 3mV.
- The guide catheter was cut away while stabilizing the lead with a finishing wire or equivalent if necessary.
- The finishing wire was removed if used.
- The lead was sutured in the vein utilizing a suture sleeve and nonabsorbable 2-0 Prolene® suture at the vein entry site.
- A subcutaneous pocket was prepared near the dorsum of the neck along the right cervical lateral area.
- The lead was tunneled to the area of the subcutaneous pocket and inserted into the pulse generator right-ventricular lead port.
- The pulse generator was inserted into the subcutaneous pocket and anchored with three non-absorbable sutures to the underlying muscle with zero Prolene® or otherwise secured as desired by the implanting veterinarian.
- Any excess lead was coiled and positioned in the subcutaneous tissue in the area of the pulse generator.
- The subcutaneous tissue was sutured closed with absorbable suture and the skin closed with surgical staples or sutures.

- Data was collected from the pulse generator during the closure process or after the area had been closed.
- Left lateral fluoroscopy and left lateral and dorsal-ventral radiographs were taken to document final lead and pulse generator location.

Each animal's coronary venous anatomy (via venogram) was saved to a CD-ROM as a cine. The final lead position was saved to a CD-ROM for lead movement reference. References of lead movement were made off radiographs however, and not fluoroscope images.

4.4.11 Periodic Lead Checks

To document lead and electrode placement and stability, radiographs were obtained immediately post-implant and at various time points throughout the study. Animals were positioned for radiographic images in left lateral and dorsal ventral position. Additionally, pacing voltage thresholds at a pulse width of 0.5 ms, pacing impedance at 5V and 0.6 ms, and R-wave amplitudes in the unipolar configuration (tip to reference electrode placed on the skin near the implant site) were collected via interrogation of the pacemaker. Radiographs and data checks were done at the following time points:

- Implant (day 0)
- Day 3 (±1 day)
- Day 7, 14, 21, 28 (±2 days)
- Day 42 (±3 days)
- Day 60 (±4 days)

4.4.12 Necropsy

The lead distal end was not removed for histopathological examination of the vein; rather, slicing after tissue fixation was done with the lead *in situ*. It was required that the lead be fixed in position within the great cardiac vein in the atrioventricular groove such that it was secured in place prior to any manipulation of the heart. The location of the tip of the lead was marked with a single suture placed on the implant vein 5 mm apically (i.e. toward the apex of the heart) from the distal end of the lead tip. This allowed assurance that the lead tip did not move between heart excision and tissue trimming.

The heart as a whole was removed from the body and, after ensuring the distal end of the lead had been secured in the great cardiac vein with a suture, the serial number of the lead was recorded in the necropsy record and the lead was cut near its entry into the SVC. The heart was immersion-fixed in 10% buffered formalin. The fixed hearts were carefully placed in rigid, fluid-filled containers of 10% neutral-buffered formalin (NBF) to help assure vessel integrity prior to histopathology evaluation. The container was large enough to ensure a 1:10 ratio, by volume, of tissue to formalin. The fixed hearts and any other collected fixed tissues were sent to the Boston Scientific Pathology Laboratory.

4.4.13 Histopathology

Trimming of tissues was performed by the study pathologist and trained histotechnologist. Whole heart radiographs or radiographs of trimmed tissue sections were used to aid in the blocking of specimens for further processing. The distance from the lead tip to the marking suture was measured prior to trimming in order to document

any shifting of the lead tip. The myocardium was trimmed on all sides of the lead leaving at least 5 mm of tissue on all sides. The lead body was cut proximal to the electrodes leaving the electrodes in place. The resulting tissue blocks were processed and embedded in SPURR epoxy resin. Radiographs of the plastic-embedded tissue blocks were taken if necessary to adequately mark the block for section preparation.

Samples which were embedded in SPURR were cut into a distal and proximal block as determined by the study pathologist. The proximal lead block was sectioned longitudinally as close to the midsagittal point (centerline) as possible in order to obtain a single section. The distal lead block was cut in order to obtain up to 4 sections. The first section was as close to the midsagittal point as possible. The depths of the other 3 sections were determined by the study pathologist in order to obtain approximate equal representation along the longitudinal axis of the lead body. Sections from SPURR embedded samples were cut at 4-5 microns. The resulting tissue sections were stained with Gomori's trichrome stain.

Overall, histological parameters of interest included trauma to the underlying myocardium, encapsulation of the lead body, encapsulation of the pacing electrode, influence of porosity of the tip electrode (test samples only), development of thrombus, identification of cell types, and evidence of necrosis. The remaining heart was examined by the pathologist. Any gross lesions were to be trimmed, processed in paraffin, and the resulting sections stained by hematoxylin and eosin and trichrome techniques as well as any special stains deemed necessary by the pathologist.

5 Results and Discussion

5.1 Chronic Animal Study Overview

Implants for this chronic animal study were performed at the Boston Scientific CRM Research and Technology Center from May 27 to May 30, 2008. The implant order was randomized, and the implants were performed by multiple implanters who were each blinded as to whether the lead being implanted was a control or test group lead. Additionally, the same implant technique was used for each lead. Each lead was delivered over a guide wire through a guide catheter into the coronary sinus and eventually into the target branch vein on the left ventricle, after which the guide wire was removed and a delivery stylet was inserted into the lead and used to push the tip of the lead as far distal as was possible ("wedging" the tip of the lead in the vein). All 16 study leads were implanted without any animal or lead replacement. Additionally, all 16 leads survived the full 60 days of the study with no complete lead dislodgements, meaning there were also no lead or animal replacements during the course of the study and a full set of data was taken for each lead.

5.1 Venography

As mentioned in Section 4.4.10, venograms of the coronary venous anatomy were taken for each animal and were saved for later reference. Using the venogram, one can note any abnormalities in the coronary venous anatomy and compare the venogram to the final implant location of the lead for reference in future determinations of lead tip movement. For reference, Figure 22 is included below, giving an example venogram image taken while injecting iodine contrast into the veins during occlusion of

the coronary sinus with a balloon catheter. This image is used as a visual "roadmap" when delivering the lead, helping the implanter guide the lead tip to the desired location. Figure 22 also shows an image of the final implant location of the lead.

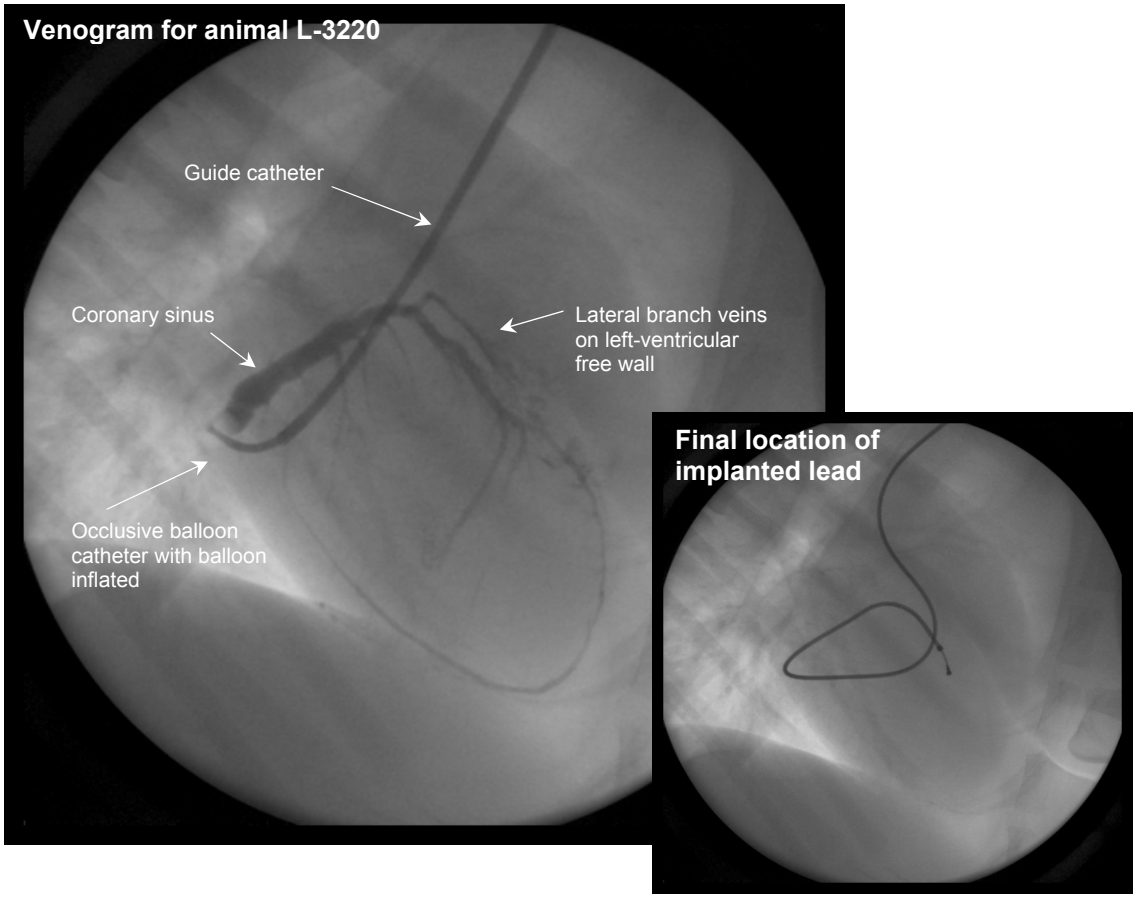

Figure 22: Occlusive venogram of animal L-3220 showing the venous anatomy from a right anterior oblique (RAO) orientation. Also shown is an image of the final location of the implanted lead.

For further reference, venogram images for each animal and images of the final location of each lead are given in Appendix C.

5.2 Lead Electrical Data

Electrical data were recorded for each lead at all of the specified time points, as given in Section 4.4.11. Figure 23 displays the pacing threshold values for each lead

over time, and Figure 24 displays the change in pacing threshold from implant for each lead (the implant threshold value is subtracted from the thresholds at each time point). The pacing vector was from the lead tip electrode to a reference electrode placed on the skin near the implant site. Though lead stability data are not specifically discussed until later, any time points where a retraction of the lead tip was noted are shown in Figure 23 and Figure 24 as a white data point instead of a solid color.

The change in threshold from implant data give the most accurate means of comparison among all leads, as the initial pacing threshold at implant can be influenced by a variety of factors not related to the lead or its electrodes. Additionally, the porosity on the tip electrodes of the test group leads would be expected to have the same threshold distribution as solid tip electrodes acutely (at implant and < 3 days thereafter), and so it makes sense to eliminate the implant thresholds as a variable in the comparison and give higher resolution to making distinctions between threshold change from implant between the groups.

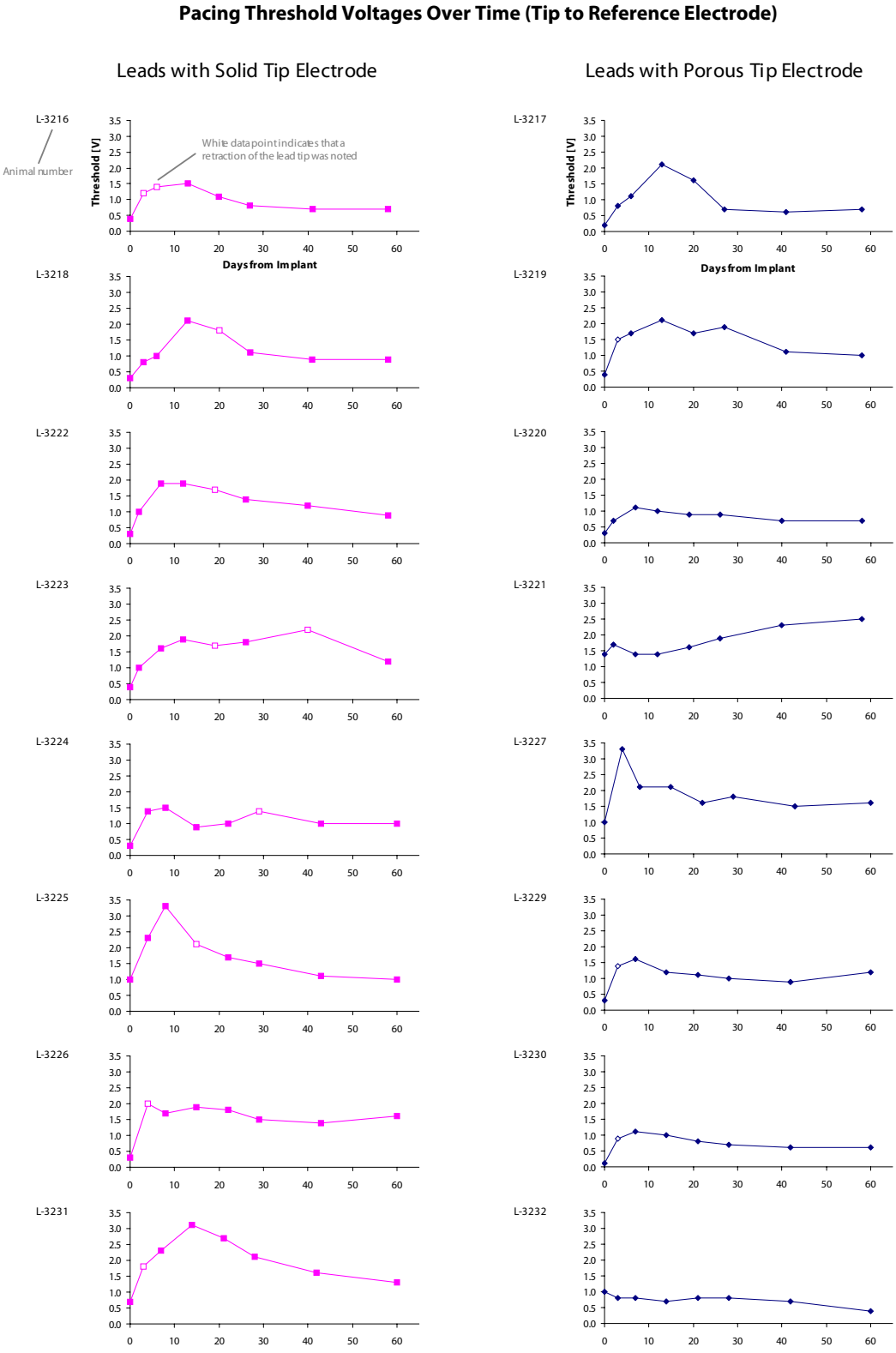

Figure 23: Pacing threshold voltages over time for each of the implanted leads included in the chronic study. Raw data for each lead is given in Appendix C.

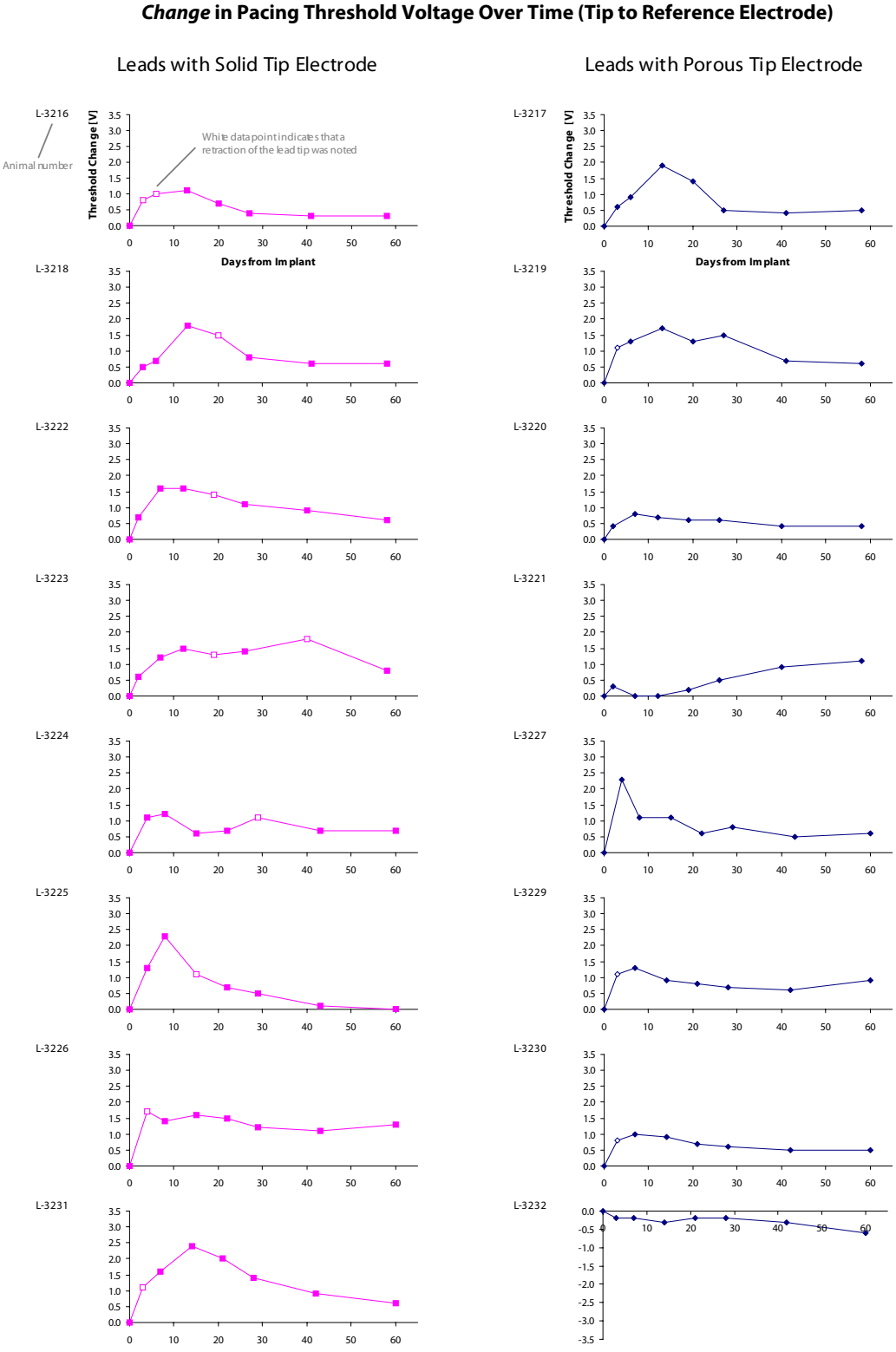

Figure 24: *Change* in pacing threshold voltages from implant for each of the implanted leads included in the chronic study. Raw data for each lead is given in Appendix C.

The characteristic threshold rise due to the foreign body response can be observed in almost every case in Figure 23 and Figure 24 in approximately the first two weeks after implant. Growth of the fibrous capsule around the lead body in the vein, including the electrode, causes the effective distance between the electrode surface and myocardial tissue to increase, requiring a higher voltage to create the minimum electric field strength to depolarize the myocardial cells. Also worthy of note is the relatively consistent threshold curve morphologies between the control group leads as compared to the test group (porous electrode) leads, which seem to have variability in magnitude of threshold rise after implant (and indeed one lead, implanted in animal L-3232, had no rise in pacing threshold after implant).

Another way to analyze the pacing threshold data is to compare the mean and standard deviation of each group at each time point. Summary data comparing the mean pacing threshold values and the change in pacing threshold from implant at each time point are shown in Figure 25.

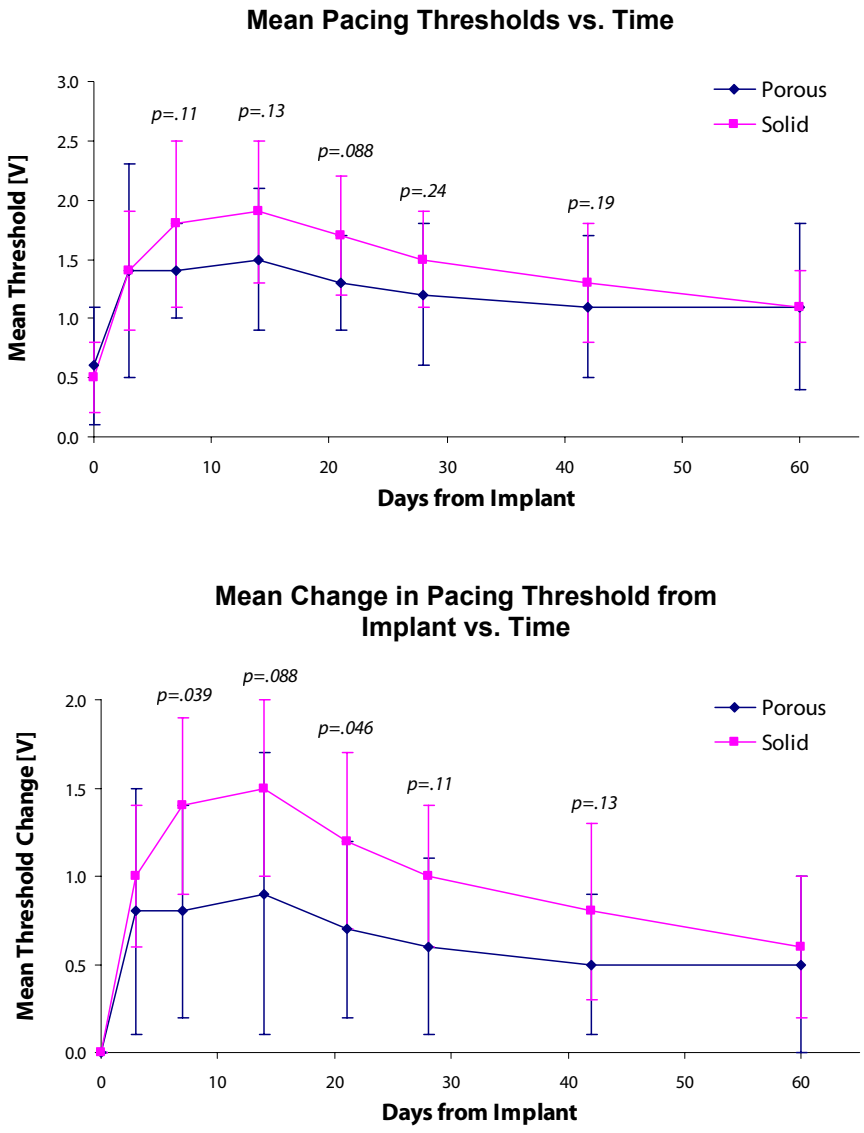

Figure 25: Plots of mean pacing threshold over time and mean change in pacing threshold from implant over time. Pacing thresholds were measured from the tip electrode to an indifferent electrode. Error bars represent +/- one standard deviation, and p-values are the result of a two sample paired t-test comparing means (p-value is for two-tail comparison) where the t-test was performed after data was normalized by doing a log transformation (group threshold data at any particular time point typically follow a lognormal distribution).

The plot of mean change in pacing threshold from implant is notable in the absolute difference in mean threshold rise between the groups. There would appear to be a departure in the mean threshold rise curves between day 3 and day 7 for the porous

electrode and solid electrode groups, and indeed the p-value for the t-test bears out this apparent difference in response (p=0.039). The p-values indicate the probability of concluding that there is a difference between the means of the two groups when in fact there is none. P-values at two time points, day 7 and day 21, are actually lower than the frequently-used threshold for statistical significance of $p \leq .05$, supporting a conclusion that the porous electrode group has a lower mean threshold rise from implant at these time points. This difference between the groups was identified despite the low sample size of the groups being compared (n=8) and the inherently low statistical power for making such conclusions for this study (due to the low sample size and multiple sources of variability). If one desired to detect a 0.5 V difference in mean threshold change from implant between the two groups assuming a 0.7 V standard deviation for each group, α=0.05, and a two-tailed test, a sample size of eight per group results in a statistical power of approximately 0.30 (much lower than what is often considered an ideal value of 0.80).

Though the p-values at the other time points shown in the lower plot of Figure 25 are greater than 0.05, this does not mean that a difference between the groups does not exist, only that no difference was detected. A study with a larger sample size (and thus a higher power) would have a higher chance of finding differences at these time points if they exist. However, in order to reach a statistical power of 0.80 in the same scenario (again assuming a desired detection of at least a 0.5 V difference between the groups with a 0.7 V standard deviation for each group), samples sizes of roughly 30 animals per group would be necessary, which is generally not feasible due to the cost and complexity of such a study.

It would seem, upon viewing Figure 25, that one factor making distinctions more difficult between the porous electrode and solid electrode groups is a higher standard deviation for the test group at many time points. As noted in the discussion of Figure 23 and Figure 24, there seems to be more variability in the morphology of the threshold curves for the porous electrode group than the solid electrode group. However, when an F-test is performed on the threshold change from implant data at each time point, looking for statistical differences in variance between the two groups, one cannot conclude that the test group has larger variances on the p-values for the tests. Figure 26 plots the individual change in threshold from implant data at each time point, and includes the p-values of each F-test performed.

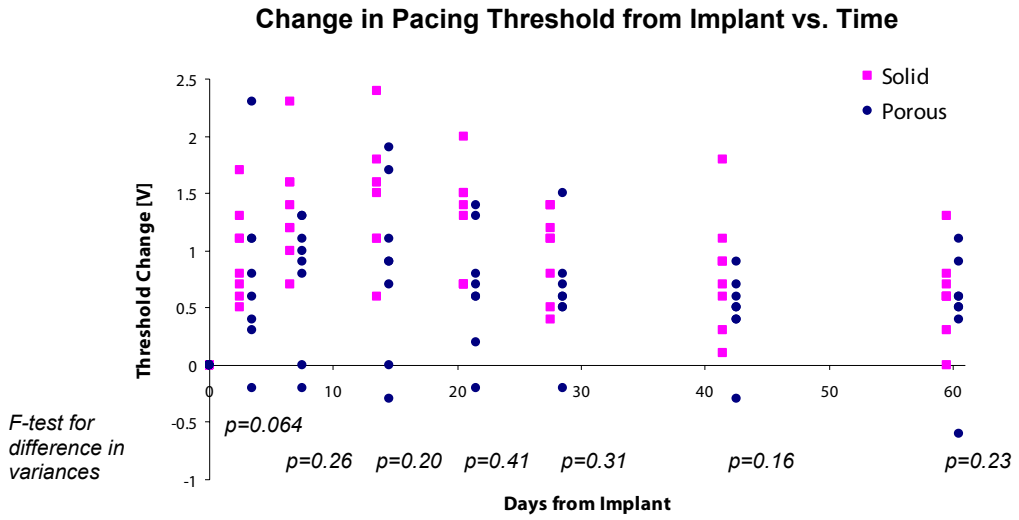

Figure 26: Plot of individual change in pacing threshold from implant data over time. Pacing thresholds were measured from the tip electrode to an indifferent electrode. Group data are slightly separated from each other in the x-axis at each time point to allow better visual comparisons to be made. P-values shown are from an F-test performed to compare the variances of the two groups at each time point.

The F-test does not take into account the morphology of each lead's threshold data curve over time; rather, the test performed treats the data at the time point as a unique

comparison with no historical information. In the end it is difficult to say if there is more variability in thresholds between groups without larger sample sizes.

Pacing impedance measurements are another set of data that can give insight into the level of foreign body response at the electrode surface. Generally speaking, the higher the impedance the better (provided a low pacing threshold voltage can be maintained) as a higher impedance saves charge stored in the pacemaker battery and extends the life of the pacemaker. Factors that influence the level of pacing impedance include the surface area of the electrode and the thickness of the fibrous capsule. Summary data comparing the mean pacing impedance values at each time point are shown in Figure 27.

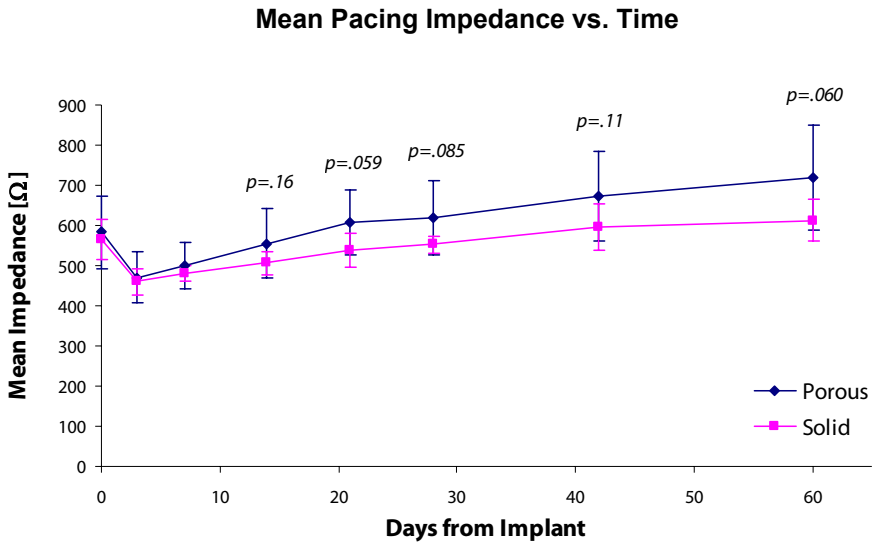

Figure 27: Plot of mean pacing impedance over time, measured from the tip electrode to an indifferent electrode during a 5 V, 0.6 ms pacing pulse. Error bars represent +/- one standard deviation, and p-values are the result of a two sample paired t-test comparing means (p-value is for two-tail comparison). No data transformations were performed for the t-test.

Here we see no statistically significant difference in mean pacing impedance between the groups at all of the time points, and this is despite the fact that the porous electrodes have a much larger surface area than the solid electrodes (approximately 64 mm^2

exposed, as compared to 7.8 mm^2 exposed for the solid electrode, as shown in Section 4.3). Larger electrode surface area normally results in lower pacing impedance simply due to the greater area for current to flow from the electrode.

In this case, the best explanation for the higher-than-expected impedance of the porous electrodes is improved biocompatibility over the solid electrodes. As discussed in Section 1.3 (in regard to Figure 3), pacing thresholds typically drop after implant due to increased vascular permeability and fluid influx, followed by a steady increase in impedance as local fluid levels decrease and phagocytic cells adjoin the electrode surface and the mature fibrous capsule forms [1]. This behavior can be readily seen in Figure 27 for both groups. However, the degree to which the impedance rises chronically depends on the persisting layer of macrophages and other phagocytic cells on the surface of the electrode. The more such cells that are near the surface of the electrode, the lower the impedance since current is conducted through cell membranes [1]. Consequently, the higher impedance for the porous electrode group is an indicator that there are fewer chronically persisting phagocytic cells at the surface of the electrode as compared to the solid electrode group. This may be due to tissue growth into the porous electrodes, and could also be due to the porosity of the electrodes activating phagocytic cells to phenotypes favorable for tissue growth and remodeling (such as an M2 phenotype for macrophages).

The sensed R-wave amplitude is another important electrical metric for a pacing system as it affects the ability of the pacemaker to sense the intrinsic electrical activity of the ventricles of the heart. The higher the sensed R-wave amplitude the easier it is for the pacemaker to recognize an intrinsically driven depolarization of the myocardial

tissue in the ventricle, allowing recognition that a ventricular contraction has occurred. Summary data comparing the mean sensed R-wave amplitude values at each time point are shown in Figure 28.

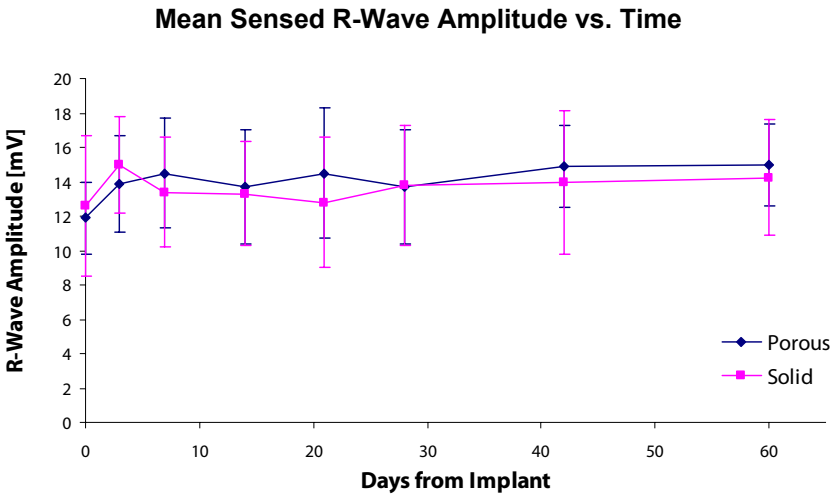

Figure 28: Plot of mean sensed R-wave amplitude over time, measured between the tip electrode and an indifferent electrode. Error bars represent +/- one standard deviation. Means were not statistically different at any of the time points.

Here there is no statistical difference between mean sensed R-wave amplitudes between the groups at any time point, and none was expected. The differences in the tip electrode designs included in this study should not affect ability to sense the intrinsic electrical activity of the heart or the magnitude of the sensed R-wave. Lack of a difference in sensed R-wave amplitude between the lead groups is also an important finding, as it points to the fact that any differences in mean change in pacing threshold from implant, or mean impedance, would be due to actual differences in biological response and not due to difference in implant locations, animal anatomy, or other variables.

5.3 Lead Stability Data

X-ray radiographs were taken of the chest area of the animals at all data check time points in order to assess the chronic stability of the lead tip. Radiographs were compared to the radiograph taken just after implant, and if necessary also compared against radiographs from other time points, and the known spacing of the tip and proximal ring electrodes (1 cm, as shown in Figure 8) was utilized to estimate the distance the lead tip had retracted from its original position. Comparing the position of the lead in one radiograph against another can be quite difficult due to the fact that the heart is beating when the radiographs are taken. Therefore, one cannot use body landmarks such as rib bones to compare relative locations of the lead tip between radiographs. Instead, the point at which the lead turns into the coronary branch vein from the great cardiac vein or coronary sinus is used as a reference landmark (if the lead tip has not moved) since the distance between this point and the tip of the lead is relatively constant despite the motion of the heart as a whole. Determination of the occurrence of a lead retraction is relatively straightforward, though the approximation of the distance of the retraction is certainly an inexact science. Besides the movement of the heart, another source of error in the approximation of the distance of lead retraction is inherent in the attempt to estimate a three-dimensional distance using a two-dimensional image. In order to mitigate this error, radiographs from the left-lateral (LL) and anterior-posterior (AP) views were both used to compare and corroborate any findings. In total, the accuracy of this method of identifying lead movements is estimated to be +/- 0.5 cm. Even with the sources of error in lead stability data, the data remains useful and an important indicator of possible performance differences between

the two lead groups. Figure 29 depicts an example of the method used to identify an occurrence of lead retraction and approximate the distance of the retraction.

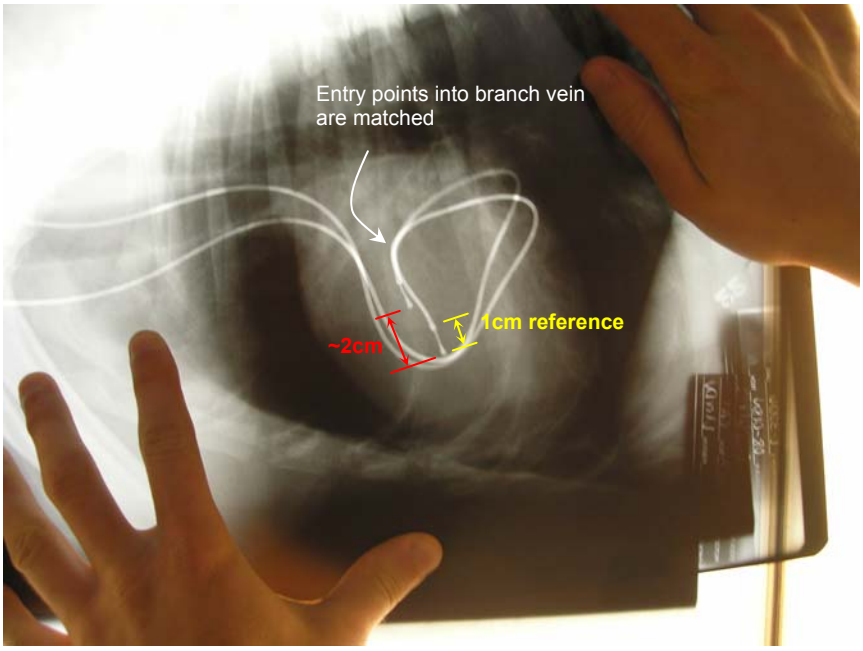

Figure 29: Example of the method used to determine the occurrence of a lead retraction between two time points and approximate the distance of the retraction. For the purposes of this example, the radiographs are twisted slightly around the points of descension into the branch vein to allow visual differentiation between the two leads. The normal procedure would be to completely overlap the lead distal ends as much as possible. The radiographs shown in this image were taken from a left-lateral (LL) view.

A summary of the lead stability data gathered during the study is shown in Figure 30. Reference Appendix C for images of the comparison of radiographs for each observation of lead retraction.

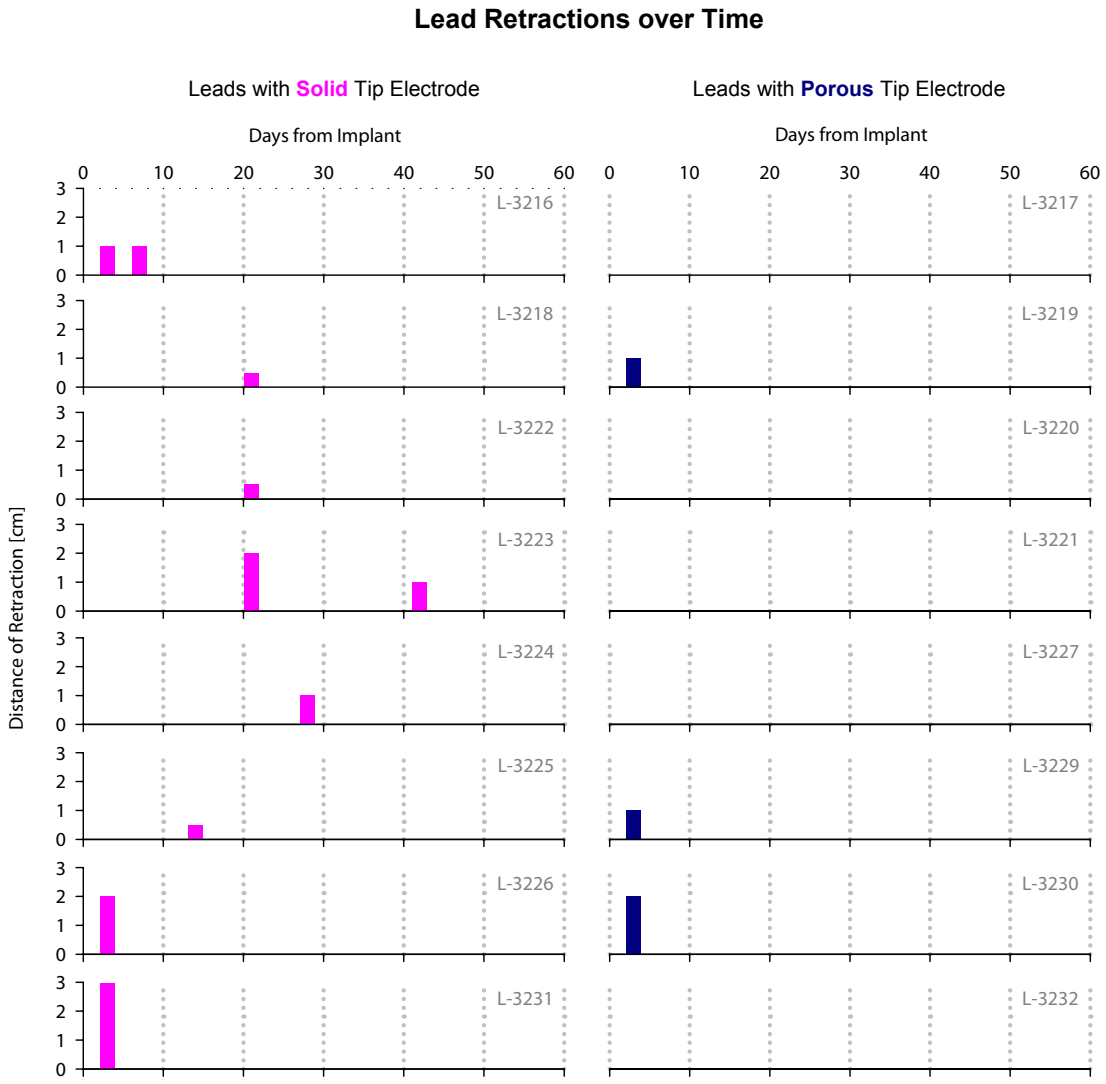

Figure 30: Summary of lead stability data from the chronic animal study. Every vertical bar shown represents a lead retraction that was observed via the radiograph taken at the time at which the bar is shown in the plot. The height of each vertical bar represents the estimated distance of the lead retraction.

Five of the eight control group leads (with solid tip electrode) were noted to have retracted at least once during the course of the study (retraction of 1 cm or greater). A retraction was also noted for the remaining three control group leads, though it was within the estimated error of the measurement method (+/- 0.5 cm). A number of the control group retractions were noted after day three of the study, with one

noted as late as the day 42 lead check. Three of the eight test group leads were noted to have retracted by day 3 of the study, but unlike the control group leads no retractions occurred in the test group after day three of the study. The lack of lead retractions after day three of the study for the test group may be due to tissue attachment and/or in-growth at the porous tip electrode acting to stabilize the leads in their respective positions. Also intriguing is that the pacing thresholds of the three porous electrode leads that retracted do not appear to have been negatively affected by the retraction (see Figure 24 for the change in threshold from implant values for these leads). If tissue attachment to the porous tip electrode after day three was a factor in increasing the stability of the leads that initially experienced a retraction, this may mean that movement of the lead tip within the vein post-implant does not affect the subsequent ability to continue the tissue attachment process.

These data all suggest that electrode porosity may be capable of chronically stabilizing the position of a coronary venous pacing lead within the vein as compared to a more standard solid electrode design. Further study with larger sample sizes would be necessary to confirm potential differences discussed here. A study of the force necessary to extract the lead from the heart using manual traction, which could be done at the animal necropsies, would also be useful in evaluating differences in lead stability. If tissue attachment to porous electrodes is in fact responsible for stabilizing the lead within the coronary vein, there may be a difference in the amount of force necessary to extract the lead as compared to leads with traditional solid electrodes.

5.4 Histopathology

Tissue sectioning for histological examination was done with the distal end of

the lead *in situ*, made possible by using SPURR epoxy resin to embed excised tissue/lead samples. Each tissue/lead block was initially cut as close as possible to the center axis of the lead, leaving two blocks that each had a face at the "zero" point relative to the lead center axis. Subsequent slices were taken in both blocks at different depths relative to the "zero" face (parallel to it) in order to get a more complete picture of the geometry of the fibrous encapsulation of the lead tip. These additional tissue sections inherently cut the lead tip and fibrous encapsulation at an oblique angle such that the further away from the zero position the smaller the lead track appears (while the fibrous encapsulation appears thicker).

No matter the location of the tissue slice, in every case the lead portion of the slice did not remain in place once the section was created. Retention of the lead with the surrounding tissue in the section was known to be improbable prior to the study. Though almost all of the sliced lead detached from the rest of the tissue section in each case, the surrounding tissue remained relatively undisturbed since it was perfused with polymer (now solidified). The exception to this was the sintered microsphere areas of the porous electrode samples. Growth of tissue into the porous electrode was visually demonstrable in many of the porous electrode tissue sections, but at the same time most of the tissue in-growth within the electrode was removed from the tissue section when the lead detached, preventing full visualization of the tissue in-growth.

For every tissue section, measurements of the thickness of the surrounding fibrous capsule were taken normal to the surface of the electrode at pre-defined points. Figure 31 graphically displays the location of the measurement points for the example case of a tissue section at "zero" with respect to the lead centerline axis.

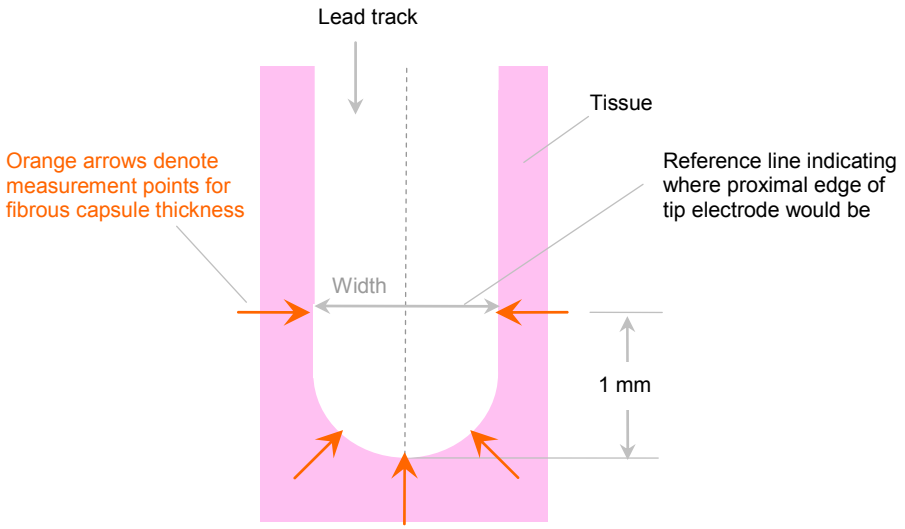

Figure 31: Graphical representations of pre-defined locations of measurement of fibrous capsule thickness normal to the tip electrode surface.

A measurement of the width of the lead track was also taken at a location 1 mm back from the distal end of the tip electrode shown in Figure 31. This measurement serves as a further means of assistance in determining the location of the tissue slice relative to the center axis of the lead, as the diameter of the electrode at the same point is known and can be compared to the measured width. Figure 32 shows an example of a section taken approximately at the center axis of a solid-electrode lead sample with all of the measurements as detailed in Figure 31. For further reference, Appendix C contains all histology images from the study.

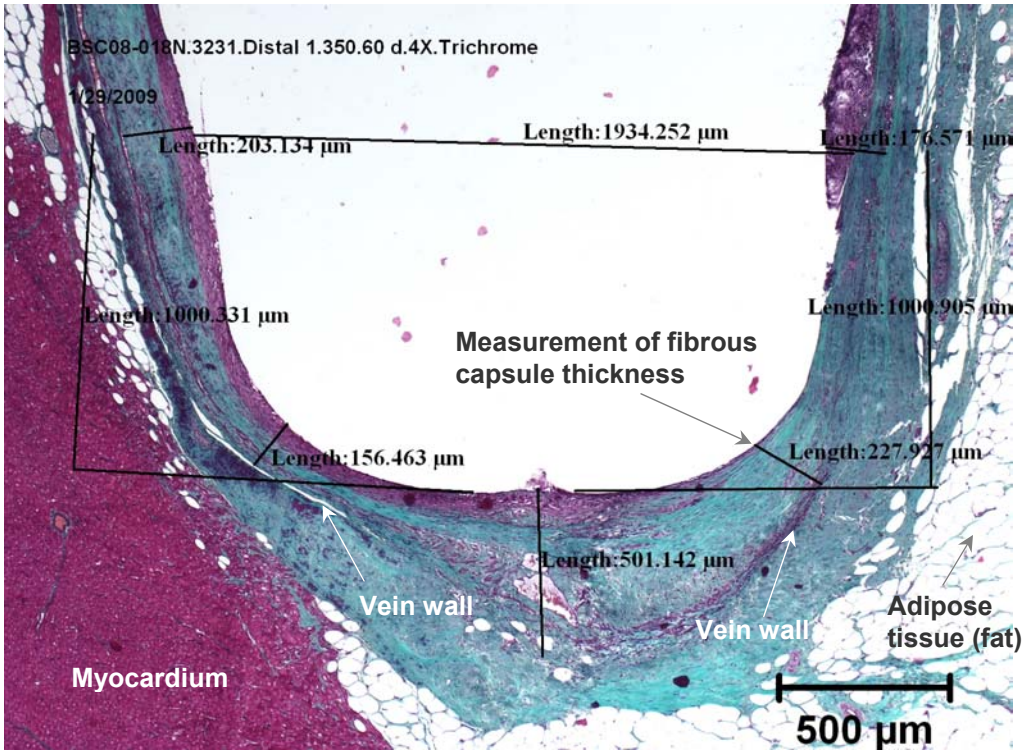

Figure 32: A histology slide of the implant site of a solid electrode (control) lead taken near the lead center axis, stained with Gomori's trichrome. The lead was implanted in animal L-3231. Measurements of the fibrous capsule thickness normal to the electrode surface, as detailed in Figure 31, can be seen above along with the measurement of lead track width 1 mm back from the distal end of the electrode.

Most tissue sections for this study were stained with Gomori's trichrome stain in order to make identification of the fibrous capsule easier. Collagenous tissue (such as mature fibrous encapsulation and the venous wall) is stained blue with Gomori's trichrome, while muscular tissue is stained red and cell nuclei are black in color. All measurements of fibrous capsule thickness were taken by the study pathologist (Bill Stoffregen, DVM, PhD), whose expertise was especially useful for identification of the demarcation between fibrous capsule and vein wall at each measurement point.

For porous electrode samples, though detachment of the lead removed in-grown tissue, there is still ample visual evidence of tissue in-growth on many of the histology

slides. Figure 33, Figure 34, Figure 35, and Figure 36 give example histology images showing tissue in-growth around microspheres that remained with the tissue section after being cut.

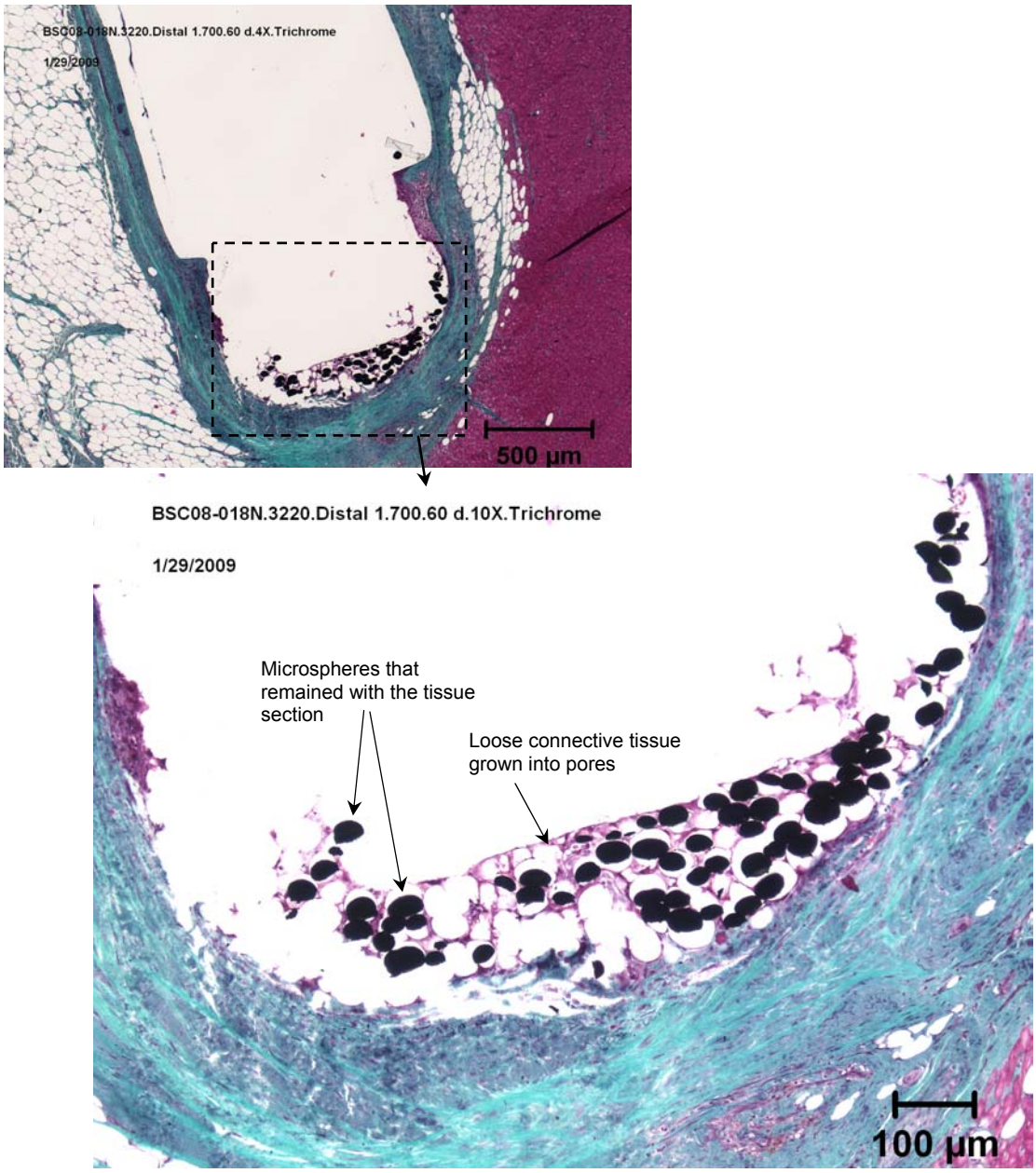

Figure 33: Section of implant site of a porous electrode lead sample (animal L-3220) taken approximately 700 µm off of the lead center axis, showing tissue in-growth into the porous electrode and surrounding microspheres that remained with the section after cutting. The tissue was stained with Gomori's trichrome; brighter blue areas are mature fibrous capsule, while dark purple areas are immature fibrous encapsulation made up of loose connective tissue, macrophages, fibroblasts, and other inflammatory cells.

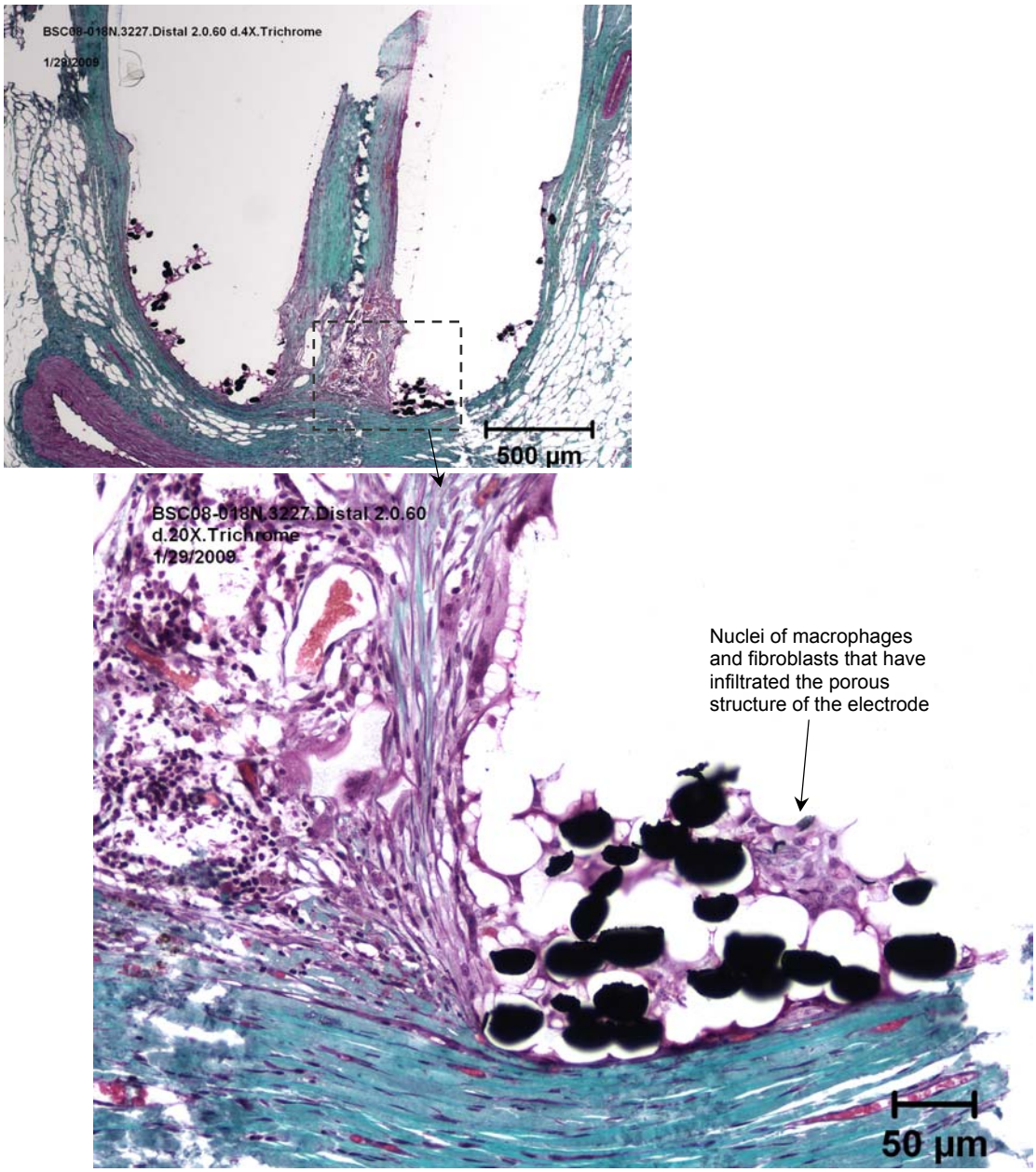

Figure 34: Section of implant site of a porous electrode lead sample (animal L-3227) taken near the lead center axis, showing tissue in-growth into the porous electrode and surrounding microspheres that remained with the section after cutting. The tissue was stained with Gomori's trichrome; brighter blue areas are mature fibrous capsule, while dark purple areas are immature fibrous encapsulation made up of loose connective tissue, macrophages, fibroblasts, and other inflammatory cells. Cells (mostly macrophages and fibroblasts) that infiltrated the porous network of the electrode are visible in the interstitial spaces of the microspheres.

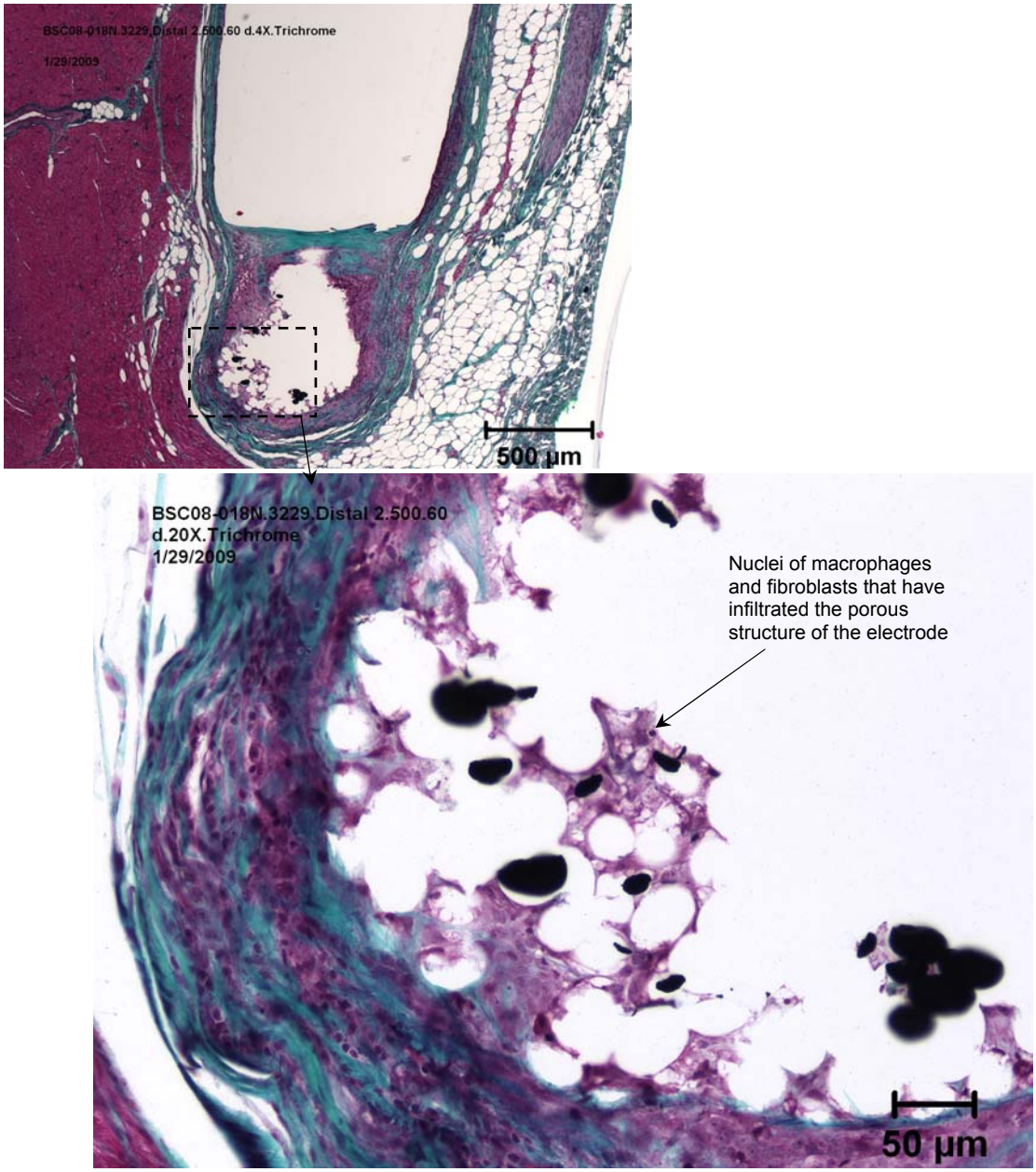

Figure 35: Section of implant site of a porous electrode lead sample (animal L-3229) taken approximately 500 µm off of the lead center axis, showing tissue in-growth into the porous electrode and surrounding microspheres that remained with the section after cutting. The tissue was stained with Gomori's trichrome; brighter blue areas are mature fibrous capsule, while dark purple areas are immature fibrous encapsulation made up of loose connective tissue, macrophages, fibroblasts, and other inflammatory cells. Cells (mostly macrophages and fibroblasts) that infiltrated the porous network of the electrode are visible in the interstitial spaces of the microspheres.

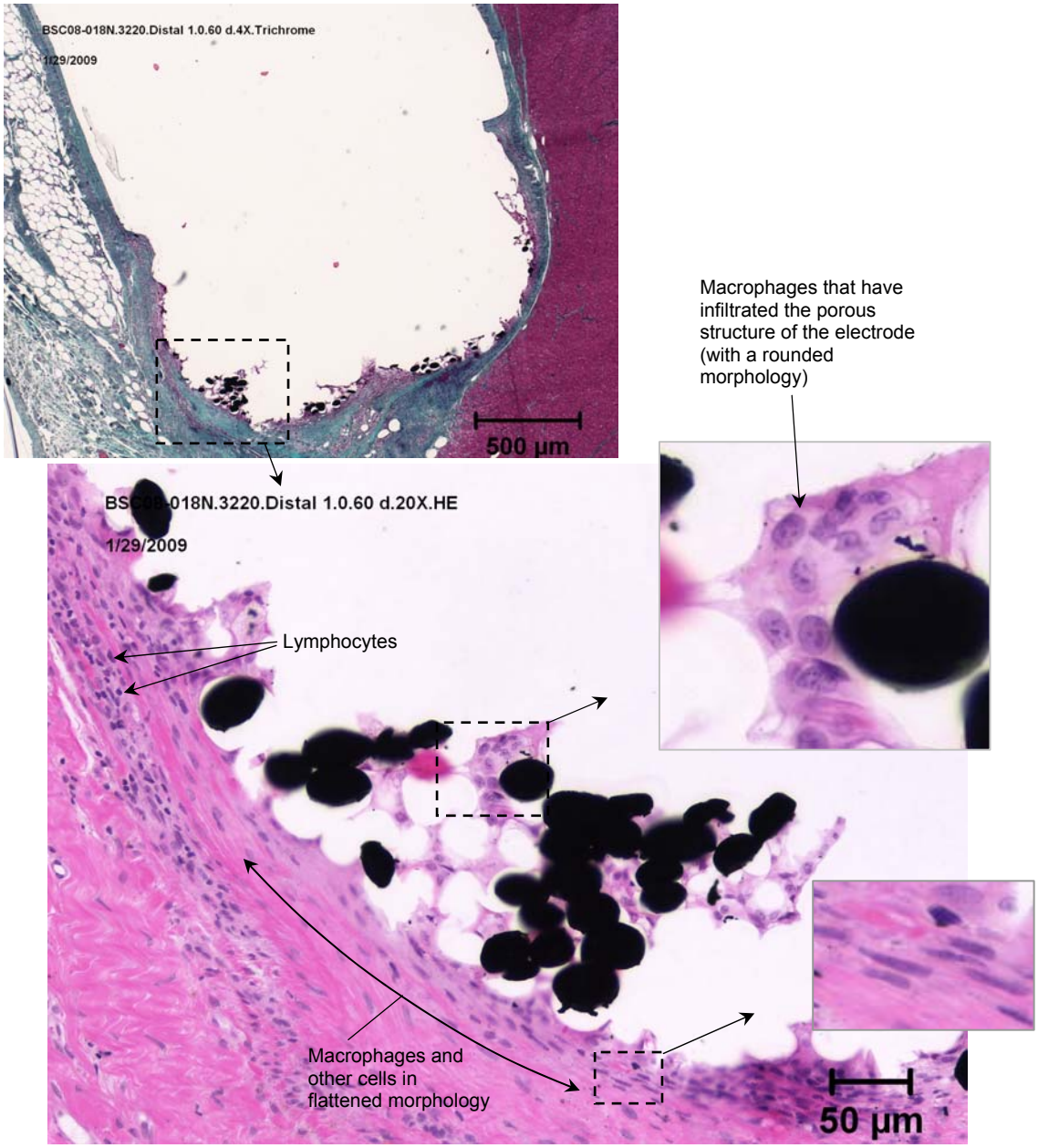

Figure 36: Section of implant site of a porous electrode lead sample (animal L-3220) taken near the lead center axis, showing tissue in-growth into the porous electrode and surrounding microspheres that remained with the section after cutting. Though this upper slide tissue was stained with Gomori's trichrome, the lower slide was stained with hemotoxylin and eosin, which allows better visualization of cell nuclei (seen as dark purple). Macrophages that infiltrated the porous network of the electrode are visible in the interstitial spaces of the microspheres and appear to be in a rounded morphology (potentially indicative of an M2 phenotype). Many macrophages and some other cells proximate to the surface of the electrode can be seen in a flattened morphology (potentially indicative of M1 phenotype, in the case of macrophages), as often seen in a classic foreign body response.

In regard to Figure 36, as noted in its caption, macrophages in a flattened morphology (such as near the surface of the electrode) and a rounded morphology (such as inside electrode pores) can be readily seen. A flattened morphology has been associated with the M1 phenotype of macrophages [47], which causes pro-inflammatory signaling and complement activation [45]. A rounded morphology has been associated with the M2 phenotypes of macrophages [47], which cause tissue growth and remodeling [45]. Activation of macrophages to a M2 phenotype, potentially caused by spatial confinement within appropriately-sized pores, has been hypothesized by Ratner [44] to be a contributing factor to the thinner fibrous capsules of porous implants (as discussed in Section 3). The visual evidence presented in Figure 36 for the potential occurrence of these differing macrophage phenotypes should not be taken as confirmation of such occurrences but simply as visual evidence. Immunohistochemical analysis such as that performed in [62] would be necessary to confirm the occurrence of the differing phenotypes. It is also not clear the role the collagenous matrix outside the electrode is playing in flattening the morphology of the cells, or whether the cells themselves are responsible for the morphological differences observed.

It is worthy of note that no evidence of endothelial cell growth into porous electrodes was found in any of the histology slides for this study. Endothelial cells line the lumenal surface of the vein wall and would come into close proximity of surface of the porous tip electrode once implanted, and it was unknown whether endothelial cells would penetrate into the electrode pores. This does not appear to have been the case. Additionally, no angiogenesis was observed within any of the porous areas that

remained with the histology slides, which require endothelial cells to form the vascular walls.

For this chronic animal study, the visual evidence of tissue growth into the porous electrode validates that the pore sizes created are within a range favorable to the body for cell infiltration and tissue formation. Further, this visual evidence provides a potential link to the lead stability data presented in Figure 30. Tissue growth into the porous electrodes is a logical explanation for the absence of any lead movement for all eight test group samples after day 3 of the study. The lead retractions prior to day 3 (three of the eight test group samples, the same number of retractions as the control group) may have occurred before the tissue in-growth process had advanced enough to secure the lead tip.

For the analysis of fibrous capsule thickness data, data from measurement points symmetrically opposite one another were pooled together, and mean and standard deviations were calculated and compared between lead groups. The thickness data taken near the lead centerline axis at the distal end of the electrode was disregarded due to fact that the central lumen in the electrode created widely varying tissue conditions depending on the tissue section being considered. For tissue sections near the centerline axis, the central lumen meant that there was actually no electrode material that created an interface with the tissue. Figure 37 summarizes how the data was pooled for analysis.

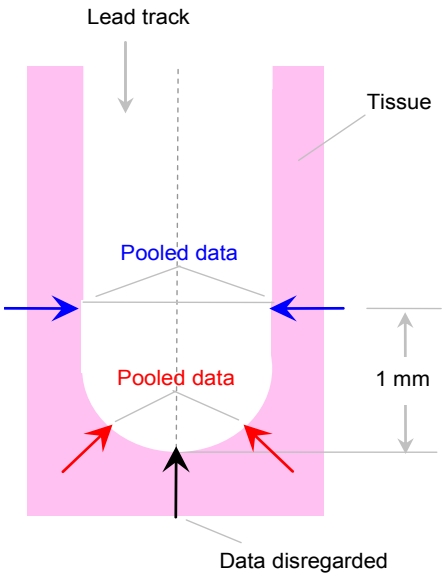

Figure 37: Summary of how data was pooled for analysis of fibrous capsule thickness. The large arrows denote pre-determined locations where fibrous capsule thickness was measured on each tissue section. Data from points symmetrically opposite one another was pooled together, while the data at the distal end of the electrode was disregarded due to the presence of the electrode's central lumen.

The pooled data from the locations depicted in Figure 37 were analyzed for tissue sections with lead track widths greater than 1500 μm. These tissue sections were deemed reasonably close to the center axis such that minimal distortion would be caused by the eccentricity of the slice. Additionally, there was some variation in the method by which the track width was measured across all of the samples (i.e. a very wide track width does not necessarily ensure that the slice was at the center axis of the lead due to some inconsistency in the points chosen for each measurement). Including all tissue sections with lead track widths greater than 1500 μm ensures the measurements taken near the lead centerline axis for both lead groups are included in the analysis within a +/- 250 μm tolerance range. Figure 38 gives a graphical

representation, to scale, of the tissue volume included in the fibrous capsule thickness analysis.

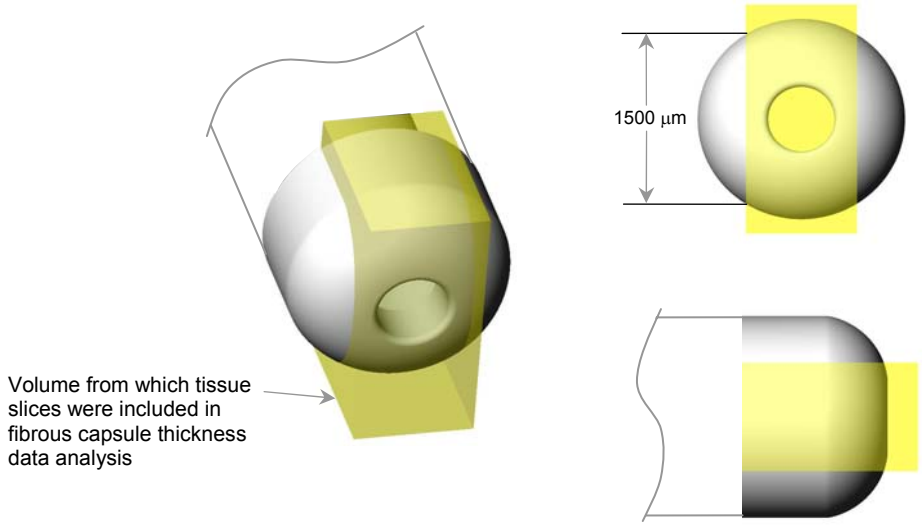

Figure 38: Graphical depiction (with CAD model of solid tip electrode, to scale) of the approximate volume from which tissue slices were included together for analysis of fibrous capsule thickness data. All histology slices with measured lea track widths greater than 1500 μm were included in the analysis.

A summary of the fibrous capsule thickness data is shown in Figure 39. For reference, the data utilized in the creation of Figure 39 is given in Appendix D.

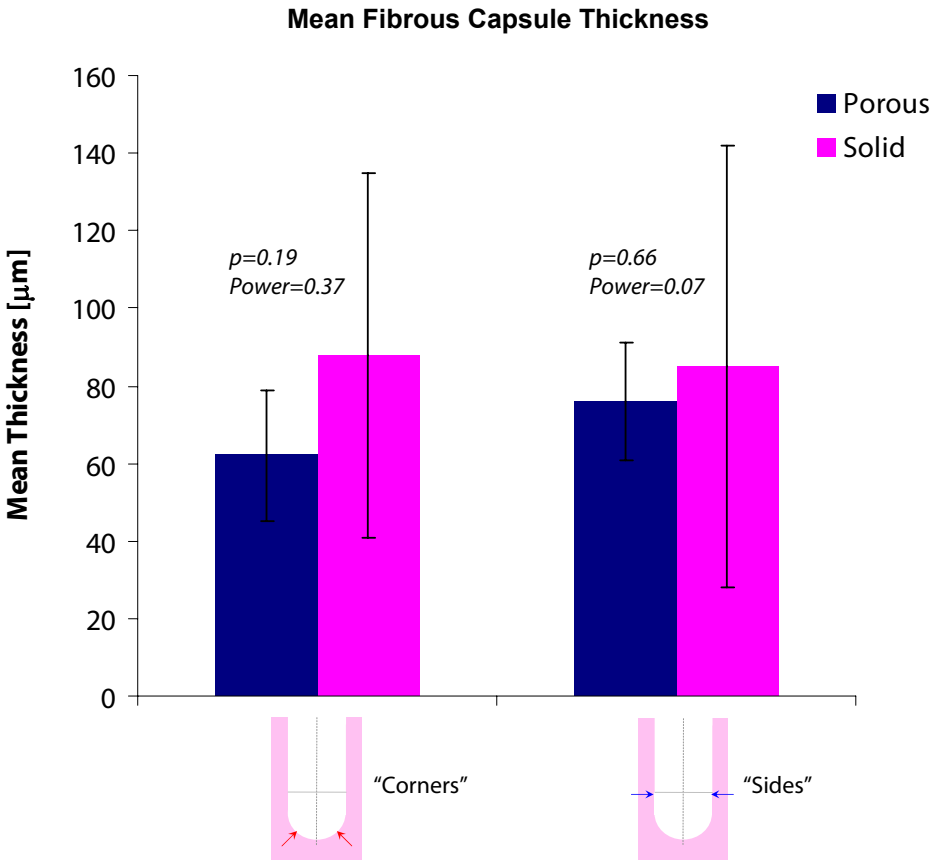

Figure 39: Mean fibrous capsule thickness at the electrode corners and sides, compared between porous and solid electrode leads (n=8 for each group). Error bars are +/- one standard deviation. Statistical comparisons were done using a t-test (normality test passed in each case) assuming unequal variances (two-tailed). For reference, the data utilized in the creation of this plot is given in Appendix D. Reported statistical power values of the performed t-test assume α=.05, a two-tailed test, and mean and standard deviation values as calculated in Appendix D for each group.

The mean fibrous capsule thickness may be lower at the electrode corners, but the power of the test is far below what would be necessary to detect differences if they exist, likely due to the low sample size and the large variability in the capsule thickness measured for the solid electrode samples. There appears to be no difference in fibrous capsule thickness at the electrode sides, but again the power of the test is very low (ideally, statistical power would be near 0.80). Further, since the pacing thresholds for

the porous and solid electrode groups (as shown in Figure 25) were essentially equal at the day 60 measurement (when the animals were euthanized), distinguishing between the thickness of the fibrous capsules for each electrode group should be more difficult than if the comparison were done at day 14 or day 21. At day 60, mature collagenous tissue has replaced acute inflammatory cells and the overall thickness of the capsule is less than it is at day 14 or day 21 (as shown schematically and discussed earlier in Figure 3). If a study was done strictly to evaluate any differences in capsule thickness during the peak of inflammation, animals could be euthanized at day 14 or day 21 and there would likely be significant differences in capsule thickness. Such differences could also be correlated to the pacing threshold differences observed at these time points.

F-tests for differences in variance were performed to confirm what seem to be differences in the variances of measured fibrous capsule thickness between the study groups. For data at the electrode corners, $p=0.007$ between groups for the F-test, and for data at the electrode sides, $p=0.001$. Both of these differences are highly significant, though the reason for the difference is not clear. One hypothesis is that the more frequent lead retractions that were observed in the solid electrode group caused more variable fibrous capsule thicknesses at day 60, since all eight of the solid electrode leads retracted at least once from their initial implant position (as shown in Figure 30).

The essentially equivalent fibrous capsule thicknesses at the electrode sides between groups is interesting for the fact that, for porous electrodes, the porosity at the electrode sides was consistently much less (if not non-existent) as compared to the electrode corners. As an example, SEM images of the proximal edge of the exposed

electrode surface of a porous electrode sample are re-presented in Figure 40. Since dip-coating is used to affix the microspheres prior to sintering, the surface tension of the binder causes a much lower volume of microspheres in this location. This is consistent across all electrode samples that were implanted in the chronic animal study (reference Appendix C for lead tip pictures).

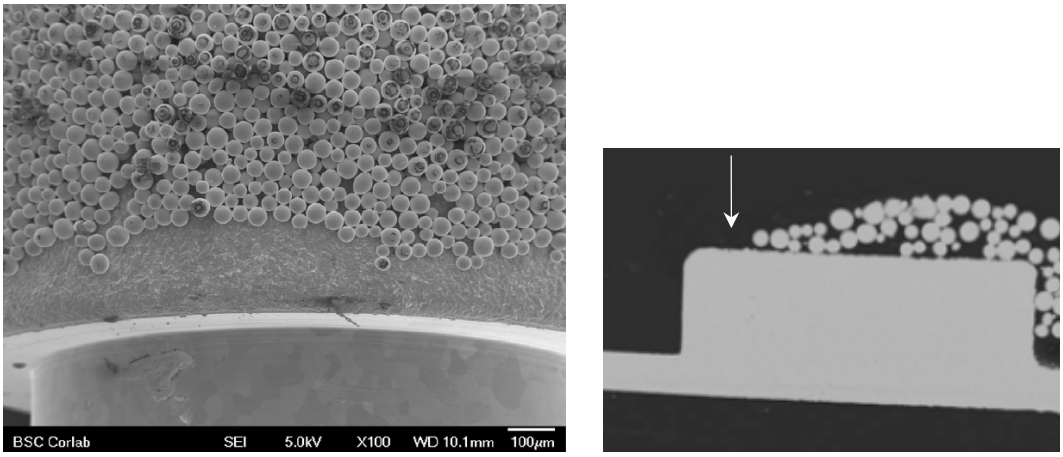

Proximal edge of porous electrode sample

Cross-section detail of proximal edge

Figure 40: SEM images of the proximal edge of a porous electrode sample showing how the porosity trails off in this area. Reference Figure 14 and Figure 16 for original images.

Porosity trailing off near the proximal edge effectively gives a non-porous area at the same location as the fibrous capsule thickness data for the electrode sides. So each porous electrode offers a chance for comparison of the capsular thickness at porous and non-porous sites for the same implant location.

For porous electrodes, a better evaluation of any differences in fibrous capsule thickness at the electrode sides and corners is to look for correlation between capsule thickness measurements across all tissue slices taken (no matter the location relative to the lead centerline axis). In such an evaluation, the actual fibrous capsule thickness

values are not necessarily important. What is of interest is whether capsule thickness at the electrode sides and corners correlate well across all tissue slices. These data are plotted in Figure 41 for both the porous electrode group and the solid electrode group. Linear regression was also performed on the data to evaluate the significance of any correlation.

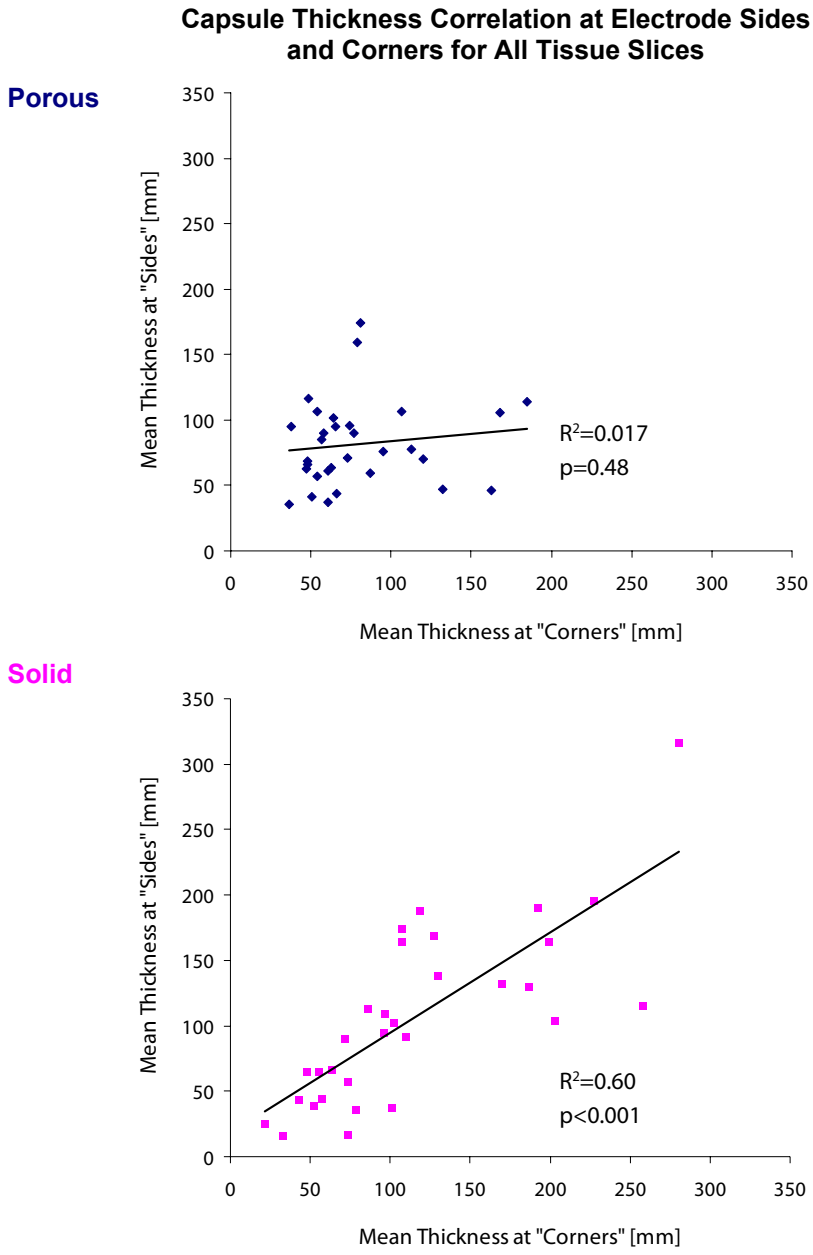

Figure 41: The plots above show that there is no correlation between fibrous capsule thickness at the electrode sides and corners for porous electrode samples, while there is good correlation for the same comparison for solid electrode samples, with high statistical significance. Linear regression was performed to obtain the correlation coefficient (R^2) and p-value for each plot.

A number of observations can be made in regard to Figure 41. The first is that there is no correlation between fibrous capsule thickness at the corners and sides of the porous electrode samples across all tissue sections taken. Additionally, there is very

good correlation for the same comparison for the solid electrode samples, with high statistical significance. This may provide further evidence that the electrode porosity causes a thinner fibrous capsule, and provides evidence that this effect is local in nature.

Due to the somewhat bulbous geometry of the porous electrodes, one cannot consider the data presented in Figure 41 as being conclusive. The relatively smaller diameter of the electrode in the area of the proximal edge compared to other areas of the electrode may have influenced the fibrous capsule thickness. Still, one can compare the two plots in Figure 41 and note the smaller spread of the data for the porous electrode samples, showing a smaller spread of fibrous capsule thicknesses for porous electrode samples. This also correlates well to a conclusion that the porous areas are influencing the local biological response and attenuating growth of fibrous encapsulation, though the effect may have been relatively stronger earlier on in the study.

5.5 Study Limitations

There are limitations to this study which should be taken into account in order to give context to the results. One such limitation is the low sample sizes in each study group, a necessity due to the complexity and expense of a chronic animal study of this nature. The low sample sizes mean that many of the analyses presented in Section 5 were low in statistical power to detect differences (though this does not invalidate any statistically significant differences that were found). In some analyses, such as the pacing threshold data, differences between groups may have had higher statistical significance if there were larger sample sizes. Another limitation of the study is inferring applicability of the results to humans. Canine coronary venous anatomy differs from human coronary venous anatomy in a number of ways, such as vein size

and tortuosity, and thus performance of the electrode and lead samples evaluated in this study cannot necessarily be generalized to humans. Aspects of the implant procedure also must be taken into account when considering the study results, such as the placement of leads as far distal as was possible in the selected branch vein (which is not always the case in normal human implants). Intentional placement of the lead tip more proximal in the selected branch vein may give differing results than those presented in this work. Finally, the Boston Scientific ACUITY^{TM} Steerable lead and its distal tip electrode design were utilized in this study, and as such it must be acknowledged that study results could be different with a different test sample or electrode design.

6 Conclusion

As a concluding discussion, a return to the research questions outlined in Section 4.4.2 is useful.

Research Question 1

After 60-day chronic implant, are there significant differences notable in biological response for the porous electrode as compared to the solid (control) electrode?

For this research question, "biological response" was thought to consist of a number of different measures, including fibrous capsule thickness and cellular response at the implant surface. There were no statistically significant differences in fibrous capsule thickness between the porous electrode and solid electrode groups, though the power to detect a meaningful difference was very low. Additionally, leads and surrounding tissue were excised at day 60 of the study when pacing thresholds between groups were similar and acute inflammation had subsided. It should also be noted that macrophages were observed to have infiltrated pores of porous electrodes in histology slides for this study, and some of the infiltrated macrophages appeared to have taken a "rounded" morphology that may be indicative of an M2 macrophage phenotype beneficial to tissue growth and remodeling [45,47].

The comparison of mean pacing impedance between the porous and solid electrode groups at each time point proved interesting, as mean pacing impedance of the porous electrode group was at least equal to that of the solid electrode group at each time point (possibly even higher by day 60, $p=0.06$) despite the much larger surface area of the porous electrodes. High pacing impedance is clinically desirable in most cases since battery life of the pacemaker can be preserved and the pacemaker can

remain in operation for a longer period of time before needing to be replaced. A possible explanation for this lack of difference in pacing impedance may be a smaller chronic inflammatory response at the surface of porous electrodes (meaning fewer cells to conduct current through cell membranes).

Research Question 2

Are there significant differences notable in electrical performance (voltage thresholds, impedance, sensed R-wave amplitude) between leads with the porous electrode as compared to leads with the solid (control) electrode?

Having just discussed pacing impedance, the remaining electrical performance data are pacing threshold and sensed R-wave amplitude. Mean pacing threshold rise from implant data were shown to be statistically different between the groups at two time points in the study (day 3 and day 21), both during the acute inflammatory stage where distance to excitable myocardial tissue is greatest. The porous electrode group had a lower mean rise in pacing threshold from implant at these time points, which was not expected given the uncontrolled anatomical factors contributing to high pacing thresholds in coronary veins and also the small sample sizes for the study groups. A lower rise in pacing threshold can also favorably impact battery life of the pacemaker since a physician typically sets the pacing voltage at implant to include a safety factor to account for threshold rise in approximately the first 30 days after implant. The ability to use a smaller safety factor with a porous electrode (and thus a lower pacing voltage) would conserve battery charge and extend pacemaker life. However, steroid-eluting collars are typically included near pacing electrodes on coronary venous pacing leads in order to attenuate acute inflammation, and no steroid collars were included on the leads in this study. It is not known whether the affect of a porous electrode would be additive

in regard to that of a steroid collar.

There were no differences noted in regard to sensed R-wave amplitude between the groups in the study, which was encouraging as it helps to validate that the lead implant environments were very similar across the groups. No differences in sensed R-wave amplitudes were expected between the groups, despite the differing tip electrode designs.

Research Question 3

Are there significant differences notable in stability of leads with the porous electrode as compared to leads with the solid (control) electrode?

While lead stability data (number of lead retractions) does not lend well to statistical tests for differences, the solid electrode group may have had more lead retractions than the porous electrode group, especially after day 3 when tissue in-growth would have begun within the porous electrodes. No porous electrode lead samples retracted after day 3 of the study, while three solid electrode leads retracted at least 1 cm after day 3 and three others were noted to have retracted 0.5 cm (a value within the error of the measurement method). For both groups, three of eight leads retracted between implant and day 3. Further study is required in order to verify any affect of tissue in-growth on lead stabilization. Tissue growth into the porous electrodes could serve to anchor the lead in place, mitigating chronic lead retractions (which are a significant problem for patients, causing repeated surgeries and safety issues).

7 Recommendations for Future Work

There are a number of investigations that would be highly useful continuations of this work. First among them is to perform a confirmatory animal study of the same nature as the one reported here, except to also include a lead group where steroid-eluting collars are included on the leads with porous electrodes. This would provide a useful comparison to a lead group with porous electrodes but no steroid collars. Such an investigation would answer the question of whether a porous electrode can provide biocompatibility and/or electrical benefits in addition to those provided by elution of steroid within the tissue. Could it be possible to nearly eliminate the characteristic rise in pacing thresholds after implant with the use of these two technologies in concert?

A second investigation that should be performed is a study of the effects of extraction of coronary venous leads with a porous electrode. The ability to extract an implanted pacing lead is a requirement for physicians, as leads can at times become infected and their removal is necessary for the safety of the patient. If tissue growth into a porous electrode is such that the lead cannot be safely or easily removed from the patient when necessary, this would compromise any benefits to pacing thresholds, impedance, or biocompatibility. Ideally, tissue in-growth would be enough to stabilize the lead chronically within the vein and prevent retractions, but would not prevent easy removal of the lead if necessary. A useful study could be done similar to that which was done in this work, but instead of immediately excising the heart for histology at the end of the study (at necropsy) the lead could be extracted and the tensile force measured and recorded (manually, or more ideally with an automated test set-up that would record

a complete plot of force over the time period of the lead extraction). After this procedure, the heart could be excised and histology done to examine the area where the lead tip was implanted to evaluate any damage to the vein wall or other tissues resulting from the extraction.

Other useful investigations would include doing *in vitro* studies of macrophage phenotypic response when seeded on porous structures in order to shed more light on the contributions of macrophages to more favorable biocompatibility. The occurrence of M1 or a M2 macrophage phenotype as a function of the average pore size of porous structures could be efficiently tested *in vitro*, with perhaps deeper understanding to be gained by isolating macrophage response from the *in vivo* environment. Another useful investigation would be to evaluate differing porous electrode geometries (possibly examining the thickness of the porosity required on the electrode to facilitate tissue in-growth and other favorable responses), and also replicating the work of Marshall and Ratner [41-43] in creation of an electrode with consistently-sized spherical pores (most usefully with a diameter of roughly 35 μm). There is the potential that the results of this work could be improved-upon with an electrode more optimally-designed for favorable biological response, as Marshall reported in regard to sphere-templated polymeric porous structures with 35 μm pore diameters [42,43]. Creation of a metallic "sphere-templated" structure would pose its own challenges as the method of accomplishing this would need to be developed.

Finally, it would also be useful to evaluate the electrical performance of porous electrodes with a so-called "capacitive coating" *in vitro* and *in vivo* (in coronary veins). The electrodes evaluated in this work were uncoated platinum iridium. Pacing lead

electrodes are often coated with a capacitive coating such as iridium oxide or titanium nitride in order to prevent dissolution of the electrode due to electrochemical reactions *in vivo*, and also to reduce polarization at the electrode surface. Application of a voltage at the pacing lead electrode causes ion layers to form (in alternating sequence of polarities) at the electrode surface, and these layers of charge must dissipate before the pacemaker can utilize the lead electrode to sense cardiac activity [21]. Formation of charge layers can also affect pacing thresholds, as higher voltages are necessary at the lead electrode in order to overcome attenuation of the electric field strength in the tissue due to the charging of these ion layers. Formation of charge layers at the electrode surface can be mitigated by increasing the electrically active surface area of the electrode, such as by increasing the surface roughness or by application of a coating with a variably surface morphology, without increasing the geometric size of the electrode [21]. Maintaining the same geometric size allows the same voltage to be applied at the electrode in order to depolarize the myocardium, while increasing the electrically active surface area decreases the density of the formed charge layers (similar to increasing the size of the parallel plates of a capacitor) and in this way decreases the attenuation of the applied electric field by these charge layers. The name "capacitive coating" comes from the fact that the capacitance of the electrode surface is increased due to the coating.

A porous electrode has a natural advantage in regard to electrode capacitance in that the porosity serves to increase the electrically active surface area of the electrode without increasing the geometric size, much in the same way as a capacitive coating. In Section 4.3 it was shown that the porous tip electrode had an approximately 720%

greater electrically active surface area as compared to the solid tip electrode. Adding a capacitive coating on top of a porous electrode would magnify the electrical surface area even further, achieving an electrical surface area that could not be achieved by a solid electrode with a capacitive coating. Figure 42 shows an example of a porous tip electrode (created in this work) with an applied capacitive coating of iridium oxide. The capacitive coating was formed on the surface of the porous electrode by sputtering of iridium in an oxygen glow discharge plasma using a magnetron sputtering system.

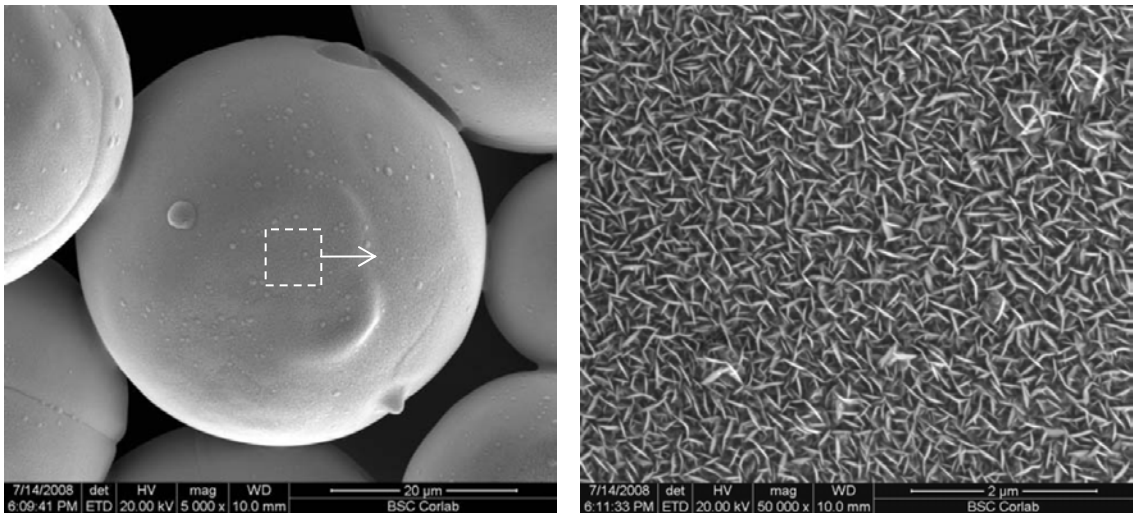

Figure 42: SEM images of sputtered iridium oxide coating the surface of a porous electrode (the same design as that investigated in the chronic animal study in this work). The iridium oxide coating increases the capacitance of the electrode surface by significantly increasing the electrically active surface area.

As can be seen, the morphology of the coating multiplies the electrically active surface area of the electrode many times over. Investigations of porous electrodes with capacitive coatings would be useful in determining if porous electrodes can have additional *in vivo* electrical performance benefits beyond those reported in this work.

Bibliography

1. Grill WM, Mortimer JT. Electrical properties of implant encapsulation tissue. *Annals of Biomedical Engineering*. 1994;22:23-33.

2. Hunt J. Foreign body response. In: *Enclyclopedia of Biomaterials and Biomedical Engineering.* 1:1 ed. Marcel Dekker, Inc.; 2004:641-648.

3. Anderson JM. Inflammation, wound healing, and the foreign body response. In: Ratner BD, Hoffman AS, Schoen FJ, Lemons JE, eds. *Biomaterials Science.* San Diego, CA: Elsevier Academic Press; 2004:296-318.

4. Pawlowski K. Host reactions. In: *Encylopedia of Biomaterials and Biomedical Engineering.* 1:1 ed. Marcel Dekker, Inc.; 2004:770-778.

5. Ratner BD, Bryant SJ. Biomaterials: Where we have been and where we are going. *Annu Rev Biomed Eng*. 2004;6:41-75.

6. Boston Scientific. Pacemaker Implantation. Available at: http://www.bostonscientific.com/procedure/ProcedureLanding.bsci/,,/navRelId/1000.1002/method/Procedure/id/10001001/seo.serve. Accessed 2/28, 2009.

7. Bobyn JD, Wilson GJ, Mycyk TR, et al. Comparison of a porous-surfaced with a totally porous ventricular endocardial pacing electrode. *Pace-Pacing and Clinical Electrophysiology*. 1981;4:405-416.

8. Amundson DC, Mcarthur W, Mosharrafa M. Porous endocardial electrode. *Pace-Pacing and Clinical Electrophysiology*. 1979;2:40-50.

9. Macgregor DC, Wilson GJ, Lixfeld W, et al. Porous-surfaced electrode - new concept in pacemaker lead design. *J Thorac Cardiovasc Surg*. 1979;78:281-291.

10. Guarda F, Galloni M, Assone F, Pasteris V, Luboz MP. Histological reactions of

porous tip endocardial electrodes implanted in sheep. *Int J Artif Organ*s. 1982;5:267-273.

11. Maccarter DJ, Lundberg KM, Corstjens JPM. Porous-electrodes - concept, technology and results. *Pace-Pacing and Clinical Electrophysiolog*y. 1983;6:427-435.
12. Beard BB, DeRosa JF, Dubin SF, Sturm L, Koerner RM. Materials characterization of implantable porous electrodes. *National Bureau of Standards.* 1974;415:55-61.
13. Hirshorn MS, Holley LK, Money DK, Spector M, Young FA, Hales JRS. Histological-evaluation of porous titanium cardiac-pacemaker electrode tips. *J Biomed Mater Re*s. 1984;18:47-60.
14. Campbell CE, von Recum AF. Microtopography and soft tissue response. *J Investig Surg*. 1989:51-74.
15. Amundson DC, Mcarthur W, Maccarter DJ, Mosharrafa M. Porous electrode-tissue interface. *Proceedings of the 6th World Symposium on Cardiac Pacing*. 1979:Chap. 29 - 16.
16. Hirshorn MS, Holley LK, Hales JRS, et al. Screening of solid and porous materials for pacemaker electrodes. *Pace-Pacing and Clinical Electrophysiolog*y. 1981;4:380-390.
17. Hayes DL, Lloyd MA, Friedman PA. *Cardiac Pacing and Defibrillation: A Clinical Approach.* Armonk, NY: Futura Pub. Co.; 2000.
18. Alberts B. The cytoskeleton. In: *Molecular Biology of the Cell.* 2nd ed. Courier Corporation; 1989:613-680.
19. Frazier DW, Krassowska W, Chen PS, et al. Extracellular field required for

excitation in three-dimensional anisotropic canine myocardium. *Circ Re*s. 1988;63:147-164.

20. Ranjan R, Thakor NV. Electrical stimulation of cardiac myocytes. *Ann Biomed En*g. 1995;23:812-821.
21. Ellenbogen KA, Wood MA. *Cardiac Pacing and ICDs.* Third Edition ed. Malden, MA: Blackwell Science; 2002.
22. Tung L, Borderies JR. Analysis of electric field stimulation of single cardiac muscle cells. *Biophys J*. 1992;63:371-386.
23. Radovsky JF, Van Fleet JF, Stokes KB, Tacker J, W.A. Paired comparisons of steroid-eluting and nonsteroid endocardial pacemaker leads in dogs: Electrical performance and morphologic alterations. *PACE*. 1988;11:1085-1094.
24. Mond HG, Stokes KB. The electrode-tissue interface: The revolutionary role of steroid elution. *PACE*. 1992;15:95-107.
25. Visible Heart Lab, University of Minnesota. Atlas of Human Cardiac Anatomy: Cardiac Veins. Available at: http://www.vhlab.umn.edu.floyd.lib.umn.edu/atlas/cv/cv.shtml. Accessed 2008.
26. Loukas M, Bilinsky S, Bilinsky E, El-Sedfy A, Anderson RH. Cardiac veins: A review of the literature. *Clinical Anatom*y. 2009;22:129-145.
27. Guidant Corporation (now part of Boston Scientific). CONTAK RENEWAL 3 Family: Cardiac Resynchronization Therapy Defibrillators. Available at: http://www.guidant.com/products/ProductTemplates/CRM/CONTAK_RENEWAL_3_US_INTRO.shtml. Accessed 2006.
28. Guidant Corporation (now part of Boston Scientific). EASYTRAK 2: Coronary

Venous Lead. Available at: http://www.guidant.com/products/ProductTemplates/CRM/easytrak2.shtml. Accessed 2006.

29. Medtronic I. Attain® Bipolar OTW Lead – Model 4194. Available at: http://www.medtronic.com/physician/hf/4194_lead.html. Accessed 2005.
30. Guidant Corporation (now part of Boston Scientific). Internal photo. © 2002.
31. Boston Scientific. Cardiac Rhythm Management. Available at: http://www.bostonscientific.com/AboutUs/BusinessGroups.bsci/,,/navRelId/1004.1011/method/BUSINESS_GROUPS_DETAIL/id/10065801/seo.serve. Accessed 5/6, 2009.
32. Medtronic I. Summary of safety and effectiveness: Medtronic® InSync® model 8040 pulse generator, attain™ LV model 2187, and attain™ CS model 2188 leads. *U.S. F.D.A. Original Pre-Market Approval P010015.* 2001. Available from: http://www.fda.gov/cdrh/pdf/P010015b.pdf. 2001.
33. Guidant Corporation (now part of Boston Scientific). Summary of safety and effectiveness: CONTAK CD® CRT-D system and EASYTRAK® coronary venous Pace/Sense lead, models 4510, 4511, 4512, 4513. *U.S. F.D.A. Original Pre-Market Approval P010012.* 2002. Available from: http://www.fda.gov/cdrh/pdf/P010012b.pdf. 2002.
34. Guidant Corporation (now part of Boston Scientific). Summary of safety and effectiveness data: SWEET TIP RX® endocardial steroid eluting pacing leads. *U.S. F.D.A. Original Pre-Market Approval P960006.* 2006. Available from: http://www.fda.gov/cdrh/pdf/P960006b.pdf. 2006.

35. Alonso C, Leclercq C, d'Allonnes FR, et al. Six year experience of transvenous left ventricular lead implantation for permanent biventricular pacing in patients with advanced heart failure: Technical aspects. *Heart*. 2001;86:405-410.

36. Zhang Z, Wang ZX, Liu SQ, Kodama M. Pore size, tissue ingrowth, and endothelialization of small-diameter microporous polyurethane vascular prostheses. *Biomaterials*. 2004;25:177-187.

37. Park H, Radisic M, Lim JO, Chang BH, Vunjak-Novakovic G. A novel composite scaffold for cardiac tissue engineering. *In Vitro Cellular & Developmental Biology-Animal*. 2005;41:188-196.

38. Jansen JA, von Recum AF. Textured and porous materials. In: Ratner BD, Hoffman AS, Schoen FJ, Lemons JE, eds. *Biomaterials Science: An Introduction to Materials in Medicine.* 2nd ed. Academic Press; 2004:218-224.

39. Sannino A, Netti PA, Madaghiele M, et al. Synthesis and characterization of macroporous poly(ethylene glycol)-based hydrogels for tissue engineering application. *J Biomed Mater Res*. 2006;79A:229-236.

40. Lowell S, Sheilds JE, Thomas MA, Thommes M. *Characterization of Porous Solids and Powders: Surface Area, Pore Size, and Density.* 4th ed. Springer; 2004.

41. Marshall A, Ratner BD. Sphere templated porous hydrogels for tissue engineering. *Trans Am Chem Soc Symp Polym Med Biol.* 2002.

42. Marshall A, Barker T, Sage EH, Hauch KD, Ratner BD. Pore size controls angiogenesis in subcutaneously implanted porous matrices. *Proceedings of the 7th World Biomaterials Congress*. Sydney, Australia. 2004.

43. Marshall AJ, Irvin CA, Barker T, Sage EH, Hauch KD, Ratner BD. Biomaterials

with tightly controlled pore size that promote vascular in-growth. *Abstracts of Papers of the American Chemical Society*. 2004;228:U386-U386.

44. Ratner BD. The engineering of heart. 2008;Presentation given to Boston Scientific CRM.
45. Mantovani A. Macrophage diversity and polarization: In vivo veritas. *Blood*. 2006;108:408-409.
46. Mantovani A, Sica A, Locati M. New vistas on macrophage differentiation and activation. *Eur J Immunol*. 2007;37:14-16.
47. Padera RF, Colton CK. Time course of membrane microarchitecture-driven neovascularization. *Biomaterials*. 1996;17:277-284.
48. Boudreau NJ, Jones PL. Extracellular matrix and integrin signaling: The shape of things to come. *Biochem J*. 1999;339:481-488.
49. Sieminski AL, Gooch KJ. Biomaterial-microvasculature interactions. *Biomaterials*. 2000;21:2233-2241.
50. Rosengren A, Danielsen N, Bjursten LM. Reactive capsule formation around soft-tissue implants is related to cell necrosis. *J Biomed Mater Res*. 1999;46:458-464.
51. Boston Scientific. Internal photo. © 2006.
52. Marshall AJ, Ratner BD. Quantitative characterization of sphere-templated porous biomaterials. *AICHE J*. 2005;51:1221-1232.
53. Woods R. *Electroanalytical Chemistry.* Vol 9. New York, NY: Marcel Dekker, Inc.; 1976.
54. Johnson Matthey. Platinum - 10.00% Iridium. Available at: http://www.platinummetalsreview.com/jmpgm/data/datasheet.do?record=1064.

Accessed 2009.

55. Davies EJ. *Conduction and Induction Heating.* London, U.K.: P. Peregrinus Ltd. on behalf of the Institution of Electrical Engineers; 1990.
56. Johnson Matthey. Pt. - Ir. Wt. loss in oxygen. Available at: http://www.platinummetalsreview.com/jmpgm/data/datasheet.do?record=122. Accessed 2009.
57. Bharadwaj SR, Tripathi SN, Chandrasekharaiah MS. The ir-pt (iridium-platinum) system. *Journal of Phase Equilibria*. 1995;16:460-464.
58. Jiang X. Summary of real surface area measurements for platinum shocking coil of RELIANCE leads (unpublished, Boston Scientific CRM internal). 2006.
59. USDA. Considerations of alternatives to painful/distressful procedures: Policy 12. In: *Animal Care Resource Guide.* 2000.
60. National Institutes of Health. Guide for the care and use of laboratory animals. *NIH Publication no. 86-23 1985.* Bethesda, Md.: National Institutes of Health; 1985.
61. American Veterinary Medical Association. 2000 report of the AVMA on euthanasia. *JAVMA*. 2001;218:669-696.
62. Ohri CM, Shikotra A, Green RH, Waller DA, Bradding P. Macrophages within NSCLC tumor islets are predominantly a cytotoxic M1 phenotype associated with extended survival. *Eur Respir J*. 2009;33:118-126.
63. Springer M. Testing report: Cyclic voltammetry for determination of real surface area increase of non-coated porous electrodes (unpublished, Boston Scientific CRM internal). 2008.

Appendix A: Cyclic Voltammetry Test Set-Up

The following description is modified slightly from that in [63]. The testing chamber was made from a 500 mL jar from I-CHEM Brand Products (Prod# 017788). Two 11/16 inch holes were bored opposite of each other on the top of the jar to act as "in" and "out" ports for nitrogen gas flow. Nitrogen gas was fed into a Cole/Parmer flow regulator (serial num 201782), which was fed through a rubber stopper that fit snugly into one of the 11/16 inch holes, and terminated in a ASTM 25-50 micron filter inside of the jar. The filter dispersed the nitrogen into the 0.5 mol/L sulfuric acid working fluid (J.T. Baker 5642-03). The "out" gas flow was fed out through a rubber stopper in the other 11/16 inch hole and into a 250 mL container of de-ionized water to visually show the nitrogen flow in the system.

Two more small holes were drilled in the top of the 500 mL jar 90 degrees from the gas ports for the working electrode and the counter electrode. The counter electrode was a modified shocking coil from a Boston Scientific RELIANCE^{TM} defibrillation lead, with the coil passed through a lead suture sleeve fitted into the hole in the jar. The working electrode was the electrode sample being tested, which was welded to a thin wire electrical connection that was passed through a small rubber stopper at the top of the jar. A MF-2052 silver-silver reference electrode was also placed in the solution through a stopper in the top of the jar. The CV testing was performed using Solartron SI 1287 electrochemical interface potentiostat, coupled with Corrware software on a PC. See Figure 43 for a schematic of the test set-up.

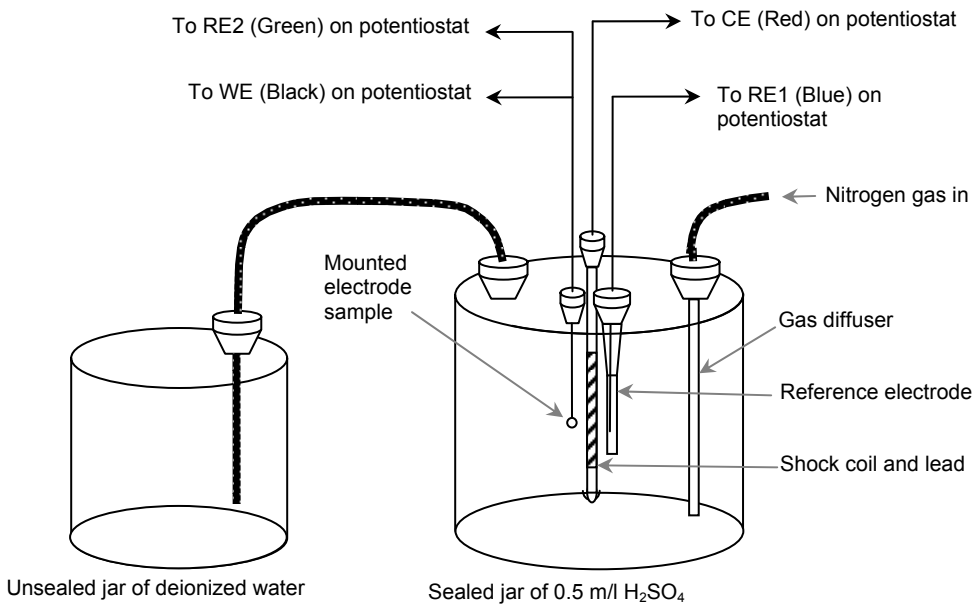

Figure 43: Schematic of cyclic voltammetry test set-up for measurement of electrode surface area [63].

Cyclic voltammetry sweeps were done as follows:

- Initial cleansing scan from -0.2000 V to 1.3800 V at a scan rate of 200 mV/sec for 100 cycles
- Final data collecting scan from -0.2000 V to 1.3800 V at a scan rate of 50 mV/sec for 10 cycles.

Integration of the hydrogen ion monolayer adsorption region, which corresponds to an approximate voltage range of -0.25 - 0.1 V in sulfuric acid on the forward sweep, was done from the current vs. voltage plot for each sweep to obtain the total charge transferred. The total charge was divided by 210 $\mu C/cm^2$, which is the amount of charge transferred during adsorption of hydrogen ions on a platinum surface [53], to obtain the surface area of the electrode sample.

Appendix B: Literature Search for Chronic Animal Study

In compliance with USDA Policy #12 [59], a literature search was performed to verify that the research described in Section 4.4 is not redundant and that animal testing is appropriate. Using predetermined keywords and wildcard variations, the titles, abstracts and major descriptor fields of three online databases (MEDLINE, EMBASE, and Biosis Previews) were searched by a Boston Scientific CRM technical librarian on March 17, 2008. The search terms and wildcards used are given below.

[File 155] **MEDLINE(R)** 1950-2008/Mar 17
[File 73] **EMBASE** 1974-2008/Mar 14
[File 5] **Biosis Previews(R)** 1926-2008/Mar W2

Set	Items	Description
S1	163926	POROSITY OR PORE? ? OR POROUS
S2	647702	LEFT(N1)(VENTRIC? OR HEART OR CARDIAC OR CHEST) OR LV OR CORONARY()(SINUS? OR VEIN? OR VESSEL? OR VENOUS? OR VASCUL?) OR CS
S3	1260029	LEAD OR LEADS OR ELECTRODE? ?
S4	269916	HEART()FAILURE OR CRT OR RESYNCYHRON? OR CRT OR CRTP OR CRTD OR RE()SYNCHRON? OR BIV OR BI()VENTRIC?
S5	174283	PACING OR PACER? ? OR PACE()(MAKE? OR MAKING?) OR PACEMAK? OR DEFIBRIL? OR (HEART OR CARDIAC)(N2)STIMULAT? OR PULSE()GENERATOR? ?
S6	**1**	**S1 AND (S2 OR S4)(N4)S3 AND S5 [not relevant]**
S7	1006605	PERMEABIL? OR ABSORPT? OR ABSORB?
S8	2	S7 AND S3(N4)(S2 OR S4) AND S5
S9	1	RD (unique items) [removes duplicate references
S10	**1**	**S9 NOT S6 [not relevant]**
S11	153	(S1 OR S7) AND (S2 OR S4) AND S5
S12	11	S11 AND S3
S13	9	RD (unique items)
S14	6	S13/ENG
S15	**4**	**S14 NOT (S6 OR S10) [one reference relevant]**
S16	18190	MICROPOR? OR MACROPOR?
S17	2	S16 AND (S2 OR S4) AND S3 AND S5
S18	1	RD (unique items)
S19	1	S18 NOT (S6 OR S10 OR S15) [one reference]

Appendix C: Chronic Animal Study Data for All Leads

This appendix serves as documentation of all available data for each implanted lead, organized such that comparisons can be made between fluoroscopy images, electrical data, radiograph images, and histology section images. Each lead data summary includes fluoroscopy images of the coronary venous anatomy and final location of the implanted lead, electrical data, images of radiograph comparisons used to determine occurrence of lead retractions, and histology images. Pictures of the lead tip prior to implantation are included for porous electrode leads.

In order to properly understand the electrical data included in each lead data summary a few explanations are necessary. The "Source" column gives the means by which the electrical data were taken. "PSA" is a Pacing System Analyzer, a system for taking electrical data during the implant surgery before the pacemaker is connected to the lead. "PG" is Pulse Generator, a phrase describing any implantable pacing device (in this case a pacemaker). Only data taken from the PG (pacemaker) is plotted in Figure 23 and Figure 24, while the PSA data is given in the tables below for reference. All PG data is taken from the tip electrode to an indifferent electrode connected to the skin of the animal during lead checks. The "Movement" column documents the magnitude of any noted lead retraction when compared to the previous time point. The "Tip Pos." or Tip Position column documents the absolute position of the tip relative to its starting position at implant.

Histology section images are given at the end of each section of lead data. To the left of each slide is a graphic showing where the slice was taken relative to the

centerline of the lead body. The stated distance relative to the lead centerline in each case is approximate, since there was no way to ensure the initial cut was exactly at the centerline of the lead. Further slices were taken from various locations parallel to the initial slice of the lead body in order to give a more complete picture of the fibrous encapsulation and surrounding tissue. The title of each slide, given near the top, will also give the magnification of the image and describe the staining method used (either Gomori's trichrome, useful for visualizing collagen (in blue) which is the main constituent of the mature fibrous capsule, or hematoxylin and eosin (HE), useful for visualizing cell nuclei and cell types within the tissue). Most histology slides are trichrome stained, though a few are HE stained.

Summary Study Information for Animal L-3216, Lead 163931 (Solid Tip Electrode)

Implant Fluoroscopy Images

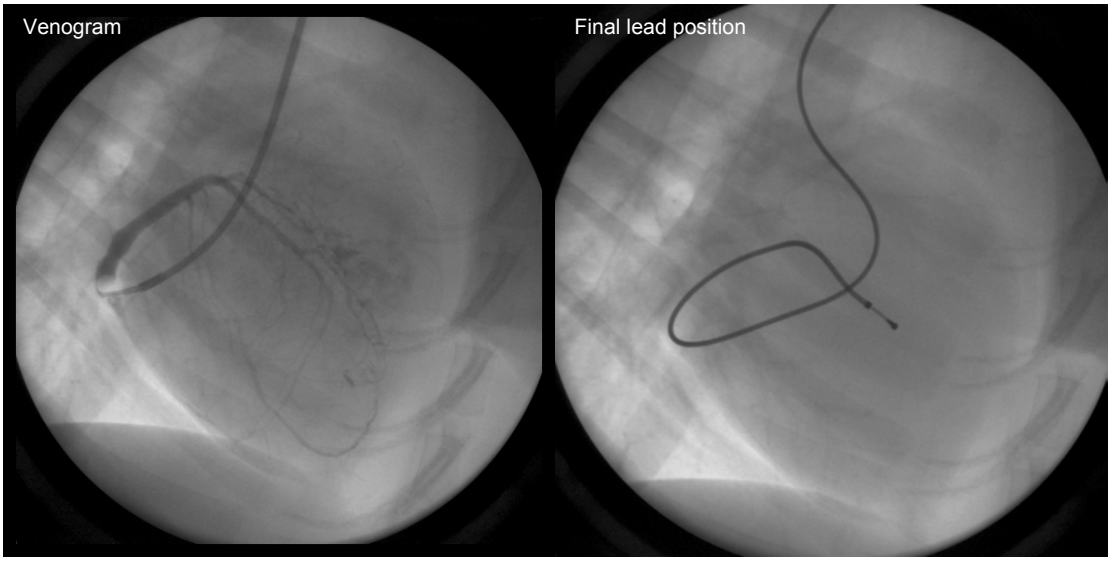

Study Data

Animal ID	Source	Date	Day	Thr. [V]	Thr. Change [V]	R-Wave [mV]	Imp. [Ω]	Movement [cm]	Tip Pos. [cm]
L-3216	PSA Ring	5/27/2008	0	0.8		25.4	1312		
Lead ID	PSA Tip	5/27/2008	0	0.6		27.2	1272		
163931	PG	5/27/2008	0	0.4	0.0	18.2	660	0	0
Tip Electrode	PG	5/30/2008	3	1.2	0.8	17.8	480	1	-1
Solid	PG	6/2/2008	6	1.4	1.0	14.1	500	1	-2
	PG	6/9/2008	13	1.5	1.1	15.5	530	0	-2
	PG	6/16/2008	20	1.1	0.7	15.0	560	0	-2
	PG	6/23/2008	27	0.8	0.4	18.2	560	0	-2
	PG	7/7/2008	41	0.7	0.3	*20.0*	600	0	-2
	PG	7/24/2008	58	0.7	0.3	15.0	640	0	-2
	PSA Ring	7/24/2008	58	1.2	0.4	25.1	886		

Lead Retractions

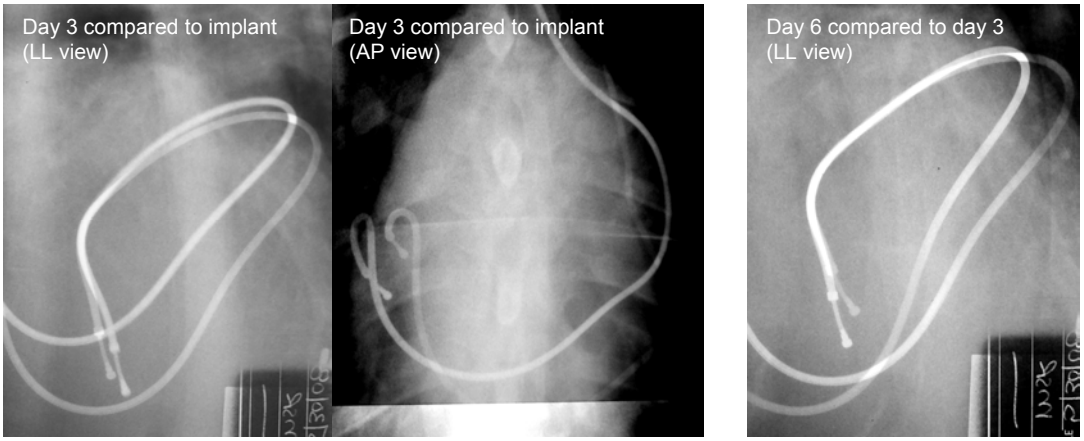

Histology

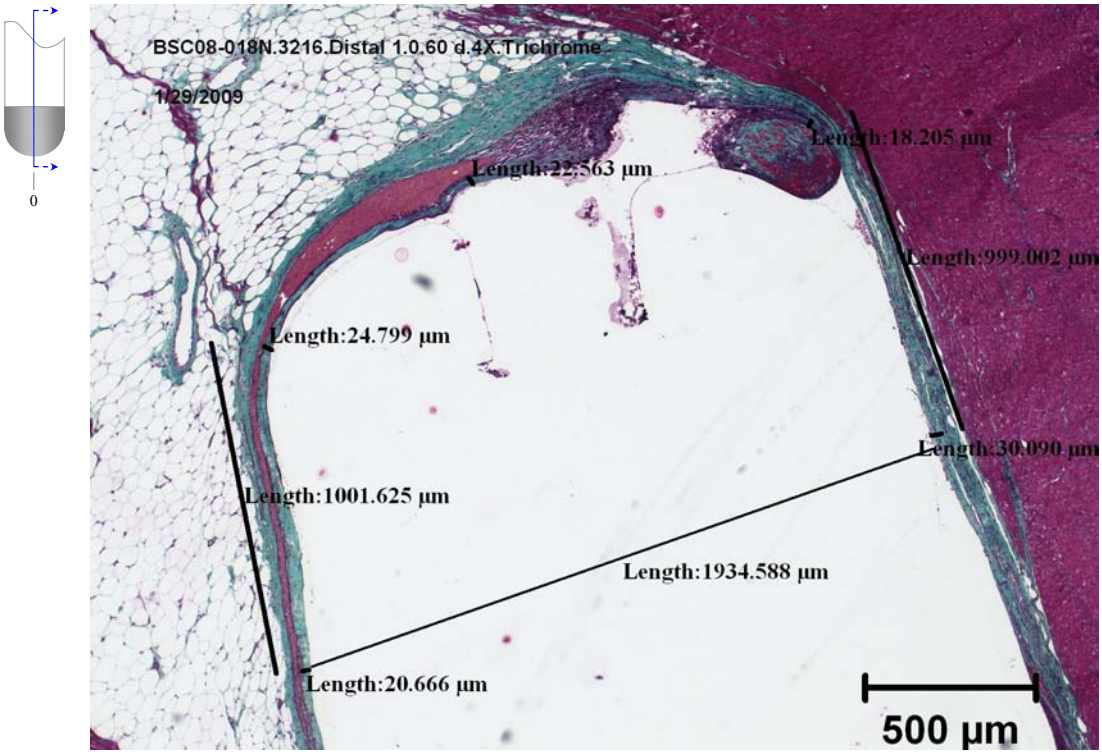
0
BSC08-018N.3216.Distal 1.0.60 d.4X.Trichrome
1/29/2009
Length:18.205 µm
Length:22.563 µm
Length:999.002 µm
Length:24.799 µm
Length:30.090 µm
Length:1001.625 µm
Length:1934.588 µm
Length:20.666 µm
500 µm

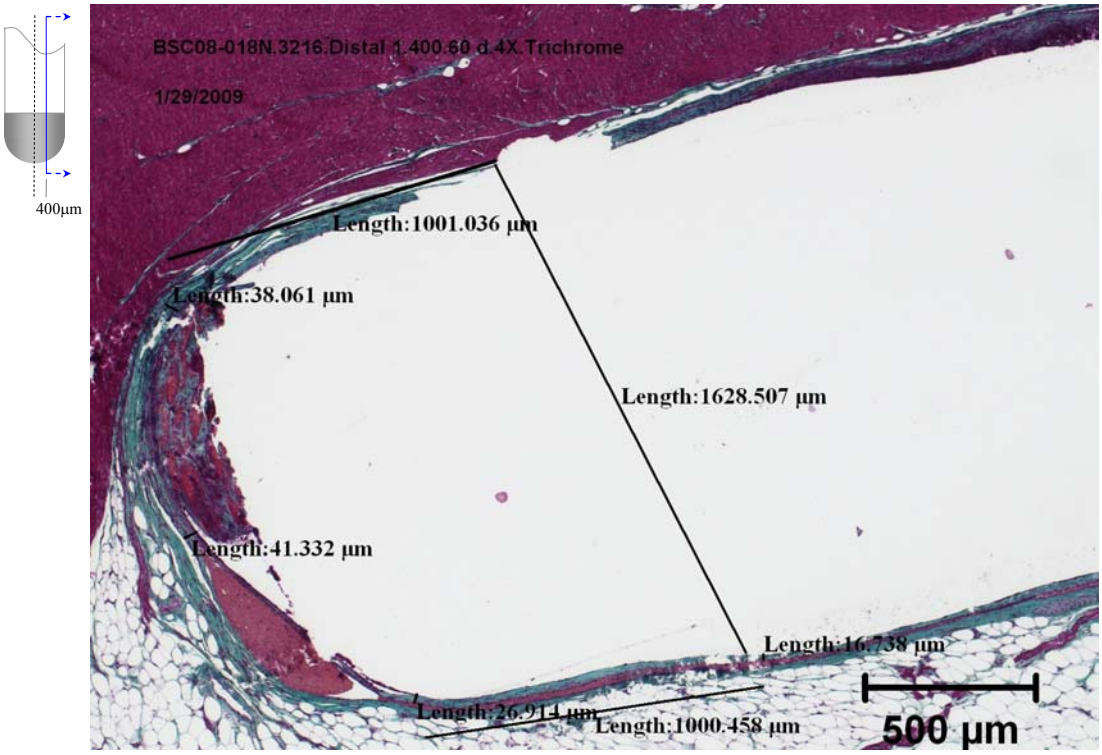
400µm
BSC08-018N.3216.Distal 1.400.60 d.4X.Trichrome
1/29/2009
Length:1001.036 µm
Length:38.061 µm
Length:1628.507 µm
Length:41.332 µm
Length:16.738 µm
Length:26.914 µm
Length:1000.458 µm
500 µm

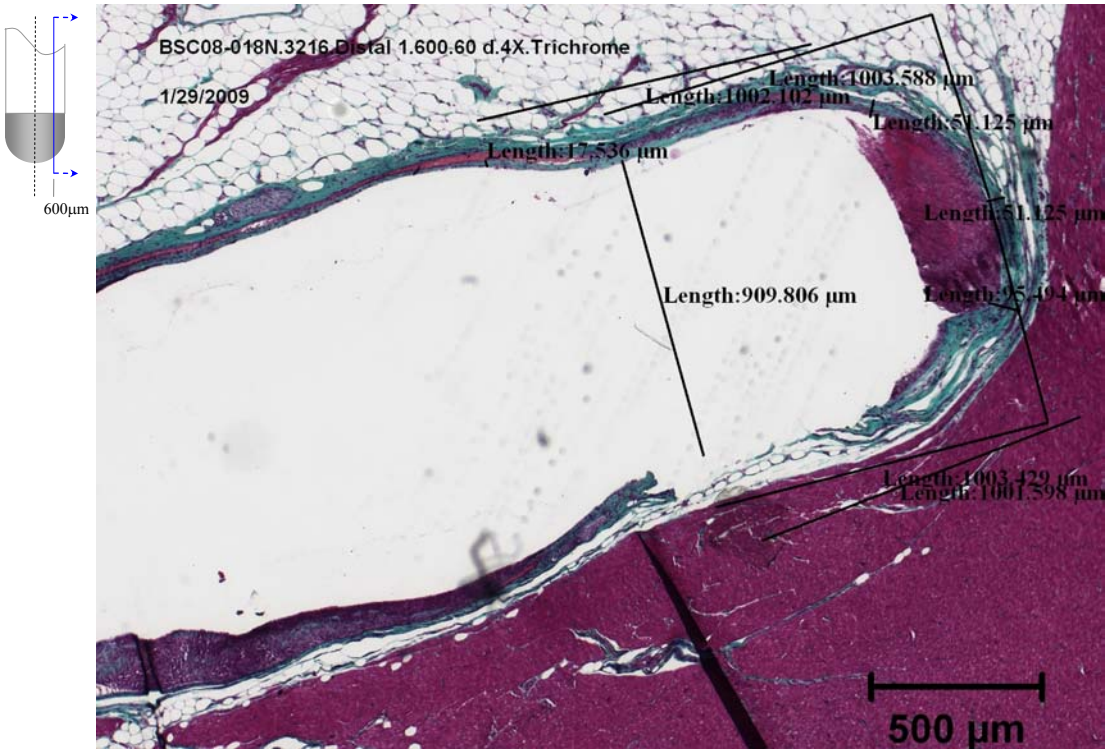
600µm
BSC08-018N.3216.Distal 1.600.60 d.4X.Trichrome
1/29/2009
Length:1003.588 µm
Length:1002.102 µm
Length:17.536 µm
Length:909.806 µm
500 µm

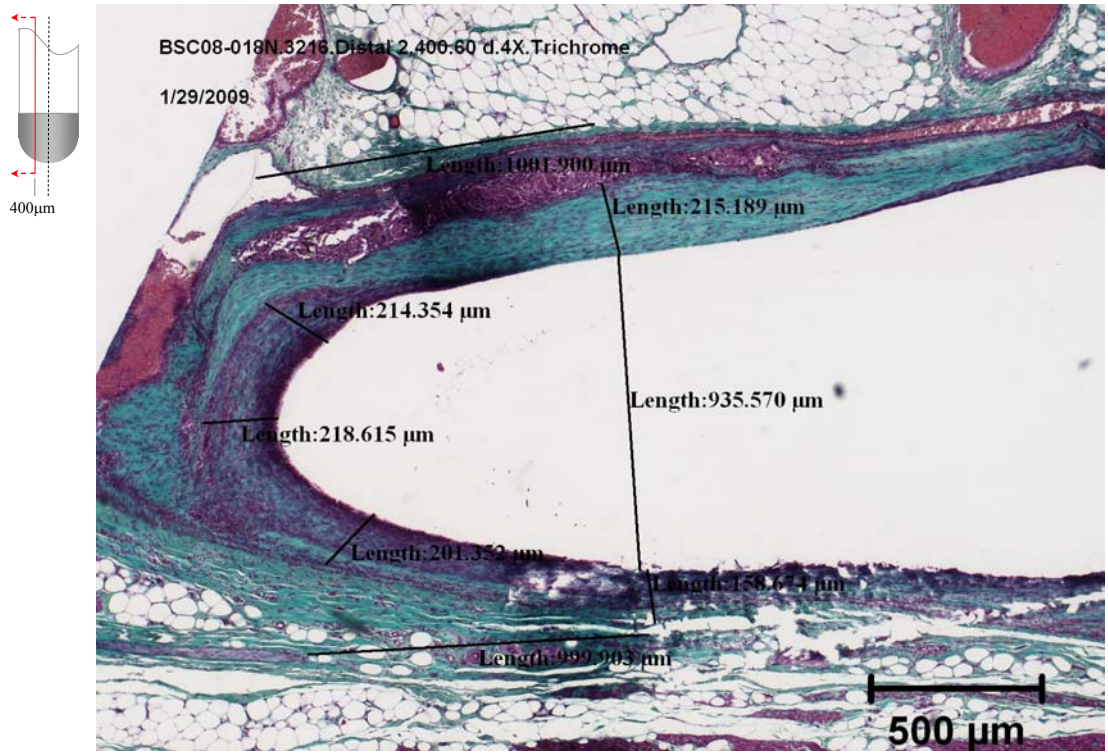
400µm
BSC08-018N.3216.Distal 2.400.60 d.4X.Trichrome
1/29/2009
Length:1001.900 µm
Length:215.189 µm
Length:214.354 µm
Length:935.570 µm
Length:218.615 µm
500 µm

Summary Study Information for Animal L-3217, Lead 164023 (Porous Tip Electrode)

Lead Tip Images*

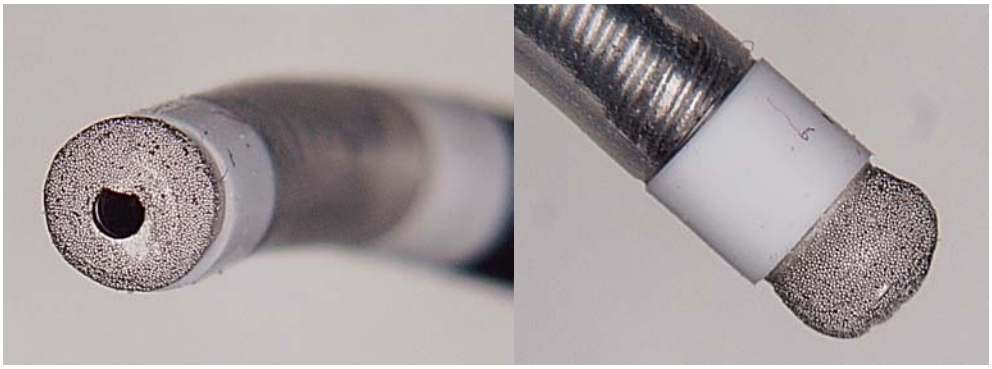

* Steroid eluting collars were initially assembled onto the lead in error (and are shown in the images), though they were later removed and replaced with silicone tubing of the same length, thickness, and diameters as the steroid collars, but with no steroid.

Implant Fluoroscopy Images

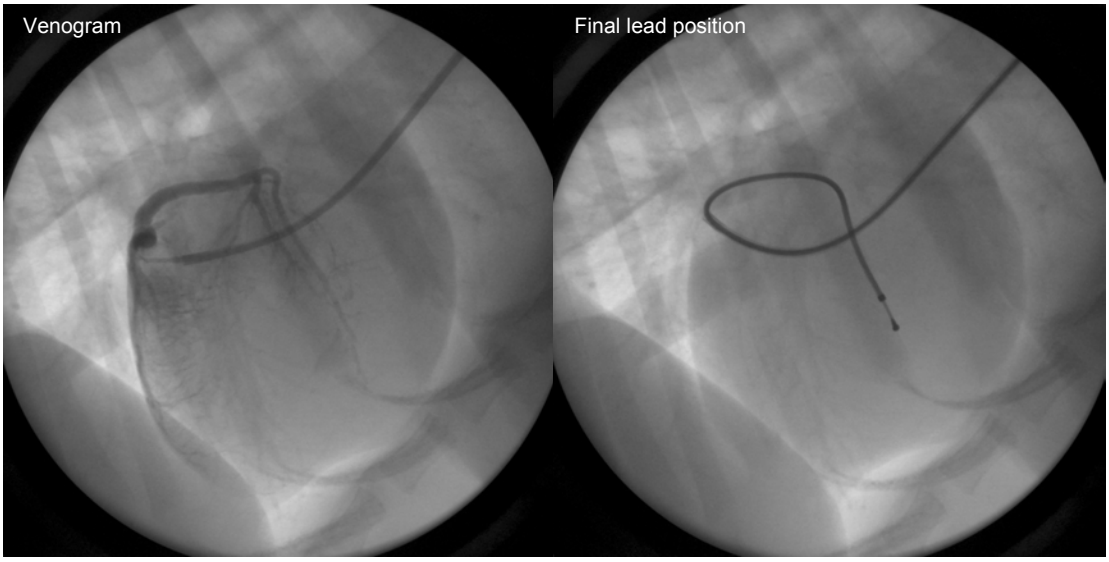

Study Data

Animal ID	Source	Date	Day	Thr. [V]	Thr. Change [V]	R-Wave [mV]	Imp. [Ω]	Movement [cm]	Tip Pos. [cm]
L-3217	PSA Ring	5/27/2008	0	1.2		19.5	942		
Lead ID	PSA Tip	5/27/2008	0	0.5		31.5	948		
164023	PG	5/27/2008	0	0.2	0.0	*12.0*	730	0	0
Tip Electrode	PG	5/30/2008	3	0.8	0.6	16.0	550	0	0
Porous	PG	6/2/2008	6	1.1	0.9	13.2	520	0	0
	PG	6/9/2008	13	2.1	1.9	17.3	460	0	0
	PG	6/16/2008	20	1.6	1.4	14.6	560	0	0
	PG	6/23/2008	27	0.7	0.5	14.6	560	0	0
	PG	7/7/2008	41	0.6	0.4	13.7	540	0	0
	PG	7/24/2008	58	0.7	0.5	16.4	560	0	0
	PSA Ring	7/24/2008	58	1.3	0.1	16.7	820		

Histology

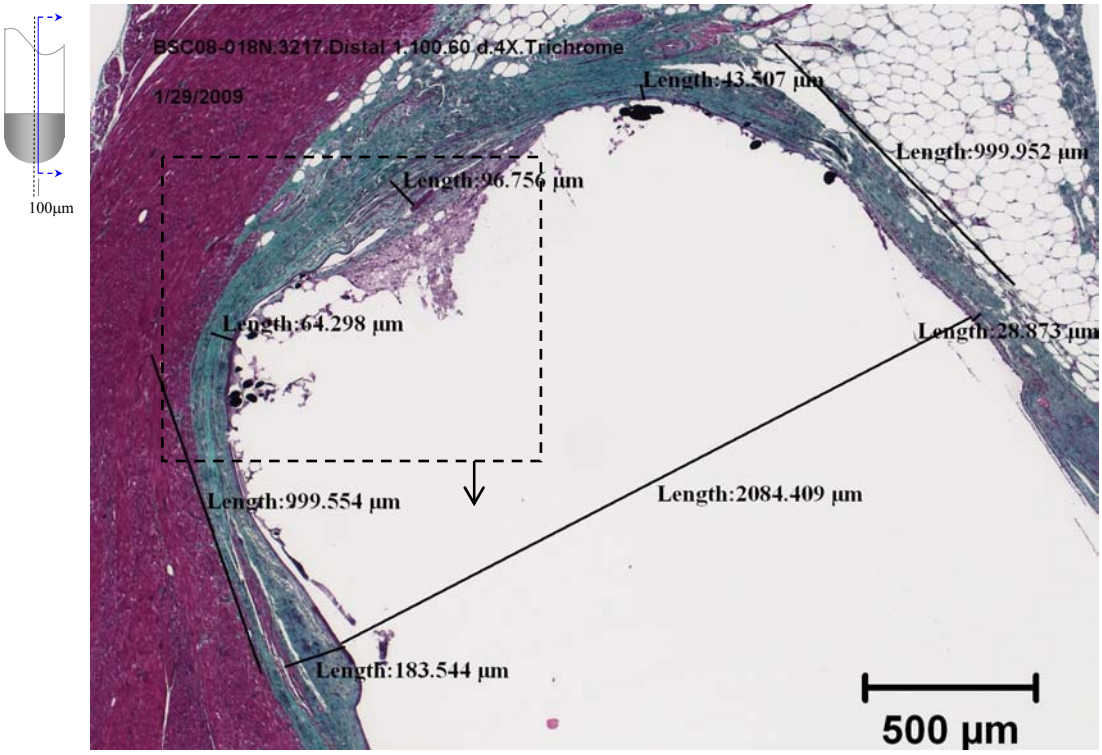
BSC08-018N.3217.Distal 1.100.60 d.4X.Trichrome
1/29/2009
Length:43.507 µm
Length:999.952 µm
Length:96.756 µm
Length:64.298 µm
Length:28.873 µm
Length:999.554 µm
Length:2084.409 µm
Length:183.544 µm
500 µm

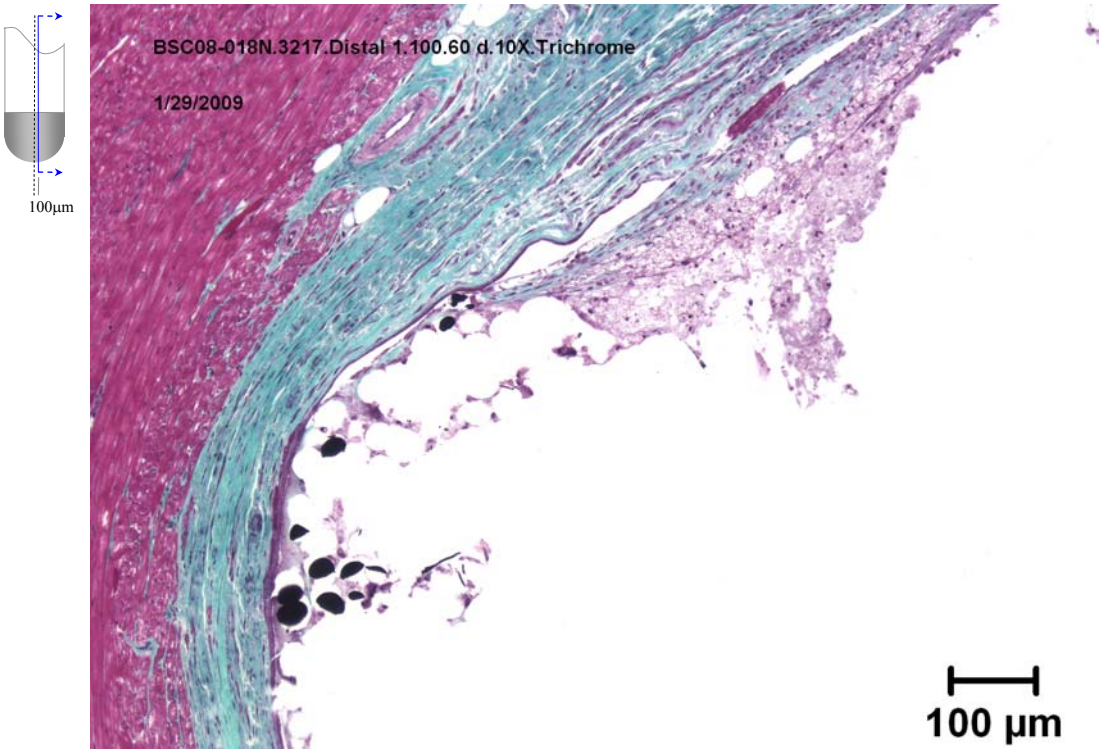
BSC08-018N.3217.Distal 1.100.60 d.10X.Trichrome
1/29/2009
100 µm

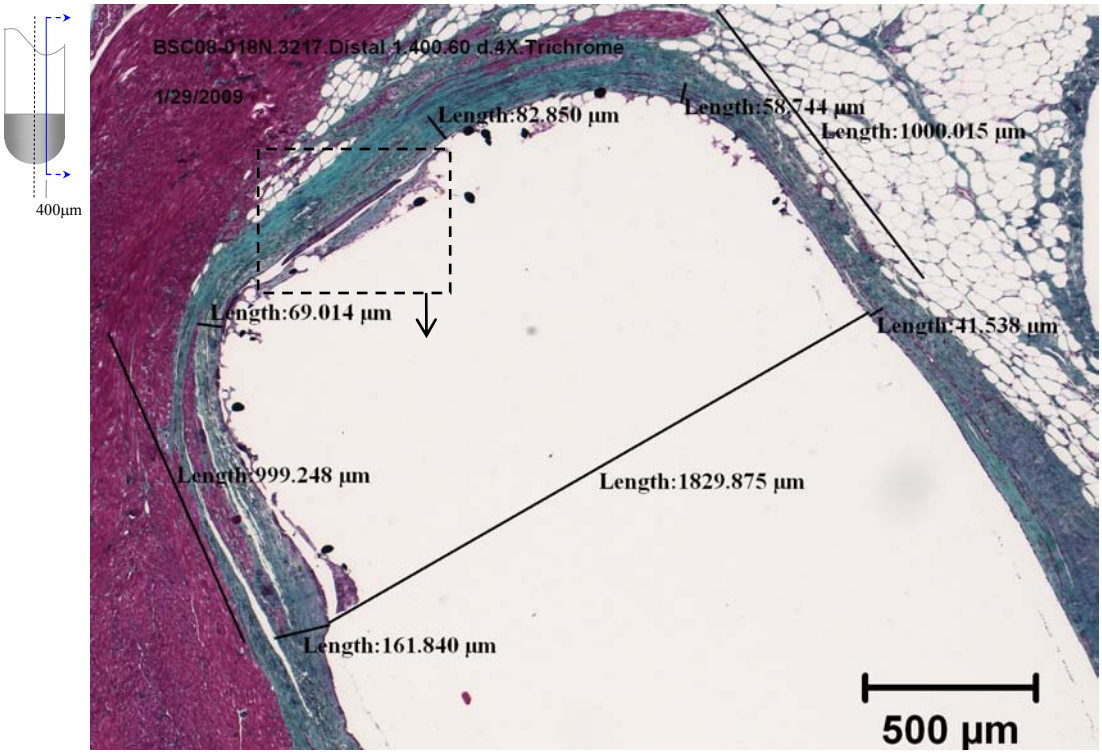
400µm
BSC08-018N.3217.Distal 1.400.60 d.4X.Trichrome
1/29/2009
Length:82.850 µm
Length:58.744 µm
Length:1000.015 µm
Length:69.014 µm
Length:41.538 µm
Length:999.248 µm
Length:1829.875 µm
Length:161.840 µm
500 µm

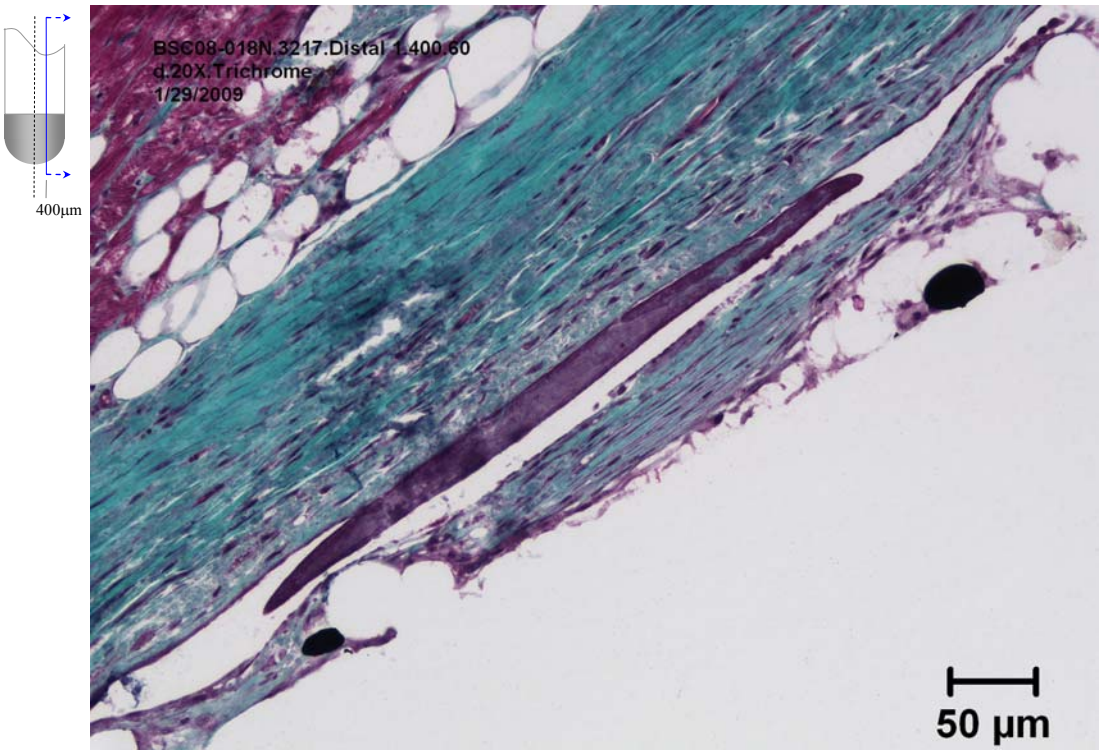
400µm
BSC08-018N.3217.Distal 1.400.60
d.20X.Trichrome
1/29/2009
50 µm

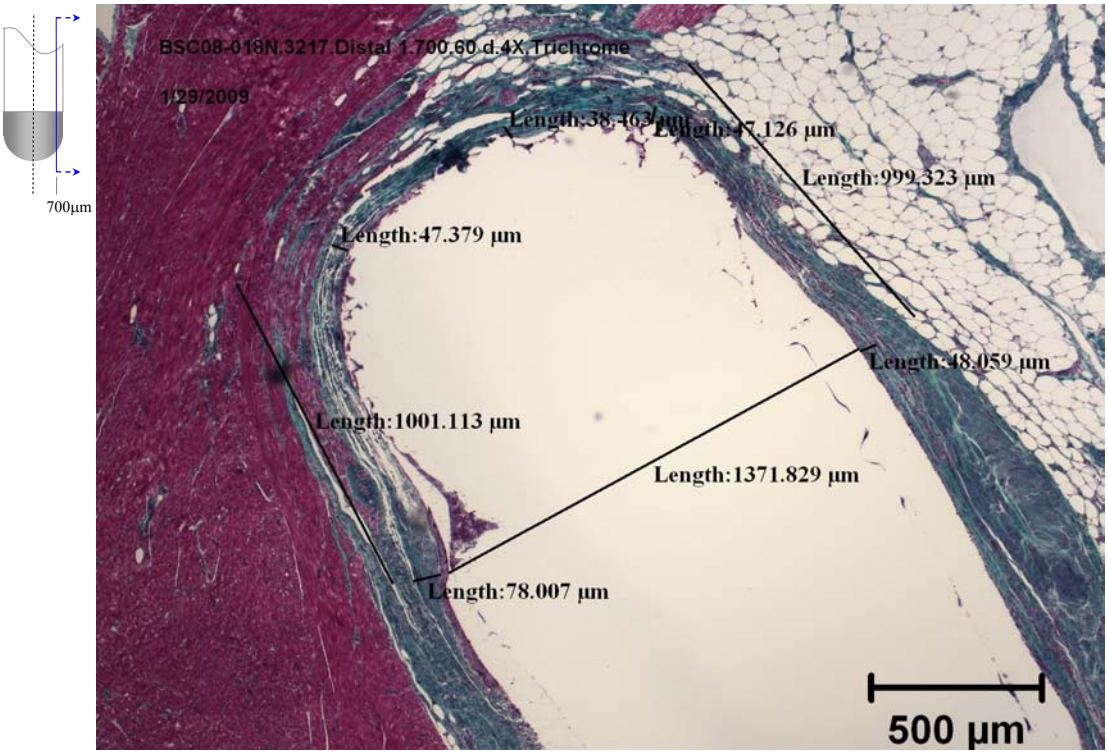
700µm
BSC08-018N.3217.Distal 1.700.60 d.4X.Trichrome
1/29/2009
Length:38.463 µm
Length:47.126 µm
Length:999.323 µm
Length:47.379 µm
Length:48.059 µm
Length:1001.113 µm
Length:1371.829 µm
Length:78.007 µm
500 µm

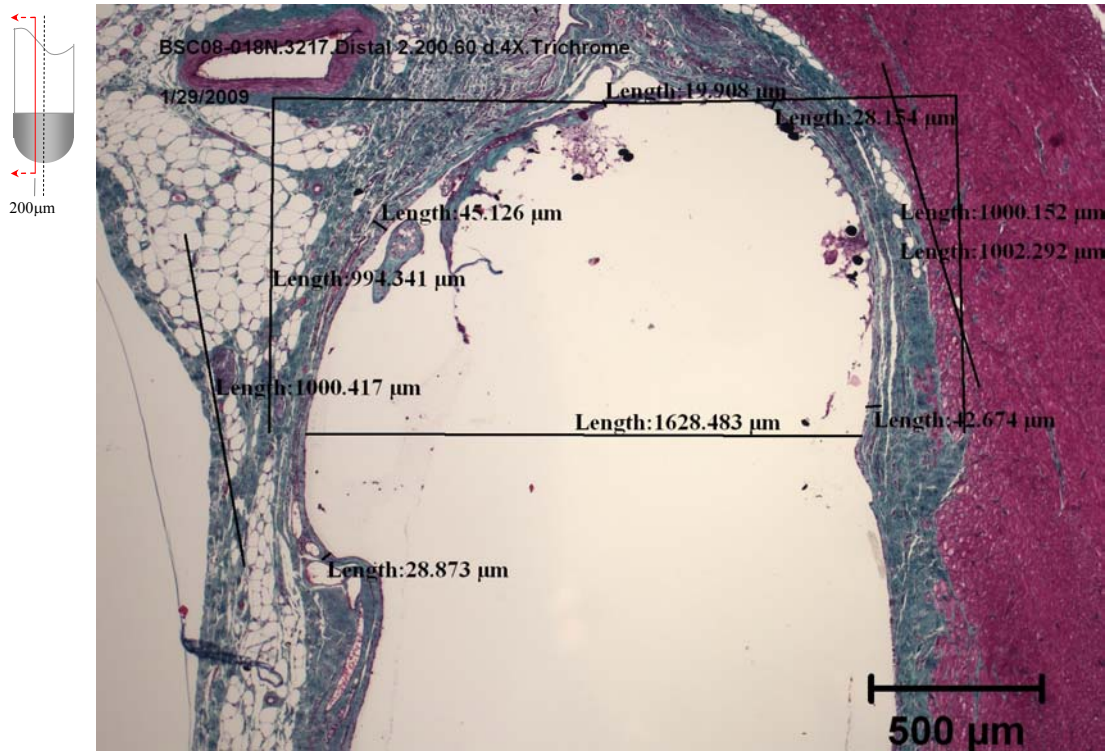
200µm
BSC08-018N.3217.Distal 2.200.60 d.4X.Trichrome
1/29/2009
Length:19.908 µm
Length:28.154 µm
Length:45.126 µm
Length:1000.152 µm
Length:1002.292 µm
Length:994.341 µm
Length:1000.417 µm
Length:1628.483 µm
Length:42.674 µm
Length:28.873 µm
500 µm

Summary Study Information for Animal L-3218, Lead 163977 (Solid Tip Electrode)

Implant Fluoroscopy Images

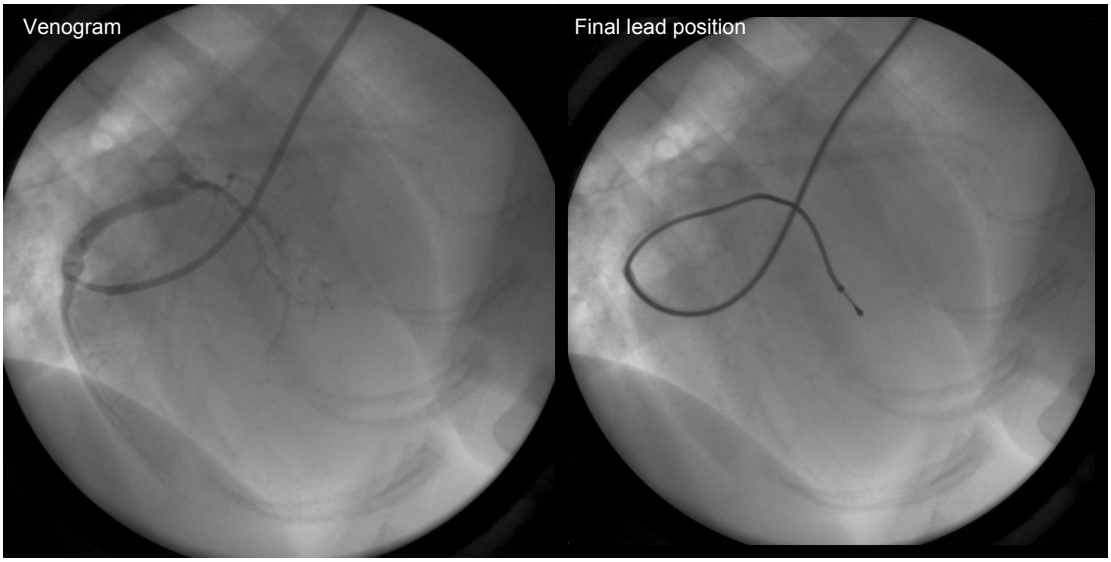

Study Data

Animal ID	Source	Date	Day	Thr. [V]	Thr. Change [V]	R-Wave [mV]	Imp. [Ω]	Movement [cm]	Tip Pos. [cm]
L-3218	PSA Ring	5/27/2008	0	0.7		20.1	852		
Lead ID	PSA Tip	5/27/2008	0	0.3		35.8	780		
163977	PG	5/27/2008	0	0.3	0.0	18.2	560	0	0
Tip Electrode	PG	5/30/2008	3	0.8	0.5	*20.0*	490	0	0
Solid	PG	6/2/2008	6	1.0	0.7	*20.0*	480	0	0
	PG	6/9/2008	13	2.1	1.8	19.2	480	0	0
	PG	6/16/2008	20	1.8	1.5	*20.0*	500	0.5	-0.5
	PG	6/23/2008	27	1.1	0.8	*20.0*	550	0	-0.5
	PG	7/7/2008	41	0.9	0.6	*20.0*	540	0	-0.5
	PG	7/24/2008	58	0.9	0.6	*20.0*	550	0	-0.5
	PSA Ring	7/24/2008	58	2.1	1.4	25.2	964		

Lead Retractions

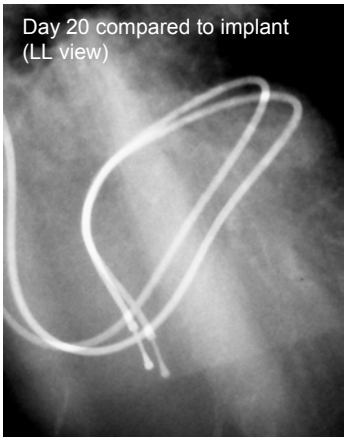

Histology

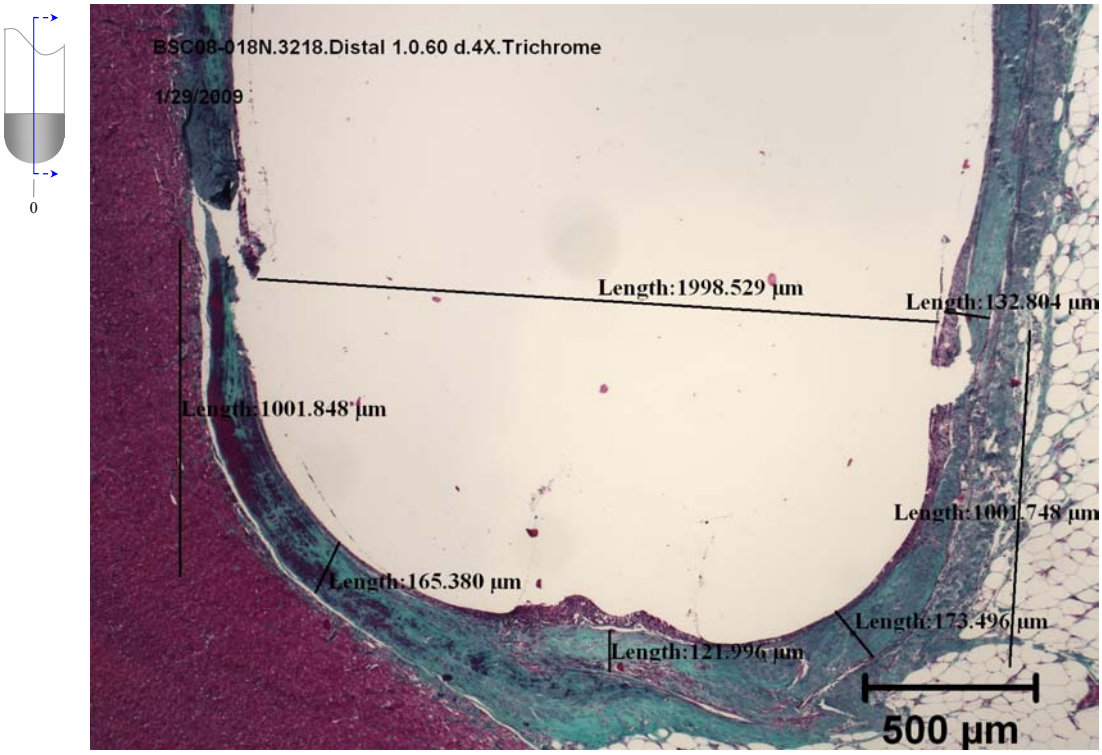
0
BSC08-018N.3218.Distal 1.0.60 d.4X.Trichrome
1/29/2009
Length:1998.529 µm
Length:132.804 µm
Length:1001.848 µm
Length:1001.748 µm
Length:165.380 µm
Length:173.496 µm
Length:121.996 µm
500 µm

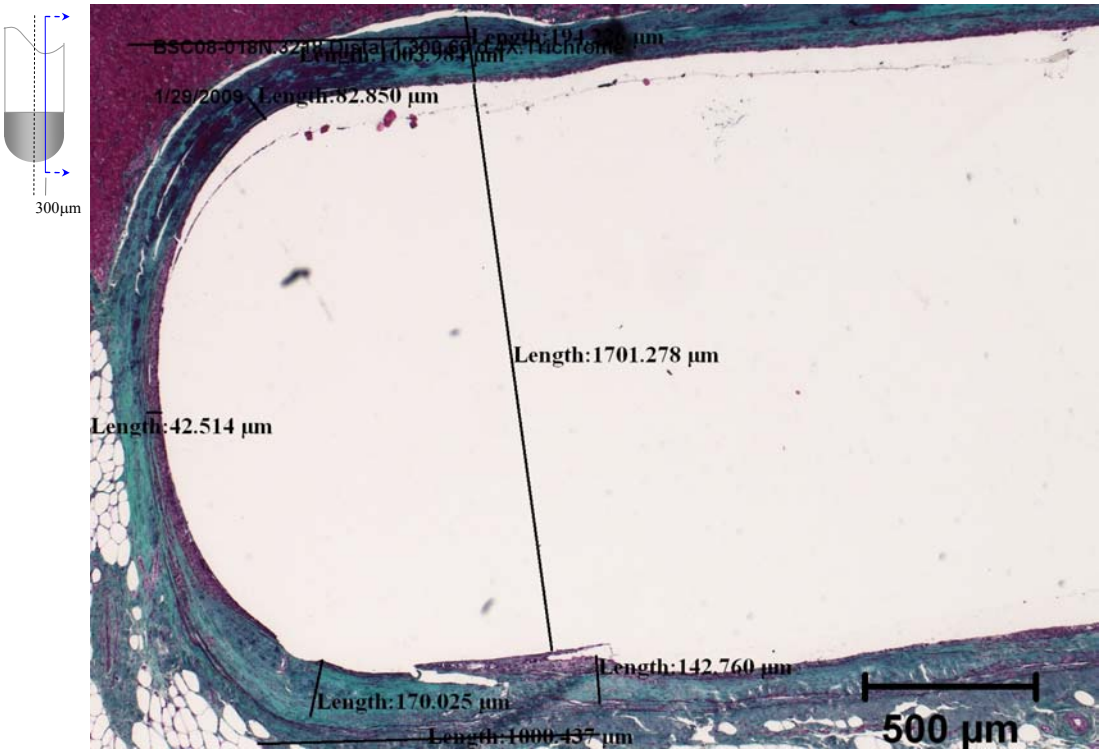
300µm
1/29/2009
Length:82.850 µm
Length:1701.278 µm
Length:42.514 µm
Length:142.760 µm
Length:170.025 µm
500 µm

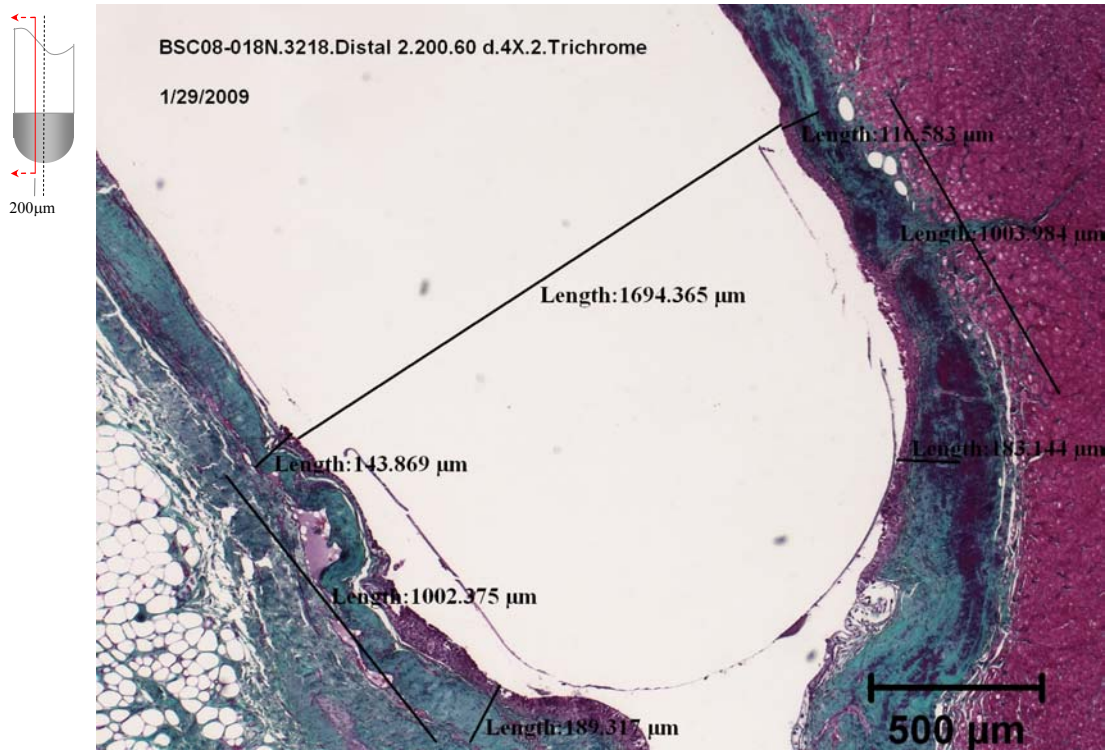
200µm
BSC08-018N.3218.Distal 2.200.60 d.4X.2.Trichrome
1/29/2009
Length:116.583 µm
Length:1003.984 µm
Length:1694.365 µm
Length:183.144 µm
Length:143.869 µm
Length:1002.375 µm
Length:189.317 µm
500 µm

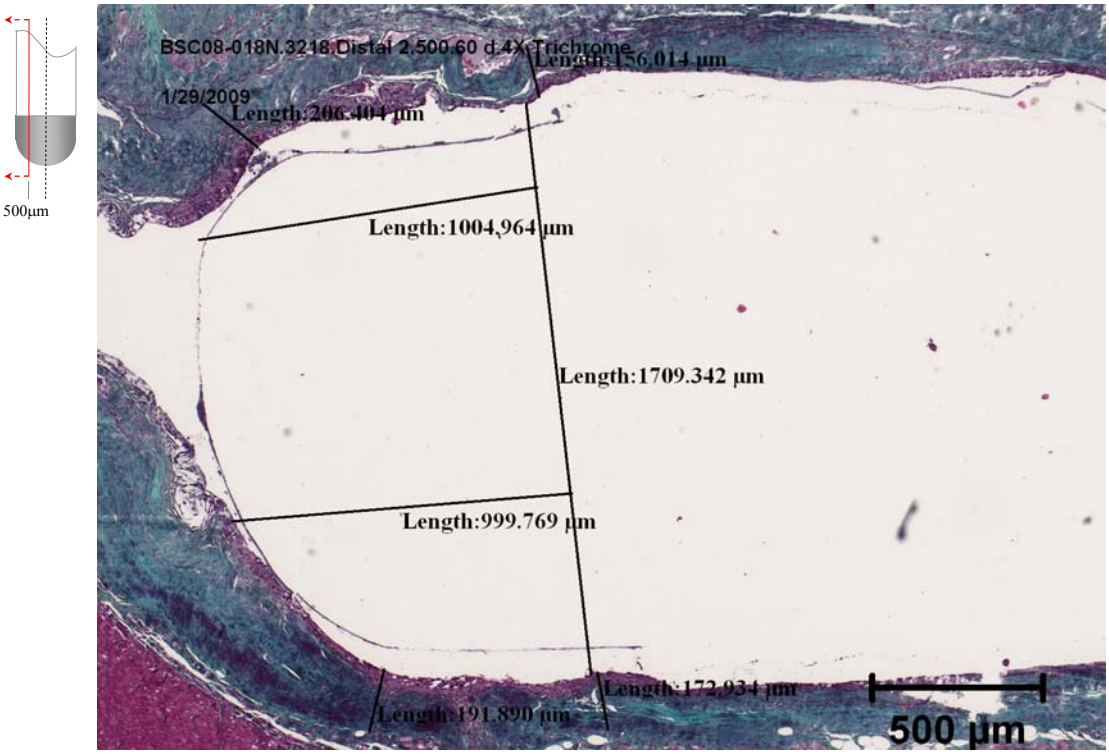
500µm
BSC08-018N.3218.Distal 2.500.60 d.4X.Trichrome
1/29/2009
Length:156.014 µm
Length:206.404 µm
Length:1004.964 µm
Length:1709.342 µm
Length:999.769 µm
Length:172.934 µm
Length:191.890 µm
500 µm

Summary Study Information for Animal L-3219, Lead 164084 (Porous Tip Electrode)

Lead Tip Images*

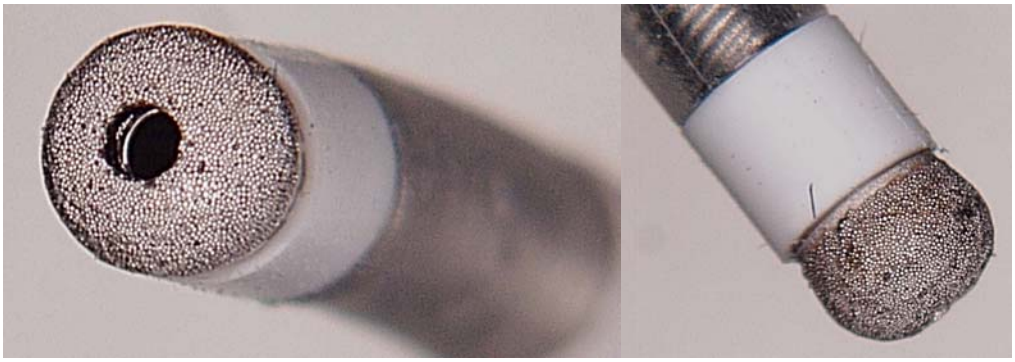

* Steroid eluting collars were initially assembled onto the lead in error (and are shown in the images), though they were later removed and replaced with silicone tubing of the same length, thickness, and diameters as the steroid collars, but with no steroid.

Implant Fluoroscopy Images

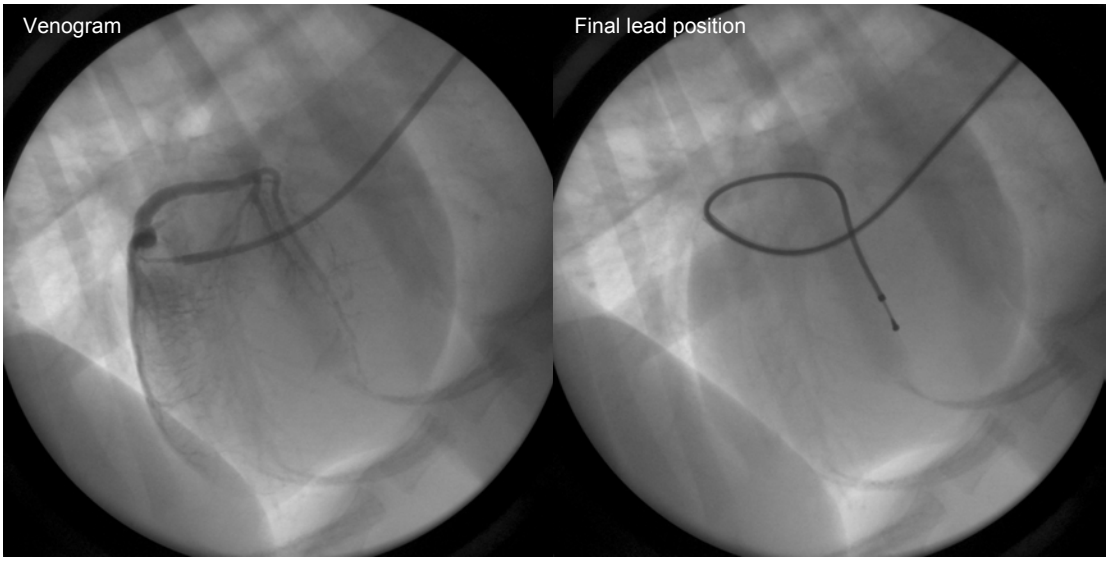

Study Data

Animal ID	Source	Date	Day	Thr. [V]	Thr. Change [V]	R-Wave [mV]	Imp. [Ω]	Movement [cm]	Tip Pos. [cm]
L-3219	PSA Ring	5/27/2008	0	1.2		16.8	792		
Lead ID	PSA Tip	5/27/2008	0	1.0		24.1	840		
164084	PG	5/27/2008	0	0.4	0.0	*12.0*	610	0	0
Tip Electrode	PG	5/30/2008	3	1.5	1.1	10.9	470	1	-1
Porous	PG	6/2/2008	6	1.7	1.3	12.3	500	0	-1
	PG	6/9/2008	13	2.1	1.7	9.1	560	0	-1
	PG	6/16/2008	20	1.7	1.3	11.4	620	0	-1
	PG	6/23/2008	27	1.9	1.5	10.0	620	0	-1
	PG	7/7/2008	41	1.1	0.7	13.7	720	0	-1
	PG	7/24/2008	58	1.0	0.6	11.9	730	0	-1
	PSA Ring	7/24/2008	58	2.7	1.5	15.2	1056		

Lead Retractions

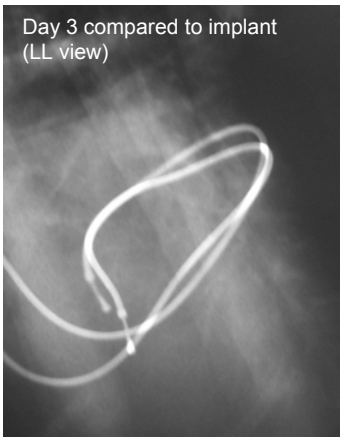

Histology

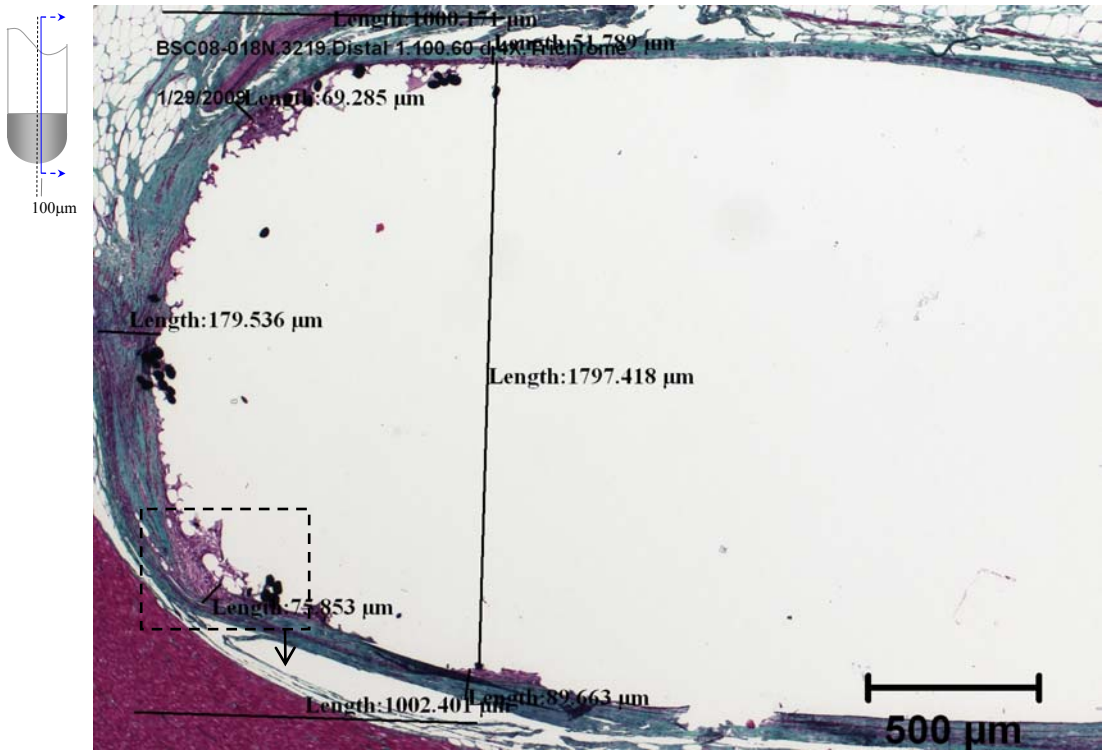

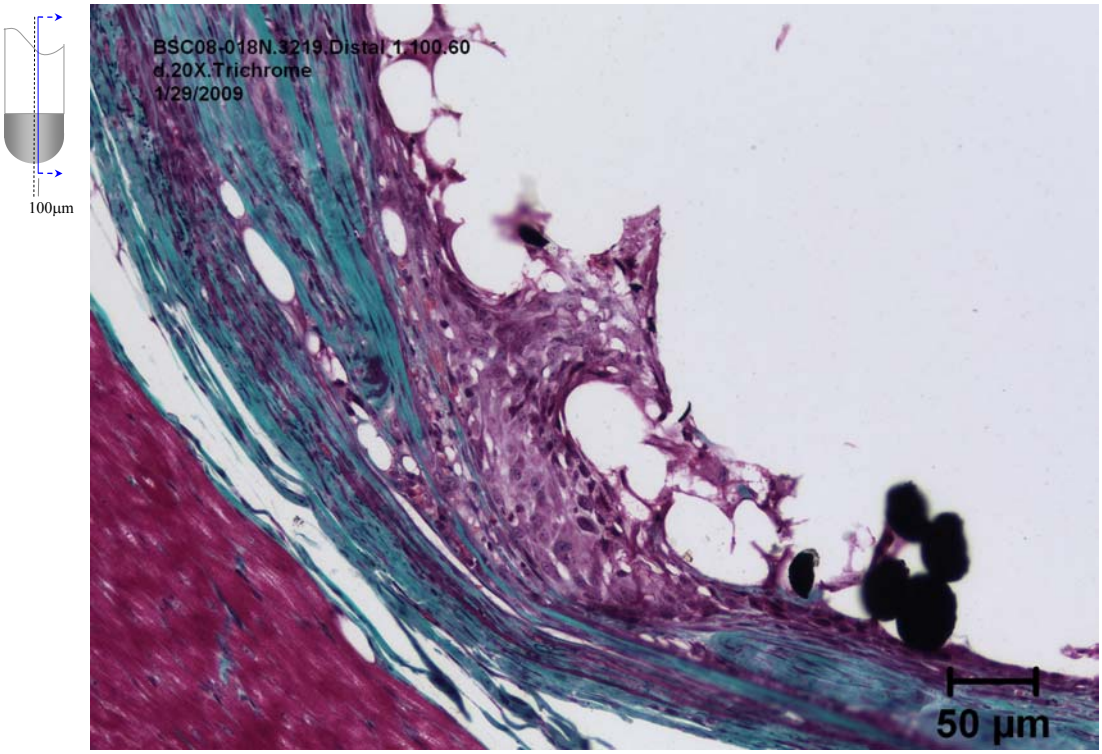
100µm
BSC08-018N.3219.Distal.1.100.60
d.20X.Trichrome
1/29/2009
50 µm

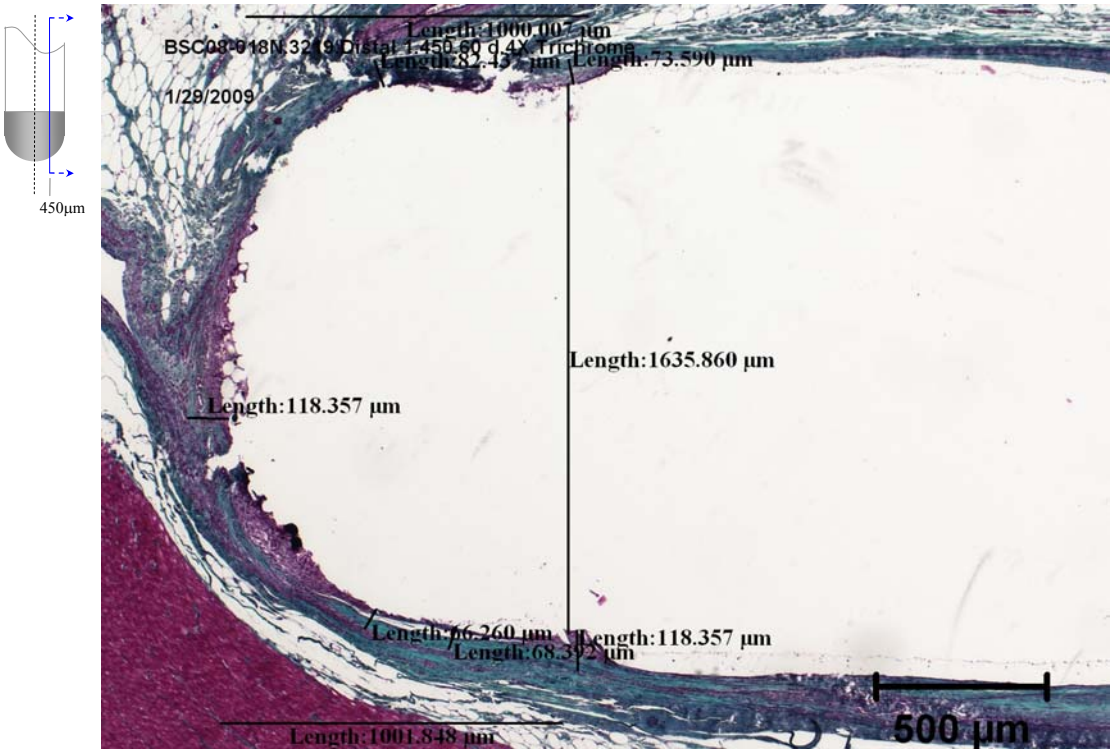
450µm
BSC08-018N.3219.Distal.1.450.60 d.4X.Trichrome
1/29/2009
Length:1000.007 µm
Length:82.432 µm
Length:73.590 µm
Length:1635.860 µm
Length:118.357 µm
Length:96.260 µm
Length:68.392 µm
Length:118.357 µm
Length:1001.848 µm
500 µm

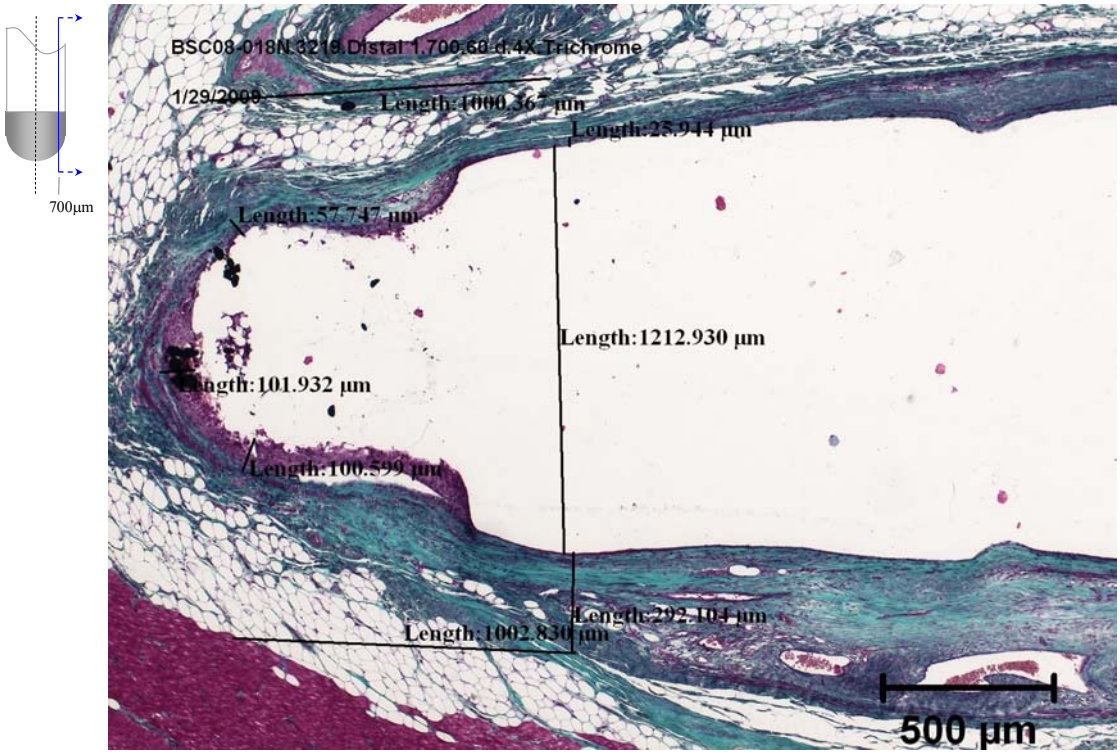
700µm
BSC08-018N.3218.Distal 1.700.60 d.4X.Trichrome
1/29/2009
Length:1000.367 µm
Length:25.944 µm
Length:57.747 µm
Length:1212.930 µm
Length:101.932 µm
Length:100.599 µm
Length:292.104 µm
Length:1002.830 µm
500 µm

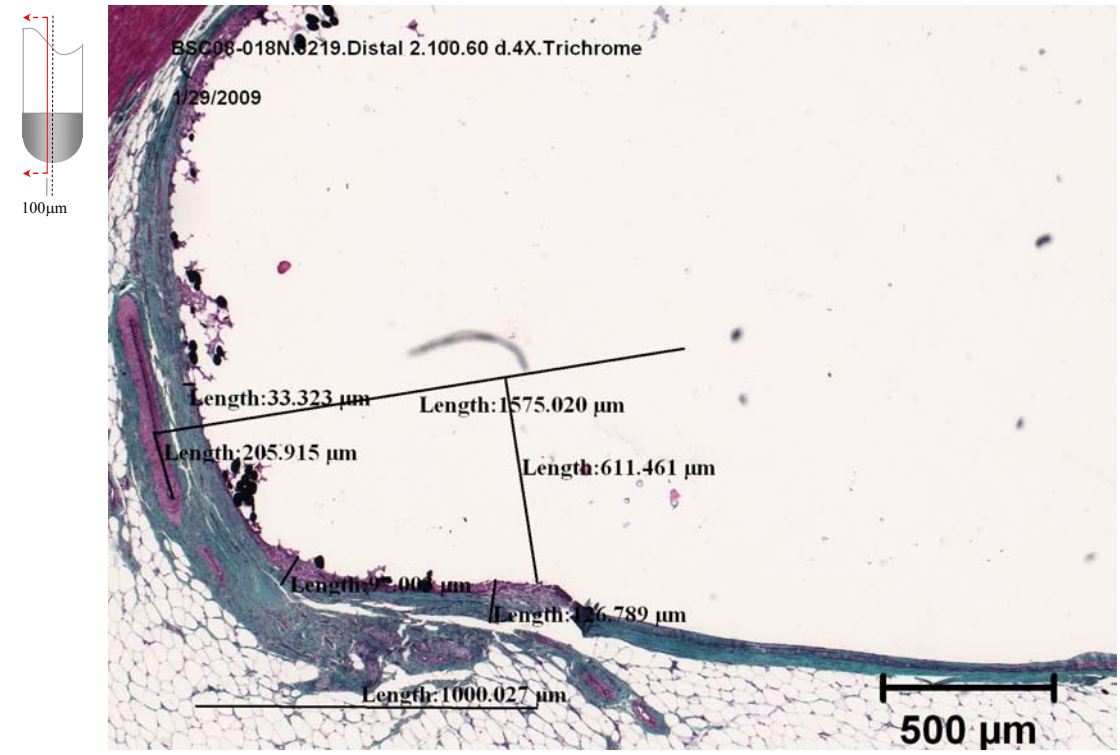
100µm
BSC08-018N.3219.Distal 2.100.60 d.4X.Trichrome
1/29/2009
Length:33.323 µm
Length:1575.020 µm
Length:205.915 µm
Length:611.461 µm
Length:97.003 µm
Length:126.789 µm
Length:1000.027 µm
500 µm

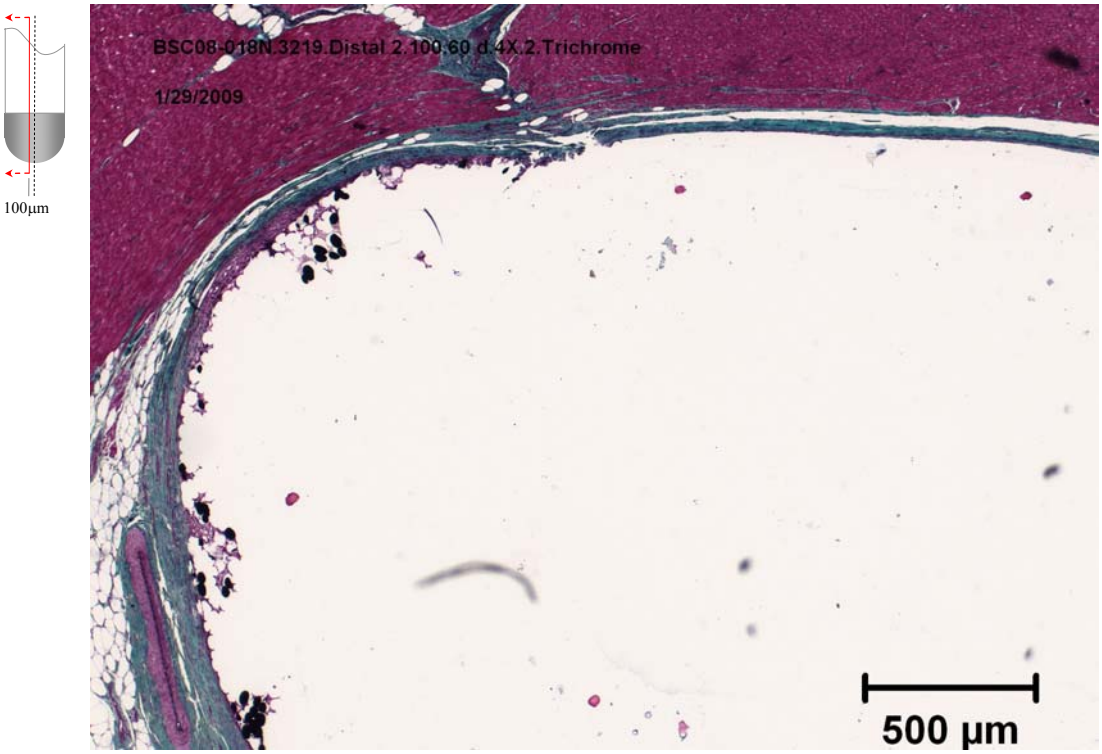
100µm
BSC08-018N.3219.Distal 2.100.60 d.4X.2.Trichrome
1/29/2009
500 µm

Summary Study Information for Animal L-3220, Lead 164021 (Porous Tip Electrode)

Lead Tip Images*

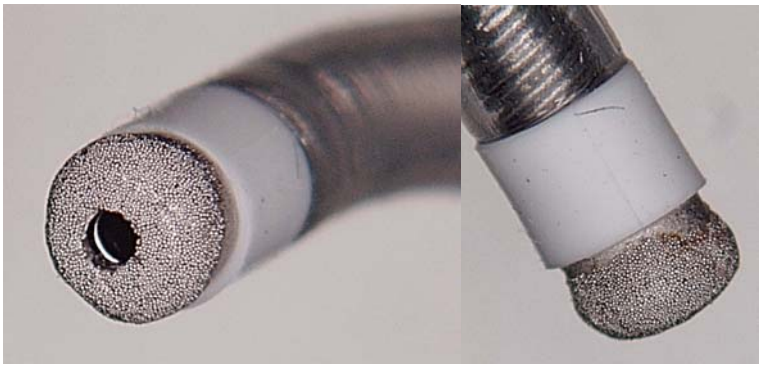

* Steroid eluting collars were initially assembled onto the lead in error (and are shown in the images), though they were later removed and replaced with silicone tubing of the same length, thickness, and diameters as the steroid collars, but with no steroid.

Implant Fluoroscopy Images

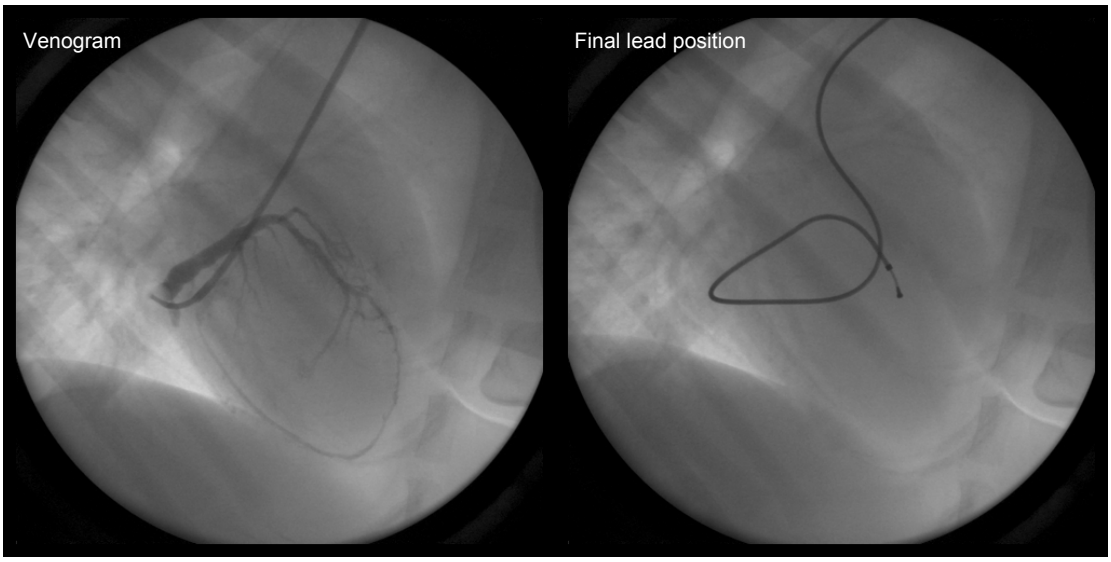

Study Data

Animal ID	Source	Date	Day	Thr. [V]	Thr. Change [V]	R-Wave [mV]	Imp. [Ω]	Movement [cm]	Tip Pos. [cm]
L-3220	PSA Ring	5/28/2008	0	0.7		14.0	916		
Lead ID	PSA Tip	5/28/2008	0	0.4		16.4	840		
164021	PG	5/28/2008	0	0.3	0.0	11.7	590	0	0
Tip Electrode	PG	5/30/2008	2	0.7	0.4	9.7	480	0	0
Porous	PG	6/4/2008	7	1.1	0.8	10.0	530	0	0
	PG	6/9/2008	12	1.0	0.7	10.5	580	0	0
	PG	6/16/2008	19	0.9	0.6	10.0	580	0	0
	PG	6/23/2008	26	0.9	0.6	11.4	620	0	0
	PG	7/7/2008	40	0.7	0.4	13.2	660	0	0
	PG	7/25/2008	58	0.7	0.4	15.5	670	0	0
	PSA Ring	7/25/2008	58	1.8	1.1	15.6	676		

Histology

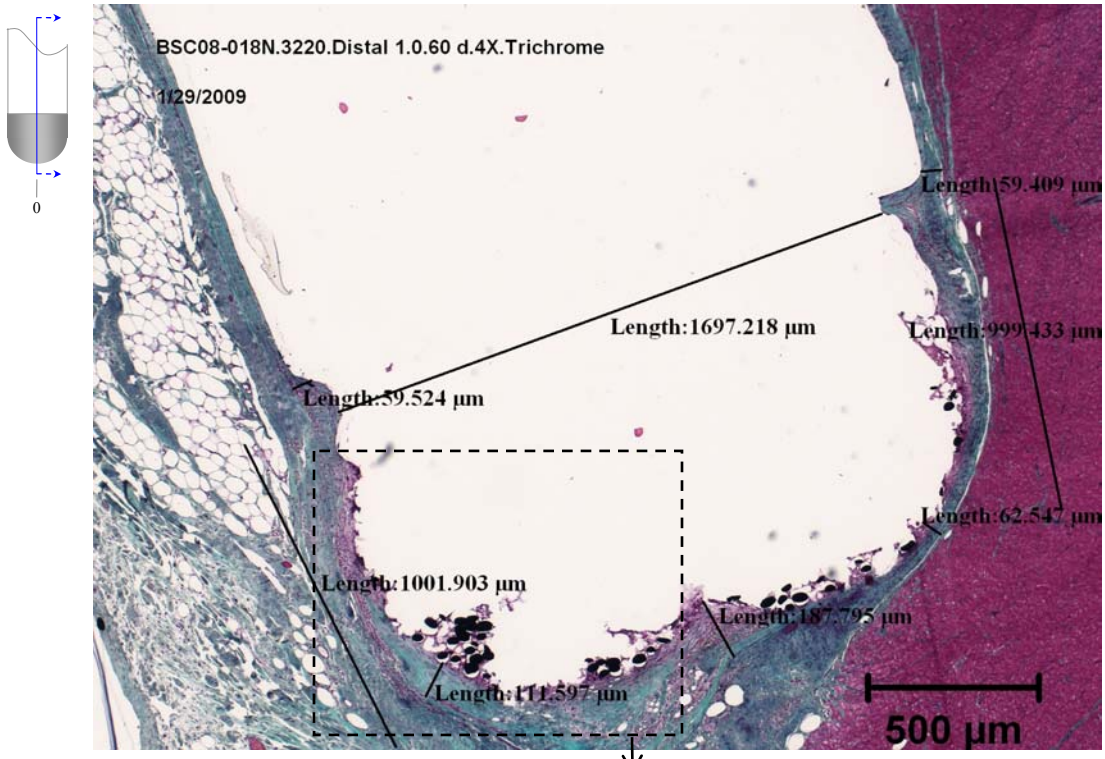
BSC08-018N.3220.Distal 1.0.60 d.4X.Trichrome
1/29/2009
Length:59.409 µm
Length:1697.218 µm
Length:999.433 µm
Length:59.524 µm
Length:62.547 µm
Length:1001.903 µm
Length:187.795 µm
Length:111.597 µm
500 µm

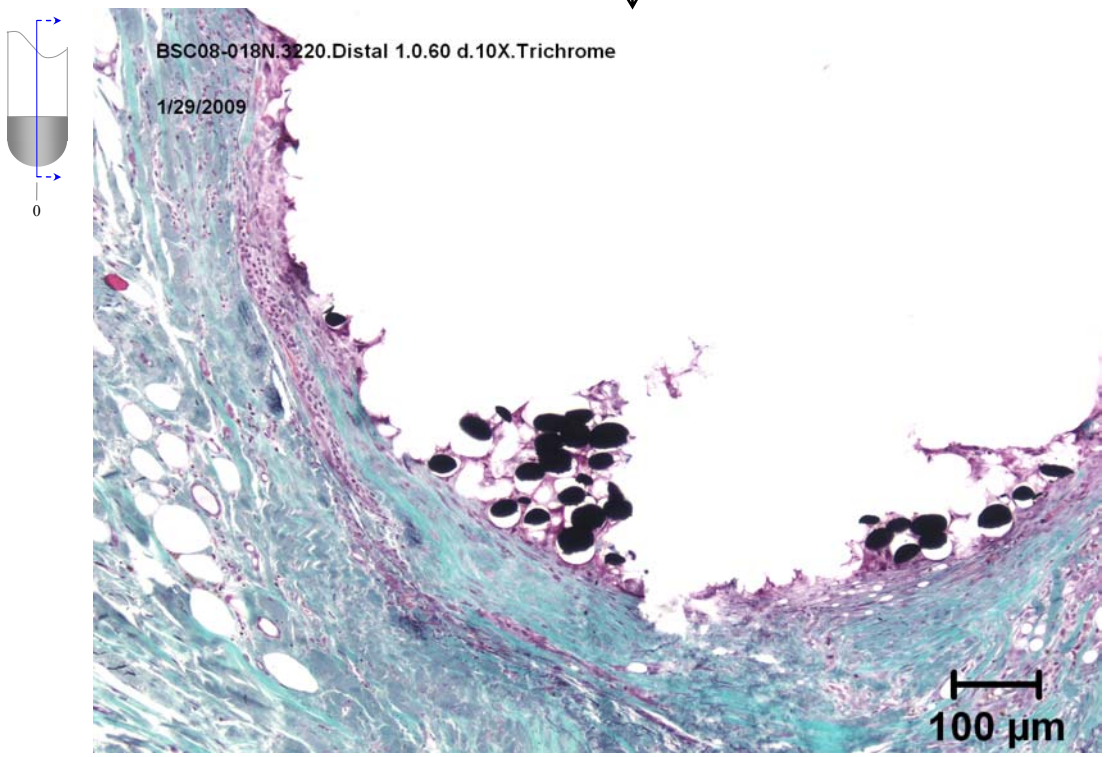
BSC08-018N.3220.Distal 1.0.60 d.10X.Trichrome
1/29/2009
100 µm

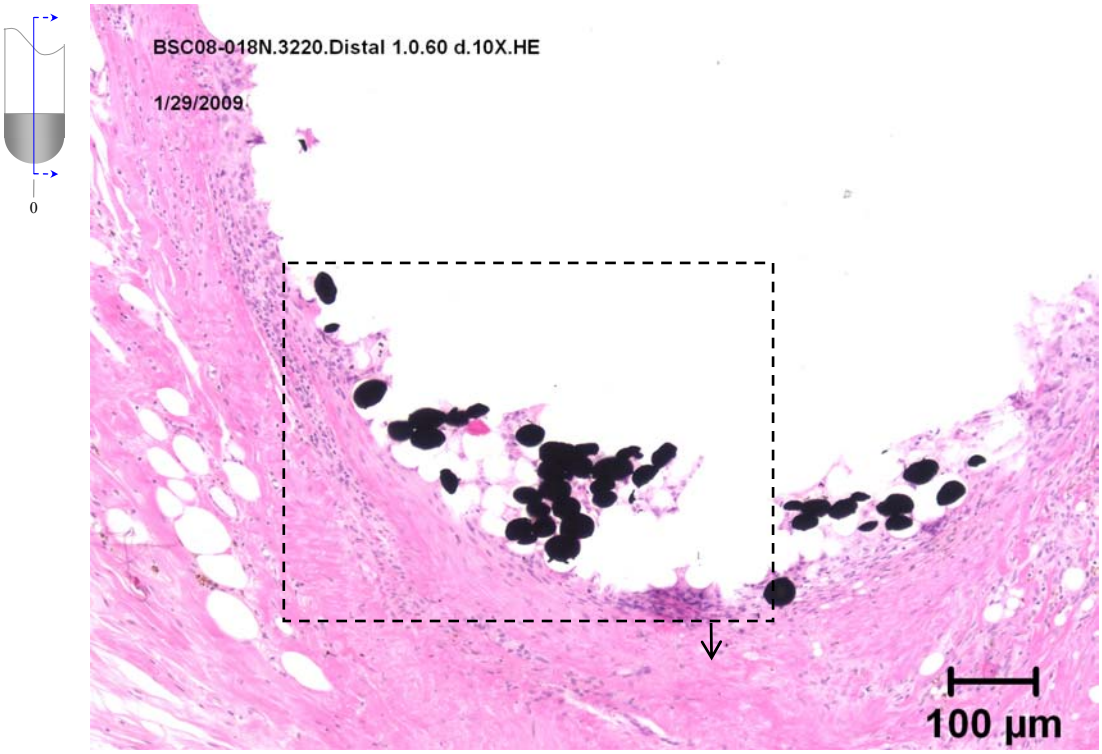
BSC08-018N.3220.Distal 1.0.60 d.10X.HE
1/29/2009
100 µm

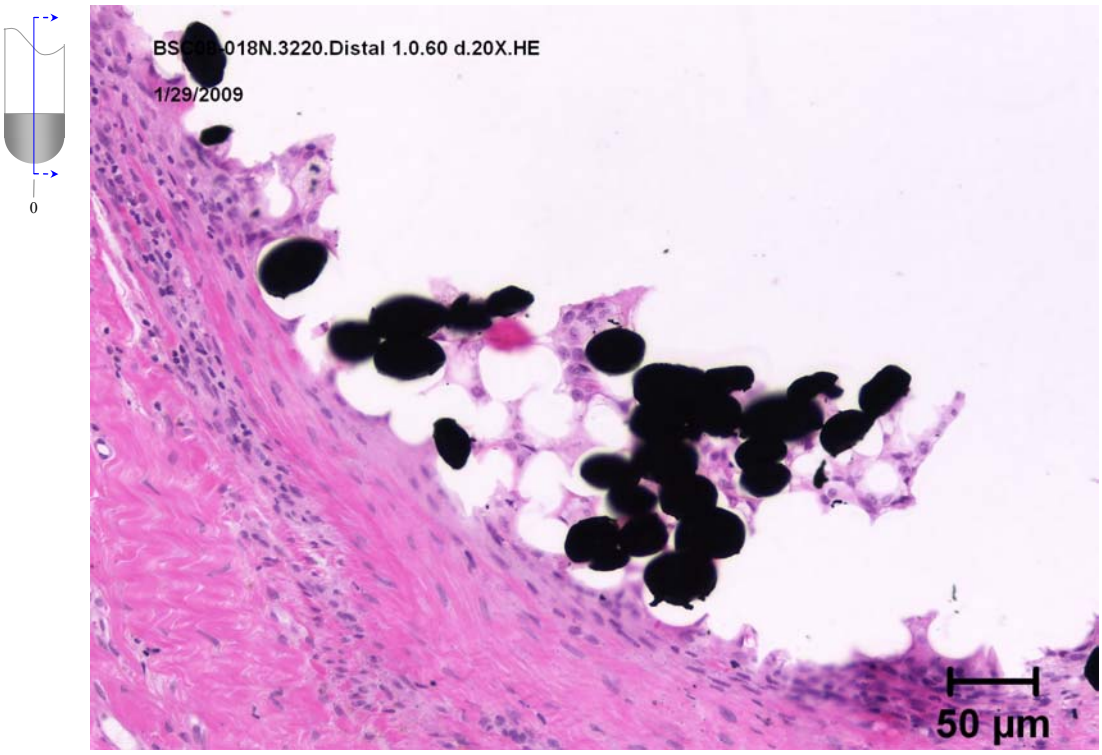
1/29/2009
50 µm

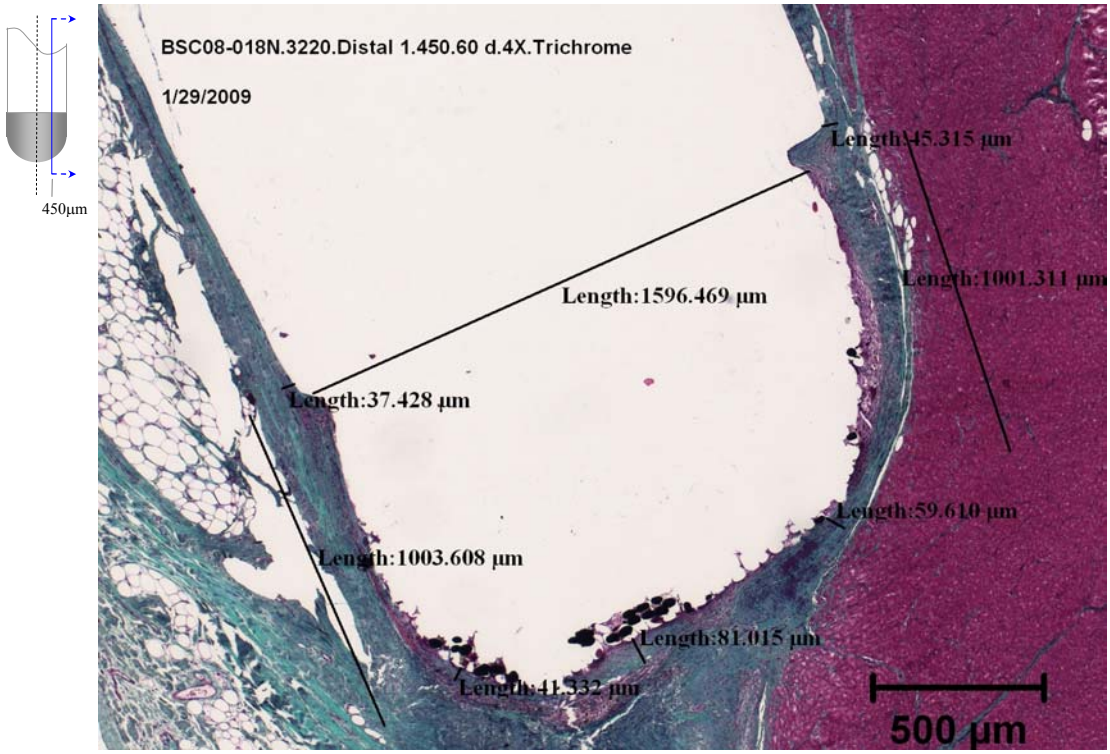
450µm
BSC08-018N.3220.Distal 1.450.60 d.4X.Trichrome
1/29/2009
Length:45.315 µm
Length:1596.469 µm
Length:1001.311 µm
Length:37.428 µm
Length:59.610 µm
Length:1003.608 µm
Length:81.015 µm
Length:41.332 µm
500 µm

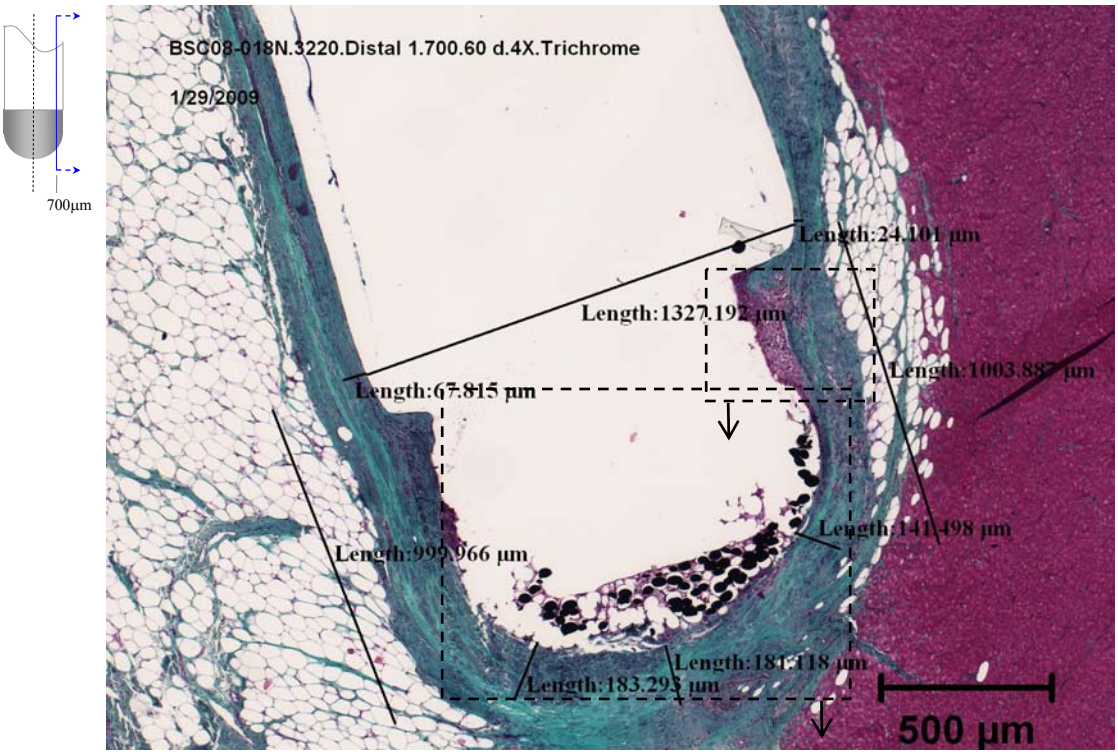
700µm
BSC08-018N.3220.Distal 1.700.60 d.4X.Trichrome
1/29/2009
Length:24.101 µm
Length:1327.192 µm
Length:1003.887 µm
Length:67.815 µm
Length:141.498 µm
Length:999.966 µm
Length:181.118 µm
Length:183.295 µm
500 µm

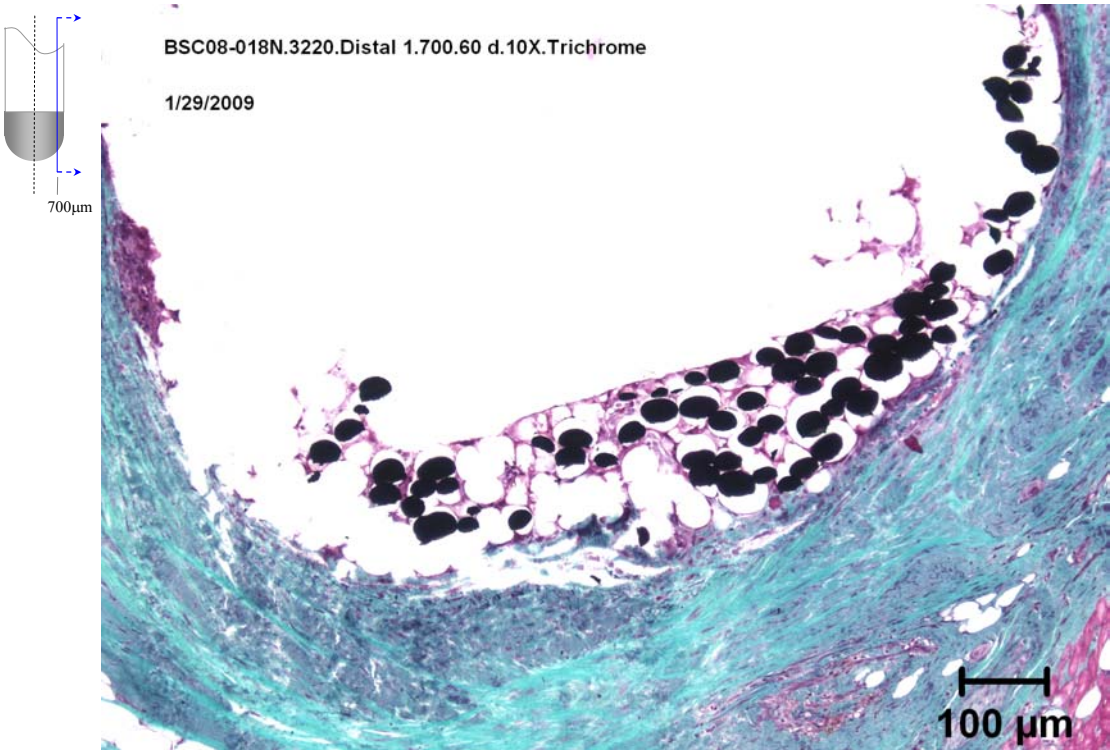
700µm
BSC08-018N.3220.Distal 1.700.60 d.10X.Trichrome
1/29/2009
100 µm

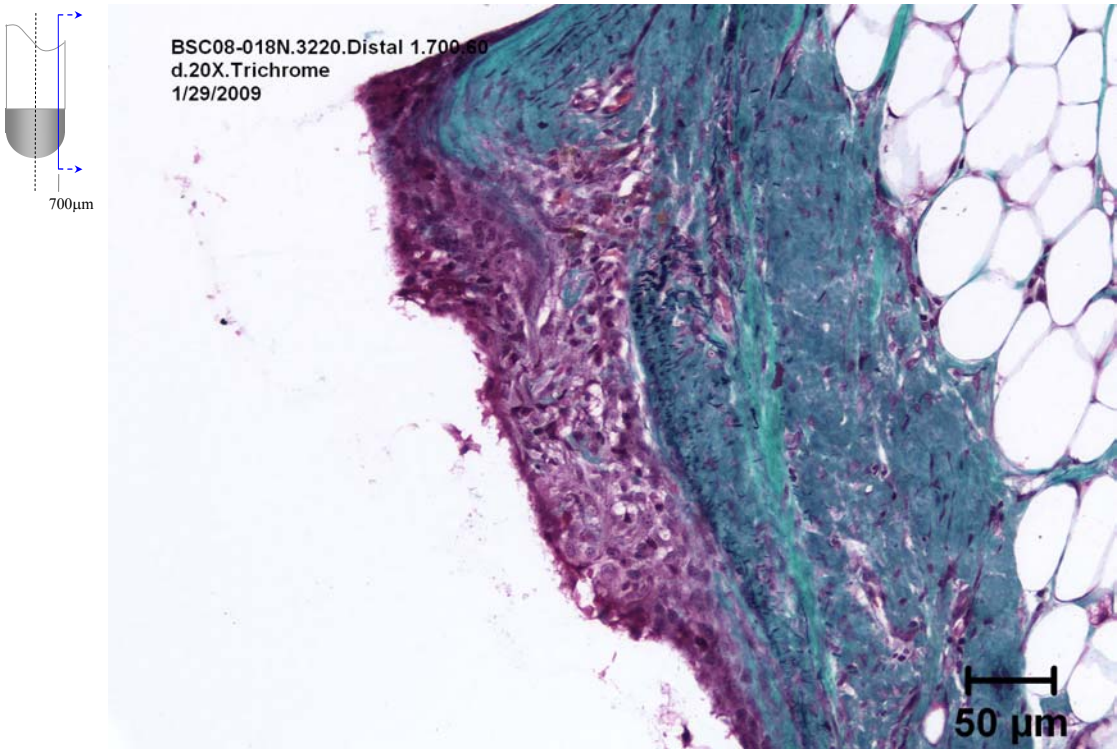
700µm
BSC08-018N.3220.Distal 1.700.60
d.20X.Trichrome
1/29/2009
50 µm

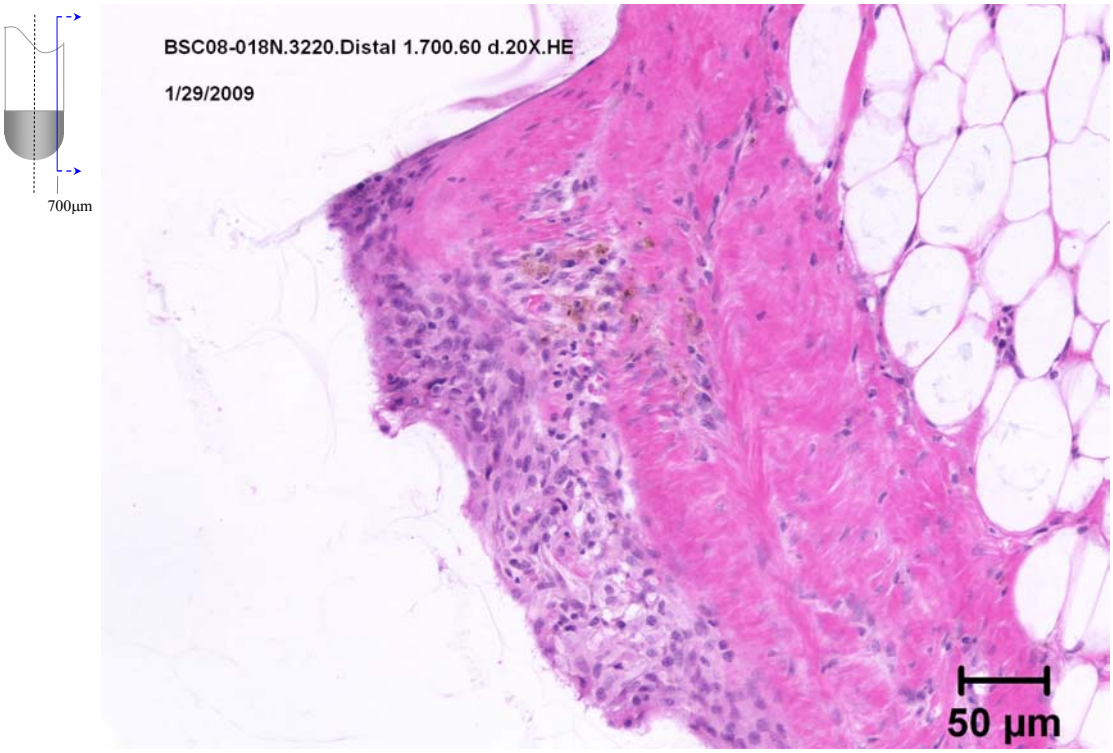
700µm
BSC08-018N.3220.Distal 1.700.60 d.20X.HE
1/29/2009
50 µm

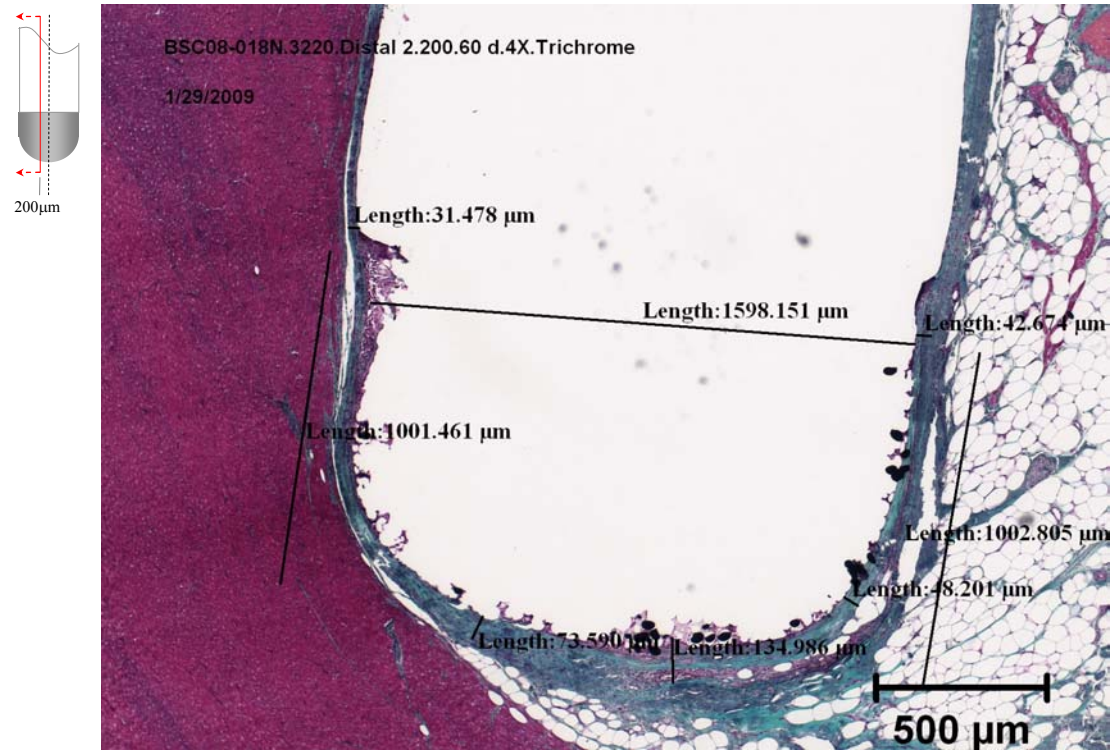
200µm
BSC08-018N.3220.Distal 2.200.60 d.4X.Trichrome
1/29/2009
Length:31.478 µm
Length:1598.151 µm
Length:42.674 µm
Length:1001.461 µm
Length:1002.805 µm
Length:48.201 µm
Length:73.590 µm
Length:134.986 µm
500 µm

Summary Study Information for Animal L-3221, Lead 164025 (Porous Tip Electrode)

Lead Tip Images*

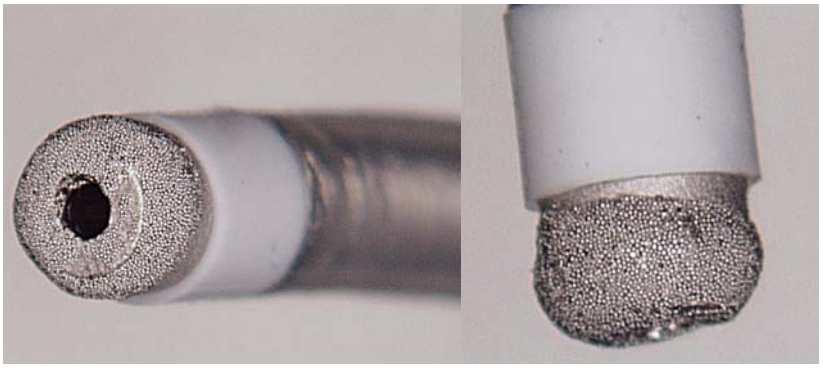

* Steroid eluting collars were initially assembled onto the lead in error (and are shown in the images), though they were later removed and replaced with silicone tubing of the same length, thickness, and diameters as the steroid collars, but with no steroid.

Implant Fluoroscopy Images

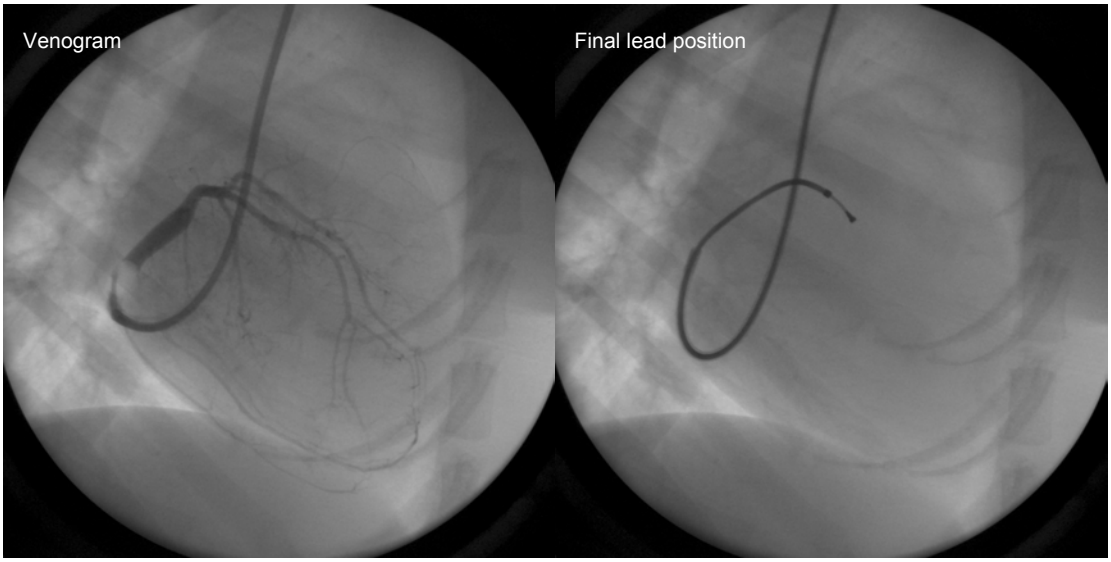

Study Data

Animal ID	Source	Date	Day	Thr. [V]	Thr. Change [V]	R-Wave [mV]	Imp. [Ω]	Movement [cm]	Tip Pos. [cm]
L-3221	PSA Ring	5/28/2008	0	2.1		11.3	1396		
Lead ID	PSA Tip	5/28/2008	0	0.9		17.0	1000		
164025	PG	5/28/2008	0	1.4	0.0	9.8	520	0	0
Tip Electrode	PG	5/30/2008	2	1.7	0.3	12.3	470	0	0
Porous	PG	6/4/2008	7	1.4	0.0	13.7	500	0	0
	PG	6/9/2008	12	1.4	0.0	11.6	560	0	0
	PG	6/16/2008	19	1.6	0.2	12.3	680	0	0
	PG	6/23/2008	26	1.9	0.5	10.0	700	0	0
	PG	7/7/2008	40	2.3	0.9	11.9	770	0	0
	PG	7/25/2008	58	2.5	1.1	11.4	880	0	0
	PSA Ring	7/25/2008	58	2.6	0.5	23.0	1188		

Histology

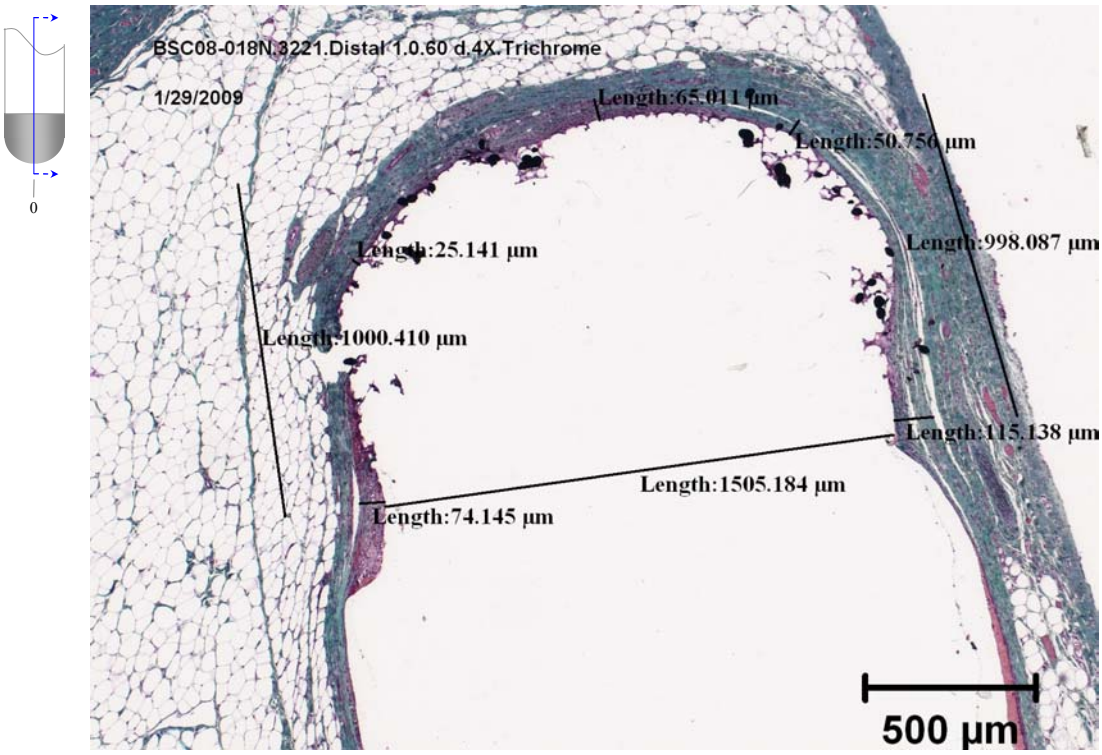
0
BSC08-018N.3221.Distal 1.0.60 d.4X.Trichrome
1/29/2009
Length:65.011 µm
Length:50.756 µm
Length:25.141 µm
Length:998.087 µm
Length:1000.410 µm
Length:115.138 µm
Length:1505.184 µm
Length:74.145 µm
500 µm

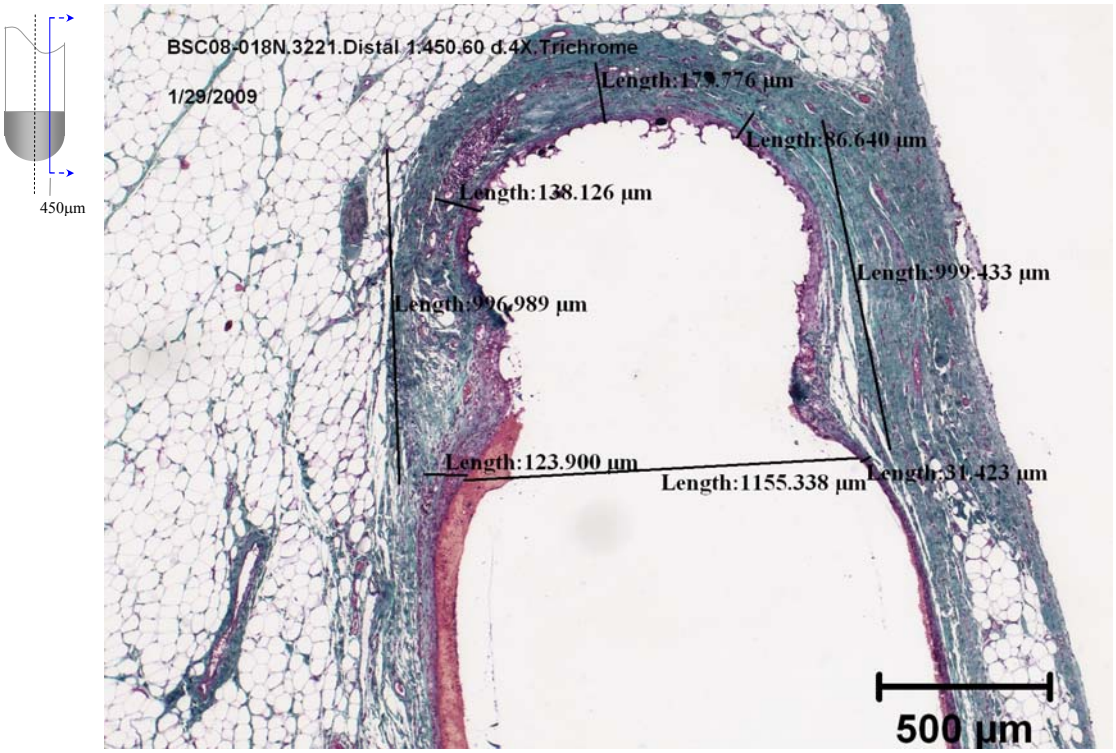
450µm
BSC08-018N.3221.Distal 1.450.60 d.4X.Trichrome
1/29/2009
Length:179.776 µm
Length:86.640 µm
Length:138.126 µm
Length:999.433 µm
Length:996.989 µm
Length:123.900 µm
Length:1155.338 µm
Length:31.423 µm
500 µm

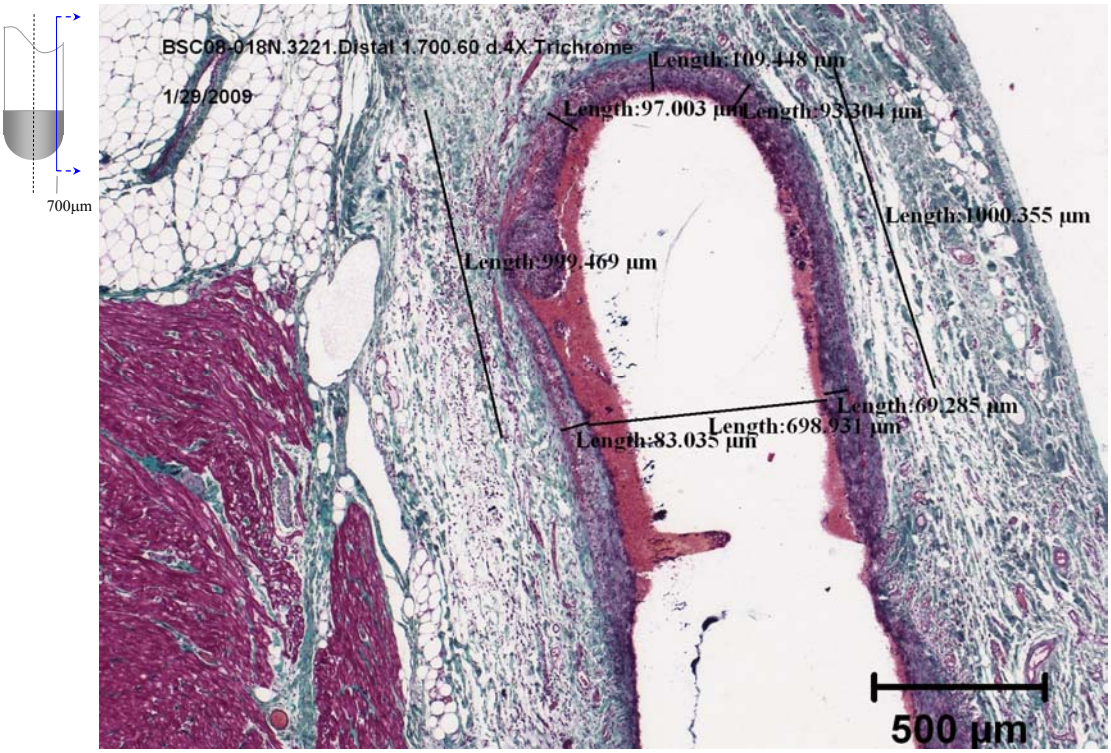
700µm
BSC08-018N.3221.Distal 1.700.60 d.4X.Trichrome
1/29/2009
Length:109.448 µm
Length:97.003 µm
Length:93304 µm
Length:1000.355 µm
Length:999.469 µm
Length:69.285 µm
Length:698.931 µm
Length:83.035 µm
500 µm

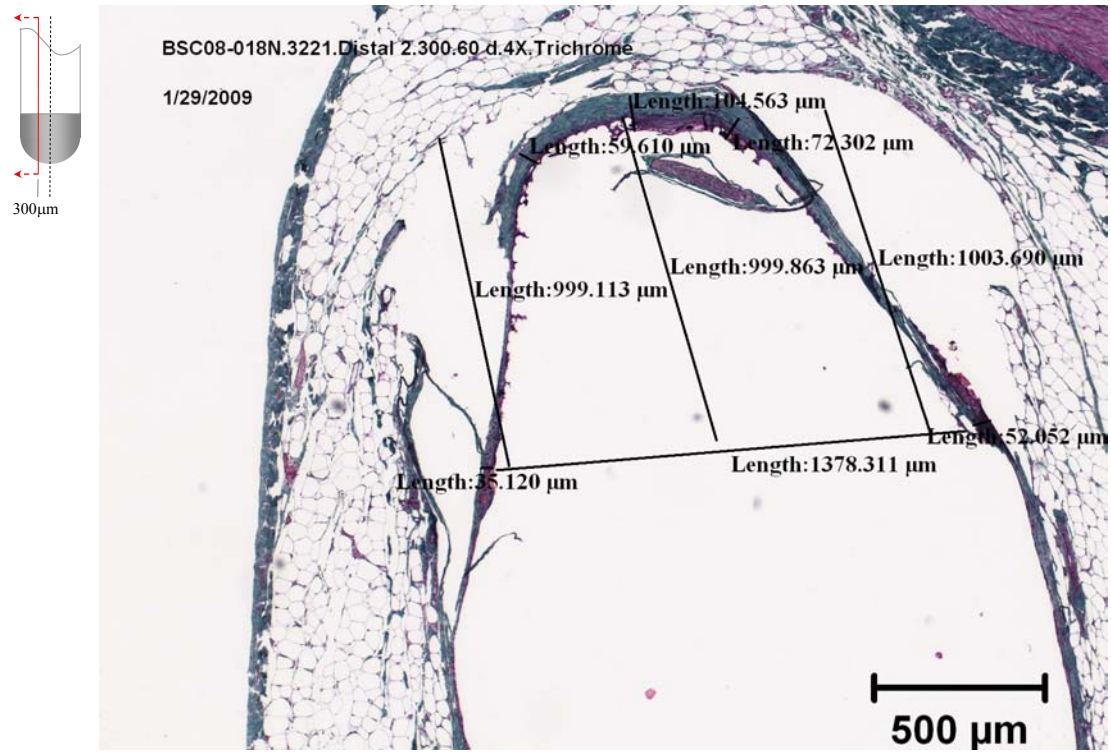
300µm
BSC08-018N.3221.Distal 2.300.60 d.4X.Trichrome
1/29/2009
Length:104.563 µm
Length:59.610 µm
Length:72.302 µm
Length:999.863 µm
Length:1003.690 µm
Length:999.113 µm
Length:52.052 µm
Length:1378.311 µm
Length:35.120 µm
500 µm

Summary Study Information for Animal L-3222, Lead 163921 (Solid Tip Electrode)

Implant Fluoroscopy Images

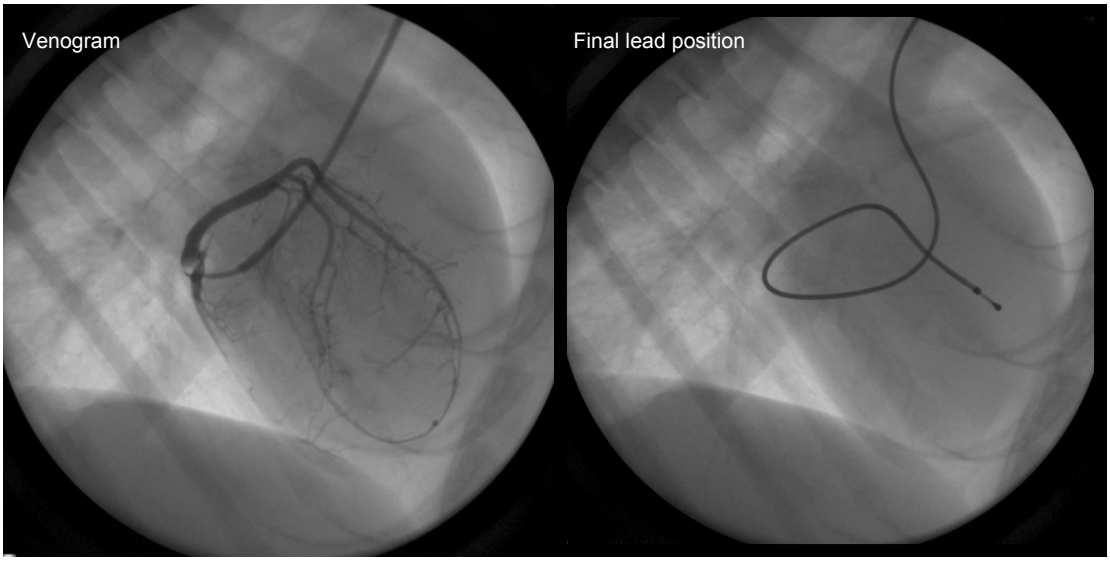

Study Data

Animal ID	Source	Date	Day	Thr. [V]	Thr. Change [V]	R-Wave [mV]	Imp. [Ω]	Movement [cm]	Tip Pos. [cm]
L-3222	PSA Ring	5/28/2008	0	0.8		16.9	1208		
Lead ID	PSA Tip	5/28/2008	0	0.5		20.6	1048		
163921	PG	5/28/2008	0	0.3	0.0	11.6	600	0	0
Tip Electrode	PG	5/30/2008	2	1.0	0.7	15.0	500	0	0
Solid	PG	6/4/2008	7	1.9	1.6	14.6	500	0	0
	PG	6/9/2008	12	1.9	1.6	12.8	490	0	0
	PG	6/16/2008	19	1.7	1.4	15.0	580	0.5	-0.5
	PG	6/23/2008	26	1.4	1.1	13.7	560	0	-0.5
	PG	7/7/2008	40	1.2	0.9	15.0	580	0	-0.5
	PG	7/25/2008	58	0.9	0.6	16.4	600	0	-0.5
	PSA Ring	7/25/2008	58	3.0	2.2	19.0	972		

Lead Retractions

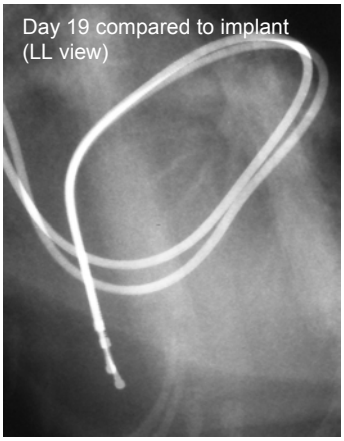

Histology

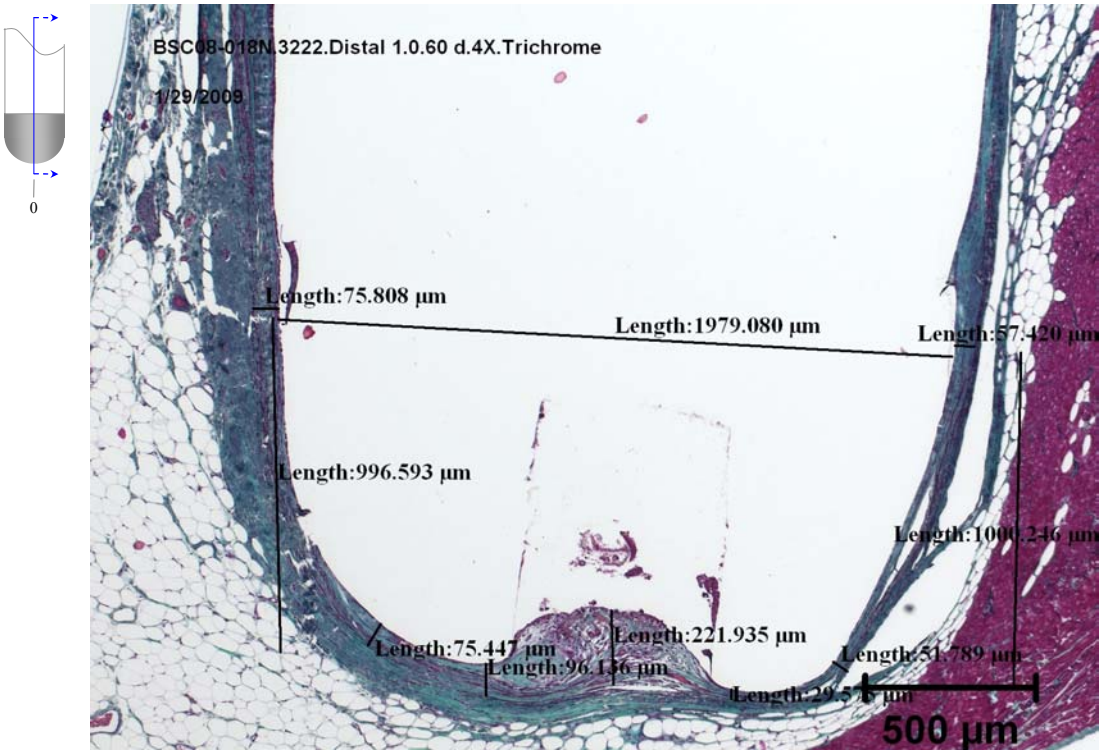
0
BSC08-018N.3222.Distal 1.0.60 d.4X.Trichrome
1/29/2009
Length:75.808 µm
Length:1979.080 µm
Length:57.420 µm
Length:996.593 µm
Length:1000.246 µm
Length:75.447 µm
Length:221.935 µm
Length:96.136 µm
Length:51.789 µm
500 µm

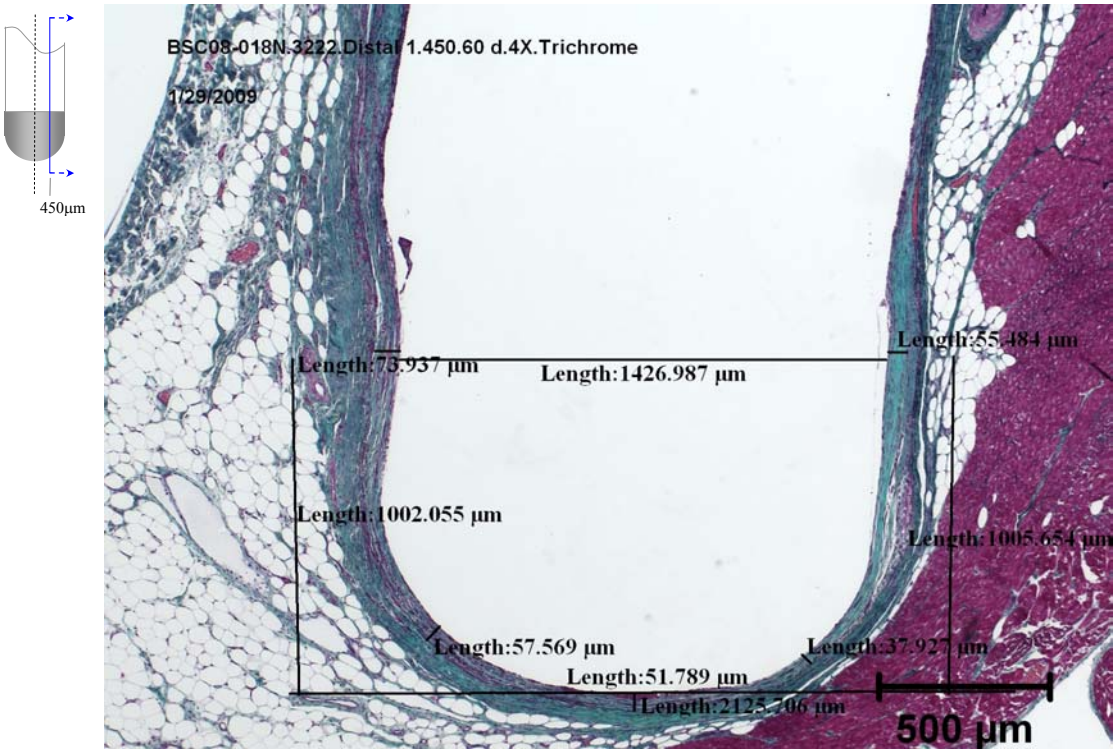
450µm
BSC08-018N.3222.Distal 1.450.60 d.4X.Trichrome
1/29/2009
Length:55.484 µm
Length:75.937 µm
Length:1426.987 µm
Length:1002.055 µm
Length:1005.654 µm
Length:57.569 µm
Length:37.927 µm
Length:51.789 µm
Length:2125.706 µm
500 µm

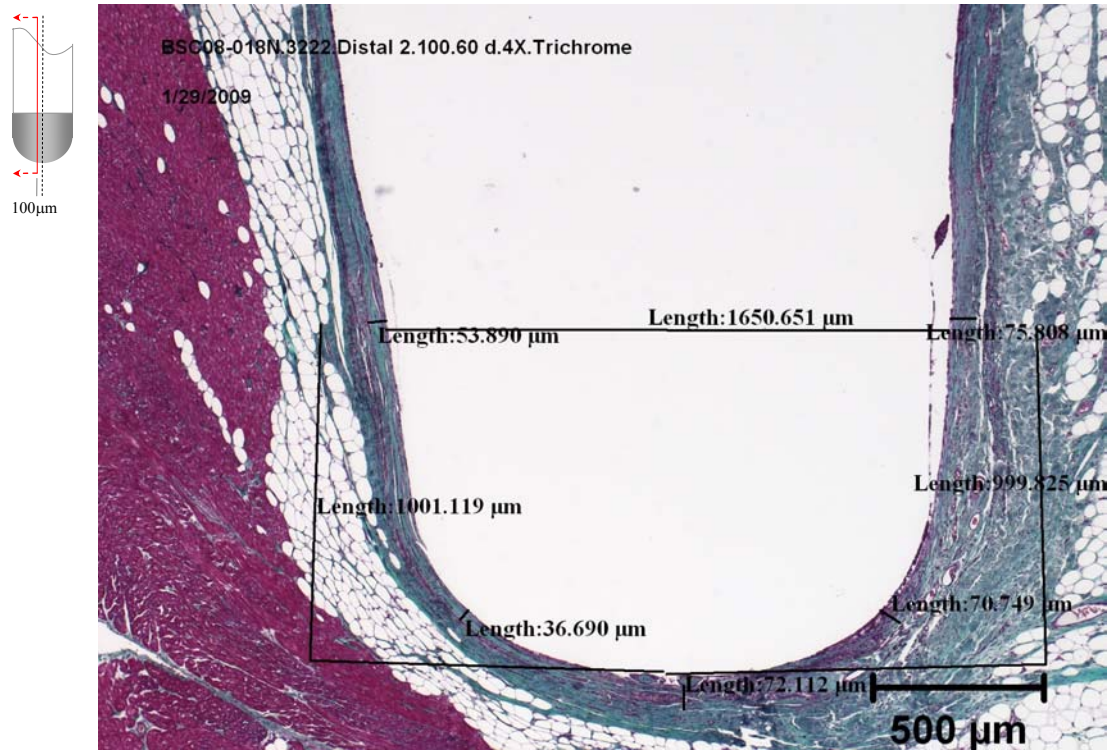
100µm
BSC08-018N.3222.Distal 2.100.60 d.4X.Trichrome
1/29/2009
Length:53.890 µm
Length:1650.651 µm
Length:75.808 µm
Length:1001.119 µm
Length:999.825 µm
Length:36.690 µm
Length:70.749 µm
Length:72.112 µm
500 µm

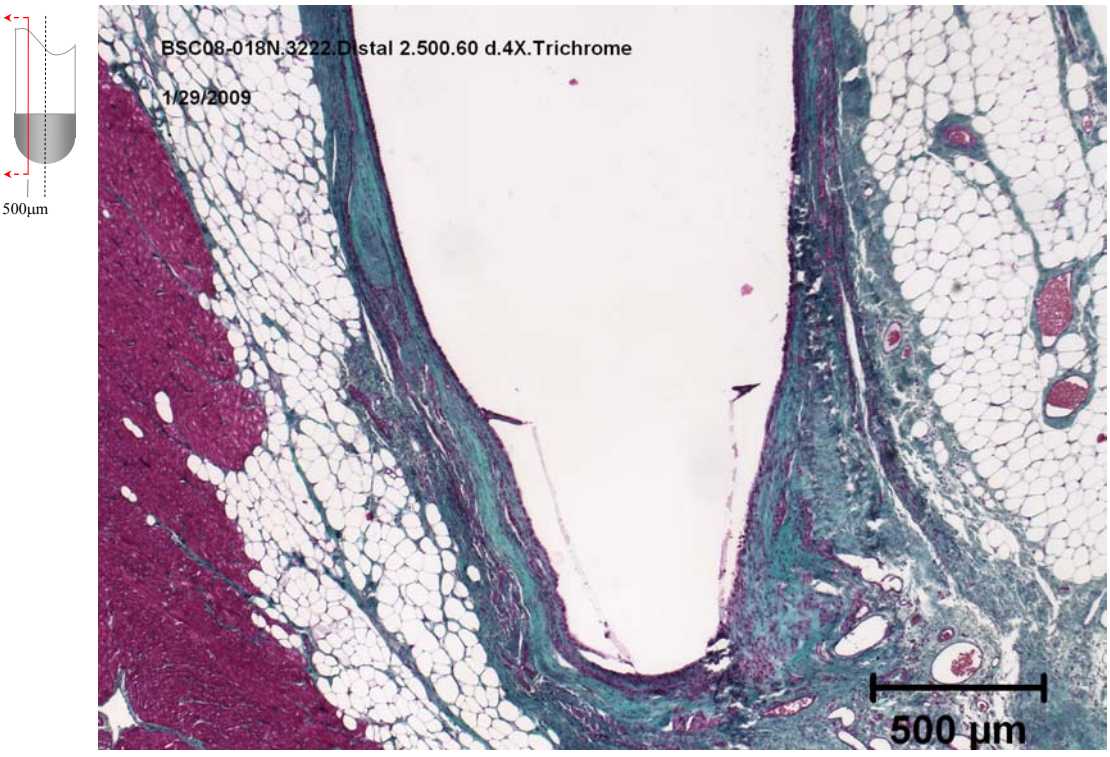
500µm
BSC08-018N.3222.Distal 2.500.60 d.4X.Trichrome
1/29/2009
500 µm

Summary Study Information for Animal L-3223, Lead 163936 (Solid Tip Electrode)

Implant Fluoroscopy Images

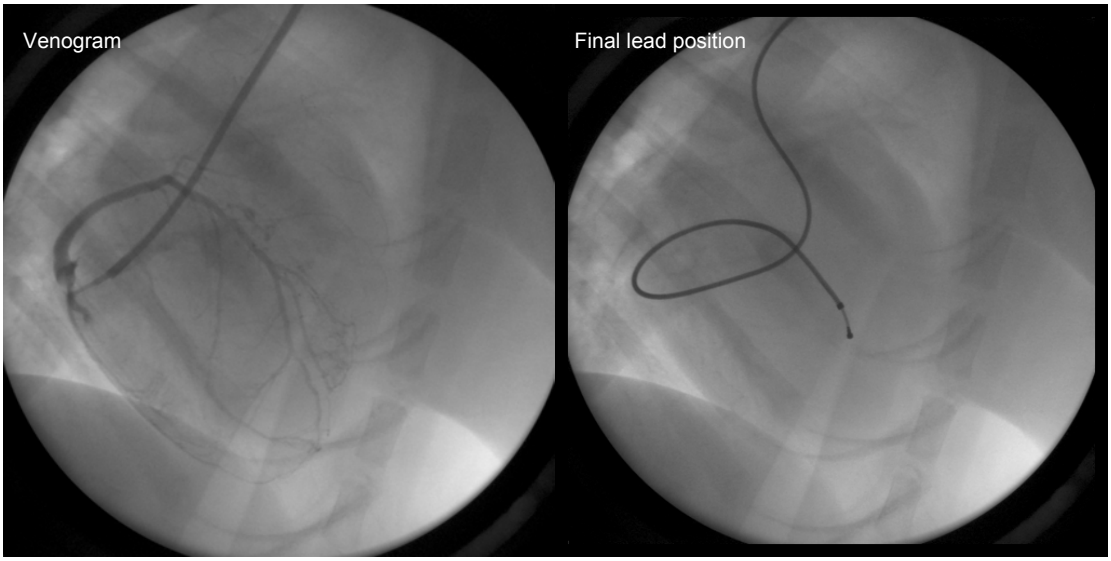

Study Data

Animal ID	Source	Date	Day	Thr. [V]	Thr. Change [V]	R-Wave [mV]	Imp. [Ω]	Movement [cm]	Tip Pos. [cm]
L-3223	PSA Ring	5/28/2008	0	1.1		15.4	1008		
Lead ID	PSA Tip	5/28/2008	0	0.6		19.1	872		
163936	PG	5/28/2008	0	0.4	0.0	*12.0*	490	0	0
Tip Electrode	PG	5/30/2008	2	1.0	0.6	14.6	410	0	0
Solid	PG	6/4/2008	7	1.6	1.2	13.7	460	0	0
	PG	6/9/2008	12	1.9	1.5	13.7	470	0	0
	PG	6/16/2008	19	1.7	1.3	9.6	480	2	-2
	PG	6/23/2008	26	1.8	1.4	11.7	530	0	-2
	PG	7/7/2008	40	2.2	1.8	10.4	640	1	-3
	PG	7/25/2008	58	1.2	0.8	11.4	660	0	-3
	PSA Ring	7/25/2008	58	3.7	2.6	14.5	880		

Lead Retractions

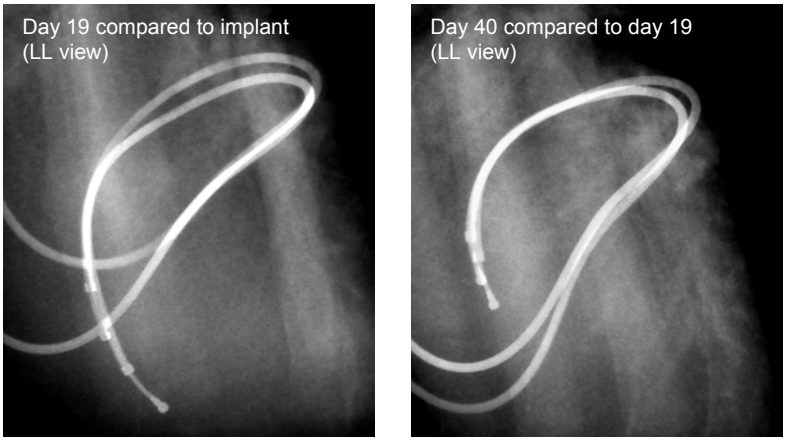

Histology

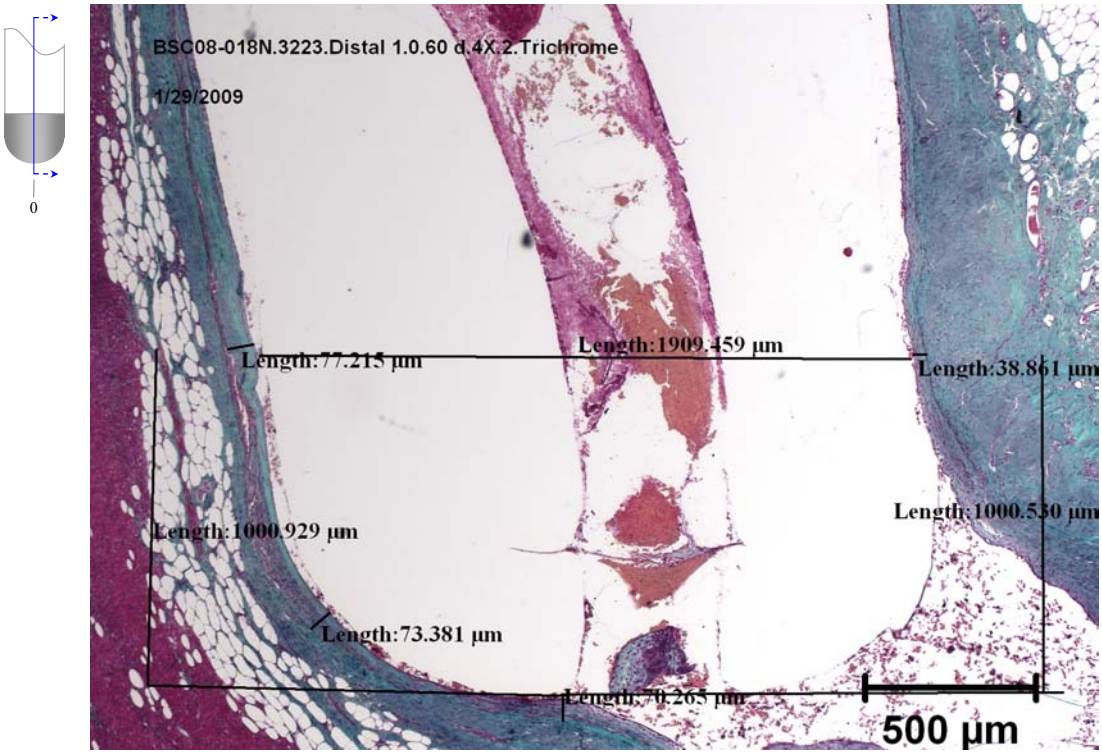
0
BSC08-018N.3223.Distal 1.0.60 d.4X.2.Trichrome
1/29/2009
Length:77.215 µm
Length:1909.459 µm
Length:38.861 µm
Length:1000.530 µm
Length:1000.929 µm
Length:73.381 µm
Length:70.265 µm
500 µm

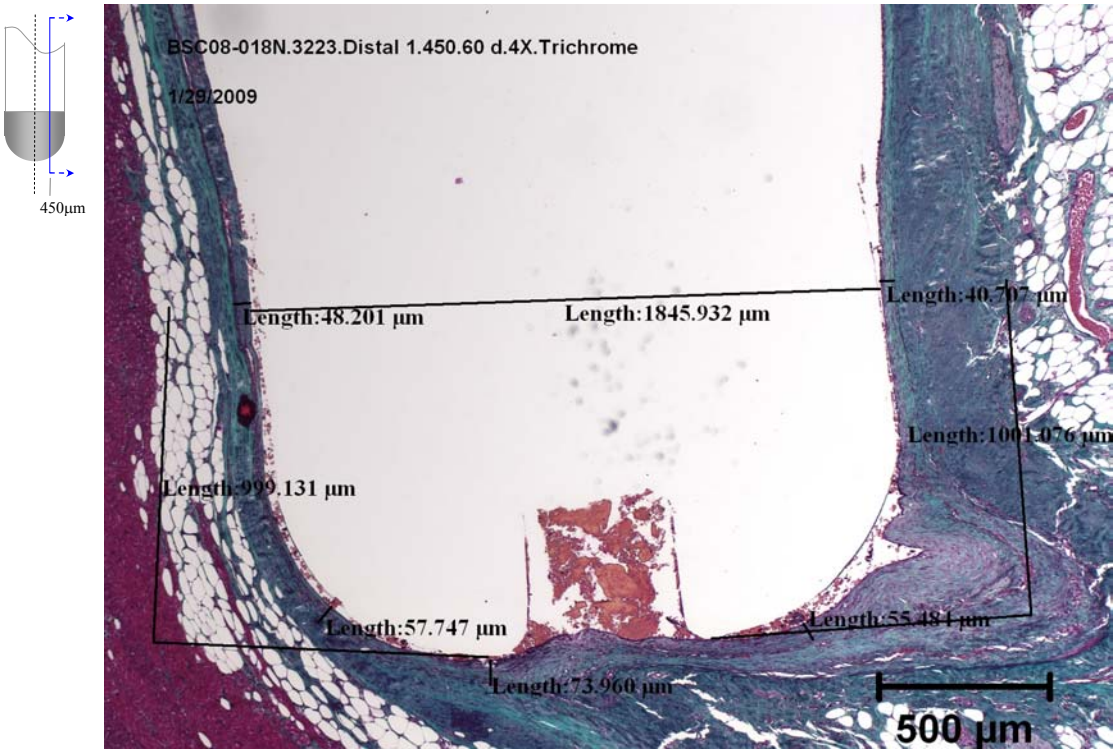
450µm
BSC08-018N.3223.Distal 1.450.60 d.4X.Trichrome
1/29/2009
Length:48.201 µm
Length:1845.932 µm
Length:40.707 µm
Length:1001.076 µm
Length:999.131 µm
Length:57.747 µm
Length:55.481 µm
Length:73.960 µm
500 µm

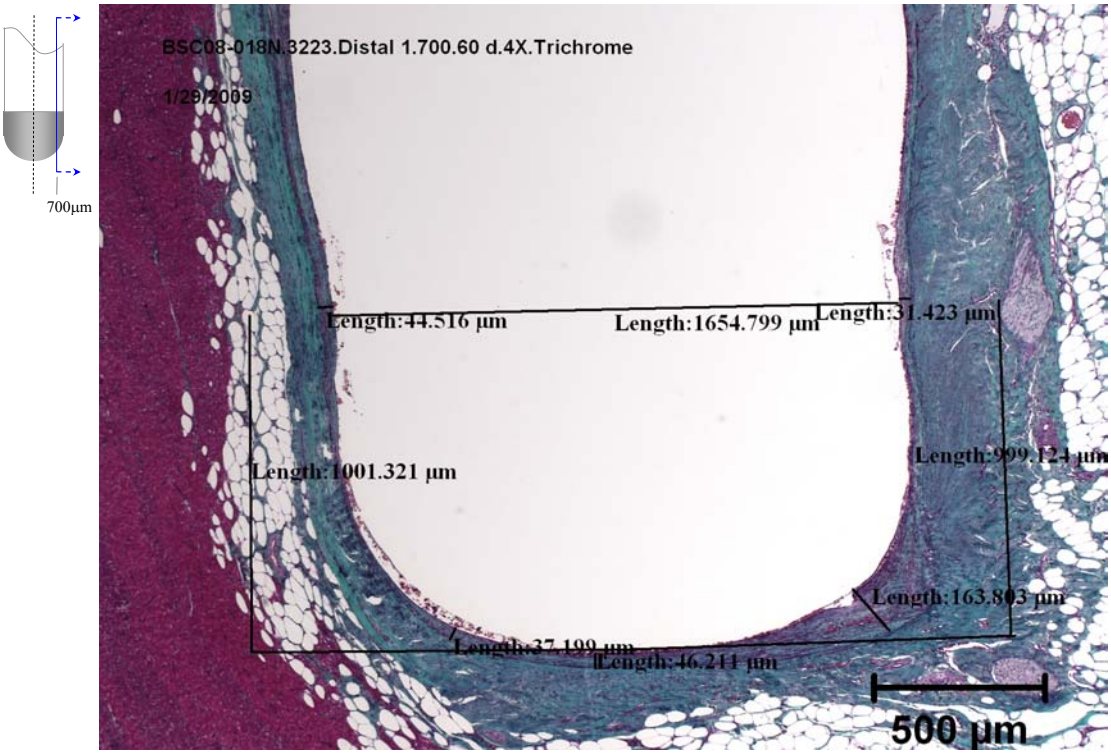
700µm
BSC08-018N.3223.Distal 1.700.60 d.4X.Trichrome
1/29/2009
Length:44.516 µm
Length:1654.799 µm
Length:31.423 µm
Length:1001.321 µm
Length:999.124 µm
Length:163.803 µm
Length:37.199 µm
Length:46.211 µm
500 µm

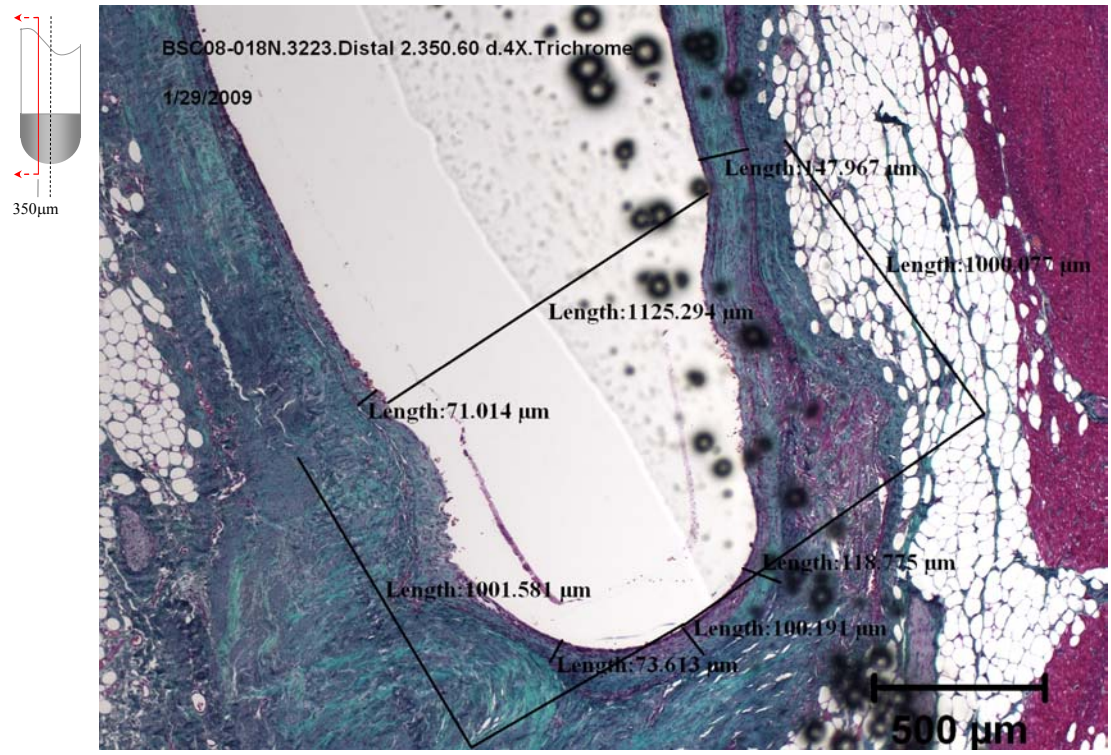
350µm
BSC08-018N.3223.Distal 2.350.60 d.4X.Trichrome
1/29/2009
Length:147.967 µm
Length:1000.077 µm
Length:1125.294 µm
Length:71.014 µm
Length:118.775 µm
Length:1001.581 µm
Length:100.191 µm
Length:73.613 µm
500 µm

Summary Study Information for Animal L-3224, Lead 163952 (Solid Tip Electrode)

Implant Fluoroscopy Images

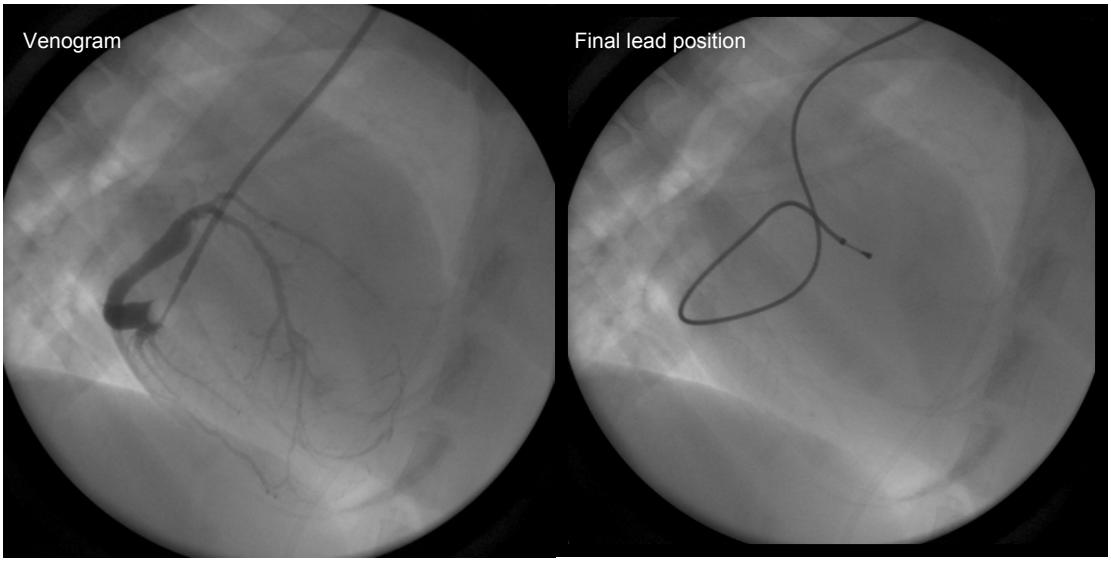

Study Data

Animal ID	Source	Date	Day	Thr. [V]	Thr. Change [V]	R-Wave [mV]	Imp. [Ω]	Movement [cm]	Tip Pos. [cm]
L-3224	PSA Ring	5/29/2008	0	1.2		15.1	1772		
Lead ID	PSA Tip	5/29/2008	0	0.8		20.3	1424		
163952	PG	5/29/2008	0	0.3	0.0	*12.0*	540	0	0
Tip Electrode	PG	6/2/2008	4	1.4	1.1	13.7	420	0	0
Solid	PG	6/6/2008	8	1.5	1.2	13.2	480	0	0
	PG	6/13/2008	15	0.9	0.6	13.2	540	0	0
	PG	6/20/2008	22	1.0	0.7	12.8	540	0	0
	PG	6/27/2008	29	1.4	1.1	13.7	550	1	-1
	PG	7/11/2008	43	1.0	0.7	13.2	540	0	-1
	PG	7/28/2008	60	1.0	0.7	16.4	550	0	-1
	PSA Ring	7/28/2008	60	9.2	8.0	16.5	1332		

Lead Retractions

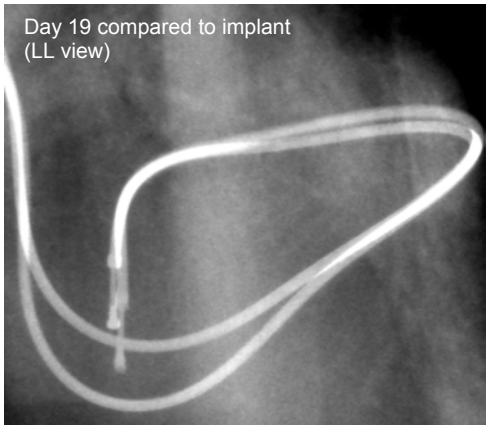

Histology

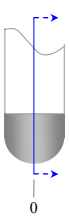
0

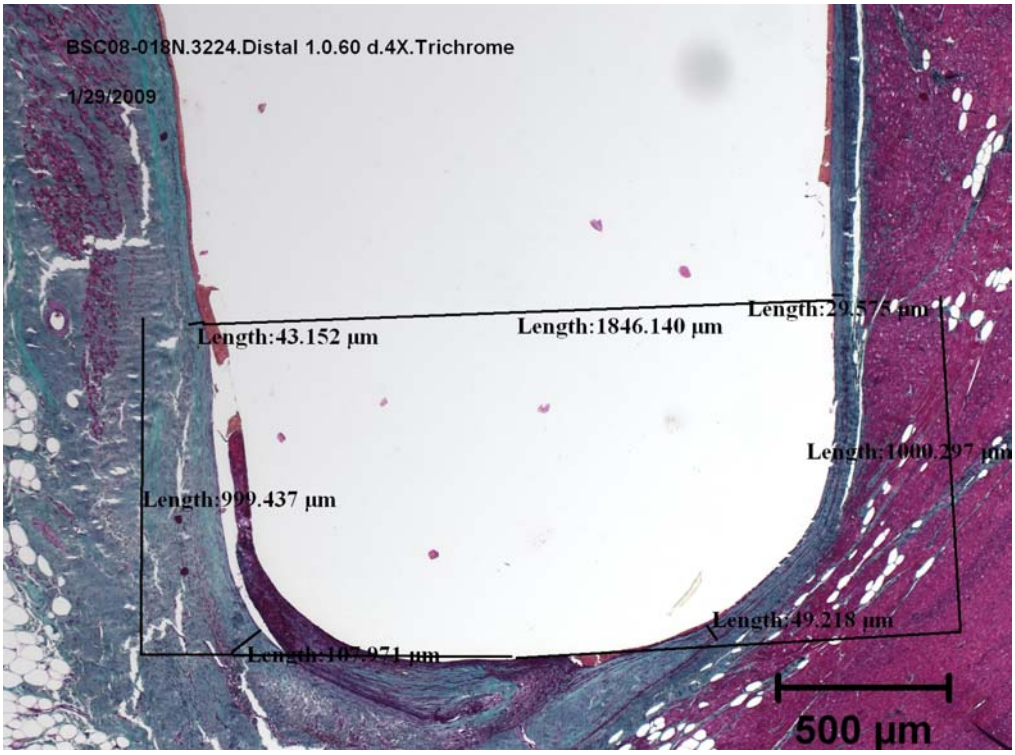
BSC08-018N.3224.Distal 1.0.60 d.4X.Trichrome
1/29/2009
Length:43.152 µm
Length:1846.140 µm
Length:29.575 µm
Length:1000.297 µm
Length:999.437 µm
Length:49.218 µm
500 µm

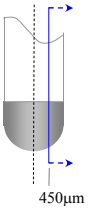
450µm

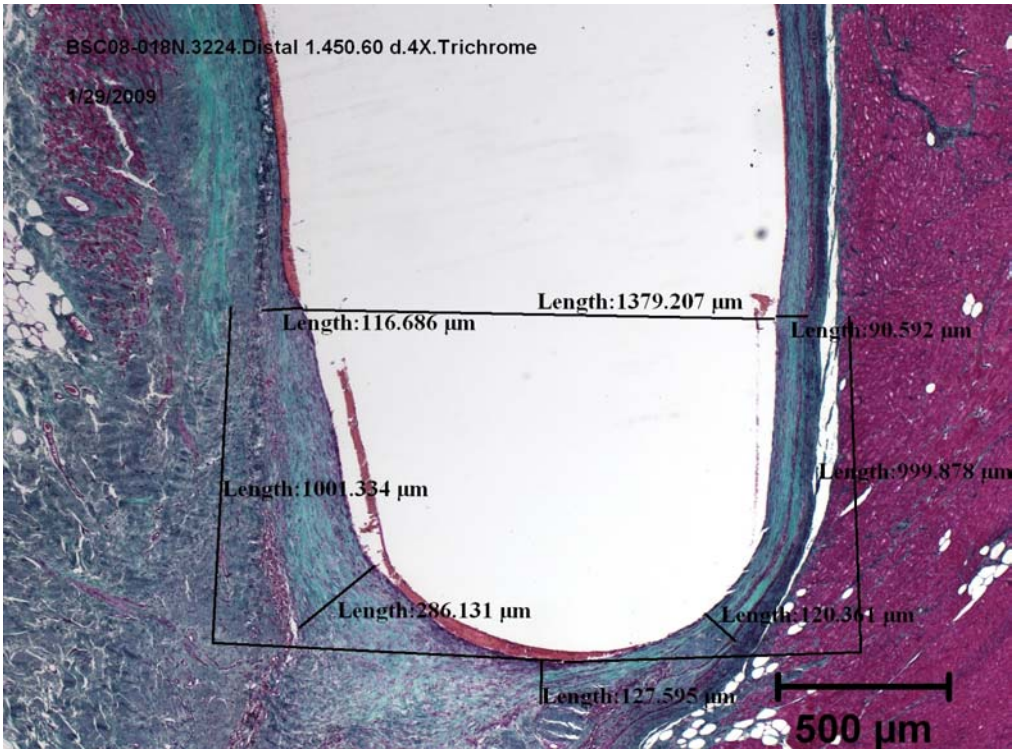
BSC08-018N.3224.Distal 1.450.60 d.4X.Trichrome
1/29/2009
Length:1379.207 µm
Length:116.686 µm
Length:90.592 µm
Length:1001.334 µm
Length:999.878 µm
Length:286.131 µm
Length:120.361 µm
Length:127.595 µm
500 µm

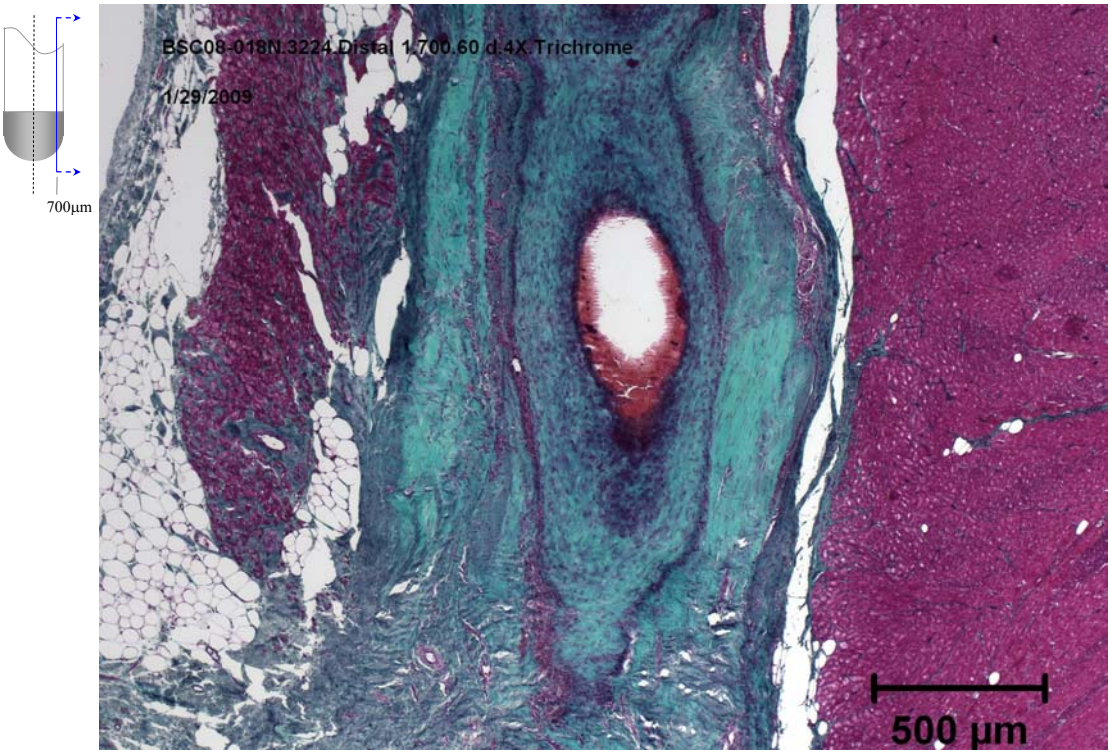
700µm
BSC08-018N.3224.Distal 1.700.60 d.4X.Trichrome
1/29/2009
500 µm

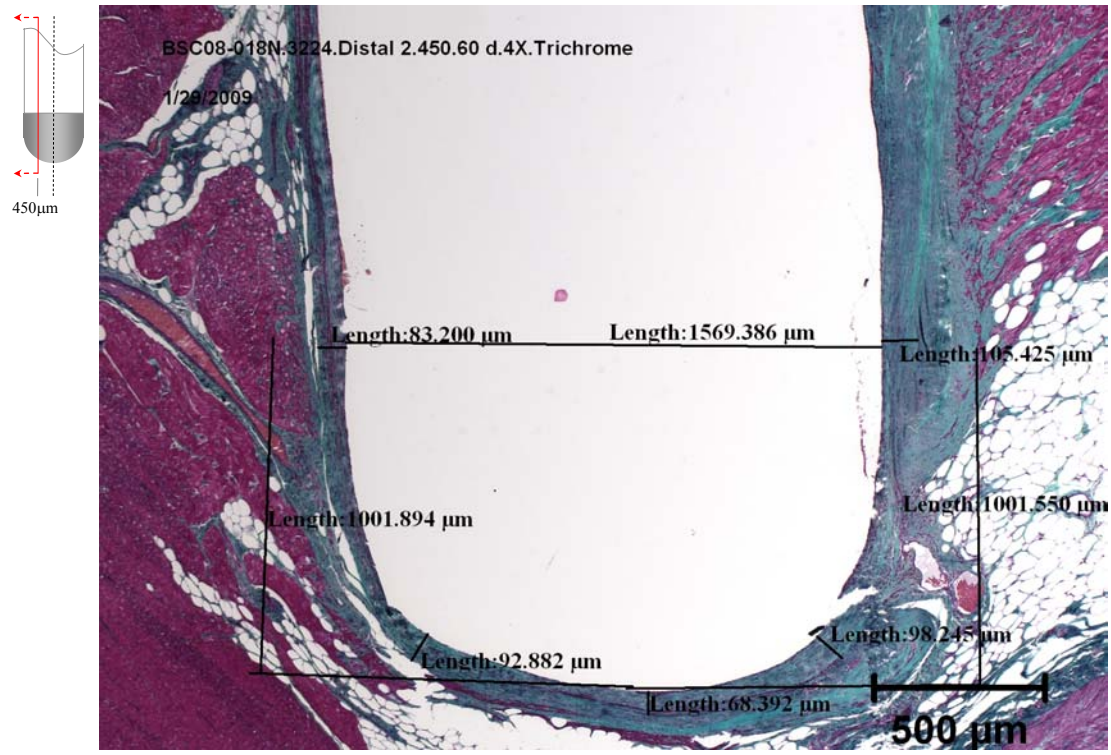
450µm
BSC08-018N.3224.Distal 2.450.60 d.4X.Trichrome
1/29/2009
Length:83.200 µm
Length:1569.386 µm
Length:105.425 µm
Length:1001.894 µm
Length:1001.550 µm
Length:98.245 µm
Length:92.882 µm
Length:68.392 µm
500 µm

Summary Study Information for Animal L-3225, Lead 163926 (Solid Tip Electrode)

Implant Fluoroscopy Images

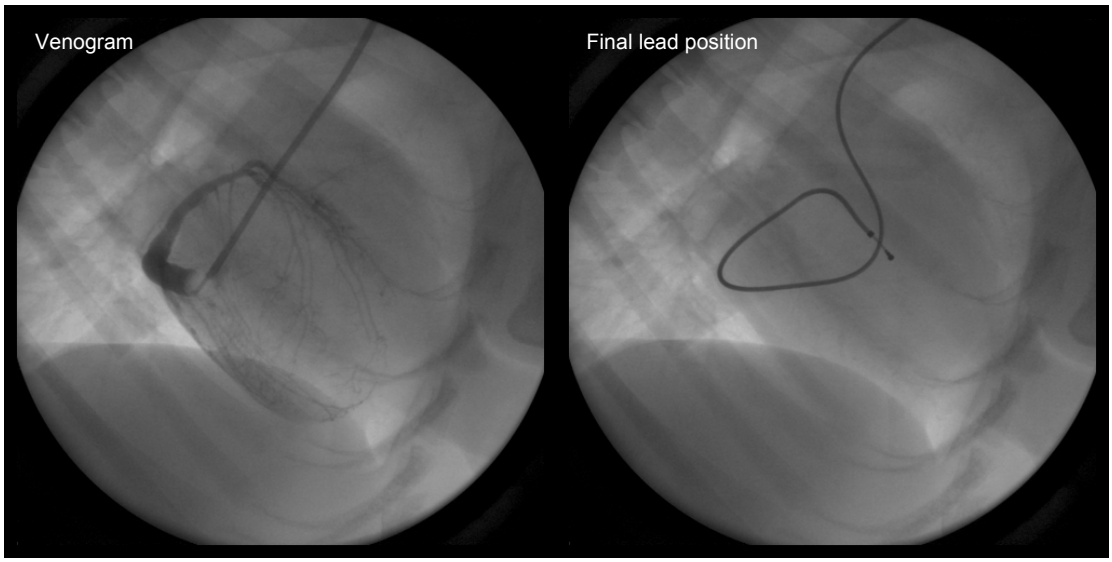

Study Data

Animal ID	Source	Date	Day	Thr. [V]	Thr. Change [V]	R-Wave [mV]	Imp. [Ω]	Movement [cm]	Tip Pos. [cm]
L-3225	PSA Ring	5/29/2008	0	1.5		12.2	1008		
Lead ID	PSA Tip	5/29/2008	0	1.1		20.9	948		
163926	PG	5/29/2008	0	1.0	0.0	11.4	580	0	0
Tip Electrode	PG	6/2/2008	4	2.3	1.3	11.2	460	0	0
Solid	PG	6/6/2008	8	3.3	2.3	11.7	460	0	0
	PG	6/13/2008	15	2.1	1.1	10.3	500	0.5	-0.5
	PG	6/20/2008	22	1.7	0.7	8.3	500	0	-0.5
	PG	6/27/2008	29	1.5	0.5	9.8	520	0	-0.5
	PG	7/11/2008	43	1.1	0.1	9.1	560	0	-0.5
	PG	7/28/2008	60	1.0	0.0	10.6	580	0	-0.5
	PSA Ring	7/28/2008	60	6.7	5.2	16.3	1376		

Lead Retractions

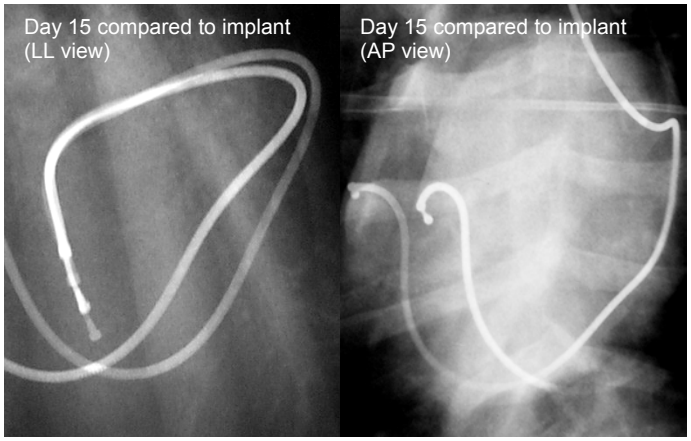

Histology

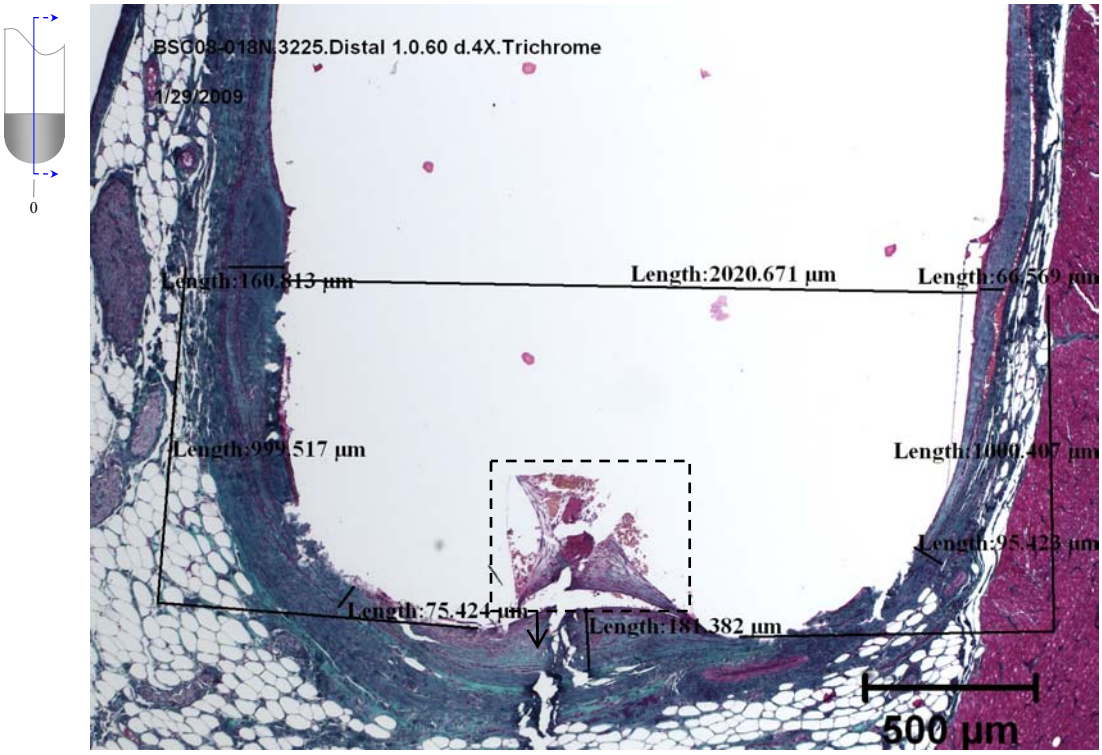
BSC08-018N.3225.Distal 1.0.60 d.4X.Trichrome
1/29/2009
Length:160.813 µm
Length:2020.671 µm
Length:999.517 µm
Length:75.424 µm
Length:181.382 µm
Length:95.423 µm
500 µm

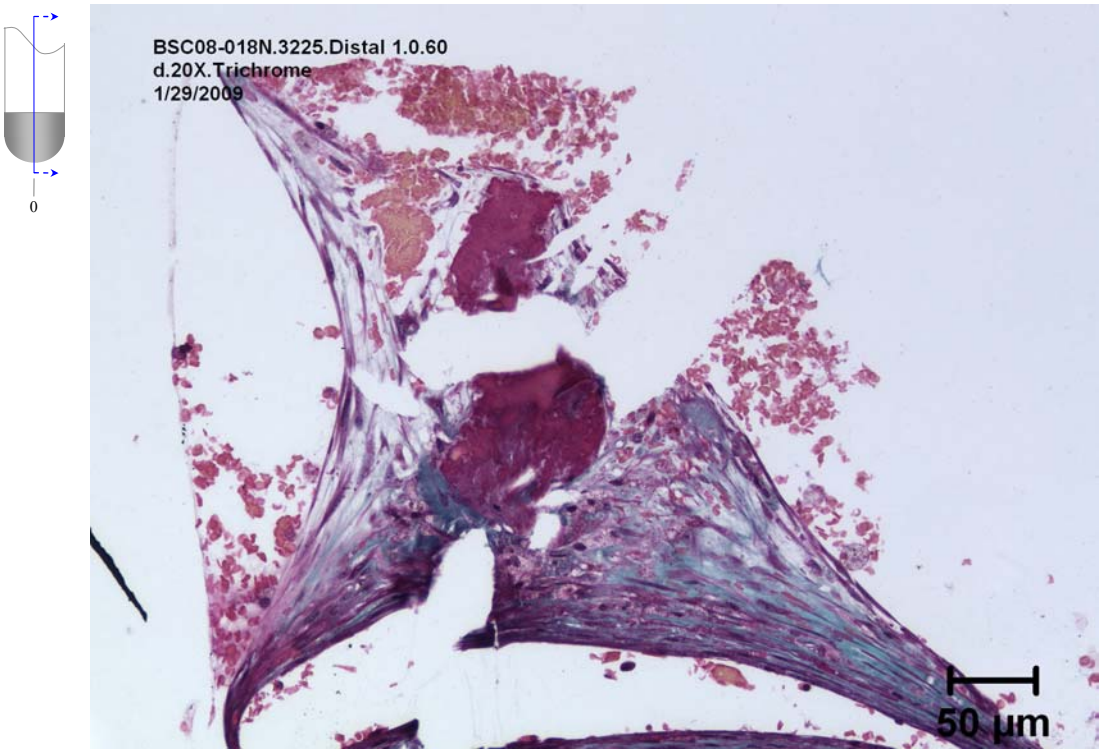
BSC08-018N.3225.Distal 1.0.60
d.20X.Trichrome
1/29/2009
50 µm

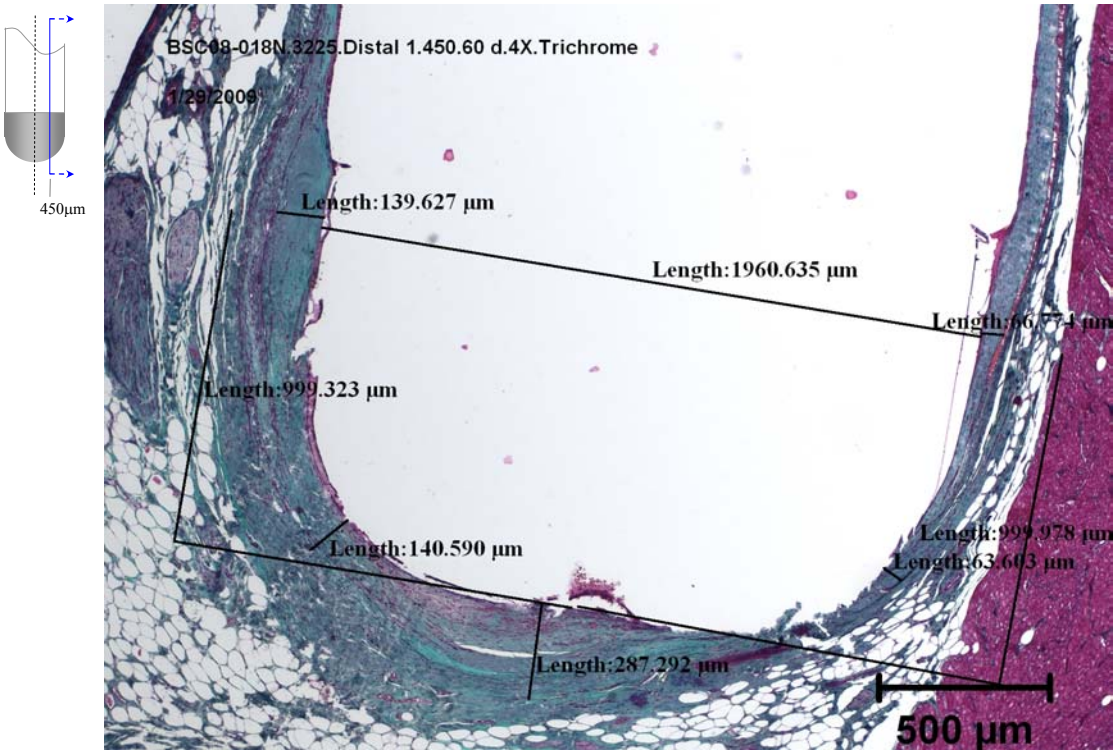
450µm
BSC08-018N.3225.Distal 1.450.60 d.4X.Trichrome
1/29/2009
Length:139.627 µm
Length:1960.635 µm
Length:999.323 µm
Length:140.590 µm
Length:287.292 µm
Length:63.603 µm
500 µm

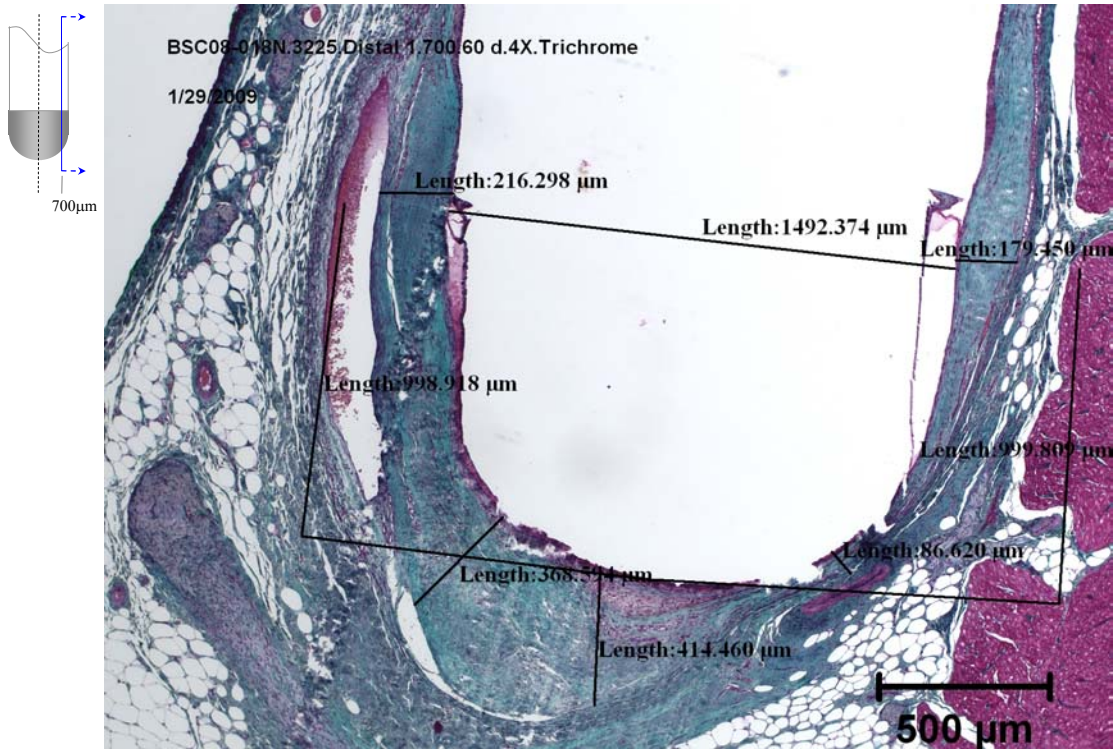
700µm
BSC08-018N.3225.Distal 1.700.60 d.4X.Trichrome
1/29/2009
Length:216.298 µm
Length:1492.374 µm
Length:998.918 µm
Length:86.620 µm
Length:414.460 µm
500 µm

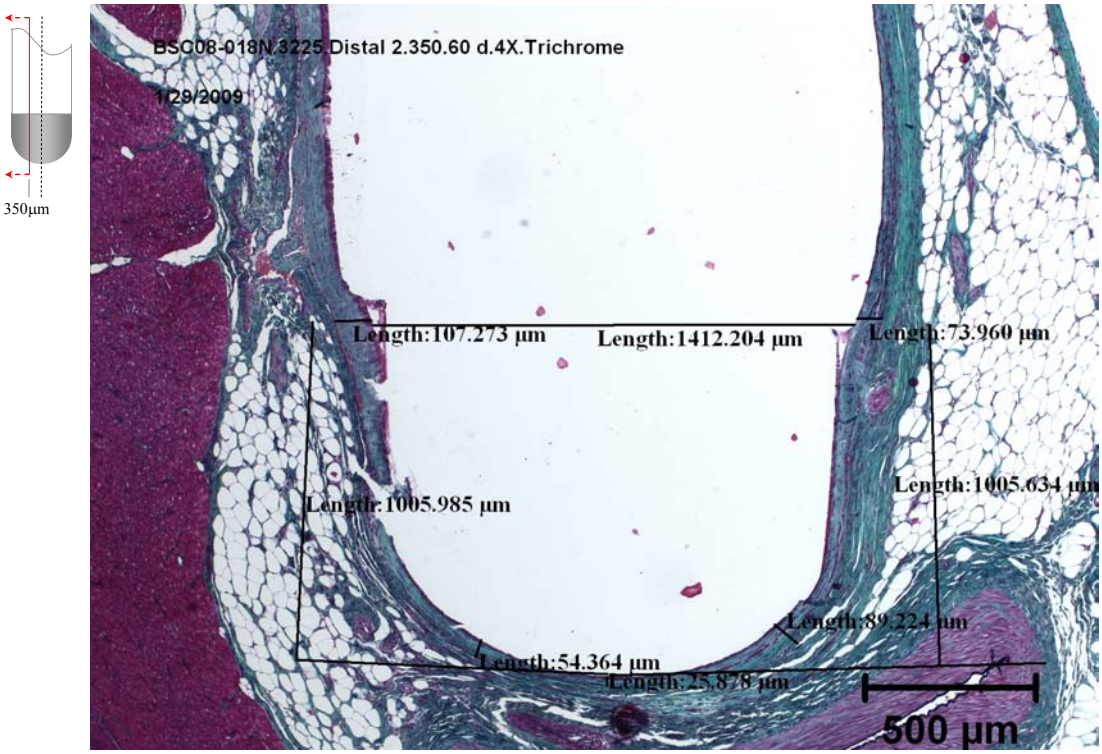
350µm
BSC08-018N.3225.Distal 2.350.60 d.4X.Trichrome
1/29/2009
Length:107.273 µm
Length:1412.204 µm
Length:73.960 µm
Length:1005.985 µm
Length:1005.634 µm
Length:89.224 µm
Length:54.364 µm
Length:25.878 µm
500 µm

Summary Study Information for Animal L-3226, Lead 164009 (Solid Tip Electrode)

Implant Fluoroscopy Images

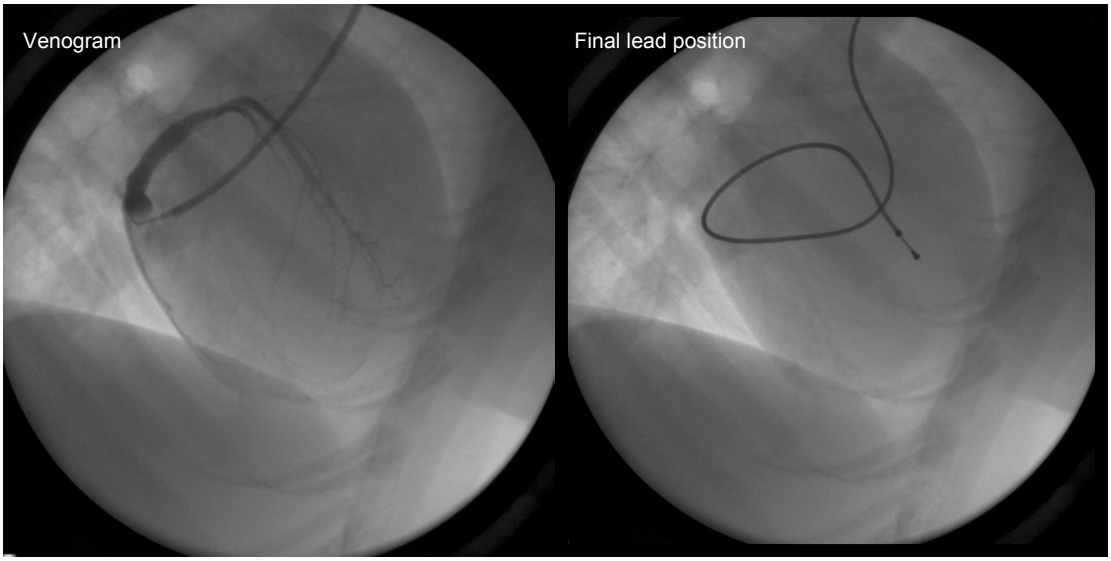

Study Data

Animal ID	Source	Date	Day	Thr. [V]	Thr. Change [V]	R-Wave [mV]	Imp. [Ω]	Movement [cm]	Tip Pos. [cm]
L-3226	PSA Ring	5/29/2008	0	0.7		14.8	1428		
Lead ID	PSA Tip	5/29/2008	0	1.4		21.6	1232		
164009	PG	5/29/2008	0	0.3	0.0	*12.0*	550	0	0
Tip Electrode	PG	6/2/2008	4	2.0	1.7	14.1	480	2	-2
Solid	PG	6/6/2008	8	1.7	1.4	11.1	500	0	-2
	PG	6/13/2008	15	1.9	1.6	10.8	550	0	-2
	PG	6/20/2008	22	1.8	1.5	11.4	560	0	-2
	PG	6/27/2008	29	1.5	1.2	11.9	560	0	-2
	PG	7/11/2008	43	1.4	1.1	12.8	590	0	-2
	PG	7/28/2008	60	1.6	1.3	13.7	620	0	-2
	PSA Ring	7/28/2008	60	2.1	1.4	16.8	828		

Lead Retractions

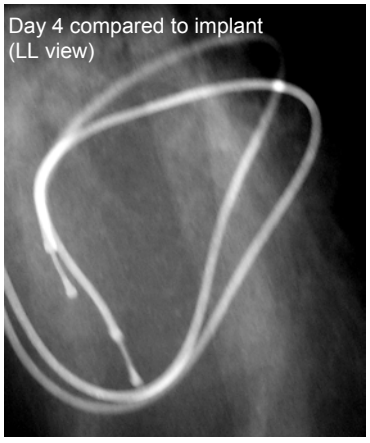

Histology

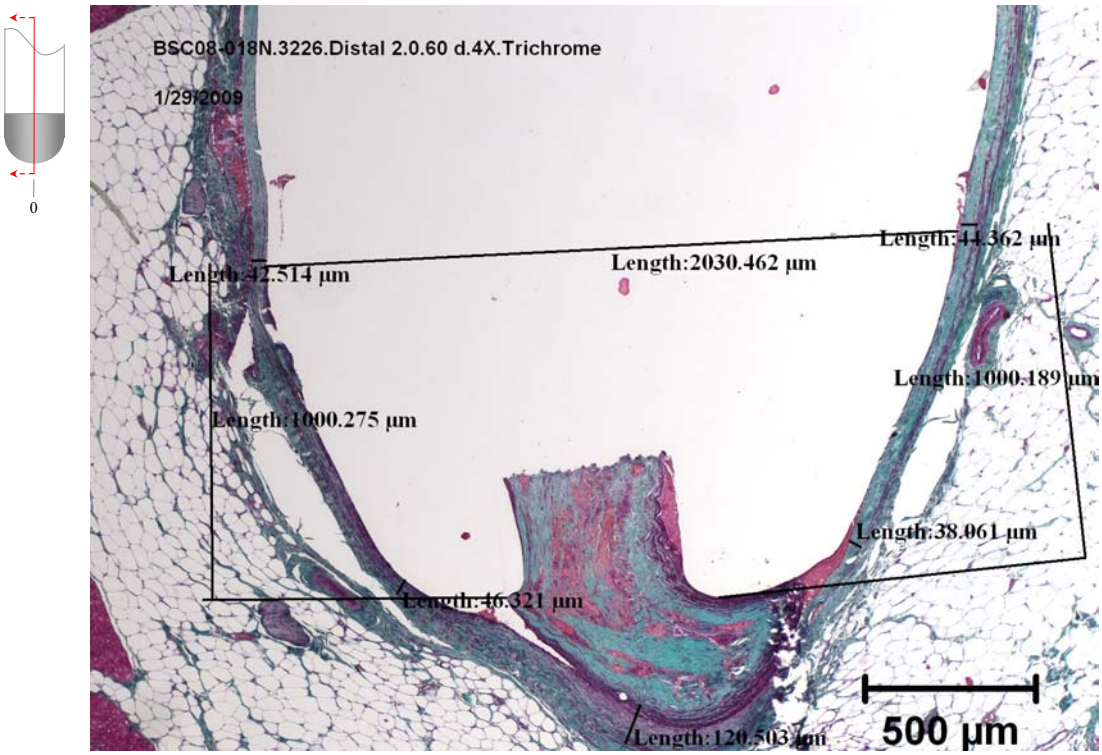
0
BSC08-018N.3226.Distal 2.0.60 d.4X.Trichrome
1/29/2009
Length:42.514 µm
Length:2030.462 µm
Length:44.362 µm
Length:1000.189 µm
Length:1000.275 µm
Length:38.061 µm
Length:46.321 µm
Length:120.503 µm
500 µm

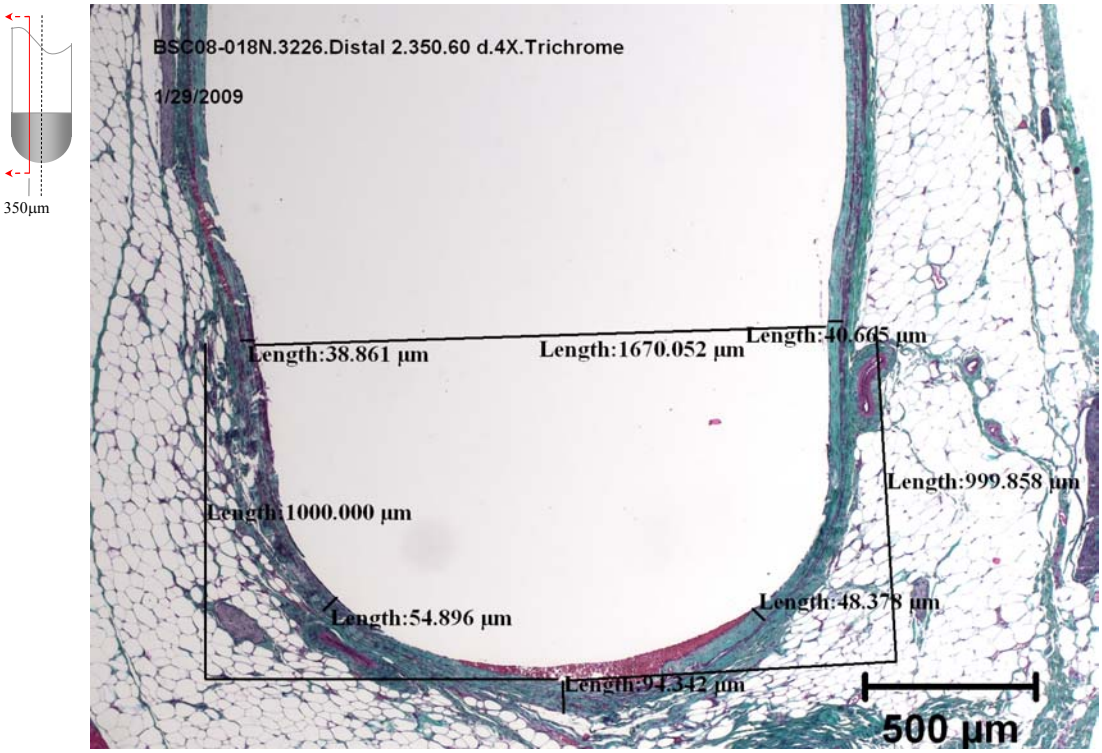
350µm
BSC08-018N.3226.Distal 2.350.60 d.4X.Trichrome
1/29/2009
Length:38.861 µm
Length:1670.052 µm
Length:40.605 µm
Length:999.858 µm
Length:1000.000 µm
Length:54.896 µm
Length:48.378 µm
Length:94.342 µm
500 µm

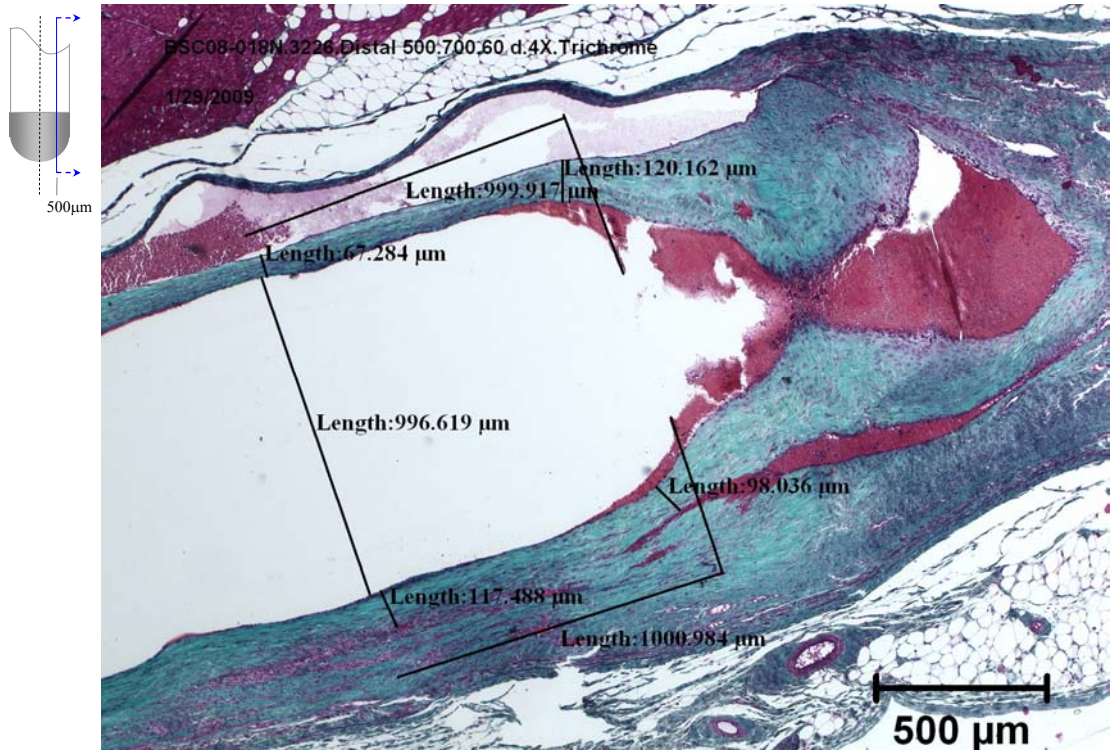
500µm
BSC08-018N.3226.Distal 500.700.60 d.4X.Trichrome
1/29/2009
Length:120.162 µm
Length:999.917 µm
Length:67.284 µm
Length:996.619 µm
Length:98.036 µm
Length:117.488 µm
Length:1000.984 µm
500 µm

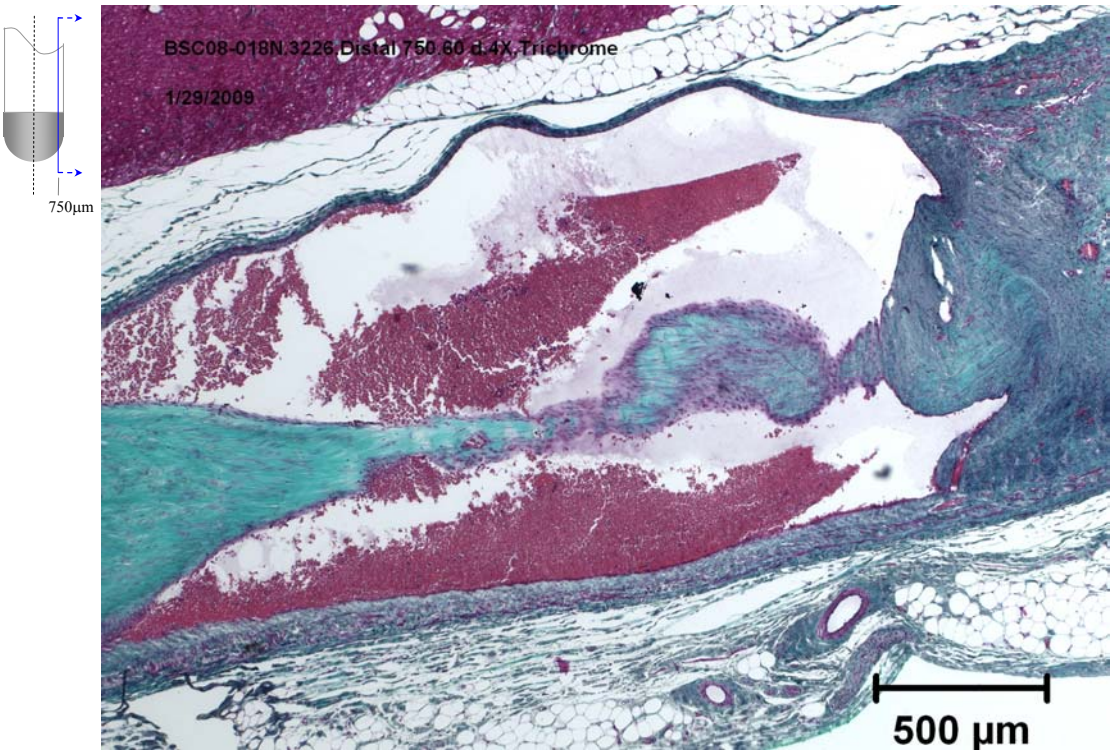
750µm
BSC08-018N.3226.Distal 750.60 d.4X.Trichrome
1/29/2009
500 µm

Summary Study Information for Animal L-3227, Lead 164098 (Porous Tip Electrode)

Lead Tip Images*

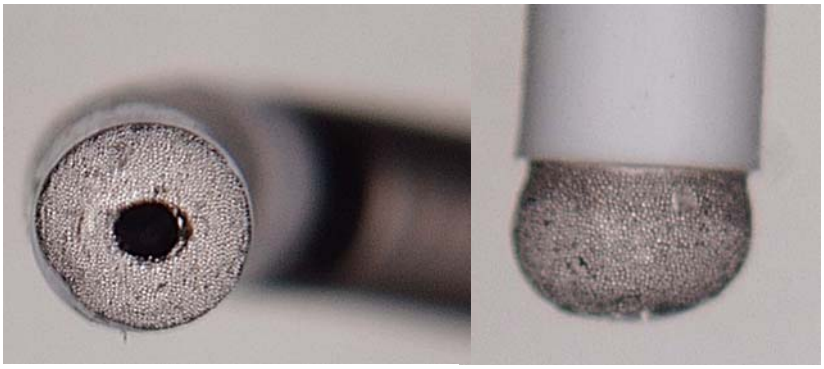

* Steroid eluting collars were initially assembled onto the lead in error (and are shown in the images), though they were later removed and replaced with silicone tubing of the same length, thickness, and diameters as the steroid collars, but with no steroid.

Implant Fluoroscopy Images

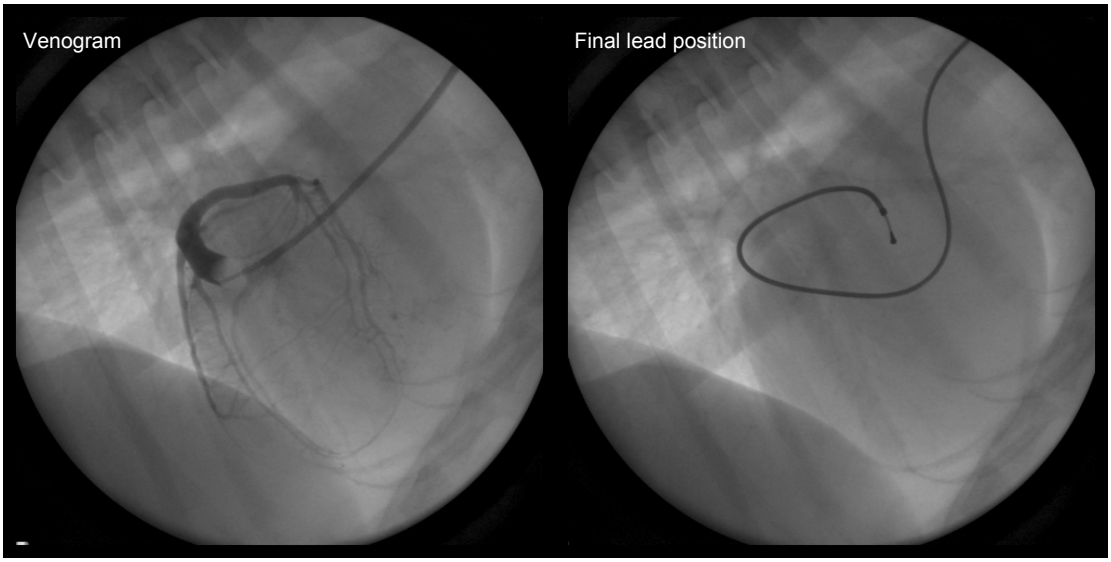

Study Data

Animal ID	Source	Date	Day	Thr. [V]	Thr. Change [V]	R-Wave [mV]	Imp. [Ω]	Movement [cm]	Tip Pos. [cm]
L-3227	PSA Ring	5/29/2008	0	1.1		11.6	792		
Lead ID	PSA Tip	5/29/2008	0	1.2		19.1	764		
164098	PG	5/29/2008	0	1.0	0.0	11.2	430	0	0
Tip Electrode	PG	6/2/2008	4	3.3	2.3	13.2	350	0	0
Porous	PG	6/6/2008	8	2.1	1.1	12.8	370	0	0
	PG	6/13/2008	15	2.1	1.1	11.4	430	0	0
	PG	6/20/2008	22	1.6	0.6	11.9	490	0	0
	PG	6/27/2008	29	1.8	0.8	12.8	490	0	0
	PG	7/11/2008	43	1.5	0.5	13.7	520	0	0
	PG	7/28/2008	60	1.6	0.6	13.7	540	0	0
	PSA Ring	7/28/2008	60	3.4	2.3	12.6	744		

Histology

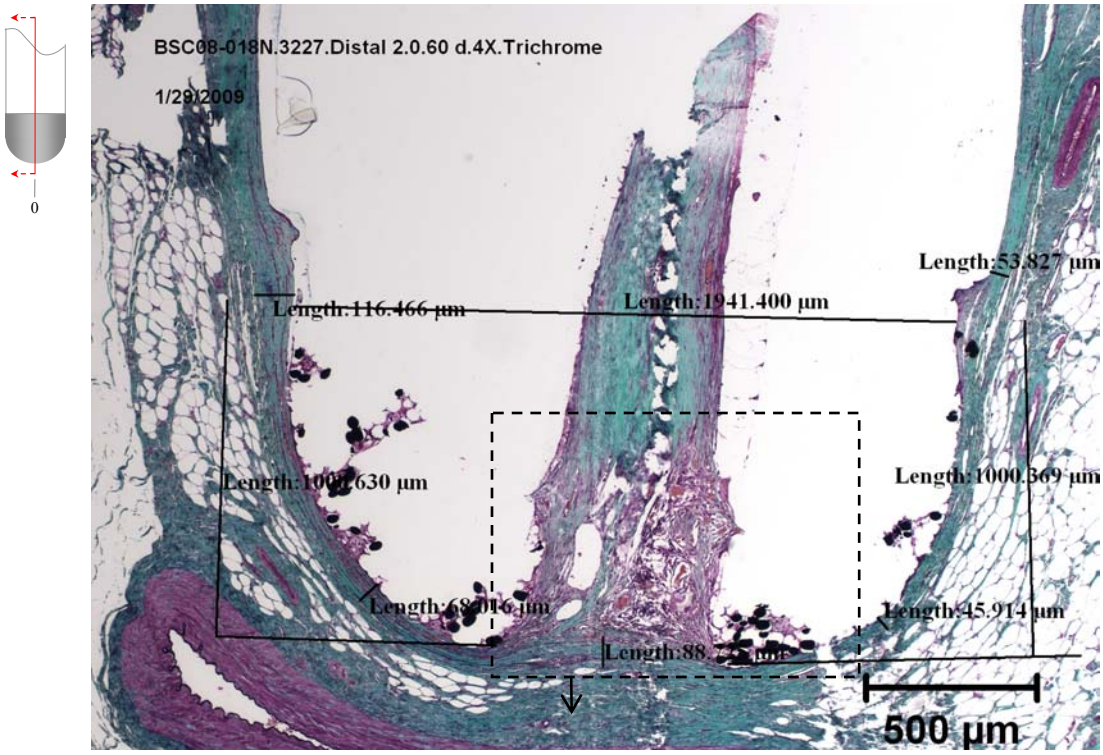
BSC08-018N.3227.Distal 2.0.60 d.4X.Trichrome
1/29/2009
Length:116.466 µm
Length:1941.400 µm
Length:53.827 µm
Length:1000.630 µm
Length:1000.369 µm
Length:45.914 µm
500 µm

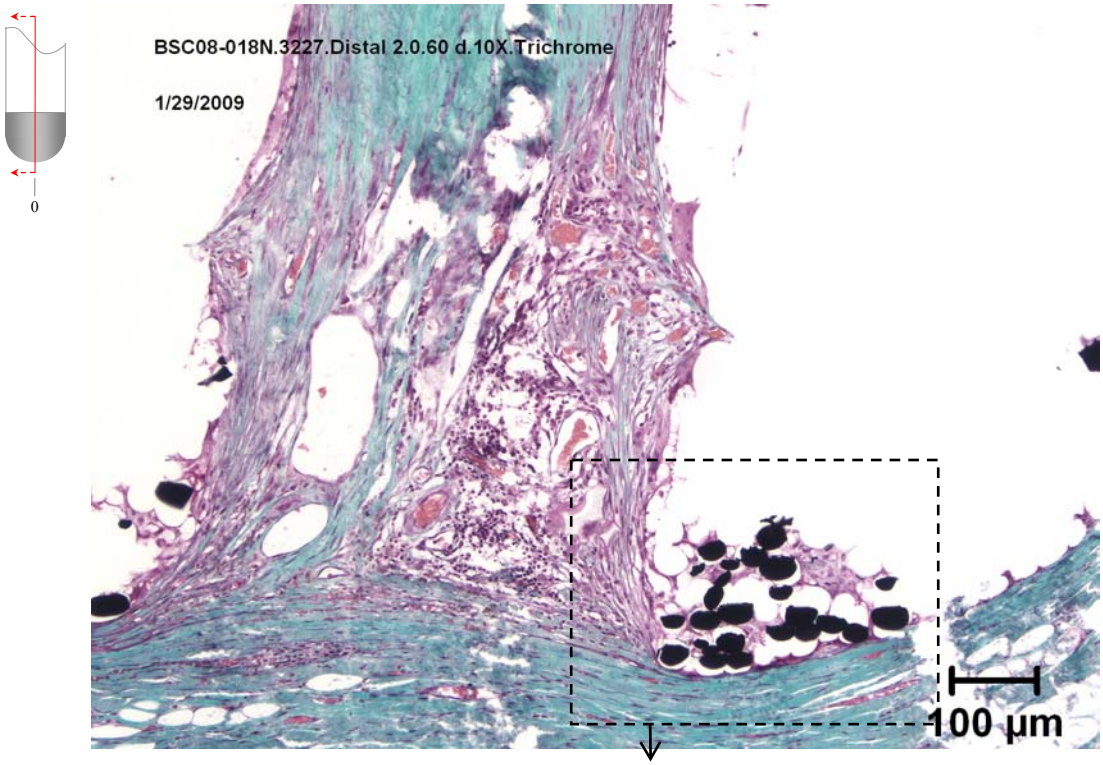
BSC08-018N.3227.Distal 2.0.60 d.10X.Trichrome
1/29/2009
100 µm

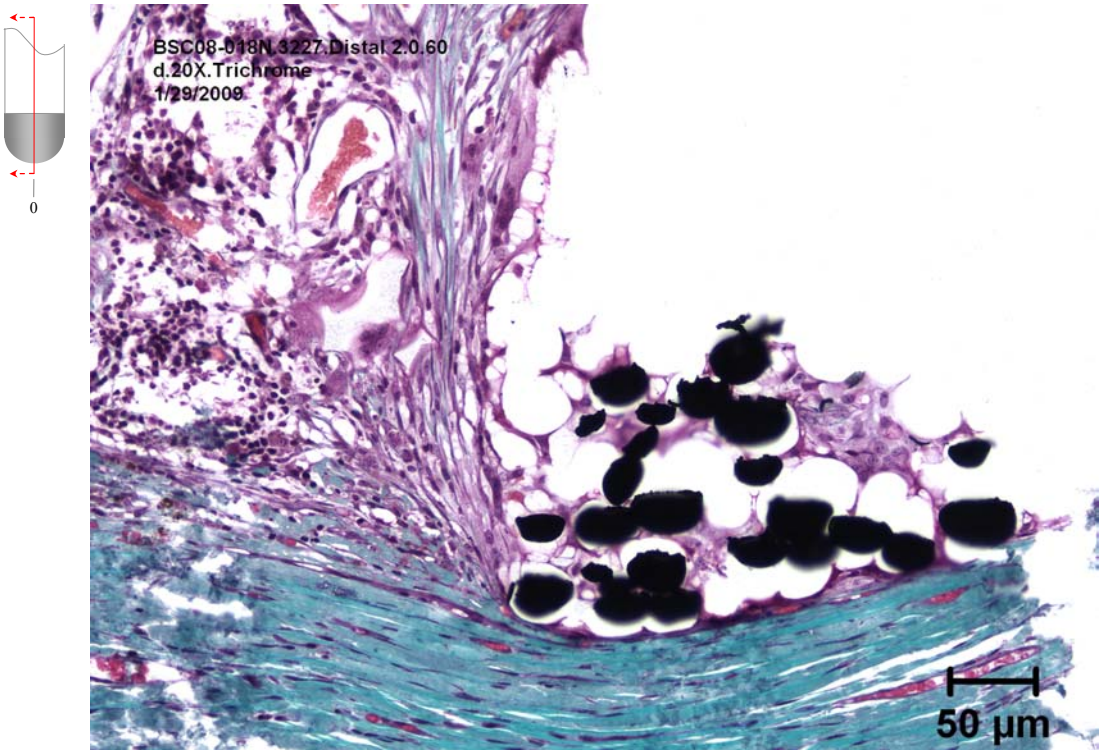
0
BSC08-018N.3227.Distal 2.0.60
d.20X.Trichrome
1/29/2009
50 µm

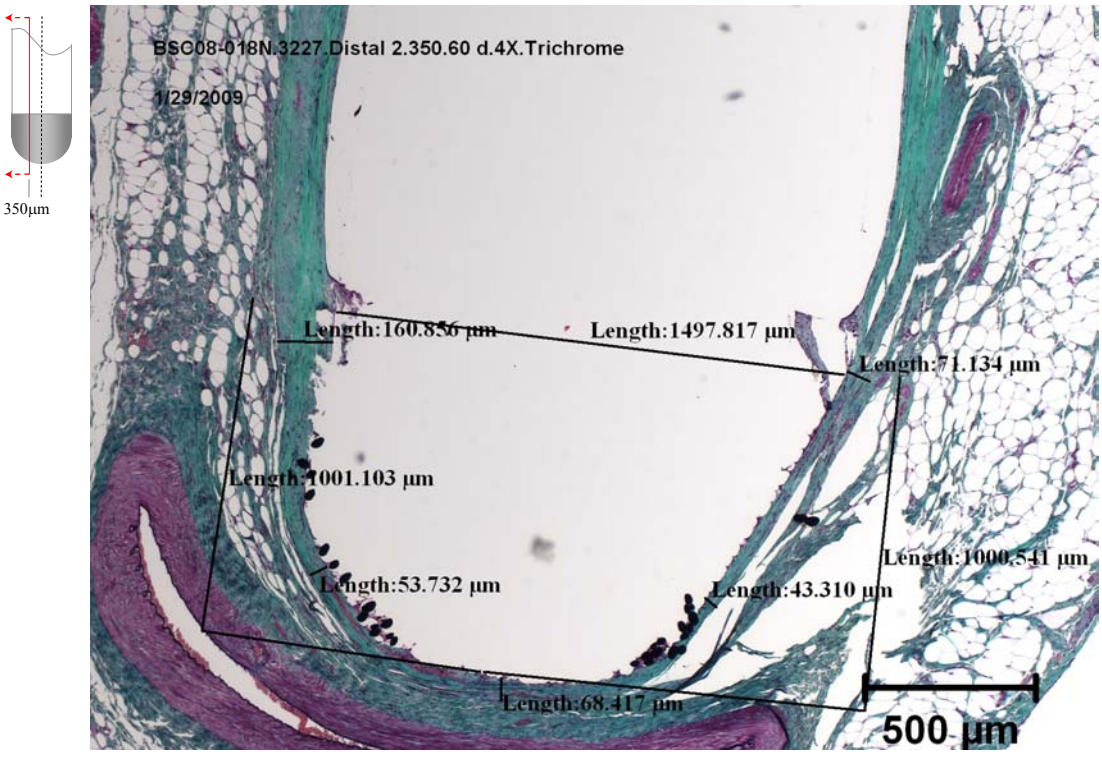
350µm
BSC08-018N.3227.Distal 2.350.60 d.4X.Trichrome
1/29/2009
Length:160.856 µm
Length:1497.817 µm
Length:71.134 µm
Length:1001.103 µm
Length:53.732 µm
Length:43.310 µm
Length:1000.541 µm
Length:68.417 µm
500 µm

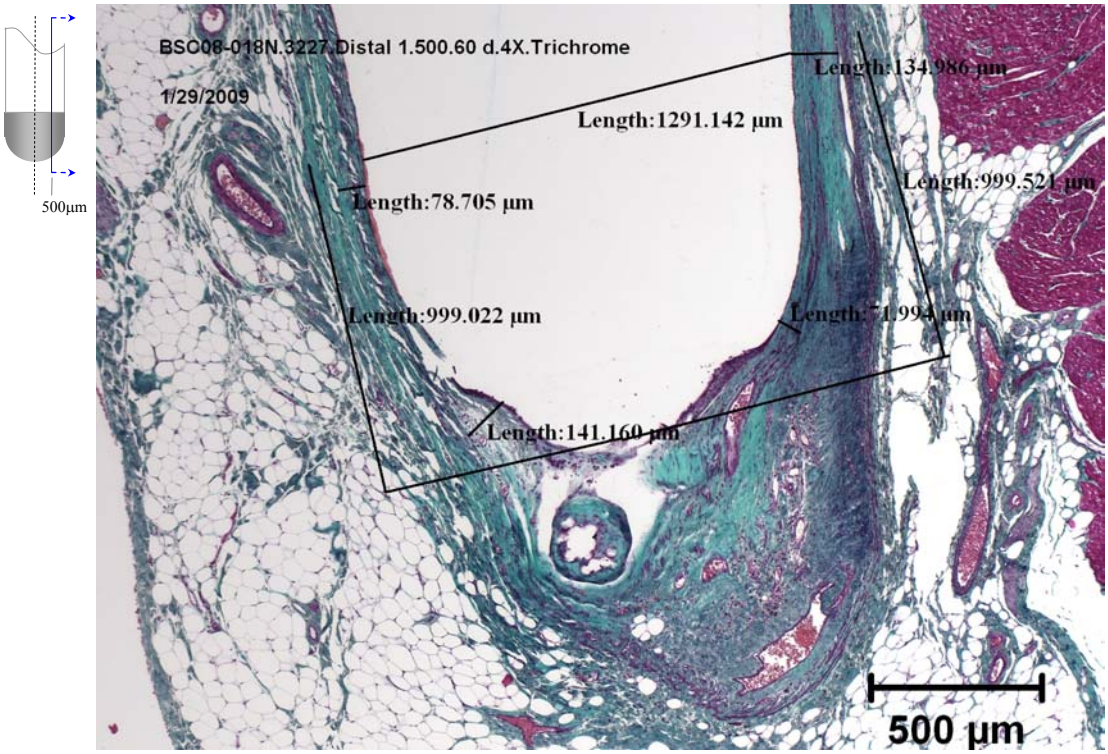
500µm
BSC08-018N.3227.Distal 1.500.60 d.4X.Trichrome
1/29/2009
Length:134.986 µm
Length:1291.142 µm
Length:999.521 µm
Length:78.705 µm
Length:999.022 µm
Length:141.160 µm
500 µm

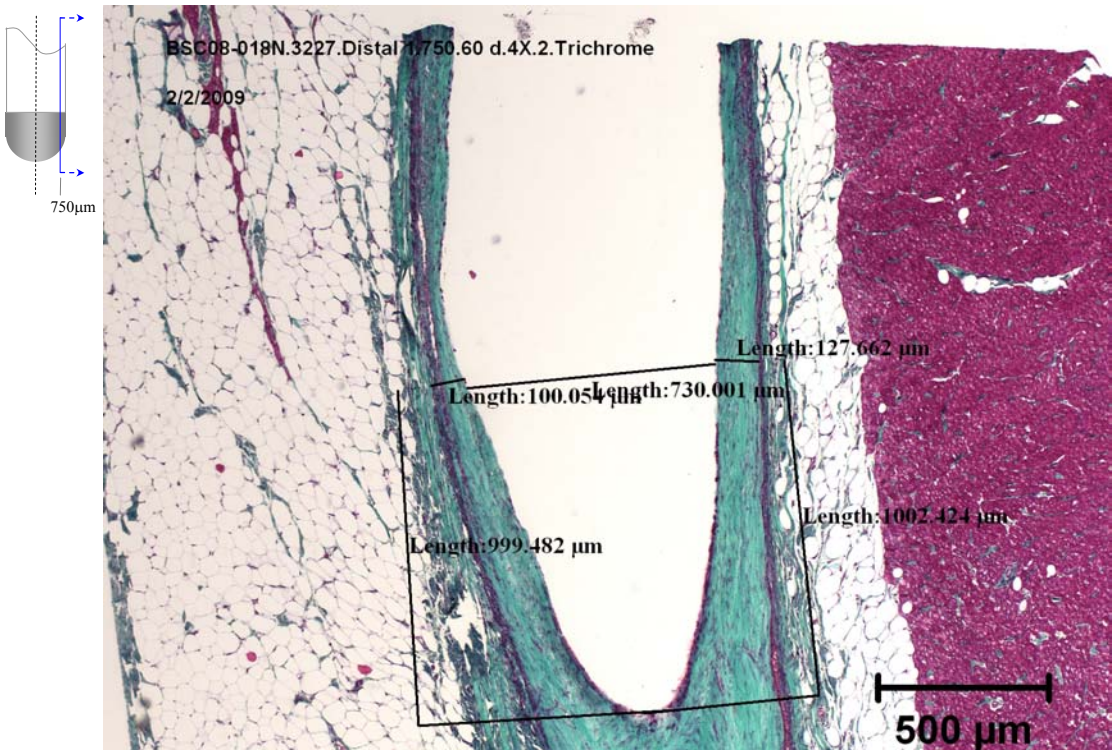
750µm
BSC08-018N.3227.Distal 1.750.60 d.4X.2.Trichrome
2/2/2009
Length:127.662 µm
Length:730.001 µm
Length:100.054 µm
Length:1002.424 µm
Length:999.482 µm
500 µm

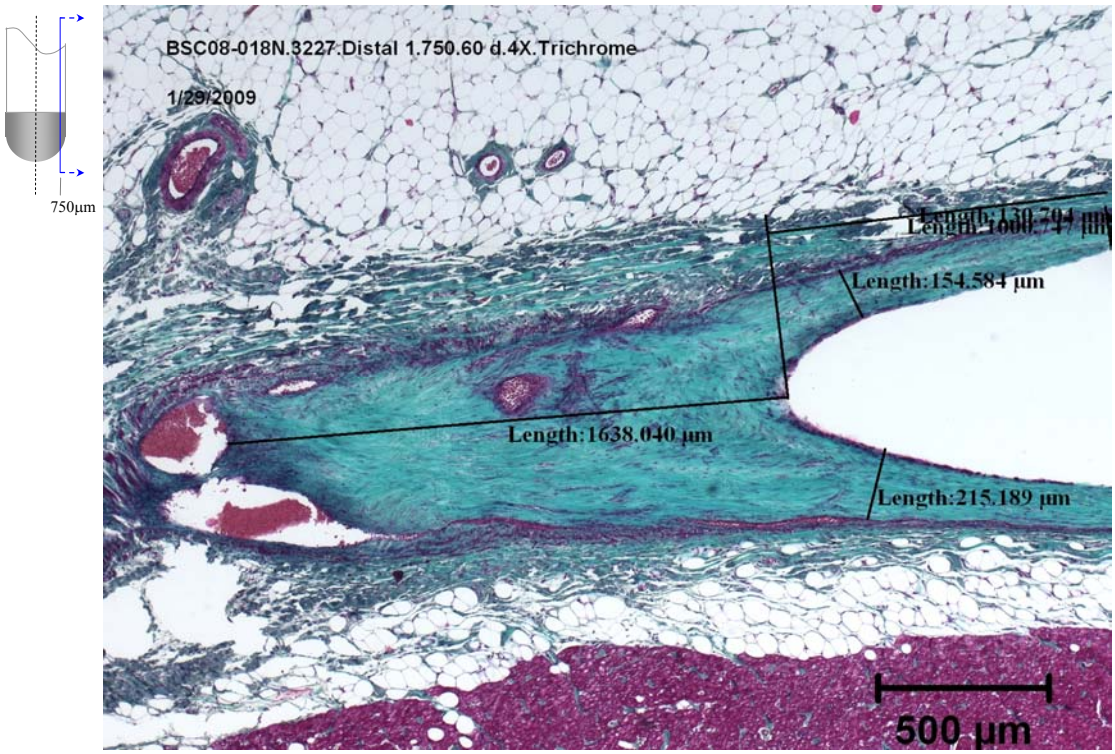
750µm
BSC08-018N.3227.Distal 1.750.60 d.4X.Trichrome
1/29/2009
Length:154.584 µm
Length:1638.040 µm
Length:215.189 µm
500 µm

Summary Study Information for Animal L-3229, Lead 164080 (Porous Tip Electrode)

Lead Tip Images*

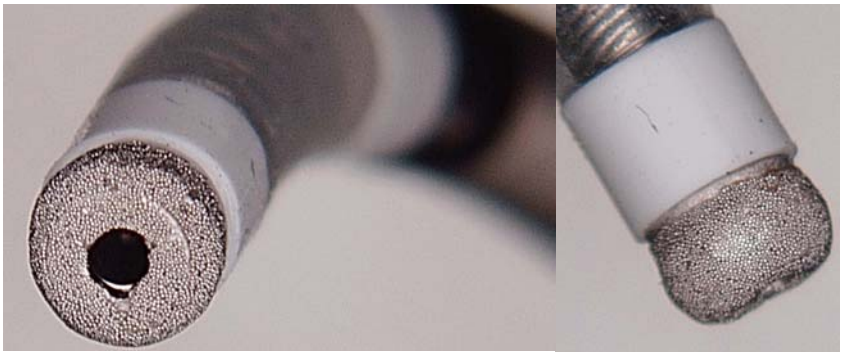

* Steroid eluting collars were initially assembled onto the lead in error (and are shown in the images), though they were later removed and replaced with silicone tubing of the same length, thickness, and diameters as the steroid collars, but with no steroid.

Implant Fluoroscopy Images

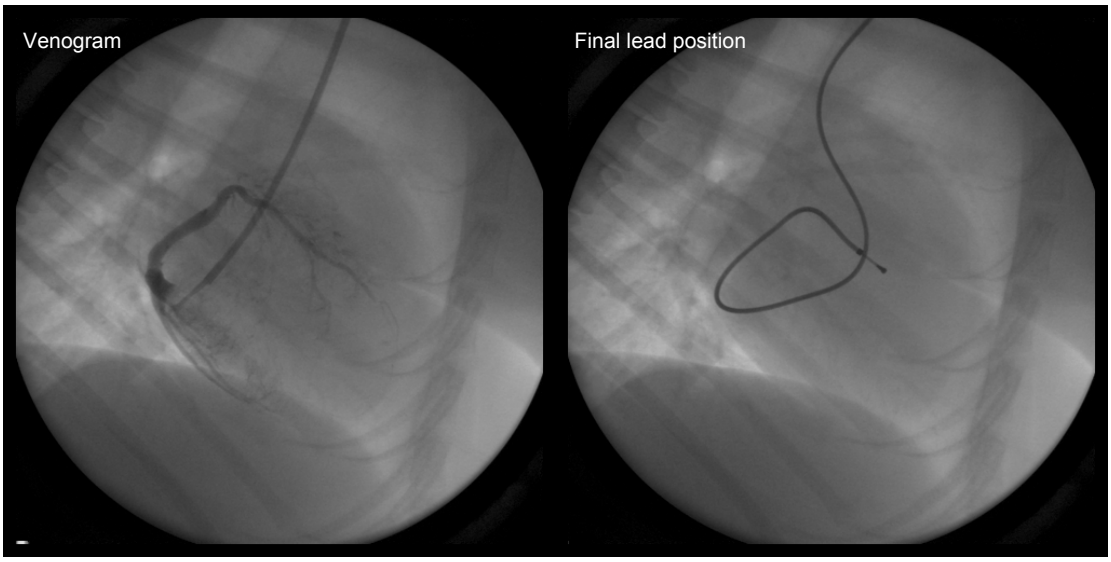

Study Data

Animal ID	Source	Date	Day	Thr. [V]	Thr. Change [V]	R-Wave [mV]	Imp. [Ω]	Movement [cm]	Tip Pos. [cm]
L-3229	PSA Ring	5/30/2008	0	2.1		22.1	1240		
Lead ID	PSA Tip	5/30/2008	0	0.5		28.2	1040		
164080	PG	5/30/2008	0	0.3	0.0	*12.0*	650	0	0
Tip Electrode	PG	6/2/2008	3	1.4	1.1	15.0	480	1	-1
Porous	PG	6/6/2008	7	1.6	1.3	16.0	540	0	-1
	PG	6/13/2008	14	1.2	0.9	16.0	710	0	-1
	PG	6/20/2008	21	1.1	0.8	*20.0*	760	0	-1
	PG	6/27/2008	28	1.0	0.7	19.2	790	0	-1
	PG	7/11/2008	42	0.9	0.6	18.2	850	0	-1
	PG	7/29/2008	60	1.2	0.9	16.9	890	0	-1
	PSA Ring	7/29/2008	60	3.4	1.3	16.7	888		

Lead Retractions

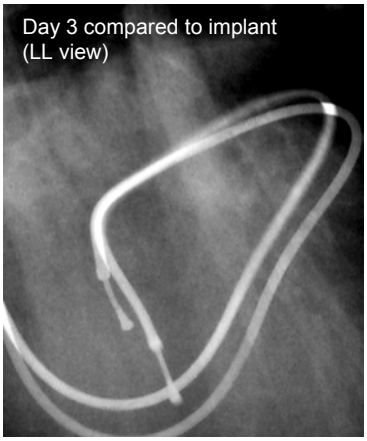

Histology

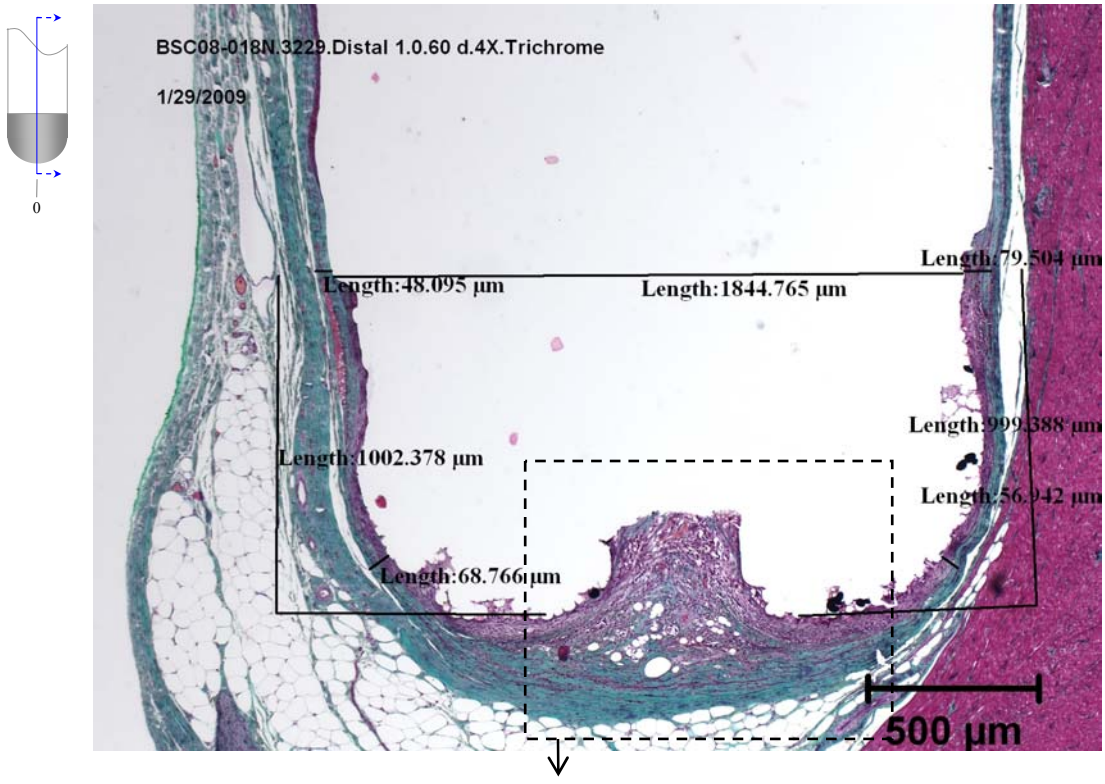

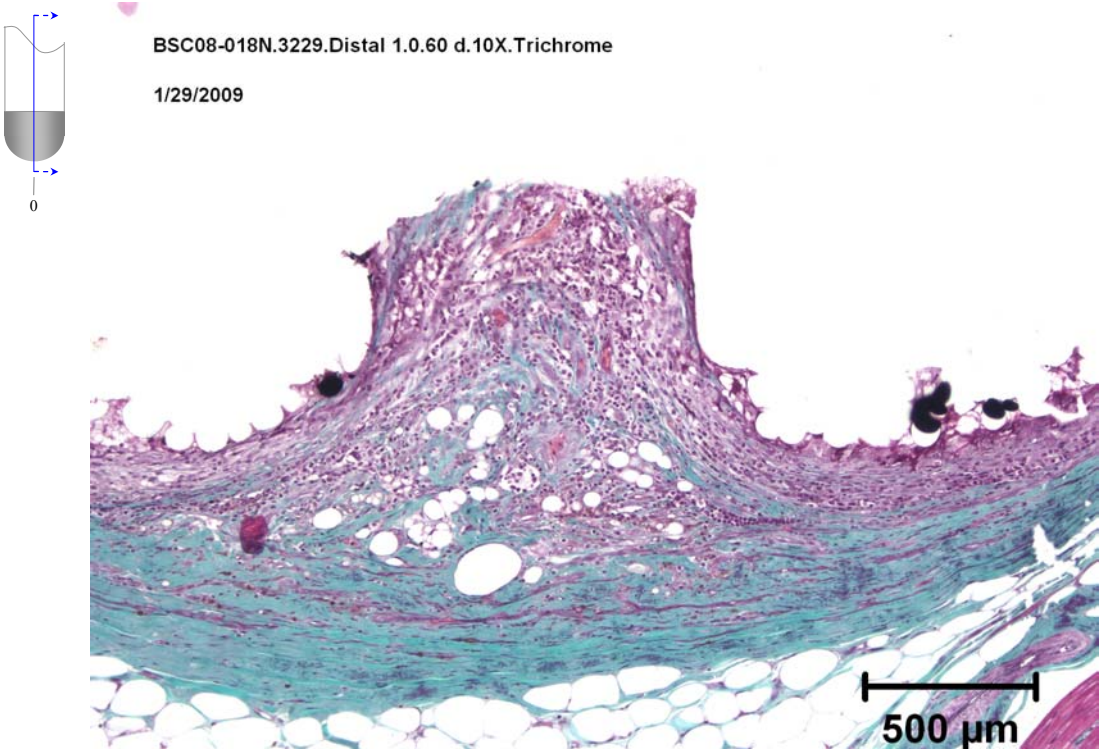
BSC08-018N.3229.Distal 1.0.60 d.10X.Trichrome
1/29/2009
0
500 µm

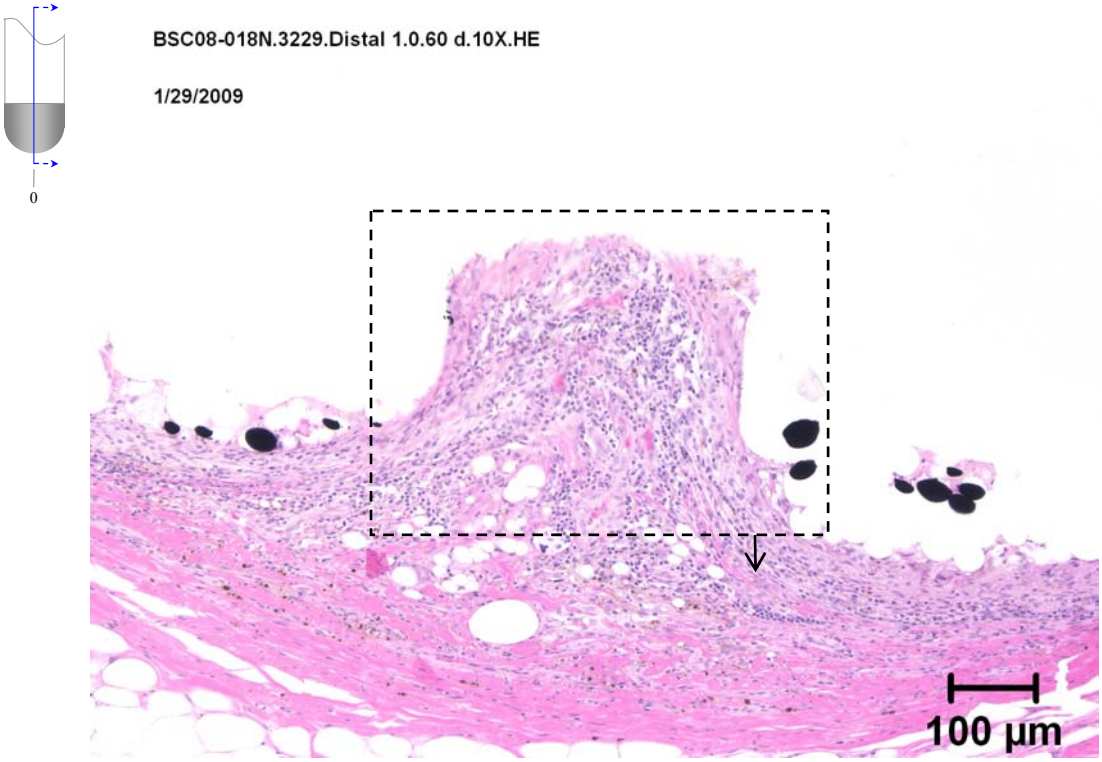
BSC08-018N.3229.Distal 1.0.60 d.10X.HE
1/29/2009
0
100 µm

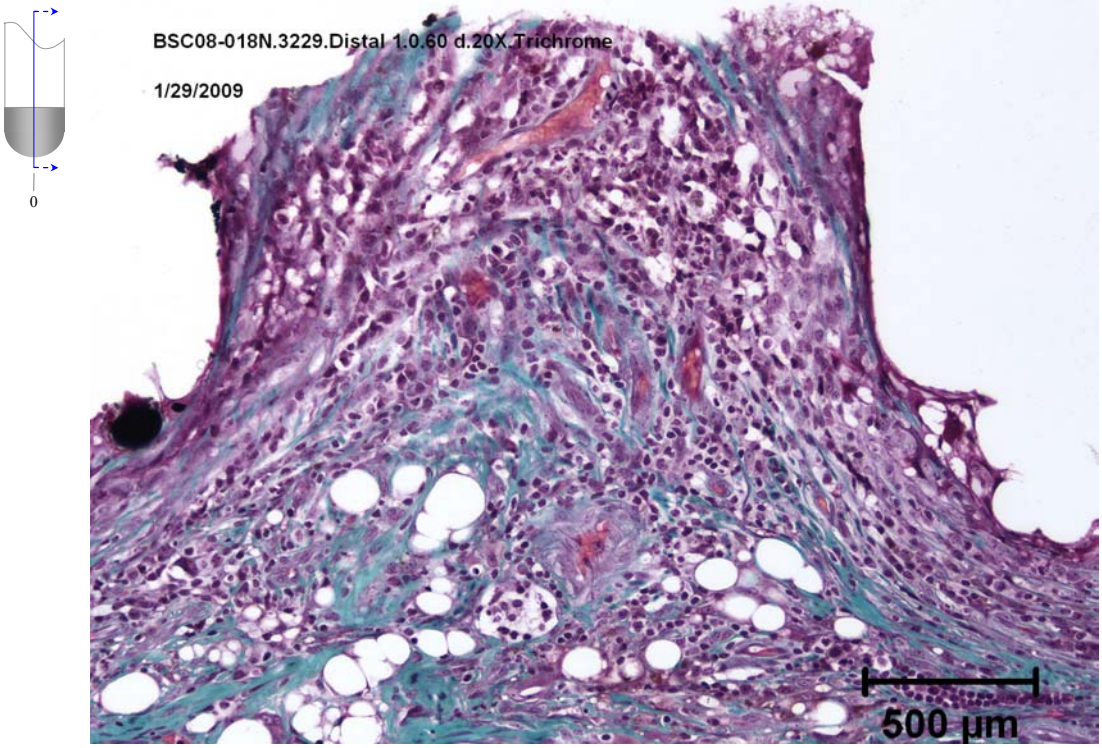
0
BSC08-018N.3229.Distal 1.0.60 d.20X.Trichrome
1/29/2009
500 µm

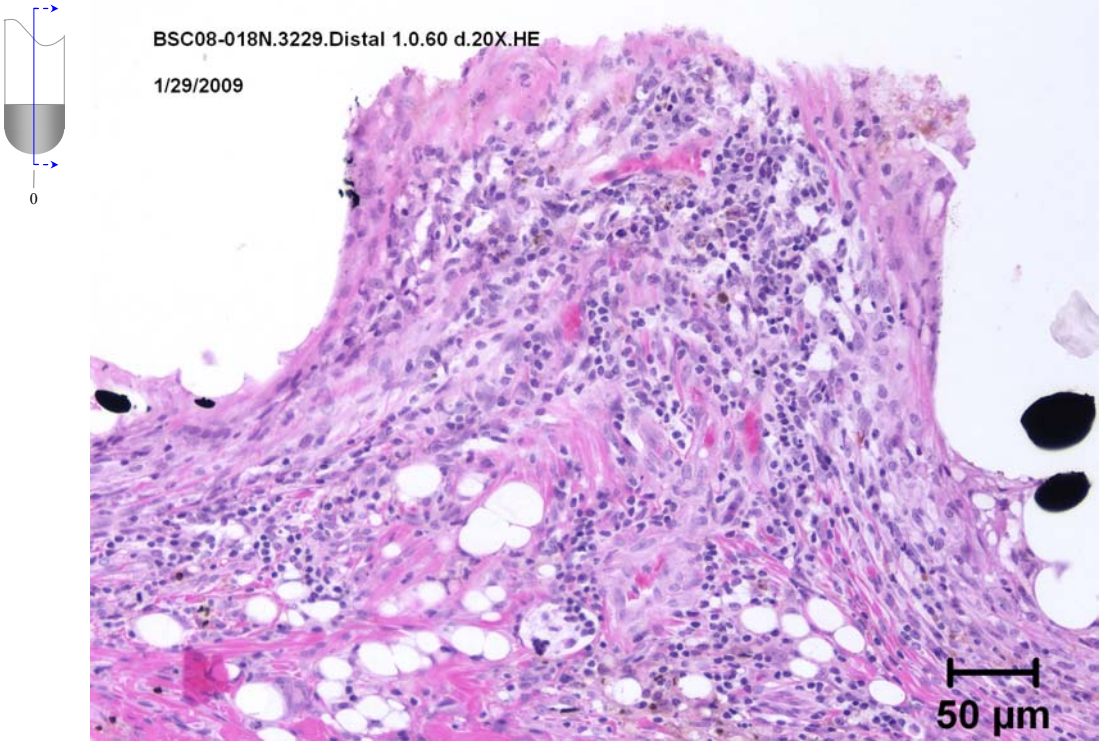
0
BSC08-018N.3229.Distal 1.0.60 d.20X.HE
1/29/2009
50 µm

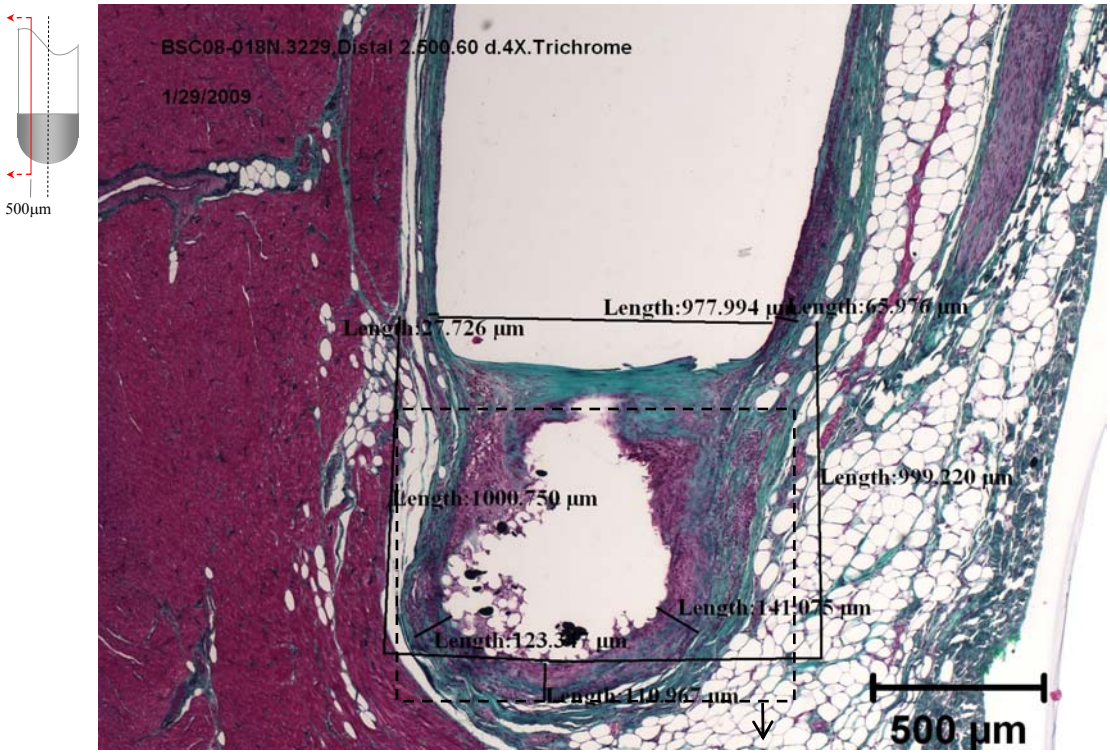
500µm
BSC08-018N.3229.Distal 2.500.60 d.4X.Trichrome
1/29/2009
Length:977.994 µm
Length:65.976 µm
Length:27.726 µm
Length:1000.750 µm
Length:999.220 µm
Length:141.075 µm
Length:123.347 µm
Length:110.967 µm
500 µm

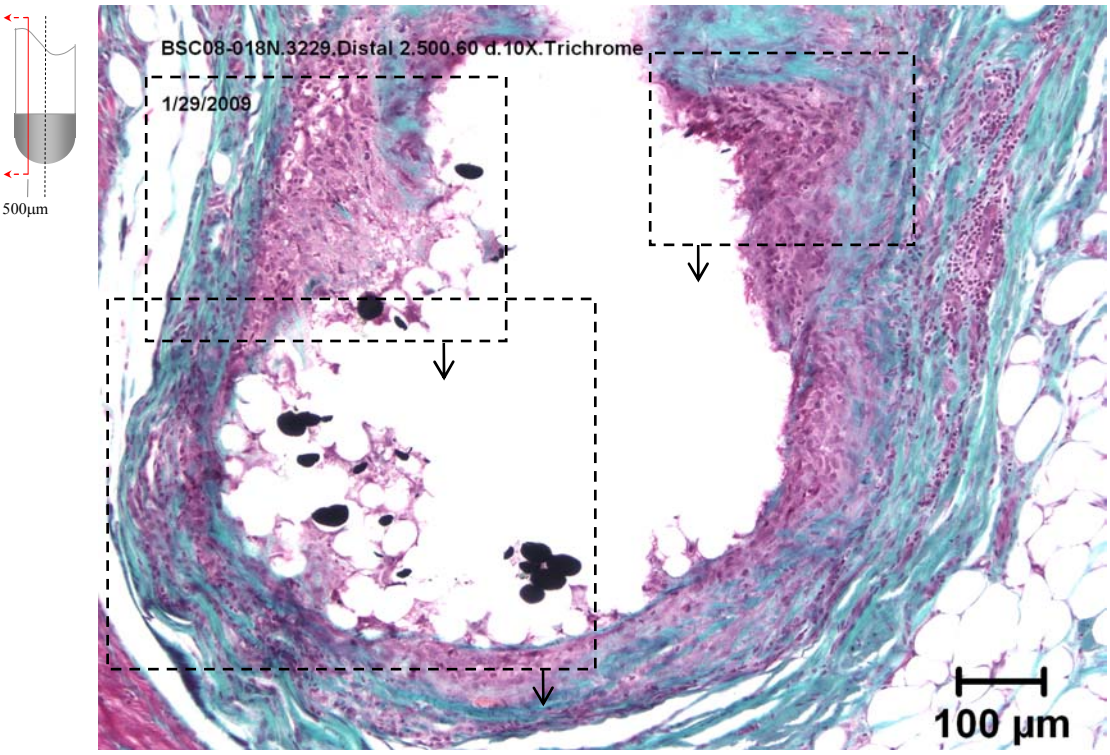
500µm
BSC08-018N.3229.Distal 2.500.60 d.10X.Trichrome
1/29/2009
100 µm

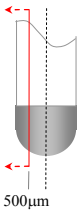
500µm

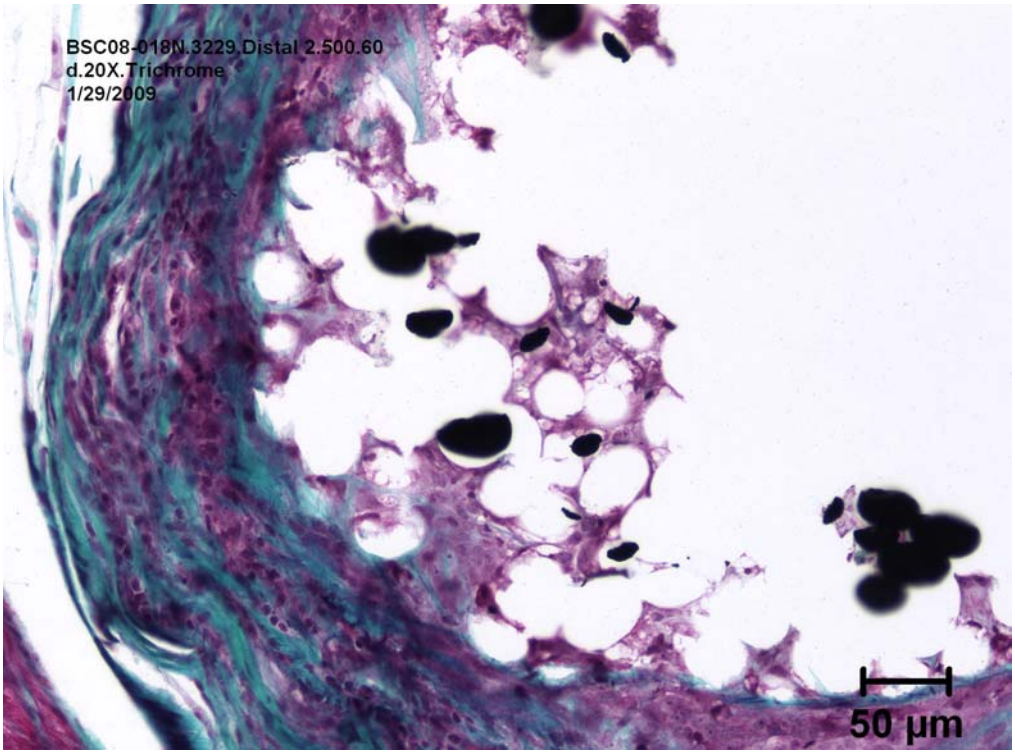
BSC08-018N.3229.Distal 2.500.60
d.20X.Trichrome
1/29/2009
50 µm

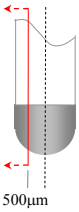
500µm

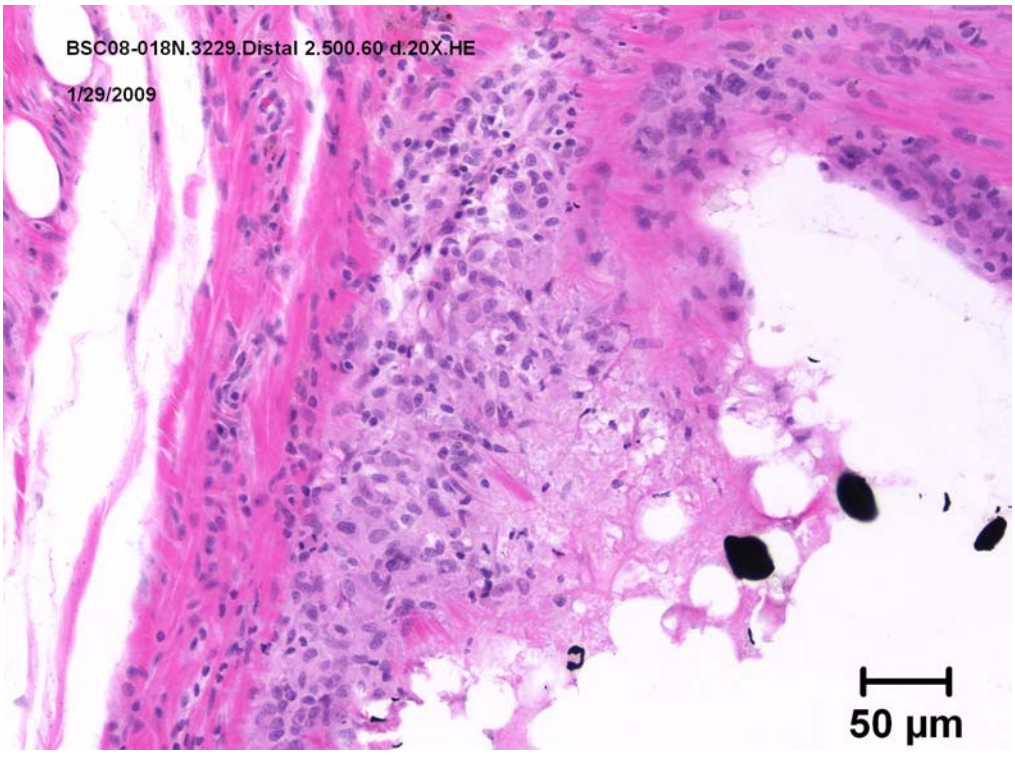
BSC08-018N.3229.Distal 2.500.60 d.20X.HE
1/29/2009
50 µm

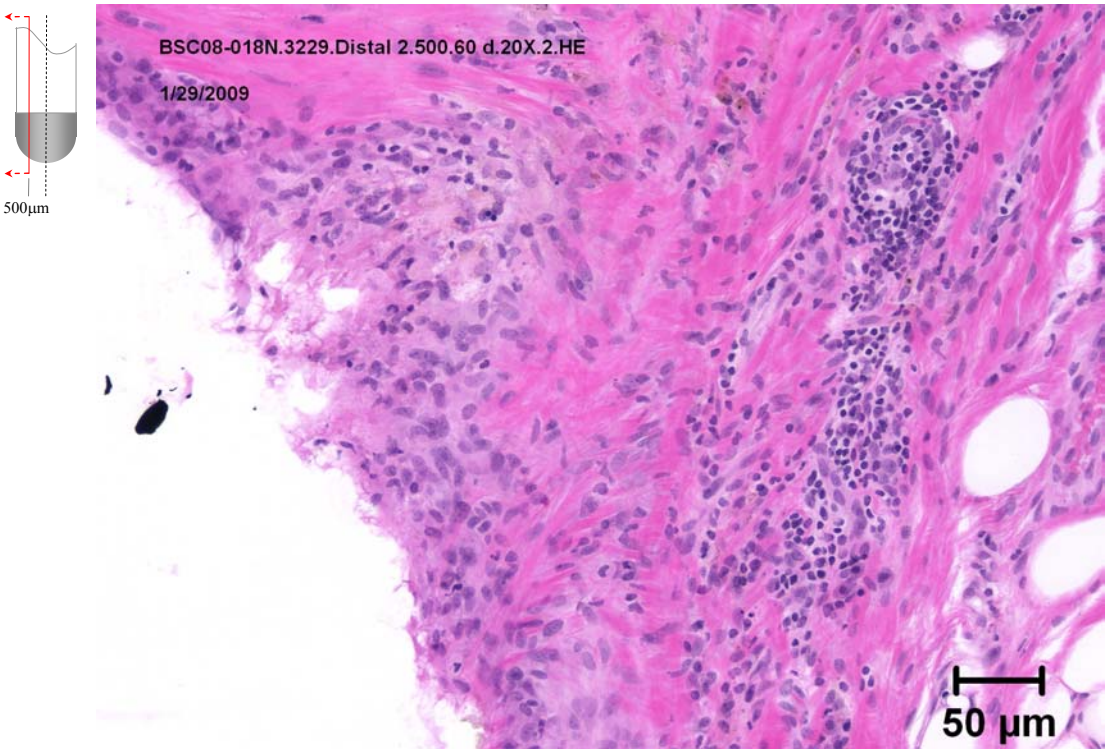
500µm
BSC08-018N.3229.Distal 2.500.60 d.20X.2.HE
1/29/2009
50 µm

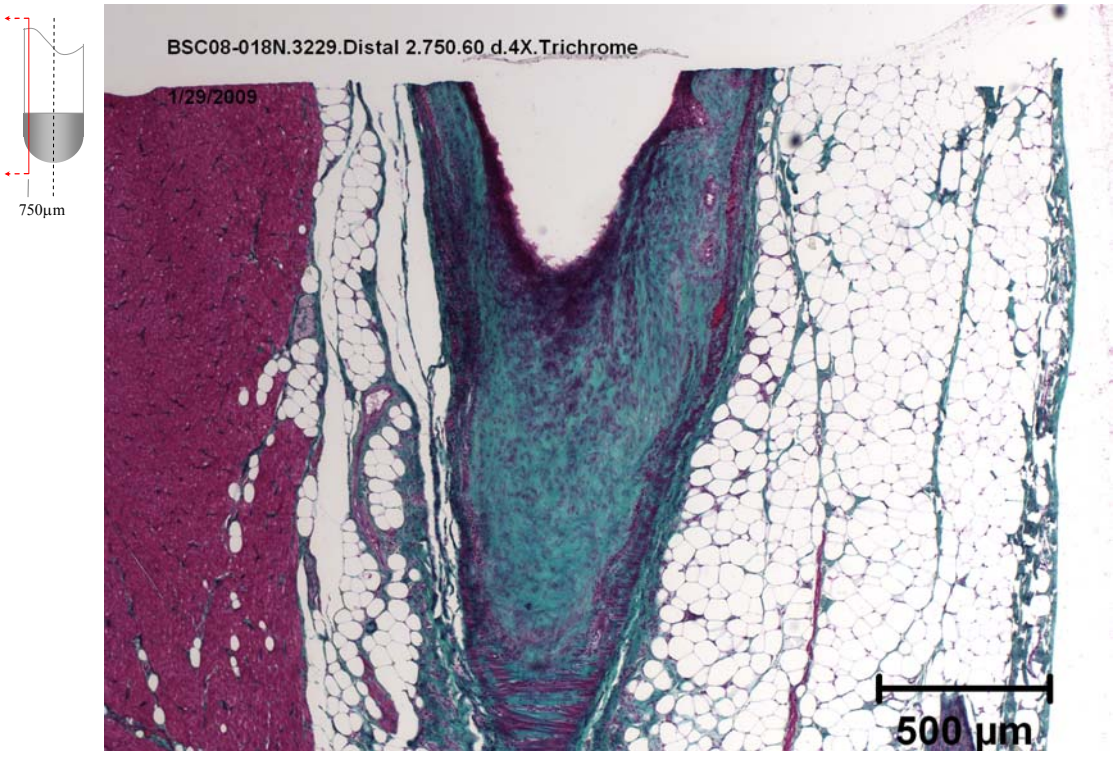
750µm
BSC08-018N.3229.Distal 2.750.60 d.4X.Trichrome
1/29/2009
500 µm

Summary Study Information for Animal L-3230, Lead 164065 (Porous Tip Electrode)

Lead Tip Images*

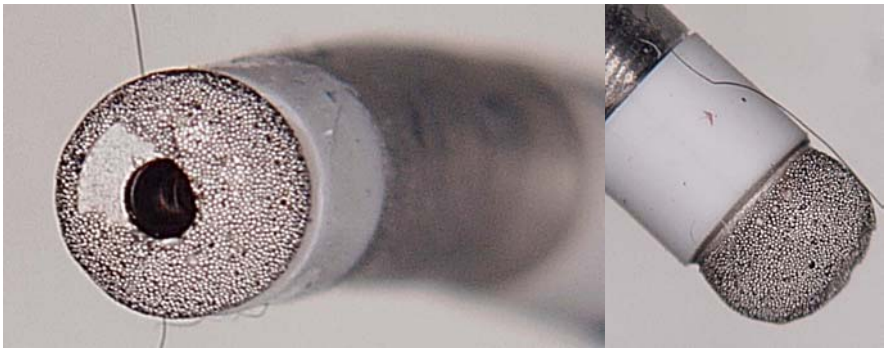

* Steroid eluting collars were initially assembled onto the lead in error (and are shown in the images), though they were later removed and replaced with silicone tubing of the same length, thickness, and diameters as the steroid collars, but with no steroid.

Implant Fluoroscopy Images

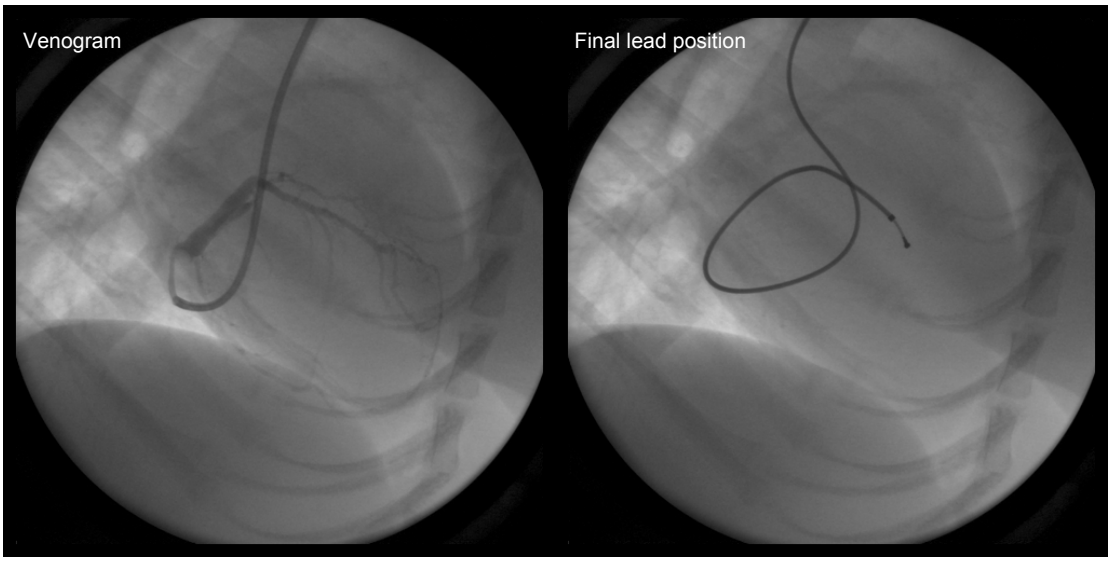

Study Data

Animal ID	Source	Date	Day	Thr. [V]	Thr. Change [V]	R-Wave [mV]	Imp. [Ω]	Movement [cm]	Tip Pos. [cm]
L-3230	PSA Ring	5/30/2008	0	0.8		12.2	964		
Lead ID	PSA Tip	5/30/2008	0	0.5		16.5	948		
164065	PG	5/30/2008	0	0.1	0.0	9.8	540	0	0
Tip Electrode	PG	6/2/2008	3	0.9	0.8	16.4	420	2	-2
Porous	PG	6/6/2008	7	1.1	1.0	18.7	480	0	-2
	PG	6/13/2008	14	1.0	0.9	16.0	540	0	-2
	PG	6/20/2008	21	0.8	0.7	19.2	580	0	-2
	PG	6/27/2008	28	0.7	0.6	14.6	550	0	-2
	PG	7/11/2008	42	0.6	0.5	16.4	620	0	-2
	PG	7/29/2008	60	0.6	0.5	17.8	700	0	-2
	PSA Ring	7/29/2008	60	6.6	5.8	17.8	1376		

Lead Retractions

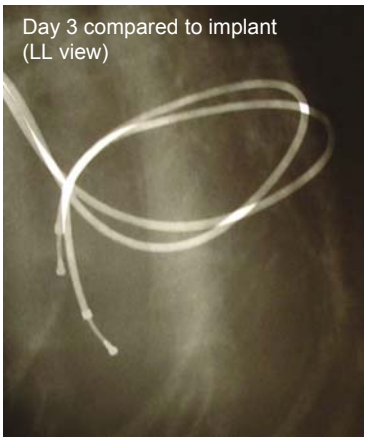

Histology

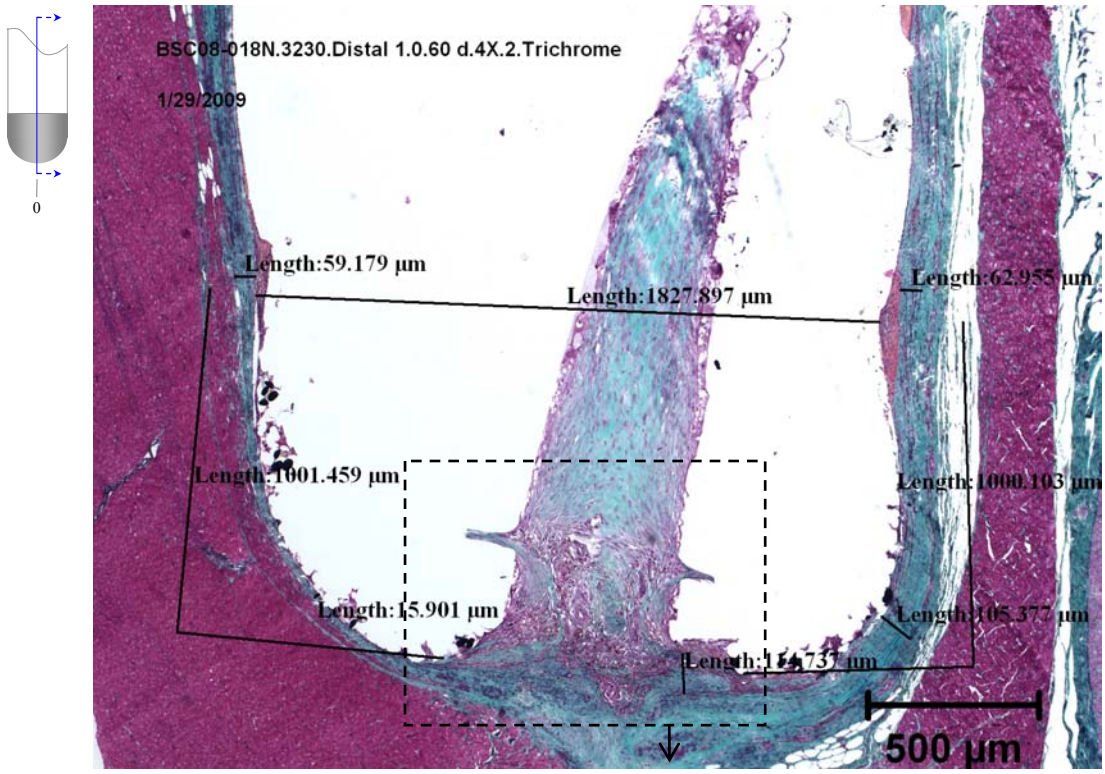

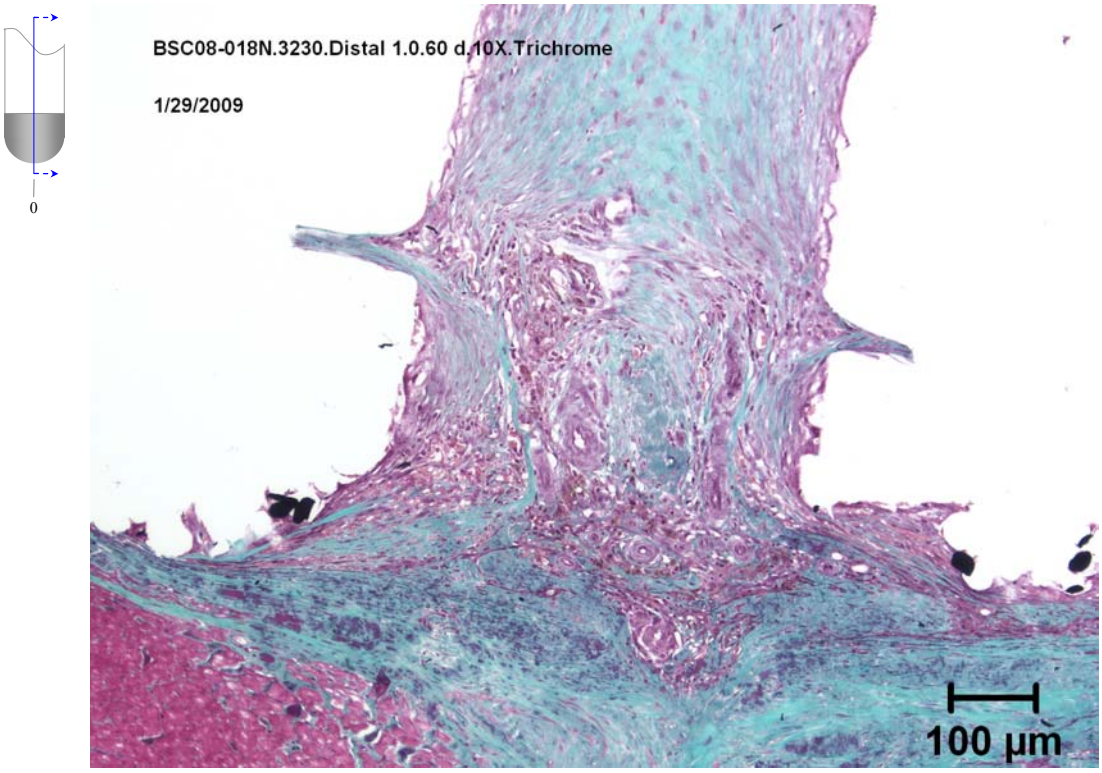
BSC08-018N.3230.Distal 1.0.60 d.10X.Trichrome
1/29/2009
100 µm

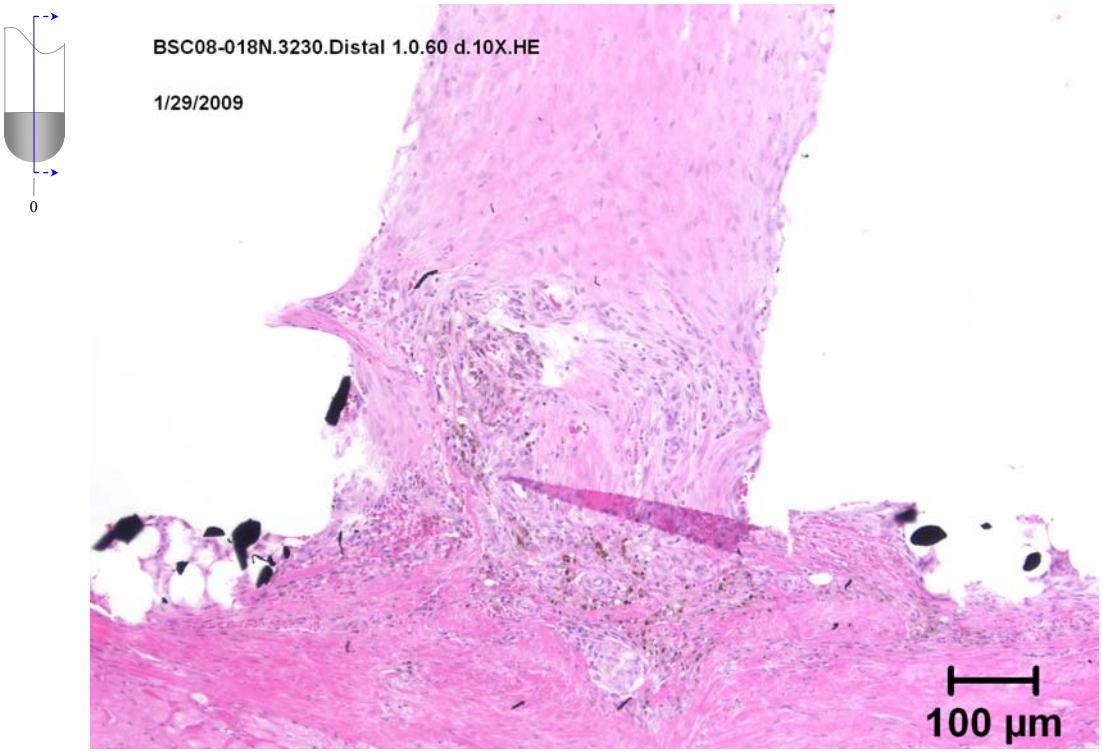
BSC08-018N.3230.Distal 1.0.60 d.10X.HE
1/29/2009
100 µm

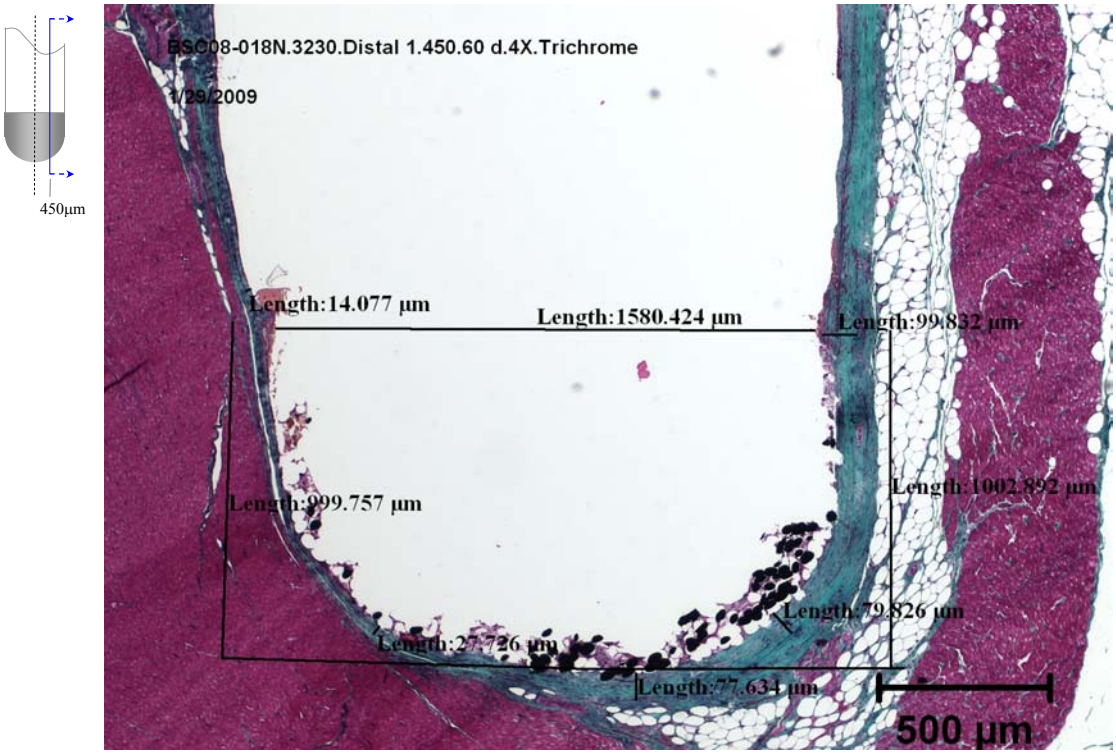
450µm
BSC08-018N.3230.Distal 1.450.60 d.4X.Trichrome
1/29/2009
Length:14.077 µm
Length:1580.424 µm
Length:99.832 µm
Length:999.757 µm
Length:1002.892 µm
Length:79.826 µm
Length:27.726 µm
Length:77.634 µm
500 µm

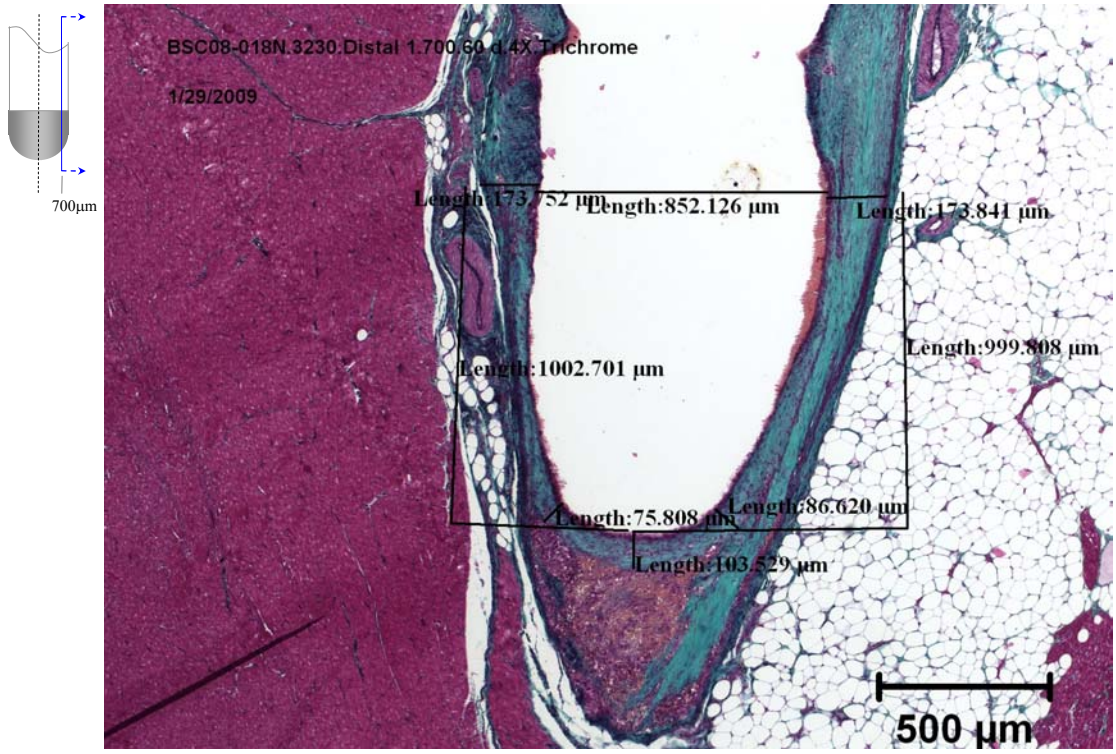
700µm
BSC08-018N.3230.Distal 1.700.60 d.4X.Trichrome
1/29/2009
Length:173.752 µm
Length:852.126 µm
Length:173.841 µm
Length:1002.701 µm
Length:999.808 µm
Length:75.808 µm
Length:86.620 µm
Length:103.529 µm
500 µm

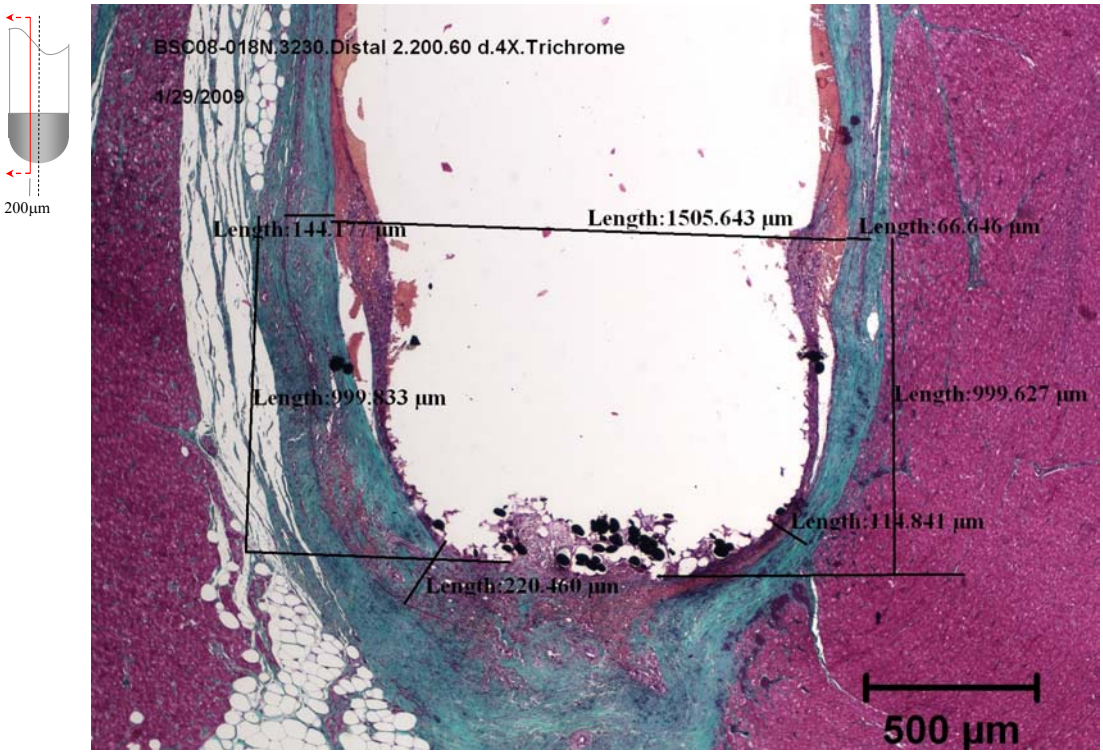
200µm
BSC08-018N.3230.Distal 2.200.60 d.4X.Trichrome
1/29/2009
Length:144.177 µm
Length:1505.643 µm
Length:66.646 µm
Length:999.833 µm
Length:999.627 µm
Length:114.841 µm
Length:220.460 µm
500 µm

Summary Study Information for Animal L-3231, Lead 164004 (Solid Tip Electrode)

Implant Fluoroscopy Images

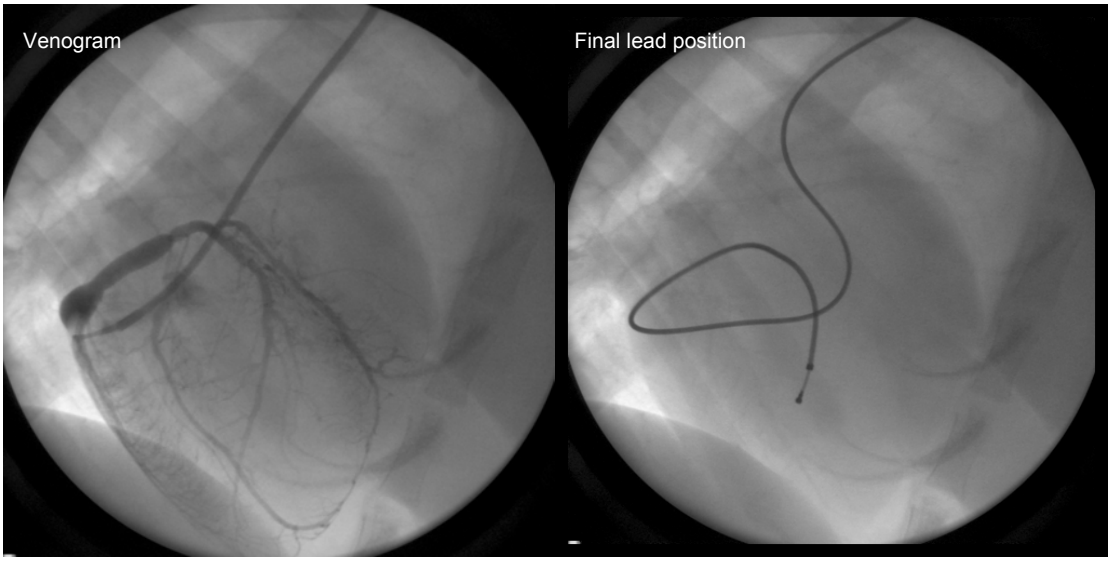

Study Data

Animal ID	Source	Date	Day	Thr. [V]	Thr. Change [V]	R-Wave [mV]	Imp. [Ω]	Movement [cm]	Tip Pos. [cm]
L-3231	PSA Ring	5/30/2008	0	0.8		9.6	2016		
Lead ID	PSA Tip	5/30/2008	0	1.9		6.0	948		
164004	PG	5/30/2008	0	0.7	0.0	5.4	550	0	0
Tip Electrode	PG	6/2/2008	3	1.8	1.1	13.2	440	3	-3
Solid	PG	6/6/2008	7	2.3	1.6	9.1	460	0	-3
	PG	6/13/2008	14	3.1	2.4	10.9	490	0	-3
	PG	6/20/2008	21	2.7	2.0	10.0	590	0	-3
	PG	6/27/2008	28	2.1	1.4	11.4	590	0	-3
	PG	7/11/2008	42	1.6	0.9	10.9	710	0	-3
	PG	7/29/2008	60	1.3	0.6	10.5	700	0	-3
	PSA Ring	7/29/2008	60	5.6	4.8	10.6	942		

Lead Retractions

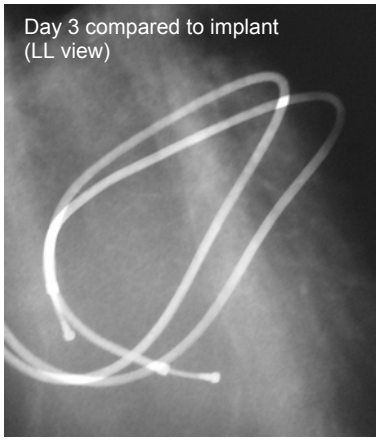

Histology

Note: The initial slice of the tissue/lead block was done off-center in this case, such that the slide labeled as being at the “zero” point in regard to the lead center axis was in fact not the slide closest to the lead center axis. The slide showing the greatest width at the point 1 mm back from the tip is the slide that was actually taken closest to the center axis of the lead. The slides below are ordered such that the slide with the largest width at the point 1 mm back from the lead tip is shown first, proceeding down to the slide with the smallest width at the same point. The first slide shown below was used in summary data for fibrous capsule thickness.

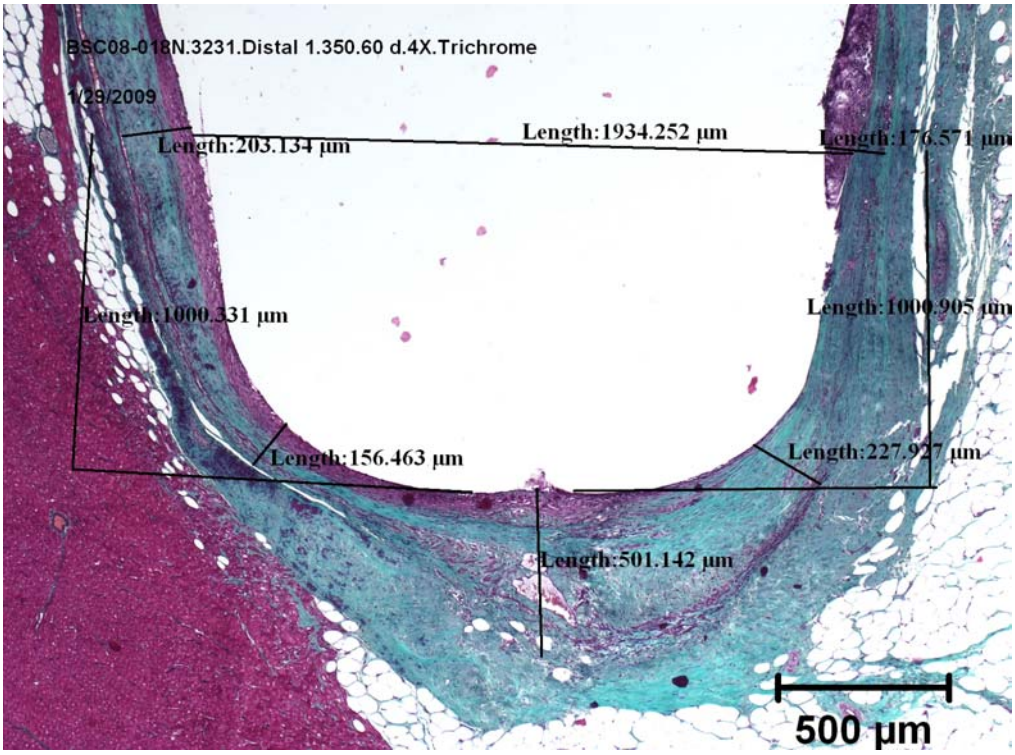

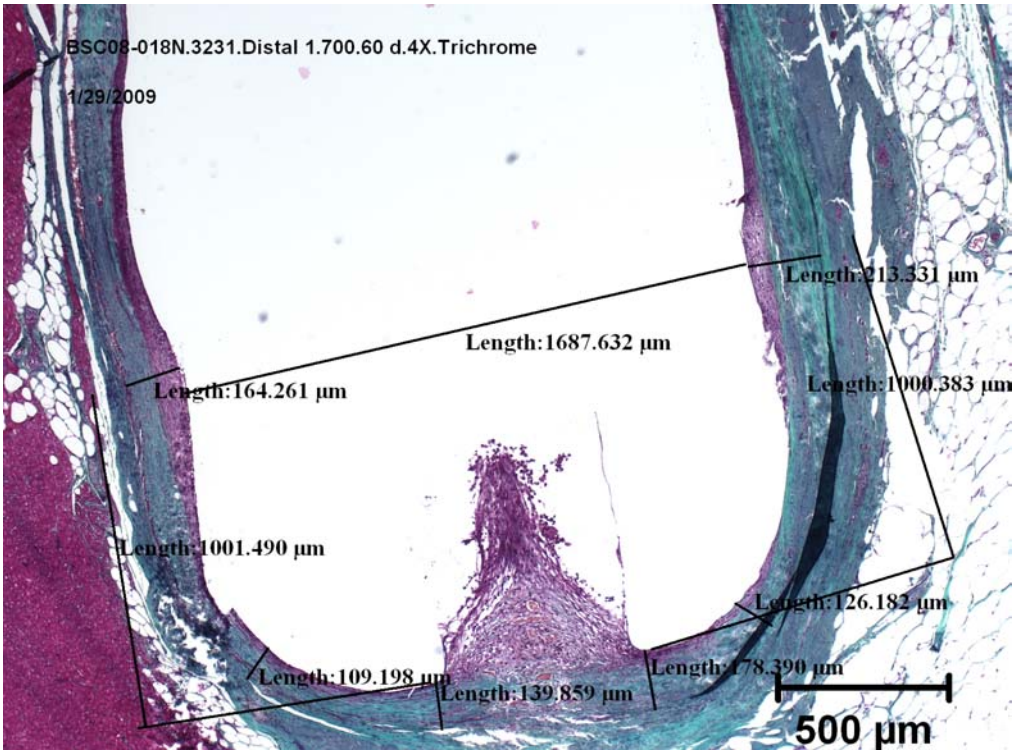
BSC08-018N.3231.Distal 1.700.60 d.4X.Trichrome
1/29/2009
Length:213.331 µm
Length:1687.632 µm
Length:164.261 µm
Length:1000.383 µm
Length:1001.490 µm
Length:126.182 µm
Length:109.198 µm
Length:139.859 µm
Length:178.390 µm
500 µm

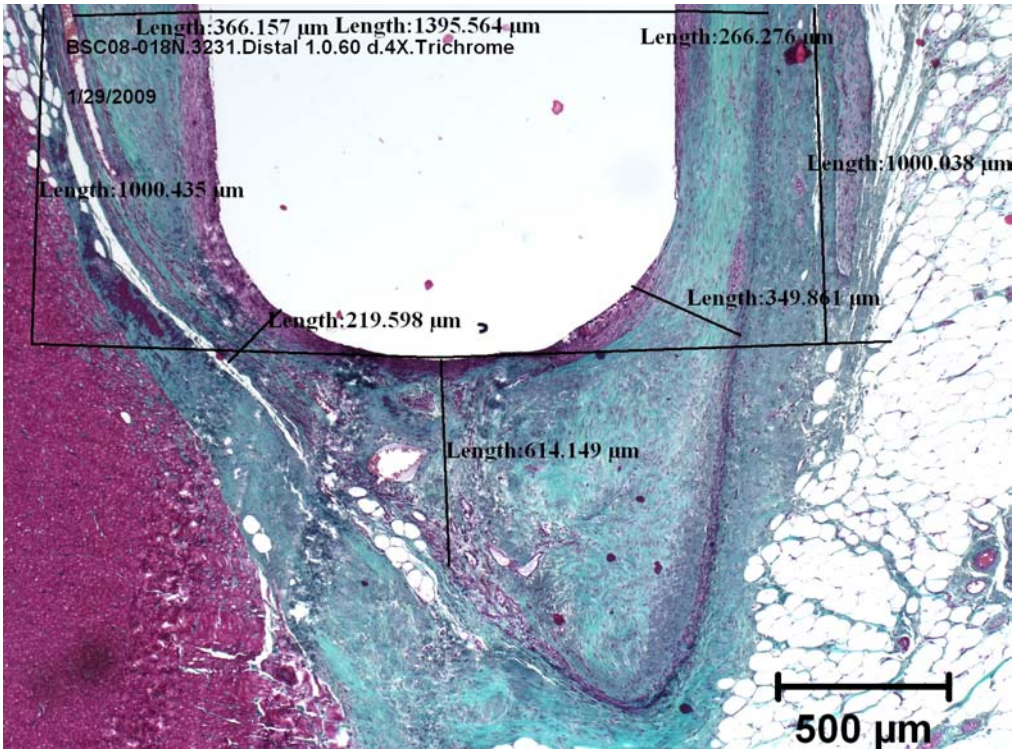
Length:366.157 µm Length:1395.564 µm
BSC08-018N.3231.Distal 1.0.60 d.4X.Trichrome
Length:266.276 µm
1/29/2009
Length:1000.038 µm
Length:1000.435 µm
Length:349.861 µm
Length:219.598 µm
Length:614.149 µm
500 µm

Summary Study Information for Animal L-3232, Lead 164017 (Porous Tip Electrode)

Lead Tip Images*

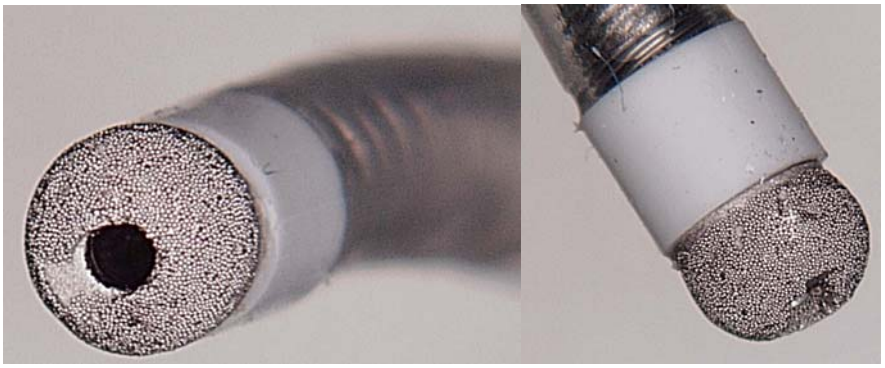

* Steroid eluting collars were initially assembled onto the lead in error (and are shown in the images), though they were later removed and replaced with silicone tubing of the same length, thickness, and diameters as the steroid collars, but with no steroid.

Implant Fluoroscopy Images

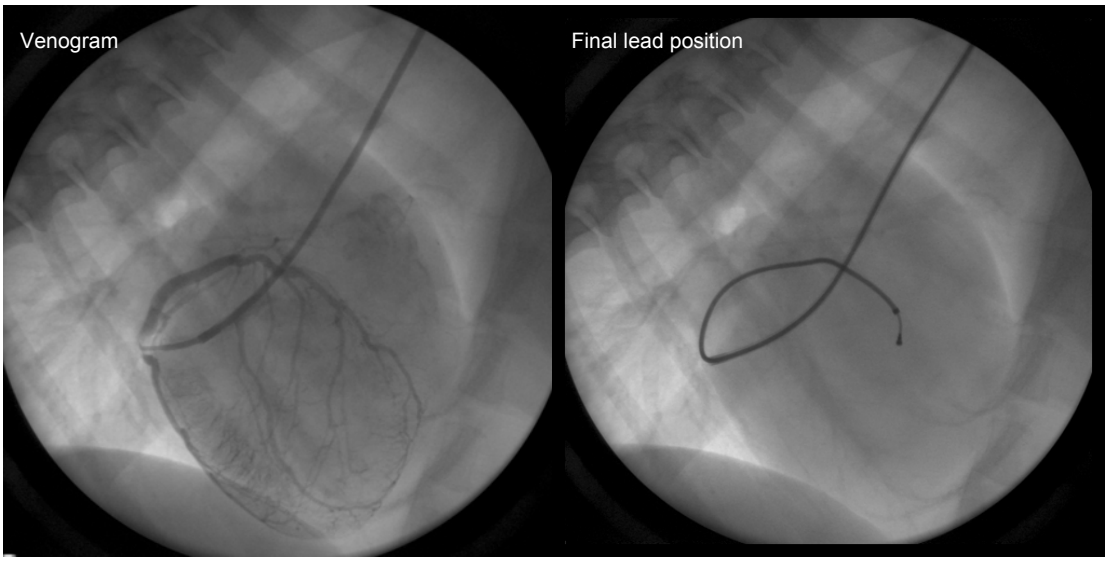

Study Data

Animal ID	Source	Date	Day	Thr. [V]	Thr. Change [V]	R-Wave [mV]	Imp. [Ω]	Movement [cm]	Tip Pos. [cm]
L-3232	PSA Ring	5/30/2008	0	3.5		16.0	1944		
Lead ID	PSA Tip	5/30/2008	0	1.0		27.5	1856		
164017	PG	5/30/2008	0	1.0	0.0	16.4	590	0	0
Tip Electrode	PG	6/2/2008	3	0.8	-0.2	17.3	540	0	0
Porous	PG	6/6/2008	7	0.8	-0.2	19.2	550	0	0
	PG	6/13/2008	14	0.7	-0.3	17.3	600	0	0
	PG	6/20/2008	21	0.8	-0.2	16.9	590	0	0
	PG	6/27/2008	28	0.8	-0.2	17.3	620	0	0
	PG	7/11/2008	42	0.7	-0.3	18.2	700	0	0
	PG	7/29/2008	60	0.4	-0.6	16.4	790	0	0
	PSA Ring	7/29/2008	60	6.8	3.3	21.0	1516		

Histology

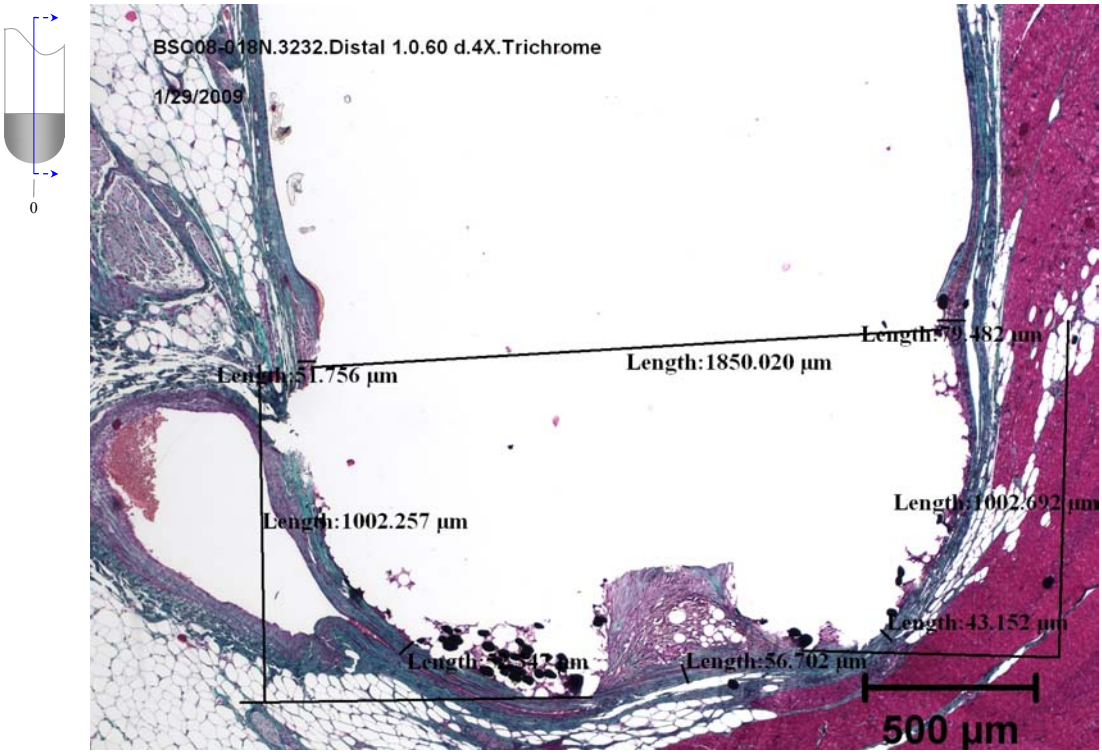
BSC08-018N.3232.Distal 1.0.60 d.4X.Trichrome
1/29/2009
0
Length:51.756 µm
Length:1850.020 µm
Length:1002.257 µm
Length:1002.692 µm
Length:43.152 µm
Length:56.702 µm
500 µm

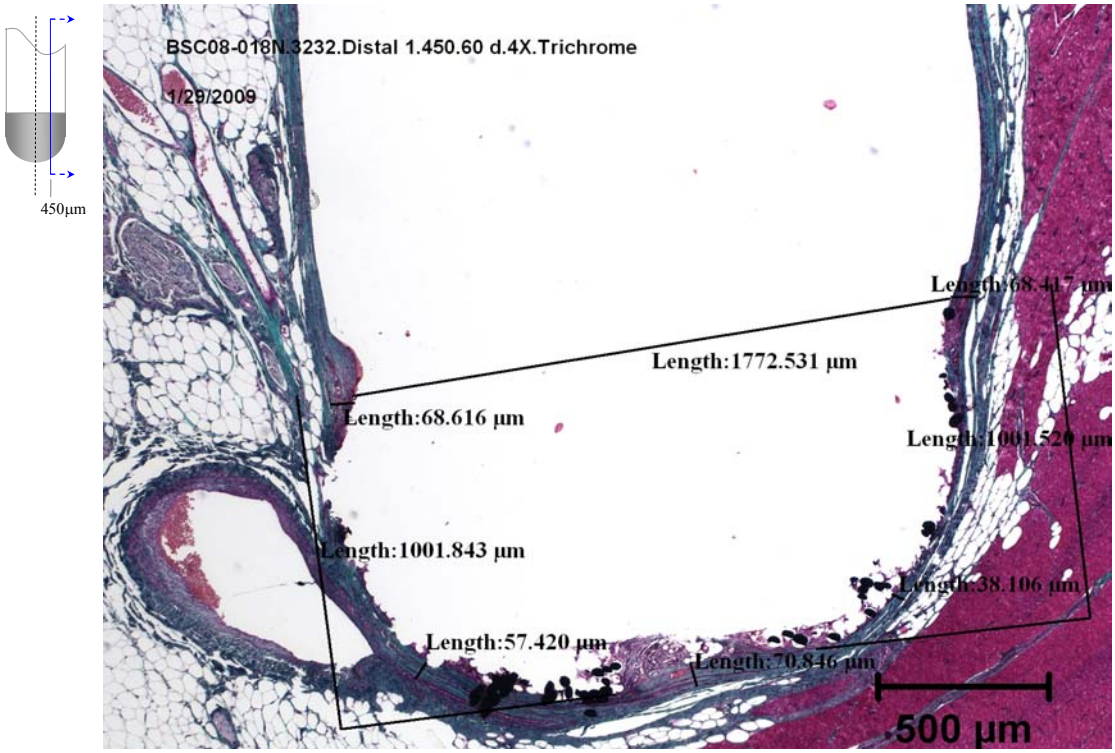
BSC08-018N.3232.Distal 1.450.60 d.4X.Trichrome
1/29/2009
450µm
Length:1772.531 µm
Length:68.616 µm
Length:1001.843 µm
Length:38.106 µm
Length:57.420 µm
Length:70.846 µm
500 µm

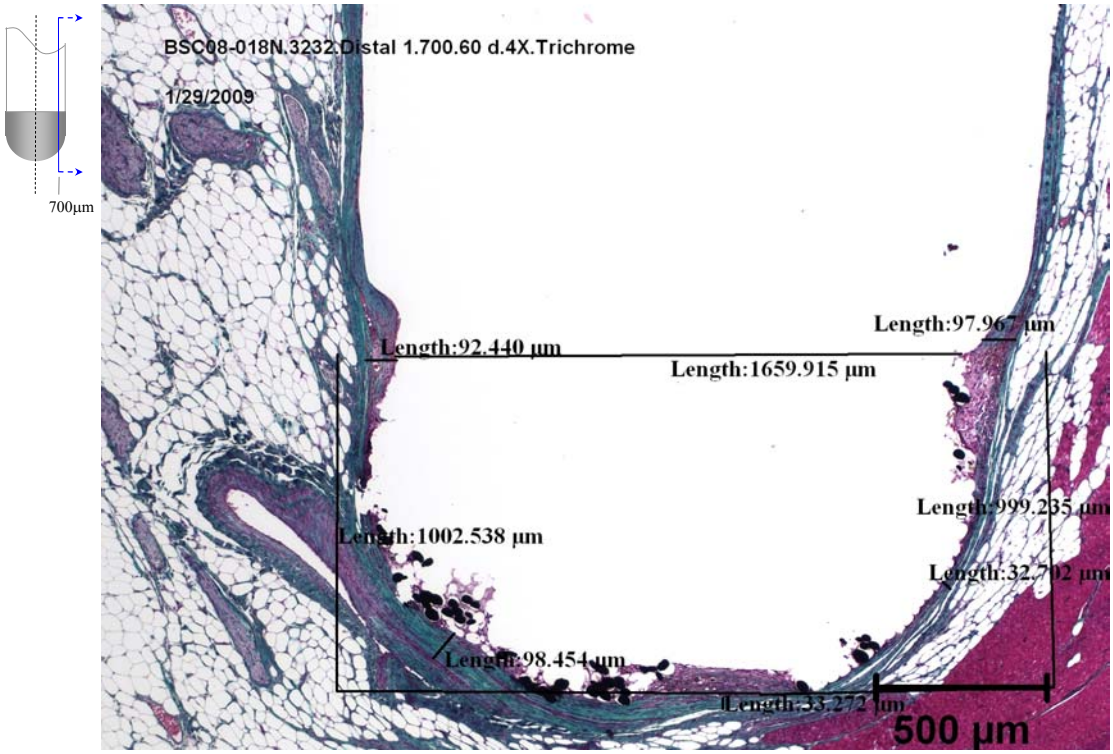
700µm
BSC08-018N.3232.Distal 1.700.60 d.4X.Trichrome
1/29/2009
Length:92.440 µm
Length:1659.915 µm
Length:97.967 µm
Length:999.235 µm
Length:1002.538 µm
Length:32.702 µm
Length:98.454 µm
Length:33.272 µm
500 µm

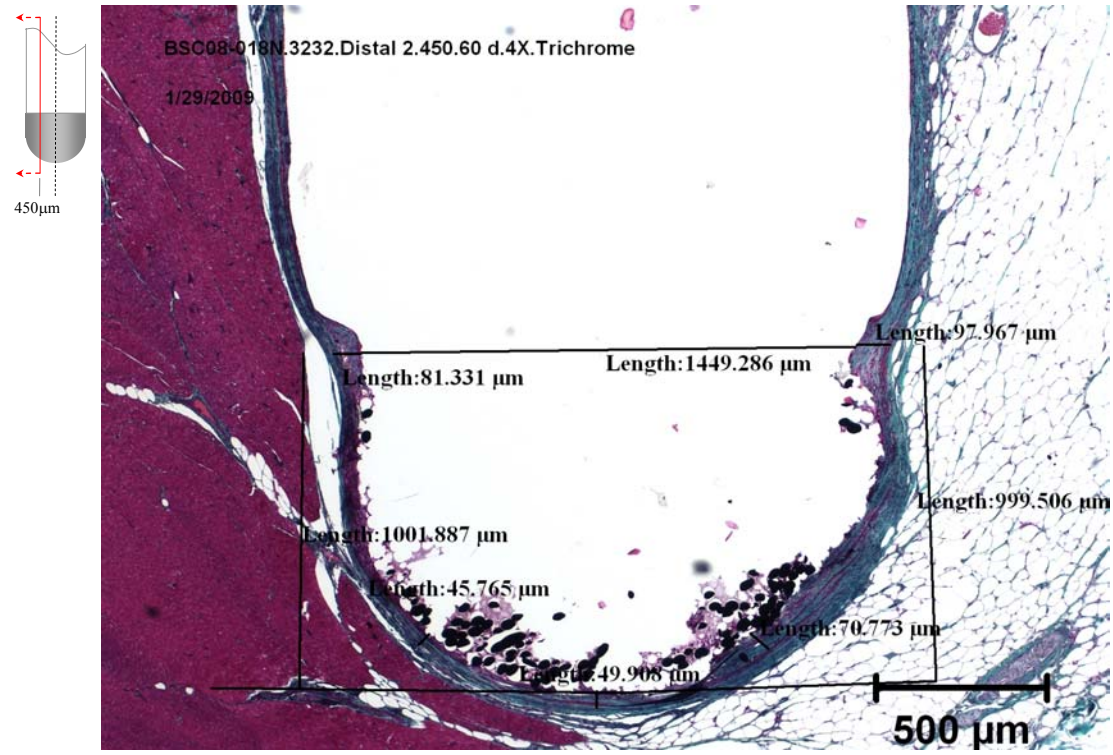
450µm
BSC08-018N.3232.Distal 2.450.60 d.4X.Trichrome
1/29/2009
Length:97.967 µm
Length:1449.286 µm
Length:81.331 µm
Length:999.506 µm
Length:1001.887 µm
Length:45.765 µm
Length:70.773 µm
Length:49.908 µm
500 µm

Appendix D: Fibrous Capsule Thickness Data

Below are the data compiled from the histology images in Appendix C which were used in the generation of Figure 39. As explained in the discussion prior to Figure 38 (and in the figure itself) only slices with measured lead track widths greater than 1500 μm were included in the fibrous capsule thickness data.

Porous Electrode Leads

		Fibrous Capsule Thickness [μm]				
Animal	Lead Track Width [μm]	"Corners" (mean within slice)	"Sides" (mean within slice)	"Corners" (mean across slices)	"Sides" (mean across slices)	
L-3217	1629	37	36			
	1830	64	102			
	2084	54	106	51	81	
L-3219	1636	74	96			
	1797	73	71			
	1918	77	90	75	86	
L-3220	1597	50	41			
	1598	61	37			
	1697	87	59	66	46	
L-3221	1505	38	95	38	95	
L-3227	1941	57	85	57	85	
L-3229	1845	63	64	63	64	
L-3230	1506	168	105			
	1580	54	57			
	1828	61	61	94	74	
L-3232	1660	66	95			
	1773	48	69			
	1850	48	66	54	76	
				62	**76**	**Mean [μm]**
				17	**15**	**St. Dev.**

Solid Electrode Leads

		Fibrous Capsule Thickness [μm]				
Animal	Lead Track Width [μm]	"Corners" (mean within slice)	"Sides" (mean within slice)	"Corners" (mean across slices)	"Sides" (mean across slices)	
L-3216	1629	33	17			
	1935	22	25	27	21	
L-3218	1694	186	130			
	1701	126	169			
	1709	199	164			
	1999	169	133	170	149	
L-3222	1651	55	65			
	1979	64	67	59	66	
L-3223	1655	101	38			
	1846	57	44			
	1910	73	58	77	47	
L-3224	1569	96	94			
	1846	79	36	87	65	
L-3225	1961	102	103			
	2021	85	114	94	108	
L-3226	1670	52	40			
	2031	42	43	47	42	
L-3231	1688	118	189			
	1832	107	175			
	1934	192	190	139	184	
				88	**85**	**Mean [μm]**
				47	**57**	**St. Dev.**